JSCSEN 88(1)1–111(2023)

ISSN 1820-7421(Online)

Journal of the Serbian Chemical Society

Electronic version

VOLUME 88

No 1

BELGRADE 2023

Available on line at

www.shd.org.rs/JSCS/

The full search of JSCS is available through

DOAJ DIRECTORY OF OPEN ACCESS JOURNALS

www.doaj.org

The **Journal of the Serbian Chemical Society** (formerly Glasnik Hemijskog društva Beograd), one volume (12 issues) per year, publishes articles from the fields of chemistry. The **Journal** is financially supported by the **Ministry of Education, Science and Technological Development of the Republic of Serbia.**

Articles published in the **Journal** are indexed in **Clarivate Analytics products: Science Citation Index-Expanded™** – accessed *via* **Web of Science®** and **Journal Citation Reports®**.

Impact Factor announced 2022: **1.100; 5-year Impact Factor**: **1.175**.

Articles appearing in the **Journal** are also abstracted by: **Scopus, Chemical Abstracts Plus (CAplus℠), Directory of Open Access Journals, Referativnii Zhurnal (VINITI), RSC Analytical Abstracts, EuroPub, Pro Quest** and **Asian Digital Library.**

Publisher:	**Serbian Chemical Society**, Karnegijeva 4/III, P. O. Box 36, 1120 Belgrade 35, Serbia tel./fax: +381–11–3370–467, E-mails: **Society** – shd@shd.org.rs; **Journal** – jscs@shd.org.rs Home Pages: **Society** – http://www.shd.org.rs/, **Journal** – http://www.shd.org.rs/JSCS/
Internet Service:	Contents, Abstracts and full papers (from Vol 64, No. 1, 1999) are available in the electronic form at the Web Site of the **Journal** (http://www.shd.org.rs/JSCS/).
Former Editors:	**Nikola A. Pušin** (1930–1947), **Aleksandar M. Leko** (1948–1954), **Panta S. Tutundžić** (1955–1961), **Miloš K. Mladenović** (1962–1964), **Đorđe M. Dimitrijević** (1965–1969), **Aleksandar R. Despić** (1969–1975), **Slobodan V. Ribnikar** (1975–1985), **Dragutin M. Dražić** (1986–2006).
Editor-in-Chief:	BRANISLAV Ž. **NIKOLIĆ**, Serbian Chemical Society (E-mail: jscs-ed@shd.org.rs)
Deputy Editor:	DUŠAN **SLADIĆ**, Faculty of Chemistry, University of Belgrade
Sub editors:	
Organic Chemistry	DEJAN **OPSENICA**, Institute of Chemistry, Technology and Metallurgy, University of Belgrade JÁNOS **CSANÁDI**, Faculty of Science, University of Novi Sad
Biochemistry and Biotechnology	OLGICA **NEDIĆ**, INEP – Institute for the Application of Nuclear Energy, University of Belgrade
Inorganic Chemistry	MILOŠ **ĐURAN**, Serbian Chemical Society
Theoretical Chemistry	IVAN **JURANIĆ**, Serbian Chemical Society
Physical Chemistry	LJILJANA **DAMJANOVIĆ-VASILIĆ**, Faculty of Physical Chemistry, University of Belgrade
Electrochemistry	SNEŽANA **GOJKOVIĆ**, Faculty of Technology and Metallurgy, University of Belgrade
Analytical Chemistry	SLAVICA **RAŽIĆ**, Faculty of Pharmacy, University of Belgrade
Polymers	BRANKO **DUNJIĆ**, Faculty of Technology and Metallurgy, University of Belgrade
Thermodynamics	MIRJANA **KIJEVČANIN**, Faculty of Technology and Metallurgy, University of Belgrade
Chemical Engineering	TATJANA **KALUĐEROVIĆ RADOIČIĆ**, Faculty of Technology and Metallurgy, University of Belgrade
Materials	RADA **PETROVIĆ**, Faculty of Technology and Metallurgy, University of Belgrade
Metallic Materials and Metallurgy	ANA **KOSTOV**, Mining and Metallurgy Institute Bor, University of Belgrade
Environmental and Geochemistry	VESNA **ANTIĆ**, Faculty of Agriculture, University of Belgrade
History of and Education in Chemistry	DRAGICA **TRIVIĆ**, Faculty of Chemistry, University of Belgrade
English Language Editors:	LYNNE **KATSIKAS**, Serbian Chemical Society VLATKA **VAJS**, Serbian Chemical Society JASMINA **NIKOLIĆ**, Faculty of Technology and Metallurgy, University of Belgrade
Technical Editors:	VLADIMIR **PANIĆ**, ALEKSANDAR **DEKANSKI**, VUK **FILIPOVIĆ**, Institute of Chemistry, Technology and Metallurgy, University of Belgrade
Journal Manager & Web Master:	ALEKSANDAR **DEKANSKI,** Institute of Chemistry, Technology and Metallurgy, University of Belgrade
Office:	VERA **ĆUŠIĆ**, Serbian Chemical Society

Editorial Board

From abroad: **R. Adžić**, Brookhaven National Laboratory (USA); **A. Casini**, University of Groningen (The Netherlands); **G. Cobb**, Baylor University (USA); **D. Douglas**, University of British Columbia (Canada); **G. Inzelt**, Etvos Lorand University (Hungary); **J. Kenny**, University of Perugia (Italy); **Ya. I. Korenman**, Voronezh Academy of Technology (Russian Federation); **M. D. Lechner**, University of Osnabrueck (Germany); **S. Macura**, Mayo Clinic (USA); **M. Spiteller**, INFU, Technical University Dortmund (Germany); **M. Stratakis**, University of Crete (Grecce); **M. Swart**, University de Girona (Cataluna, Spain); **G. Vunjak-Novaković**, Columbia University (USA); **P. Worsfold**, University of Plymouth (UK); **J. Zagal**, Universidad de Santiago de Chile (Chile).

From Serbia: **B. Abramović**, **V. Antić**, **V. Beškoski**, **J. Csanadi**, **Lj. Damjanović-Vasilić**, **A. Dekanski**, **V. Dondur**, **B. Dunjić**, **M. Đuran, S. Gojković**, **I. Gutman**, **B. Jovančićević**, **I. Juranić**, **T. Kaluđerović Radioičić**, **L. Katsikas**, **M. Kijevčanin**, **A. Kostov**, **V. Leovac**, **S. Milonjić**, **V.B. Mišković-Stanković**, **O. Nedić**, **B. Nikolić**, **J. Nikolić**, **D. Opsenica**, **V. Panić**, **M. Petkovska**, **R. Petrović**, **I. Popović**, **B. Radak**, **S. Ražić**, **D. Sladić**, **S. Sovilj**, **S. Šerbanović**, **B. Šolaja**, **Ž. Tešić**, **D. Trivić**, **V. Vajs**.

Subscription: The annual subscription rate is **150.00 €** including postage (surface mail) and handling. For Society members from abroad rate is **50.00 €**. For the proforma invoice with the instruction for bank payment contact the Society Office (E-mail: shd@shd.org.rs) or see JSCS Web Site: http://www.shd.org.rs/JSCS/, option Subscription.

Godišnja pretplata: Za članove SHD: **2.500,00 RSD**, za penzionere i studente: **1000,00 RSD**, a za ostale: **3.500,00 RSD**:za organizacije i ustanove: **16.000,00 RSD**. Uplate se vrše na tekući račun Društva: **205-13815-62**, poziv na broj **320**, sa naznakom "pretplata za JSCS".

Nota: Radovi čiji su svi autori članovi SHD prioritetno se publikuju.

Odlukom Odbora za hemiju Republičkog fonda za nauku Srbije, br. 66788/1 od 22.11.1990. godine, koja je kasnije potvrđena odlukom Saveta Fonda, časopis je uvršten u kategoriju međunarodnih časopisa (**M-23**). Takođe, aktom Ministarstva za nauku i tehnologiju Republike Srbije, 413-00-247/2000-01 od 15.06.2000. godine, ovaj časopis je proglašen za publikaciju od posebnog interesa za nauku. **Impact Factor** časopisa objavljen 2022. godini iznosi **1,100**, a petogodišnji **Impact Factor 1,175**.

INSTRUCTIONS FOR AUTHORS (2021)

GENERAL

The *Journal of the Serbian Chemical Society* (the *Journal* in further text) is an international journal publishing papers from all fields of chemistry and related disciplines. Twelve issues are published annually. The Editorial Board expects the editors, reviewers, and authors to respect the well-known standard of professional ethics.

Types of Contributions

Original scientific papers	(up to 15 typewritten pages, including Figures, Tables and References) report original research which must not have been previously published.
Short communications	(up to 8 pages) report unpublished preliminary results of sufficient importance to merit rapid publication.
Notes	(up to 5 pages) report unpublished results of short, but complete, original research
Authors' reviews	(up to 40 pages) present an overview of the author's current research with comparison to data of other scientists working in the field
Reviews[a]	(up to 40 pages) present a concise and critical survey of a specific research area. Generally, these are prepared at the invitation of the Editor
Surveys	(about 25 pages) communicate a short review of a specific research area.
Book and Web site reviews	(1 - 2 pages)
Extended abstracts	(about 4 pages) of Lectures given at meetings of the Serbian Chemical Society Divisions
Letters to the Editor	report miscellaneous topics directed directly to the Editor

[a]Generally, Authors' reviews, Reviews and Surveys are prepared at the invitation of the Editor.

Research Data Policy

The Journal of the Serbian Chemical Society (JSCS) encourages that all supporting data sets and the results, which were used for discussion and making conclusions in the presented paper, should be available to readers. We strongly support authors to deposits their datasets in free available repositories. Read more at https://www.shd-pub.org.rs/index.php/JSCS/DataPolicy.

PrePrint Policy

Authors are allowed to store a preprint version of their manuscript on a recognized preprint server such as ChemRxiv, arXiv, or on any repository that provides a public identifier (e.g. DOI) prior to submission. Read more at https://www.shd-pub.org.rs/index.php/JSCS/Preprint.

ORCID

The journal requires from corresponding authors to submit ORCID upon registration, while co-authors are forwarded an ORCID attribution request upon manuscript submission, and upon potential acceptance of the paper for publication. Read more at https://www.shd-pub.org.rs/index.php/JSCS/Orcid.

Submission of manuscripts

Manuscripts should be submitted using the **OnLine Submission Form**, available on the JSCS Web Site (**http://www.shd-pub.org.rs/index.php/JSCS**). The manuscript must be uploaded as a Word.doc or .rtf file, with tables and figures (including the corresponding captions – above Tables and below Figures), placed within the text to follow the paragraph in which they were mentioned for the first time.

Please note that **Full Names (**First Name, Last Name), **Full Affiliation** and **Country** (from drop down menu) of **ALL OF AUTHORS** (written in accordance with English spelling rules - the first letter capitalized) must be entered in the manuscript Submission Form (Step 3). Manuscript Title, authors' names and affiliations, as well as the Abstract, **WILL APPEAR** in the article listing, as well as in **BIBLIOGRAPHIC DATABASES (WoS, SCOPUS...)**, in the form and in the order entered in the author details

Graphical abstract

Graphical abstract is a one-image file containing the main depiction of the authors work and/or conclusion and must be supplied along with the manuscript. It must enable readers to quickly gain the main message of the paper and to encourage browsing, help readers identify which papers are most relevant to their research interests. Authors must provide an image that clearly represents the research described in the paper. The most relevant figure from the work, which summarizes the content, can also be submitted. The image should be submitted as a separate file in **Online Submission Form - Step 2**.

Specifications: The graphical abstract should have a clear start and end, reading from top to bottom or left to right. Please omit unnecessary distractions as much as possible.

- **Image size:** minimum of 500×800 pixels (W×H) and a minimum resolution of 300 dpi. If a larger image is sent, then please use the same ratio: 16 wide × 9 high. Please note that your image will be scaled proportionally to fit in the available window in TOC; a 150x240 pixel rectangle. Please be sure that the quality of an image cannot be increased by changing the resolution from lower to higher, but only by rescanning or exporting the image with a higher resolution, which can be set in usual "settings" option.
- **Font:** Please use Calibri and Symbol font with a large enough font size, so it is readable even from the image of a smaller size (150 × 240 px) in TOC.
- **File type:** JPG and PNG only.

No additional text, outline or synopsis should be included. Please do not use white space or any heading within the image.

Cover Letter

Manuscripts must be accompanied by a cover letter (strictly uploaded in **Online Submission Step 2**) in which the type of the submitted manuscript and a warranty as given below are given. The Author(s) has(have) to warranty that the manuscript submitted to the *Journal* for review is original, has been written by the stated author(s) and has not been published elsewhere; is currently not being considered for publication by any other journal and will not be submitted for such a review while under review by the *Journal*; the manuscript contains no libellous or other unlawful statements and does not contain any materials that violate any personal or proprietary rights of any other person or entity. All manuscripts will be acknowledged on receipt (by e-mail).

Illustrations

Illustrations (Figs, schemes, photos…) in TIF or EPS format (JPG format is acceptable for colour and greyscale photos, only), must be additionally uploaded (Online Submission Step 2) as a separate file or one archived (.zip, .rar or .arj) file. Figures and/or Schemes should be prepared according to the **Artwork Instructions -** http://www.shd.org.rs/JSCS/jscs-pdf/Artwork_Instructions.pdf!

For any difficulties and questions related to **OnLine Submission Form -** https://www.shd-pub.org.rs/index.php/JSCS/submission/wizard, please refer to **User Guide -** https://openjournal-systems.com/ojs-3-user-guide/ , Chapter **Submitting an Article -** https://openjournalsystems.com/ojs-3-user-guide/submitting-an-article/. If difficulties still persist, please contact JSCS Editorial Office at **JSCS@shd.org.rs**

A manuscript not prepared according to these instructions will be returned for resubmission without being assigned a reference number.

Conflict-of-Interest Statement*: Public trust in the peer review process and the credibility of published articles depend in part on how well a conflict of interest is handled during writing, peer review, and editorial decision making. A conflict of interest exists when an author (or the author's institution), reviewer, or editor has financial or personal relationships that inappropriately influence (bias) his or her actions (such relationships are also known as dual commitments, competing interests, or competing loyalties). These relationships vary from those with negligible potential to those with great potential to influence judgment, and not all relationships represent true conflict of interest. The potential for a conflict of interest can exist whether or not an individual believes that the relationship affects his or her scientific judgment. Financial relationships (such as employment, consultancies, stock ownership, honoraria, paid expert testimony) are the most easily identifiable conflicts of interest and the most likely to undermine the credibility of the journal, the authors, and of science itself. However, conflicts can occur for other reasons, such as personal relationships, academic competition, and intellectual passion.

Informed Consent Statement*: Patients have a right to privacy that should not be infringed without informed consent. Identifying information, including patients' names, initials, or hospital numbers, should not be published in written descriptions, photographs, and pedigrees unless the information is essential for

*International Committee of Medical Journal Editors ("Uniform Requirements for Manuscripts Submitted to Biomedical Journals"), February 2006

scientific purposes and the patient (or parent or guardian) gives written informed consent for publication. Informed consent for this purpose requires that a patient who is identifiable be shown the manuscript to be published. Authors should identify Individuals who provide writing assistance and disclose the funding source for this assistance. Identifying details should be omitted if they are not essential. Complete anonymity is difficult to achieve, however, and informed consent should be obtained if there is any doubt. For example, masking the eye region in photographs of patients is inadequate protection of anonymity. If identifying characteristics are altered to protect anonymity, such as in genetic pedigrees, authors should provide assurance that alterations do not distort scientific meaning and editors should so note. The requirement for informed consent should be included in the journal's instructions for authors. When informed consent has been obtained it should be indicated in the published article.

Human and Animal Rights Statement* When reporting experiments on human subjects, authors should indicate whether the procedures followed were in accordance with the ethical standards of the responsible committee on human experimentation (institutional and national) and with the Helsinki Declaration of 1975, as revised in 2000 (5). If doubt exists whether the research was conducted in accordance with the Helsinki Declaration, the authors must explain the rationale for their approach, and demonstrate that the institutional review body explicitly approved the doubtful aspects of the study. When reporting experiments on animals, authors should be asked to indicate whether the institutional and national guide for the care and use of laboratory animals was followed.

PROCEDURE

All contributions will be peer reviewed and only those deemed worthy and suitable will be accepted for publication. The Editor has the final decision. To facilitate the reviewing process, authors are encouraged to suggest up to three persons competent to review their manuscript. Such suggestions will be taken into consideration but not always accepted. If authors would prefer a specific person not be a reviewer, this should be announced. The Cover Letter must be accompanied by these suggestions. Manuscripts requiring revision should be returned according to the requirement of the Editor, within 60 days upon reception of the reviewing comments by e-mail.

The *Journal* maintains its policy and takes the liberty of correcting the English as well as false content of manuscripts **provisionally accepted** for publication in the first stage of reviewing process. In this second stage of manuscript preparation by JSCS Editorial Office, the author(s) may be required to supply some **additional clarifications and corrections**. This procedure will be executed during copyediting actions, with a demand to author(s) to perform corrections of unclear parts before the manuscript would be published OnLine as **finally accepted manuscript (OLF Section of the JSCS website)**. Please note that the manuscript can receive the status of **final rejection** if the author's corrections would not be satisfactory.

When finally accepted manuscript is ready for printing, the corresponding author will receive a request for proof reading, which should be performed within 2 days. Failure to do so will be taken as the authors agree with any alteration which may have occurred during the preparation of the manuscript for printing.

Accepted manuscripts of active members of the Serbian Chemical Society (all authors) have publishing priority.

MANUSCRIPT PRESENTATION

Manuscripts should be typed in English (either standard British or American English, but consistent throughout) with 1.5 spacing (12 points Times New Roman; Greek letters in the character font Symbol) in A4 format leaving 2.5 cm for margins. For Regional specific, non-standard characters that may appear in the text, save documents with Embed fonts Word option: *Save as -> (Tools) -> Save Options… -> Embed fonts in the text.*

The authors are requested to seek the assistance of competent English language expert, if necessary, to ensure their English is of a reasonable standard. The Serbian Chemical Society can provide this service in advance of submission of the manuscript. If this service is required, please contact the office of the Society by e-mail (jscs-info@shd.org.rs).

Tables, figures and/or schemes must be embedded in the main text of the manuscript and should follow the paragraph in which they are mentioned for the first time. **Tables** must be prepared with the aid of the **WORD table function**, without vertical lines. The minimum size of the font in the tables should be **10 pt**. Table columns must not be formatted using multiple spaces. Table rows must not be formatted using any returns (enter key; ↵ key) and are **limited to 12 cm width**. Tables should not be incorporated as graphical objects. **Footnotes to Tables** should follow them and are to be indicated consequently (in a single line) in superscript letters and separated by semi-column.

Table caption must be placed above corresponding Table, while **Captions of the Illustrations** (Figs. Schemes...) must follow the corresponding item. **The captions, either for Tables or Illustrations**, should make the items comprehensible without reading of the main text (but clearly referenced in), must follow numerical order (Roman for Tables, Arabic for Illustrations), and should not be provided on separate sheets or as separate files.

High resolution Illustrations (named as Fig. 1, Fig. 2… and/or Scheme 1, Scheme 2…) in **TIF or EPS format** (JPG format is acceptable for photos, only) **must be additionally uploaded as a separate files or one archived (.zip, .rar) file.**

Illustrations should be prepared according to the ARTWORK INSTRUCTIONS - http://www.shd.org.rs/JSCS/jscs-pdf/Artwork_Instructions.pdf. **!**

All pages of the manuscript must be numbered continuously.

DESIGNATION OF PHYSICAL QUANTITIES AND UNITS

IUPAC recommendations for the naming of compounds should be followed. SI units, or other permissible units, should be employed. The designation of physical quantities must be in italic throughout the text (including figures, tables and equations), whereas the units and indexes (except for indexes having the meaning of physical quantities) are in upright letters. They should be in Times New Roman font. In graphs and tables, a slash should be used to separate the designation of a physical quantity from the unit (example: p / kPa, j / mA cm^{-2}, t / °C, T_0 / K, τ / h, ln (j / mA cm^{-2})…). Designations such as: p (kPa), t [min]…, are not acceptable. However, if the full name of a physical quantity is unavoidable, it should be given in upright letters and separated from the unit by a comma (example: Pressure, kPa; Temperature, K; Current density, mA cm^{-2}…). Please do not use the axes of graphs for additional explanations; these should be mentioned in the figure captions and/or the manuscript (example: "pressure at the inlet of the system, kPa" should be avoided). The axis name should follow the direction of the axis (the name of y-axis should be rotated by 90°). Top and right axes should be avoided in diagrams, unless they are absolutely necessary.

Latin words, as well as the names of species, should be in *italic*, as for example: *i.e.*, *e.g.*, *in vivo*, *ibid*, *Calendula officinalis* L., *etc*. The branching of organic compound should also be indicated in *italic*, for example, *n*-butanol, *tert*-butanol, *etc*.

Decimal numbers must have decimal points and not commas in the text (except in the Serbian abstract), tables and axis labels in graphical presentations of results. Thousands are separated, if at all, by a comma and not a point.

Mathematical and chemical equations should be given in separate lines and must be numbered, Arabic numbers, consecutively in parenthesis at the end of the line. All equations should be embedded in the text Complex equations (fractions, integrals, matrix…) should be prepared with the aid of the **Microsoft Equation 3.0** (or higher) or **MathType** (Do not use them to create simple equations and labels). **Using the Insert -> Equation option, integrated in MS Office 2010 and MS Office 2013, as well as insertion of equation objects within paragraph text IS NOT ALLOWED.**

ARTICLE STRUCTURE

- TITLE PAGE
- MAIN TEXT – including Tables and Illustrations with corresponding captions
- SUPPLEMENTARY MATERIAL (optional**)**

Title page

- **Title** in bold letters, should be clear and concise, preferably 12 words or less. The use of non-standard abbreviations, symbols and formulae is discouraged.
- AUTHORS' NAMES in capital letters with the full first name, initials of further names separated by a space and surname. Commas should separate the author's names except for the last two names when 'and' is to be used. In multi-affiliation manuscripts, the author's affiliation should be indicated by an Arabic number placed in superscript after the name and before the affiliation. Use * to denote the corresponding author(s).
- *Affiliations* should be written in italic. The e-mail address of the corresponding author should be given after the affiliation(s).

- *Abstract:* A one-paragraph abstract written of 150 – 200 words in an impersonal form indicating the aims of the work, the main results and conclusions should be given and clearly set off from the text. Domestic authors should also submit, on a separate page, an Abstract - Izvod, the author's name(s) and affiliation(s) in Serbian (Cyrillic letters). (Домаћи аутори морају доставити Извод (укључујући имена аутора и афилијацију) на српском језику, исписане ћирилицом, иза Захвалнице, а пре списка референци.) For authors outside Serbia, the Editorial Board will provide a Serbian translation of their English abstract.
- *Keywords:* Up to 6 keywords should be given. Do not use words appearing in the manuscript title
- RUNNING TITLE: A one line (maximum five words) short title in capital letters should be provided.

Main text – should have the form:

- **INTRODUCTION,**
- **EXPERIMENTAL (RESULTS AND DISCUSSION),**
- **RESULTS AND DISCUSSION (EXPERIMENTAL),**
- **CONCLUSIONS,**
- **NOMENCLATURE (optional) and**
- ***Acknowledgements*: If any.**
- REFERENCES (Citation of recent papers published in chemistry journals that highlight the significance of work to the general readership is encouraged.)

The sections should be arranged in a sequence generally accepted for publication in the respective fields. They subtitles should be in capital letters, centred and NOT numbered.

- The INTRODUCTION should include the aim of the research and a concise description of background information and related studies directly connected to the paper.
- The EXPERIMENTAL section should give the purity and source of all employed materials, as well as details of the instruments used. The employed methods should be described in sufficient detail to enable experienced persons to repeat them. Standard procedures should be referenced and only modifications described in detail. On no account should results be included in the experimental section.

Chemistry

Detailed information about instruments and general experimental techniques should be given in all necessary details. If special treatment for solvents or chemical purification were applied that must be emphasized.

Example: Melting points were determined on a Boetius PMHK or a Mel-Temp apparatus and were not corrected. Optical rotations were measured on a Rudolph Research Analytical automatic polarimeter, Autopol IV in dichloromethane (DCM) or methanol (MeOH) as solvent. IR spectra were recorded on a Perkin-Elmer spectrophotometer FT-IR 1725X. ^{1}H and ^{13}C NMR spectra were recorded on a Varian Gemini-200 spectrometer (at 200 and 50 MHz, respectively), and on a Bruker Ultrashield Advance III spectrometer (at 500 and 125 MHz, respectively) employing indicated solvents (*vide infra*) using TMS as the internal standard. Chemical shifts are expressed in ppm (δ / ppm) values and coupling constants in Hz (J / Hz). ESI-MS spectra were recorded on Agilent Technologies 6210 Time-Of-Flight LC-MS instrument in positive ion mode with CH_3CN/H_2O 1/1 with 0.2 % HCOOH as the carrying solvent solution. Samples were dissolved in CH_3CN or MeOH (HPLC grade purity). The selected values were as follows: capillary voltage = 4 kV, gas temperature = 350 °C, drying gas flow 12 L min^{-1}, nebulizer pressure = 310 kPa, fragmentator voltage = 70 V.The elemental analysis was performed on the Vario EL III- C,H,N,S/O Elemental Analyzer (Elementar Analysensysteme GmbH, Hanau-Germany). Thin-layer chromatography (TLC) was performed on precoated Merck silica gel 60 F254 and RP-18 F254 plates. Column chromatography was performed on Lobar LichroPrep Si 60 (40-63 μm), RP-18 (40-63 µm) columns coupled to a Waters RI 401 detector, and on Biotage SP1 system with UV detector and FLASH 12+, FLASH 25+ or FLASH 40+ columns pre packed with KP-SIL [40-63 µm, pore diameter 6 nm (60 Å)], KP-C18-HS (40-63 µm, pore diameter 9 nm (90 Å) or KP-NH [40-63 µm, pore diameter 10 nm (100 Å)] as adsorbent. Compounds were analyzed for purity (HPLC) using a Waters 1525 HPLC dual pump system equipped with an Alltech, Select degasser system, and dual λ 2487 UV-VIS detector. For data processing, Empower software was used (methods A and B). Methods C and D: Agylent Technologies 1260 Liquid Chromatograph equipped with Quat Pump (G1311B), Injector (G1329B) 1260 ALS, TCC 1260 (G1316A) and Detector 1260 DAD VL+ (G1315C). For data processing, LC OpenLab CDS ChemStation software was used. For details, see Supporting Information.

1. Synthesis experiments

Each paragraph describing a synthesis experiment should begin with the name of the product and any structure number assigned to the compound in the Results and Discussions section. Thereafter, the compound should be identified by its structure number. Use of standard abbreviations or unambiguous molecular formulas for reagents and solvents, and of structure numbers rather than chemical names to identify starting materials and intermediates, is encouraged.

When a new or improved synthetic method is described, the yields reported in key experimental examples, and yields used for comparison with existing methods, should represent amounts of isolated and purified products, rather than chromategraphically or spectroscopically determined yields. Reactant quantities should be reported in weight and molar units and for product yields should be reported in weight units; percentage yields should only be reported for materials of demonstrated purity. When chromatography is used for product purification, both the support and solvent should be identified.

2. Microwave experiments

Reports of syntheses conducted in microwave reactors must clearly indicate whether sealed or open reaction vessels were used and must document the manufacturer and model of the reactor, the method of monitoring the reaction mixture temperature, and the temperature-time profile. Reporting a wattage rating or power setting is not an acceptable alternative to providing temperature data. Manuscripts describing work done with domestic (kitchen) microwave ovens will not be accepted except for studies where the unit is used for heating reaction mixtures at atmospheric pressure.

3. Compound characterization

The Journal upholds a high standard for compound characterization to ensure that substances being added to the chemical literature have been correctly identified and can be synthesized in known yield and purity by the reported preparation and isolation methods. For **all new** compounds, evidence adequate to establish both **identity** and **degree of purity** (homogeneity) must be provided.

Identity *- Melting point.* All homogeneous solid products (*e.g.* not mixtures of isomers) should be characterized by melting or decomposition points. The colors and morphologies of the products should also be noted.

Specific rotations. Specific rotations based on the equation $[\alpha]^{t};D = (100\ \alpha) / (l\ c)$ should be reported as unitless numbers as in the following example: $[\alpha]^{20}$; D = -25.4 (c 1.93, $CHCl_3$), where c / g mL^{-1} is concentration and l / dm is path length. The units of the specific rotation, (deg mL) / (g dm), are implicit and are not included with the reported value.

Spectra/*Spectral Data.* Important IR adsorptions should be given.

For all new diamagnetic substances, NMR data should be reported (^1H, ^{13}C, and relevant heteronuclei). ^1H NMR chemical shifts should be given with two digits after the decimal point. Include the number of protons represented by the signal, signal multiplicity, and coupling constants as needed (*J* italicized, reported with up to one digit after the decimal). The number of bonds through which the coupling is operative, ^{x}J, may be specified by the author if known with a high degree of certainty. ^{13}C NMR signal shifts should be rounded to the nearest 0.01 ppm unless greater precision is needed to distinguish closely spaced signals. Field strength should be noted for each spectrum, not as a comment in the general experimental section. Hydrogen multiplicity (C, CH, CH_2, CH_3) information obtained from routine DEPT spectra should be included. If detailed signal assignments are made, the type of NOESY or COSY methods used to establish atom connectivity and spatial relationships should be identified in the Supporting Information. Copies of spectra should also be included where structure assignments of complex molecules depend heavily on NMR interpretation. Numbering system used for assignments of signals should be given in the Supporting Information with corresponding general structural formula of named derivative.

HPLC/LCMS can be substituted for biochemistry papers where the main focus is not on compound synthesis.

HRMS/*elemental analysis.* To support the molecular formula assignment, HRMS data accurate within 5 ppm, or combustion elemental analysis [carbon and hydrogen (and nitrogen, if present)] data accurate within 0.5 %, should be reported for new compounds. HRMS data should be given in format as is usually given for combustion analysis: calculated mass for given formula following with observed mass: (+)ESI-HRMS *m*/*z*: [molecular formula + H]$^+$ calculated mass, observed mass. Example: (+)ESI-HRMS *m*/*z*: calculated for [$C_{13}H_8BrCl_2N$ + H^+] 327.92899, observed 327.92792.

NOTE: in certain cases, a crystal structure may be an acceptable substitute for HRMS/elemental analysis.

Biomacromolecules. The structures of biomacromolecules may be established by providing evidence about sequence and mass. Sequences may be inferred from the experimental order of amino acid, saccharide, or nucleotide coupling, from known sequences of templates in enzyme-mediated syntheses, or through standard sequencing techniques. Typically, a sequence will be accompanied by MS data that establish the molecular weight.

Example: Product was isolated upon column chromatography [dry flash (SiO_2, eluent EA, EA/MeOH gradient 95/5 → 9/1, EA/MeOH/NH_3 gradient 18/0.5/0.5 → 9/1/1, and flash chromatography (Biotage SP1, RP column, eluent MeOH/H_2O gradient 75/25 → 95/5, N-H column, eluent EA/Hex gradient 6/3 → EA). was obtained after flash column chromatography (Biotage SP NH column, eluent hexane/EA 4:6 → 2:6). Yield 968.4 mg (95 %). Colorless foam softens at 96-101 °C. $[\alpha]^{20}$; D = +0,163 (c =2.0×10^{-3} g/mL, CH_2Cl_2). IR (ATR): 3376w, 2949m, 2868w, 2802w, 1731s, 1611w, 1581s, 1528m, 1452m, 1374s, 1331w, 1246s, 1171m, 1063w, 1023m, 965w, 940w, 881w, 850w, 807w, cm^{-1}. ^{1}H NMR (500 MHz, $CDCl_3$, δ): 8.46 (*d*, 1H, J = 5.4, H-2'), 7.89 (*s*, 1H, J = 2.0, H-8'), 7.71 (*d*, 1H, J = 8.9, H-5'), 7.30 (*dd*, 1H, J_1 = 8.8, J_2 = 2.1, H-6'), 6.33 (*d*, 1H, J = 5.4, H-3'), 6.07 (*s*, HN-Boc, exchangeable with D_2O), 5.06 (*s*, 1H, H-12), 4.92-4.88 (*m*, 1H, H-7), 4.42 (*bs*, H-3), 3.45 (*s*,CH_3-N), 3.33 (*bs*, H-9'), 3.05-2.95 (*m*, 2H, H-11'), 2.70-2.43 (*m*, 2H, H-24) and HN, exchangeable with D_2O), 2.07 (*s*, CH_3COO), 2.04 (*s*, CH_3COO), 1.42 (*s*, 9H, $(CH_3)_3$C-N(Boc)), 0.88 (*s*, 3H, CH_3-10), 0.79 (*d*, 3H,J = 6.6, CH_3-20), 0.68 (*s*, 3H, CH_3-13). ^{13}C NMR (125 MHz, $CDCl_3$, δ): 170.34, 170.27, 151.80, 149.92, 148.87, 134.77, 128.36, 125.11, 121.43, 117.29, 99.98, 75.41, 70.82, 50.43, 49.66, 47.60, 47.33, 44.97, 43.30, 41.83, 41.48, 37.65, 36.35, 35.44, 34.89, 34.19, 33.23, 31.24, 28.79, 28.35, 27.25, 26.45, 25.45, 22.74, 22.63, 21.57, 21.31, 17.85, 12.15. (+)ESI-HRMS (*m*/*z*): calculated for $[C_{45}H_{67}ClN_4O_6 + H]^+$ 795.48219, observed 795.48185. Combustion analysis for $C_{45}H_{67}ClN_4O_6$: Calculated. C 67.94, H 8.49, N 7.04; found C 67.72, H 8.63, N 6.75. HPLC purity: method A: RT 1.994, area 99.12 %; method C: RT 9.936, area 98.20 %.

Purity - Evidence for documenting compound purity should include one or more of the following:

a) Well-resolved high field 1D ^{1}H NMR spectrum showing at most only trace peaks not attributable to the assigned structure and a standard 1D proton-decoupled ^{13}C NMR spectrum. Copies of the spectra should be included as figures in the Supporting Information.
b) Quantitative gas chromatographic analytical data for distilled or vacuum-transferred samples, or quantitative HPLC analytical data for materials isolated by column chromatography or separation from a solid support. HPLC analyses should be performed in two diverse systems. The stationary phase, solvents (HPLC), detector type, and percentage of total chromatogram integration should be reported; a copy of the chromatograms may be included as a figure in the Supporting Information.
c) Electrophoretic analytical data obtained under conditions that permit observing impurities present at the 5 % level.

HRMS data may be used to support a molecular formula assignment **but cannot be used as a criterion of purity**.

4. Biological Data

Quantitative biological data are required for all tested compounds. Biological test methods must be referenced or described in sufficient detail to permit the experiments to be repeated by others. Detailed descriptions of biological methods should be placed in the experimental section. Standard compounds or established drugs should be tested in the same system for comparison. Data may be presented as numerical expressions or in graphical form; biological data for extensive series of compounds should be presented in tabular form. Tables consisting primarily of negative data will not usually be accepted; however, for purposes of documentation they may be submitted as supporting information. Active compounds obtained from combinatorial syntheses should be resynthesized and retested to verify that the biology conforms to the initial observation.

Statistical limits (statistical significance) for the biological data are usually required. If statistical limits cannot be provided, the number of determinations and some indication of the variability and reliability of the results should be given. References to statistical methods of calculation should be included. Doses and concentrations should be expressed as molar quantities (*e.g.*, mol/kg, μmol/kg, M, mM). The routes of administration of test compounds and vehicles used should be indicated, and any salt forms used (hydrochlorides, sulfates, *etc.*) should be noted. The physical state of the compound dosed (crystalline, amorphous; solution, suspension) and the formulation for dosing (micronized, jet-milled, nanoparticles) should be indicated. For those compounds found to be inactive, the highest concentration (*in vitro*) or dose level (*in vivo*) tested should be indicated.

- The RESULTS AND DISCUSSION should include concisely presented results and there significance discussed and compared to relevant literature data. The results and discussion may be combined or kept separate.
- The inclusion of a CONCLUSION section, which briefly summarizes the principal conclusions, is recommended.
- NOMENCLATURE is optional but, if the authors wish, a list of employed symbols may be included.
- REFERENCES should be numbered sequentially as they appear in the text. Please note that any reference numbers appearing in the Illustrations and/or Tables and corresponding captions must follow the numbering sequence of the paragraph in which they appear for the first time. When cited, the reference number should be superscripted in Font 12, following any punctuation mark. In the reference list, they should be in normal position followed by a full stop. Reference entry must not be formatted using Carriage returns (enter key; ↵ key) or multiple space key. The formatting of references to published work should follow the *Journal*'s style as follows:

Journals[a]:	A. B. Surname1, C. D. Surname2, *J. Serb. Chem. Soc.* **Vol** (Year) first page Number (https://doi.org/doi)[b]
Books:	A. B. Surname1, C. D. Surname2, *Name of Book*, Publisher, City, Year, pp. 100-101 (https://doi.org/doi)[b]
Compilations:	A. B. Surname1, C. D. Surname2, in *Name of Compilation*, A. Editor1, C. Editor2, Ed(s)., Publisher, City, Year, p. 100 (https://doi.org/doi)[b]
Proceedings:	A. B. Surname1, C. D. Surname2, in *Proceedings of Name of the Conference or Symposium*, (Year), Place of the Conference, Country, *Title of the Proceeding*, Publisher, City, Year, p. or Abstract No. 100
Patents:	A. B. Inventor1, C. D. Inventor2, (Holder), Country Code and patent number (registration year)
Chemical Abstracts:	A. B. Surname1, C. D. Surname2, *Chem. Abstr*. CA 234 567a; For non-readily available literature, the Chemical Abstracts reference should be given in square brackets: [C.A. 139/2003 357348t] after the reference
Standards:	EN ISO 250: *Name of the Standard* (Year)
Websites:	Title of the website, URL in full (date accessed)

[a] When citing Journals, the International Library Journal abbreviation is required. Please consult, *e.g.*, https://images.webofknowledge.com/WOK46/help/WOS/A_abrvjt.html

[b] doi should be replaced by doi number of the Article, for example: http://dx.doi.org/10.2298/JSC161212085B (as active link). If doi do not exist, provide the link to the online version of the publication.

Only the last entry in the reference list should end with a full stop.

The names of all authors should be given in the list of references; the abbreviation *et al.* may only be used in the text. The original journal title is to be retained in the case of publications published in any language other than English (please denote the language in parenthesis after the reference). Titles of publications in non-Latin alphabets should be transliterated. Russian references are to be transliterated using the following transcriptions:

ж→zh, х→kh, ц→ts, ч→ch, ш→sh, щ→shch, ы→y, ю→yu, я→ya, э→e, й→i, ь→'.

Supplementary material

Authors are encouraged to presentthe information and results non-essential to the understanding of their paper as SUPPLEMENTARY MATERIAL (can be uploaded inStep 4 of Online Submission). This material may include as a rule, but is not limited to, the presentation of analytical and spectral data demonstrating the identity and purity of synthesized compounds, tables containing raw data on which calculations were based, series of figures where one example would remain in the main text, etc. The Editorial Board retain the right to assign such information and results to the Supplementary material when deemed fit. Supplementary material does not appear in printed form but can be downloaded from the web site of the JSCS.

Mathematical and chemical equations should be given in separate lines and must be numbered, Arabic numbers, consecutively in parenthesis at the end of the line. All equations should be embedded in the text Complex equations (fractions, integrals, matrix…) should be prepared with the aid of the

Microsoft Equation 3.0 (or higher) or MathType (Do not use them to create simple equations and labels). Using the Insert -> Equation option, integrated in MS Office 2010 and MS Office 2013, as well as insertion of equation objects within paragraph text IS NOT ALLOWED.

Deposition of crystallographic data

Prior to submission, the crystallographic data included in a manuscript presenting such data should be deposited at the appropriate database. Crystallographic data associated with organic and metal-organic structures should be deposited at the Cambridge Crystallographic Data Centre (CCDC) by e-mail to **deposit@ccdc.cam.ac.uk**

Crystallographic data associated with inorganic structures should be deposited with the Fachinformationszentrum Karlsruhe (FIZ) by e-mail to **crysdata@fiz-karlsruhe.de**. A deposition number will then be provided, which should be added to the reference section of the manuscript.

For detailed instructions please visit the JSCS website:
https://www.shd-pub.org.rs/index.php/JSCS/Instructions

ARTWORK INSTRUCTIONS

JSCS accepts only **TIFF** or **EPS** formats, as well as **JPEG** format (only for colour and greyscale photographs) for electronic artwork and graphic files. **MS files** (Word, PowerPoint, Excel, Visio) **NOT acceptable**. Generally, scanned instrument data sheets should be avoided. Authors are responsible for the quality of their submitted artwork. Every single Figure or Scheme, as well as any part of the Figure (A, B, C…) should be prepared according to following instructions (every part of the figure, A, B, C…, must be submitted as an independent single graphic file):

TIFF

Virtually all common artwork and graphic creation software is capable of saving files in TIFF format. This 'option' can normally be found under 'the 'Save As...' or 'Export...' commands in the 'File' menu.

TIFF (Tagged Image File Format) is the recommended file format for bitmap, greyscale and colour images.

- Colour images should be in the RGB mode
- When supplying TIFF files, please ensure that the files are supplied at the correct resolution:
    1. Line artwork: minimum of 1000 dpi
    2. RGB image: minimum of 300 dpi
    3. Greyscale image: minimum of 300 dpi
    4. Combination artwork (line/greyscale/RGB): minimum of 500 dpi
- Images should be tightly cropped, without frame and any caption.
- If applicable please re-label artwork with a font supported by JSCS (Arial, Helvetica, Times, Symbol) and ensure it is of an appropriate font size.
- Save an image in TIFF format with LZW compression applied.
- It is recommended to remove Alpha channels before submitting TIFF files.
- It is recommended to flatten layers before submitting TIFF files.

Please be sure that quality of an image cannot be increased by changing the resolution from lower to higher, but only by rescanning or exporting the image with higher resolution, which can be set in usual "settings" facilities.

EPS

Virtually all common artwork creation software, such as Canvas, ChemDraw, CorelDraw, SigmaPlot, Origin Lab…, are capable of saving files in EPS format. This 'option' can normally be found under the 'Save As...' or 'Export...' commands in the 'File' menu.

For vector graphics, EPS (Encapsulated PostScript) files are the preferred format as long as they are provided in accordance with the following conditions:

- when they contain bitmap images, the bitmaps should be of good resolution (see instructions for TIFF files)
- when colour is involved, it should be encoded as RGB
- an 8-bit preview/header at a resolution of 72 dpi should always be included
- embed fonts should always included and only the following fonts should be used in artwork: Arial, Helvetica, Times, Symbol
- the vertical space between the parts of an illustration should be limited to the bare necessity for visual clarity
- no data should be present outside the actual illustration area
- line weights should range from 0.35 pt to 1.5 pt
- when using layers, they should be reduced to one layer before saving the image (Flatten Artwork)

JPEG

Virtually all common artwork and graphic creation software is capable of saving files in JPEG format. This 'option' can normally be found under 'the 'Save As...' or 'Export...' commands in the 'File' menu.

JPEG (Joint Photographic Experts Group) is the acceptable file format **only for colour and greyscale photographs**. JPEG can be created with respect to photo quality (low, medium, high; from 1 to 10), ensuring file sizes are kept to a minimum to aid easy file transfer. Images should have a minimum resolution of 300 dpi. Image width: minimum 3.0 cm; maximum 12.0 cm.

Please be sure that quality of an image cannot be increased by changing the resolution from lower to higher, but only by rescanning or exporting the image with higher resolution, which can be set in usual "settings" facilities.

SIZING OF ARTWORK

- JSCS aspires to have a uniform look for all artwork contained in a single article. Hence, it is important to be aware of the style of the journal.
- Figures should be submitted in black and white or, if required, colour (charged). If coloured figures or photographs are required, this must be stated in the cover letter and arrangements made for payment through the office of the Serbian Chemical Society.
- As a general rule, the lettering on an artwork should have a finished, printed size of 11 pt for normal text and no smaller than 7 pt for subscript and superscript characters. Smaller lettering will yield a text that is barely legible. This is a rule-of-thumb rather than a strict rule. There are instances where other factors in the artwork, (for example, tints and shadings) dictate a finished size of perhaps 10 pt. Lines should be of at least 1 pt thickness.
- When deciding on the size of a line art graphic, in addition to the lettering, there are several other factors to address. These all have a bearing on the reproducibility/readability of the final artwork. Tints and shadings have to be printable at the finished size. All relevant detail in the illustration, the graph symbols (squares, triangles, circles, *etc*.) and a key to the diagram (to explain the explanation of the graph symbols used) must be discernible.
- The sizing of halftones (photographs, micrographs,...) normally causes more problems than line art. It is sometimes difficult to know what an author is trying to emphasize on a photograph, so you can help us by identifying the important parts of the image, perhaps by highlighting the relevant areas on a photocopy. The best advice that can be given to graphics suppliers is not to over-reduce halftones. Attention should also be paid to magnification factors or scale bars on the artwork and they should be compared with the details inside. If a set of artwork contains more than one halftone, again please ensure that there is consistency in size between similar diagrams.

General sizing of illustrations which can be used for the Journal of the Serbian Chemical Society:

- Minimum fig. size: 30 mm width
- Small fig. size - 60 mm width
- Large fig. size - 90 mm width
- Maximum fig. size - 120 mm width

Pixel requirements (width) per print size and resolution for bitmap images:

	Image width	A	B	C
Minimal size	30 mm	**354**	**591**	**1181**
Small size	60 mm	**709**	**1181**	**2362**
Large size	90 mm	**1063**	**1772**	**3543**
Maximal size	120 mm	**1417**	**2362**	**4724**

A: 300 dpi > RGB or Greyscale image
B: 500 dpi > Combination artwork (line/greyscale/RGB)
C: 1000 dpi> Line artwork

The designation of physical quantities and graphs formatting

The designation of physical quantities on figures must be in italic, whereas the units are in upright letters. They should be in Times New Roman font. In graphs a slash should be used to separate the designation of a physical quantity from the unit (example: p / kPa, t °C, T_0 / K, τ / h, ln (j / mA cm^{-2})…). Designations such as: p (kPa), t [min]…, are not acceptable. However, if the full name of a physical quantity is unavoiable, it should be given in upright letters and separated from the unit by a comma (example: Pressure, kPa, Temperature, K…). Please do not use the axes of graphs for additional explanations; these should be mentioned in the figure captions and/or the manuscript (example: "pressure at the inlet of the system, kPa" should be avoided). The axis name should follow the direction of the axis (the name of y-axis should be rotated by 90°). Top and right axes should be avoided in diagrams, unless they are absolutely necessary. Decimal numbers must have decimal points and not commas in the axis labels in graphical presentations of results. Thousands are separated, if at all, by a comma and not a point.

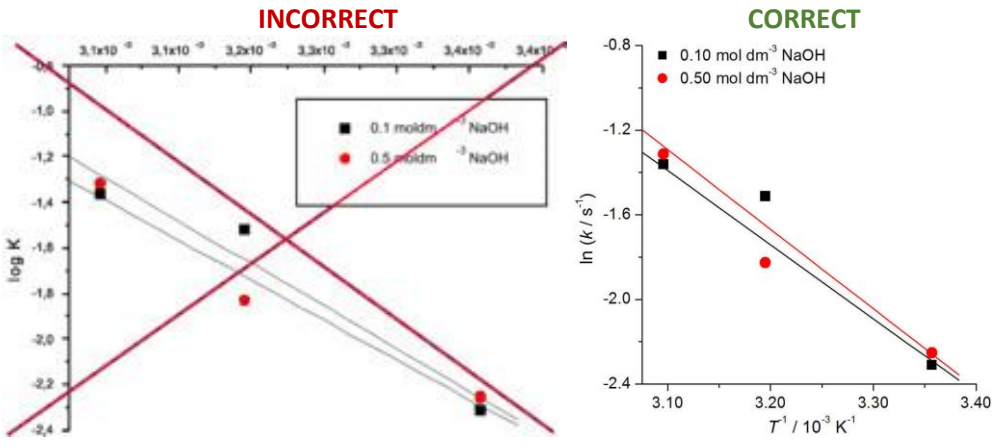

Journal of the Serbian Chemical Society
JSCS-info@shd.org.rs • www.shd.org.rs/JSCS

J. Serb. Chem. Soc. Vol. 88, No. 1 (2023)

CONTENTS*

Published by the Serbian Chemical Society
Karnegijeva 4/III, P.O. Box 36, 11120 Belgrade, Serbia
Printed by the Faculty of Technology and Metallurgy
Karnegijeva 4, P.O. Box 35-03, 11120 Belgrade, Serbia

* For colored figures in this issue please see electronic version at the Journal Home Page: http://www.shd.org.rs/JSCS/

Journal of the Serbian Chemical Society
JSCS@tmf.bg.ac.rs • www.shd.org.rs/JSCS
J. Serb. Chem. Soc. *88* (1) 1–9 (2023)
JSCS–5606
Original scientific paper
Published 18 November 2022

Green chemical principles based regioselective functionalization of 2,4,6-trichloropyrimidine-5-carbaldehyde: Application in the synthesis of new pyrimidines and pyrrolopyrimidine

ALLU UDAYASRI[1], MANCHIKANTI M. CHANDRASEKHAR[1], BRAHMESWARARAO M. V. NAGA[2], GANESH VARANASI[2] and DUGGIRALA S. RAMAKRISHNA[1]*

[1]*Department of Chemistry, Veer Surendra Sai University of Technology, Burla-768018, Odisha, India and* [2]*Prodev Pharma (OPC) Pvt. Ltd, ALEAP Industrial Estate, Hyderabad-500090, India*

(Received 4 August 2021, revised 6 July, accepted 29 July 2022)

Abstract: The present work reports the synthesis of three new nitrogen-containing heteronuclear molecules (two pyrimidines and one pyrrolopyrimidine). Based on the 12 principles of green chemistry, chemical methodologies are planned and executed. Various phase transfer catalysts were examined in the crucial step to execute C–N bond formation (through the SnAr mechanism), TBAI was found to be a better option than those of TBAB and CTAB. The one-pot synthetic methodology was optimized involving Wittig olefination and bromination to achieve a key precursor for the synthesis of a new pyrrolopyrimidine.

Keywords: twelve principles of green chemistry; phase transfer catalysis; one-pot synthesis; Wittig olefination; synthesis of new *N*-heterocyclic compounds; halogen solvent-free processes; catalytic reactions.

INTRODUCTION

In the DNA and RNA structures, pyrimidine is a common structural motif present in the form of different nucleobases, such as cytosine, thymine and uracil. Scaffolds containing tetra substituted pyrimidines occupy a prominent position based on their biological applications.[1–10] Recently, 2,4,6-trichloro-pyrimidine-5-carbaldehydes having cholesterol moiety are used for gelation.[11] Interest in the studies based on the derivatives of pyrrolo[2,3-*d*]pyrimidines has increased significantly after the introduction of nucleoside antibiotics, such as tubercidin, toyocamycin and sangivamycin.[12] In addition these tetra substituted pyrimidines are acting as precursors in the synthesize of new biologically active pyrrolo[2,3-

* Corresponding author. E-mail: ramakrishnads_chem@vssut.ac.in
https://doi.org/10.2298/JSC210804063U

-*d*]pyrimidines. A few representative pyrimidines and pyrrolo[2,3-*d*]pyrimidine structural motifs containing examples are shown in Fig. 1.

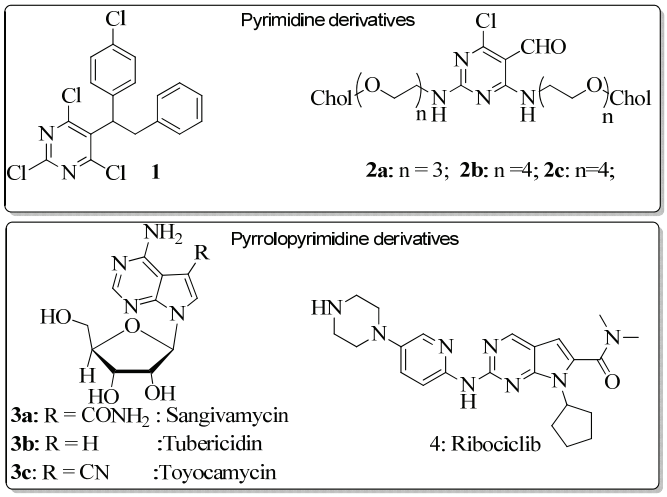

Fig. 1. Representative examples of pyrimidine and pyrrolopyrimidine derivatives.

EXPERIMENTAL

General procedures

All reactions were performed under a nitrogen atmosphere using anhydrous techniques unless otherwise stated. All commercially available materials and solvents were used directly without further purification. ^{1}H-NMR (400 MHz) and ^{13}C-NMR (100 MHz) were recorded on a Bruker Avance NMR spectrometer using TMS as the internal standard in $CDCl_3$ or DMSO-d_6 solution. The mass spectra were determined on a THERMO LTQ (ESI) or Agilent 5973 MSD (EI) spectrometer. The IR spectra were recorded on Perkin–Elmer model 683 or 1310 spectrometers with sodium chloride optics or KBr pellets. All reactions were monitored by thin-layer chromatography (TLC) employing 0.25 mm Merck silica gel plates (60F-254). Column chromatography was performed using Acme silica gel (60–120 mesh). Visualization of the spots on the TLC plates was achieved either by exposure to UV light, and iodine vapor or by dipping the plates in phosphomolybdic acid–ceric (IV) sulfate–sulfuric acid solution (PMA solution) and heating the plates at 120 °C. All the products were purified by column chromatography. The structures were characterized by analysis of spectra data, namely ^{1}H-NMR, ^{13}C-NMR, IR and mass spectra.

Analytical and spectral data are given in Supplementary material to this paper.

2,4-Dichloro-6-(cyclopentylamino)pyrimidine-5-carbaldehyde (7). To a stirred solution of 2,4,6-trichloro-pyrimidine-5-carbaldehyde **5** (5.0 g, 23.6 mmol) in a mixture of toluene (10 ml) and water (40 ml) was added cyclopentyl amine 6 (2.01 g, 23.6 mmol), $CsCO_3$ (4.0 g, 40 mmol) and a catalytic amount of TBAB (0.35 g, 1.08 mmol) at 25 to 35 °C. The reaction mass was maintained for 2–3 h at 25 to 35 °C. The organic layer was separated from the aqueous layer, washed with brine solution and dried over anhydrous Na_2SO_4. The organic layer was concentrated under vacuum to give a thick oily residue that was purified by column chromatography to give **7** (5.53 g, 90 %).

*Methyl (Z)-2-bromo-3-(2,4-dichloro-6-(cyclopentylamino)pyrimidin-5-yl)acrylate (**9**)*. To a stirred solution of (methoxycarbonyl methyl)triphenylphosphoniumbromide, **8** (15.8 g, 38.0 mmol) in a mixture of dioxane (9 ml) and water (45 ml) was added *N*-bromosuccinamide (7.5 g, 42.1 mmol) at 0–5 °C. The mixture was stirred at 0–5 °C for 45 to 60 min. The temperature of the reaction mass was raised to 25 °C and then compound **7** (9.0 g, 34.5 mmol) was added followed by $CsCO_3$ (14.83 g, 46.01 mmol). After keeping the reaction mass at 25 °C for 2 to 3 h. it was dried over anhydrous Na_2SO_4 and then concentrated under reduced pressure to obtain a yellow crude oil. The crude residue was purified by column chromatography to give **9** (12.29 g, 85 %)

*Methyl 2,4-dichloro-7-cyclopentyl-7H-pyrrolo[2,3-d]pyrimidine-6-carboxylate (**10**)*. To a stirred solution of compound **9** (4.0 g, 10.1 mmol), K_2CO_3 (7.0 g, 50.6 mmol) and DABCO (0.56 g, 5.06 mmol) in 1,4 dioxane (20 ml) was added CuI (0.385 g, 2.02 mmol) under a nitrogen atmosphere at 25 °C. The temperature of the reaction mass was raised to reflux and maintained for 16.0 h under a nitrogen atmosphere. Then reaction mass was filtered and the filtrate washed with dioxane (4 ml). The filtrate was dried over anhydrous Na_2SO_4 and then concentrated to obtain a thick yellow syrup. Using columns chromatographic technique. The product **10** was purified by column chromatography (2.92 g, 90 %)

RESULTS AND DISCUSSION

Synthesis of pyrimidine and pyrrolopyrimidine

The synthesis of new and diversified pyrrolopyrimidines using pyrimidine precursors was unexplored to date. Thus, it was intend to synthesize a series of N-heterocyclic compounds having a pyrimidine moiety as a common structural entity and to prepare new pyrrolo[2,3-*d*]pyrimidines based on the execution of green chemical approaches. In continuation of the execution of green chemical methodologies based on twelve principles of chemistry, in the current work, these advanced methodologies were extended to the synthesize N-heterocyclic compounds.[13–18] The importance of one pot synthetic methodology is increasing in a fast manner.[19–21] Extending new synthetic methodologies to the synthesis of a series of pyrimidine analogues and their characterization were the main objectives of this work. For this purpose, the synthesis a common intermediate having functionalizable groups on each carbon of pyrimidine was envisaged. The envisaged synthetic strategy involved the usage of reliable and high yield producing reactions such as C–N bond formation (through the S_NAr mechanism), the Wittig reaction and cyclization. To generate new and different analogs having pyrimidine moiety, compound 2,4,6-trichloropyrimidine-5-carbaldehyde was chosen which is having four functionalizable sites, *i.e.*, three chloro substituents and one aldehyde functionality. Compound **5** can be synthesized using barbituric acid as the starting material since it is a cheap commercially available material. The synthesis was initiated with barbituric acid that was converted into **5** using $POCl_3$ in DMF (Vilsmeier–Haack reaction conditions), the required pyrimidine derivative having four functionalizable groups was synthesized in 85 % yield (Scheme 1).[22]

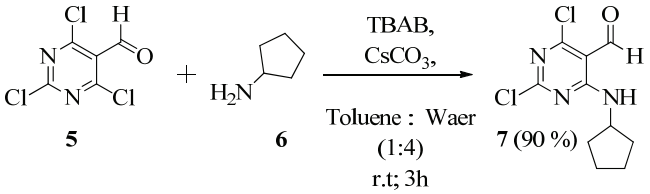

Scheme 1. C–N bond formation reaction.

After obtaining the required intermediate, functionalization of the 2nd/6th position was explored using cyclopentyl amine to generate a new C–N bond. The main difficulty involved in this reaction is that there may be a chance of the formation of imine product using aldehyde and amine through condensation reaction (a parallel reaction) instead of a C–N bond formation reaction.

A similar reaction with this substrate **5** using toluene solvent was reported.[23] Though toluene is a preferable solvent in synthetic organic chemistry in comparison with other organic solvents, such as chlorinated solvents (DCM, CCl_4) or benzene, it still has some negative impacts on nature. The usage of organic solvents should be reduced to a bare minimum by employing/increasing ecofriendly solvents, such as water, to carry out the reaction. This reaction was optimized with the higher solvent contribution of water (80 %) as the major solvent in comparison with that of toluene (20 %) solvent as the minor solvent. The other advantage of using higher amounts of water is to diminish the formation of imine products that could be obtained from aldehyde and amine. Water was not only a solvent but also a byproduct in this parallel imine condensation reaction. Hence, the Lechleiter principle was applied, *i.e.*, by increasing the concentration of water, the formation of imine product can be reduced. The role of water in this reaction is not only to decrease the usage of the toluene solvent but also to lessen the production of imine product. The reaction was optimized based on the following parameters shown in Table I. Different phase transfer catalysts were examined, such as TBAB, TBAI and CTAB. Different bases, such as K_2CO_3, $KHCO_3$, Na_2CO_3, $NaHCO_3$ and $CsCO_3$, were employed to obtain higher yields of the required product in various solvent combinations. Based on careful experimentation of the reaction under various conditions (Table I), a higher yield of the product was obtained using $CsCO_3$ as the base, TBAB as PTC, and solvents ratio toluene:water of 1:4. The required product was obtained in good yield using TBAB in comparison with other phase transfer catalysts (Scheme 1).

Compound **7** was characterized based on its ^{1}H-NMR spectrum, the appearance of cyclopentyl amine structure representing protons signals ranging from δ 1.5 to 4.5 ppm, the NH proton was observed at δ 9.30 ppm and this peak was absent in its D_2O exchanged ^{1}H-NMR spectrum. In addition compound **7** was confirmed by the appearance of its mass peak at *m*/*z* 260.0 (M+1) over mass

chromatogram with dichloro mass pattern in positive scan mode. The spectral data of **7** was in full agreement with the assigned structure.

TABLE I. Optimization of the S_NAr reaction; equivalence of base and PTC were calculated concerning the equivalence of substrates 2 and 3

S. No.	PTC (4.5 mol. %, equivalence)	Base (1.7 equivalence)	Isolated yield, % (equivalence)
1	TBAI	K_2CO_3	80
2	TBAI	$KHCO_3$	65
3	TBAI	Na_2CO_3	75
4	TBAI	$CsCO_3$	70
5	**TBAB**	**$CsCO_3$**	**90**
6	TBAB	$KHCO_3$	80
7	TBAB	Na_2CO_3	70
8	TBAB	$NaHCO_3$	50
9	CTAB	K_2CO_3	60
10	CTAB	$KHCO_3$	50
11	CTAB	Na_2CO_3	60
12	CTAB	$CsCO_3$	50

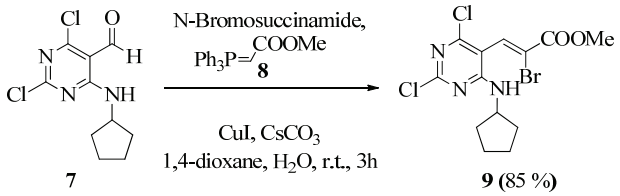

Scheme 2. One pot Wittig and bromination reaction.

Although one-pot bromination and Wittig reactions were optimized previously with simple substrates such as aliphatic, and aromatic compounds most of the reactions used organic solvents such as DCM or DMSO only.[24] The main drawback in those reaction conditions was the non-aqueous media. To implement green chemical methodology by using an aqueous solvent along with increasing the yield of the product, the reaction conditions in the aqueous media containing a biphasic system were optimized. In this way, the usage of organic solvents was reduced by employing an eco-friendly aqueous solvent. Wittig olefination of compound **7** using **8** and Na_2CO_3 at 25 °C resulted in olefin **9** in 65 % yield. For improving the yield of the conversion of **7** into **8**, each parameter of the reaction was systematically examined (as shown in Table II). From Table II, it is very clear that the availability of K_2CO_3 to the reactants was greater in a bi-phasic mixture of 1,4-dioxane + water, which made the reaction faster with more complete transformation of **7** into **8** and higher yields (Scheme 2). After completion of the reaction, MTBE was used in the purification step, for extraction purposes,

TPP oxide by-products can be removed selectively from the reaction mixture and in this way the usage of a hazardous organic solvent was reduced to some extent.

TABLE II. Optimization of the Wittig reaction

S. No.	Solvent	Base	Reaction temperature, °C	Reaction time, h	Isolated yield, %
1	CH_2Cl_2	K_2CO_3	–20	> 48	~35
2	Benzene	K_2CO_3	–20	> 48	~ 40
3	Methanol	Na_2CO_3	–20	> 48	~ 45
4	Toluene + methanol	Na_2CO_3	–20	> 48	~ 40
5	1,4-Dioxane	Na_2CO_3	–20	7	50
6	1,4-Dioxane	Na_2CO_3	0	5	55
7	1,4-Dioxane + water	Na_2CO_3	–20	3	80
8	1,4-Dioxane + water	Na_2CO_3	0	2	85
9	1,4-Dioxane + water	$CsCO_3$	25	1	85

Compound **9** was analyzed using ^{1}H-NMR by the appearance of the cyclopentyl amine structure representing protons signals ranging from δ 1.5 to 4.5 ppm, the NH proton was observed at 7.45 ppm and this peak was absent in the D_2O exchanged ^{1}H-NMR spectrum. In addition, compound **9** was confirmed by the appearance of its mass peaks at *m*/*z* 394 and 396 over mass chromatogram with bromo and dichloro mass pattern in positive scan mode. The spectral data of **9** was in full agreement with the assigned structure.

Compound **9** was converted to **10** using copper iodide, Na_2CO_3 and DABCO in 1,4-dioxane with a 92 % yield (Scheme 3).[25] As shown in Table III, the best conversion of the reaction from **9** to **10** was achieved with Na_2CO_3 in 1,4-dioxane at 110 °C. It was observed that inorganic bases were more effective in obtaining better cyclization conditions than the organic base diisopropylethylamine (DIPEA).[26] After finalizing the conversion, compound **10** was purified using column chromatography. Compound **10** was characterized based on ^{1}H-NMR by the appearance of proton signal of the cyclized five-membered ring alkene at δ 7.4 ppm, in addition to the appearance of its mass peaks at *m*/*z* 314 over mass chromatogram with a dichloro mass pattern in positive scan mode. The spectral data of **10** was in full agreement with the assigned structure.

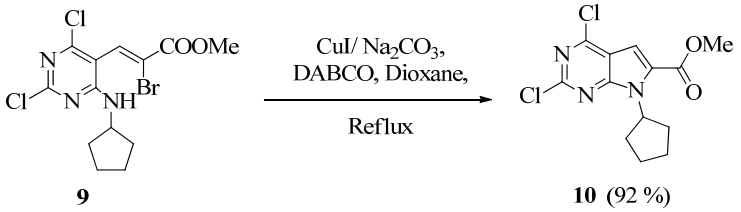

9 **10** (92 %)

Scheme 3. Cyclization reaction.

TABLE III. Optimization of the cyclization reaction

S. No.	Solvent	Base	Temperature, °C	Reaction time, h	Isolated yield, %
1	Dichloromethane	K_2CO_3	35	No reaction	-
2	Tetrahydrofuran	K_2CO_3	65	> 36	30
3	Toluene	K_2CO_3	110	> 36	60
4	Toluene	Na_2CO_3	110	> 36	60
5	Toluene	KO^tBu	110	> 36	25
6	1,4-dioxane	Et_3N	110	> 36	25
7	1,4-dioxane	DIPEA	110	> 36	20
8	1,4-dioxane	Na_2CO_3	110	12	92

CONCLUSIONS

The outstanding features of this synthetic methodology are: *i*) two aqueous phase transformations such as C–N bond formation and Wittig reaction, *ii*) one pot synthetic methodology that includes both Wittig reaction and bromination, *iii*) one phase transfer catalytic reaction using TBAB in C–N bond formation reaction, *iv*) all reactions are carried out by catalysts such as TBAB and CuI as two-room temperature reactions and *v*) all reactions and procedures are halogen solvent free processes.

SUPPLEMENTARY MATERIAL

Additional data and information are available electronically at the pages of journal website: https://www.shd-pub.org.rs/index.php/JSCS/article/view/11028, or from the corresponding author on request.

ИЗВОД

РЕГИОСЕЛЕКТИВНА ФУНКЦИОНАЛИЗАЦИЈА 2,4,6-ТРИХЛОРПИРИМИДИН-5-КАРБАЛДЕХИДА НА АПРИНЦИПИМА ЗЕЛЕНЕ ХЕМИЈЕ: ПРИМЕНА У СИНТЕЗИ НОВИХ ПИРИМИДИНА И ПИРОЛОПИМИДИНА

ALLU UDAYASRI[1], MANCHIKANTI M. CHANDRASEKHAR[1], BRAHMESWARARAO M. V. NAGA[2], GANESH VARANASI[2] и DUGGIRALA S. RAMAKRISHNA[1]

[1]*Department of Chemistry, Veer Surendra Sai University of Technology, Burla-768018, Odisha, India и* [2]*Prodev Pharma (OPC) Pvt. Ltd, ALEAP Industrial Estate, Hyderabad-500090, India*

У овом раду приказана је синтеза три нова хетероциклична једињења азота (два деривата пиримидина и један дериват пиролопиримидина). План хемијске методологије синтезе је заснован на 12 принципа зелене хемије и план је реализован. Испитани су различити катализатори преноса између фаза у најважнијем реакционом кораку, формирања C–N везе (S_NAr механизмом) и утврђено је да је најбољи резултат постигнут коришћењем TBAI у поређењу са TBAB и CTAB. Оптимизована је нова ситетичка методологија која укључује Витихову (Wittig) олефинацију и бромовање за добијање најважнијег прекурсора у синтези нових пиролпиримидина.

(Примљено 4. августа 2021, ревидирано 6. јула, прихваћено 29. јула 2022)

REFERENCES

1. P. K. Maji, *Curr. Org. Chem* **24** (2020) 1055 (https://doi.org/10.2174/1385272824999200507123843)
2. A. Mahapatra, T. Prasad, T. Sharma, *Futur. J. Pharm. Sci.* **7** (2021) 1 (https://doi.org/10.1186/s43094-021-00274-8)
3. H. K. Akula, H. Kokatla, G. Andrei, R. Snoeck, D. Schols, J. Balzarini, L. Yang, M. K. Lakshman, *Org. Biomol. Chem.* **15** (2017) 1130 (https://doi.org/10.1039/C6OB02334G)
4. S. Kumar, B. Narasimhan, *Chem. Central J.* **12** (2018) 38 (https://doi.org/10.1186/s13065-018-0406-5)
5. A. Frank,F. Meza-Arriagada, C. O. Salas, C. Espinosa-Bustos, H. Stark, *Bioorg. Med. Chem.* **27** (2019) 3194 (https://doi.org/10.1016/j.bmc.2019.05.042)
6. A. Ali, M. Khalid, M. F. U Rehman, S. Haq, A. Ali, M. N. Tahir, M. Ashfaq, F. Rasool, A. C. Braga, *ACS Omega* **5** (2020) 15115 (https://doi.org/10.1021/acsomega.0c00975)
7. A. Ali, M. Khalid, M. N. Tahir, M. Imran, M. Ashfaq, R. Hussain, M. A. Assiri, I. Khan, *ACS Omega* **6** (2021) 7047 (https://doi.org/10.1021/acsomega.0c06323)
8. A. Ali, A. Kuznetsov, M. Ashfaq, M. N. Tahir, M. Khalid, M. Imran, A. Irfan, *J. Mol. Struct.* **1243** (2021) 130789 (https://doi.org/10.1016/j.molstruc.2021.130789)
9. M. Khalid, A. Ali, S. Haq, M. N. Tahir, J. Iqbal, A. A. C. Braga, M. Ashfaq, S. U. H. Akhtar, *J. Mol. Struct.* **1224** (2021) 129308 (https://doi.org/10.1016/j.molstruc.2020.129308)
10. M. Ashfaq, A. Ali, A. Kuznetsov, M. N. Tahir, M. Khalid, *J. Mol. Struct.* **1228**(2021) 129445 (https://doi.org/10.1016/j.molstruc.2020.129445)
11. S. Datta, S. Bhattacharya, *Soft Matter.* **11** (2015) 1945 (https://doi.org/10.1039/C4SM02792B)
12. P. K. Gu, S. Daunert, M. R. Nassiri, L. L. Wotring, J. C. Drach, L. B. Townsend, *J. Med. Chem.* **32**(1989) 402 (https://doi.org/10.1021/jm00122a019)
13. D. S. Ramakrishna, *Chem. Data Collect.* **33** (2021) 100685 (https://doi.org/10.1016/j.cdc.2021.100685)
14. D. S. Ramakrishna, *Chem. Data Collect.* **32** (2021) 100667 (https://doi.org/10.1016/j.cdc.2021.100667).
15. D. S. Ramakrishna, A. Pradhan, *ARKIVOC* **2021** (2021) 1 (https://doi.org/10.24820/ark.5550190.p011.519)
16. G. Kumaraswamy, D. Ramakrishna, K. Santhakumar, *Tetrahedron: Asymmetry* **21** (2010) 544 (https://doi.org/10.1016/j.tetasy.2010.02.024)
17. G. Kumaraswamy, K. Sadaiah, D. S. Ramakrishna, N. Police, B. Sridhar, J. Bharatam, *Chem. Commun.* (2008) 5324 (https://doi.org/10.1039/B810770J)
18. G. Kumaraswamy, A. Pitchaiah, G. Ramakrishna, D. S. Ramakrishna, K. Sadaiah, *Tetrahedron Lett.* **47** (2006) 2013 (https://doi.org/10.1016/j.tetlet.2006.01.050)
19. H. P. Kokatla, M. K. Lakshman, *Org. Lett.* **20** (2010) 4478 (https://doi.org/10.1021/ol101655h)
20. R. Meesala, Y. K. Lee, A. S. Md. I. Abdullah, Md. N. Mordi, N. A. Rahman, *Synlett* **31** (2020) 2054 (DOI: 10.1055/s-0040-1706477)
21. R. Meesala, A. S. Md. Arshad, Md. N. Mordi, S. M. Mansor, *Tetrahedron* **72** (2016) 8537 (https://doi.org/10.1016/j.tet.2016.10.069)
22. J. M. Hatcher, J. Zhang, 'H. G. Choi, G. Ito, D. R. Alessi, N. S. Gray, *ACS Med. Chem. Lett.* **6** (2015) 584 (https://doi.org/10.1021/acsmedchemlett.5b00064)
23. R. L. Beingessner, B. L. Deng, P. E. Fanwick, H. Fenniri, *J. Org. Chem.***73** (2008) 931 (https://doi.org/10.1021/jo7021422)

24. U. Karama, R. Mahfouz, Z. Al-Othman, I. Warad,A.Almansour, *Synth. Comm*. **43** (2013) 893(https://doi.org/10.1080/00397911.2011.614712)
25. Y. H. Jang, S. W. Youn, *Org. Lett.* **16** (2014) 3720 (https://doi.org/10.1021/ol5015398)
26. A. Udayasri, M. M. Chandrasekhar, M. V. N. Brahmeswararao, G. Varanasi, P. L. Praveen, D. S. Ramakrishna, *TopCatal*. (2022) (https://doi.org/10.1007/s11244-022-01602-9).

Journal of the Serbian Chemical Society
JSCS@tmf.bg.ac.rs • www.shd.org.rs/JSCS
J. Serb. Chem. Soc. **88** (1) S1–S9 (2023) *Supplementary material*

SUPPLEMENTARY MATERIAL TO

Green chemical principles based regioselective functionalization of 2,4,6-trichloropyrimidine-5-carbaldehyde: Application in the synthesis of new pyrimidines and pyrrolopyrimidine

ALLU UDAYASRI[1], MANCHIKANTI M. CHANDRASEKHAR[1], BRAHMESWARARAO M. V. NAGA[2], GANESH VARANASI[2] and DUGGIRALA S. RAMAKRISHNA[1]*

[1]*Department of Chemistry, Veer Surendra Sai University of Technology, Burla-768018, Odisha, India and* [2]*Prodev Pharma (OPC) Pvt. Ltd, ALEAP Industrial Estate, Hyderabad-500090, India*

J. Serb. Chem. Soc. **88** (1) (2023) 1–9

SPECTRAL AND ANALYTICAL DATA FOR THE NEW COMPOUNDS

*2,4-Dichloro-6-(cyclopentylamino) pyrimidine-5-carbaldehyde (**7**)*

White powder; m.p.: 121-122 ºC; ^{1}H-NMR (400 MHz, DMSO-d_6, δ / ppm): 10.20 (*s*, 1H), 9.30 (*s*, 1H), 4.4 (*m*, 1H), 2.03-1.90 (*m*, 2H), 1.80-1.55 (*m*, 6H); ^{13}C-NMR (100 MHz, DMSO, δ / ppm): 190.77, 165.09, 163.41, 160.94, 112.38, 52.84, 32.17, 31.77, 23.35, 23.22; IR (cm^{-1}): 3260.00, 2951.11, 1713.14; MS (ESI): *m/z*: $(M+H)^+$: 260; Anal. Calcd for $C_{10}H_{11}Cl_2N_3O$: C, 46.17; H, 4.26; Cl, 27.26; N, 16.15. Found: C, 46.16; H, 4.27; Cl, 27.25; N, 16.13.

*Methyl (Z)-2-bromo-3-(2,4-dichloro-6-(cyclopentylamino)pyrimidin-5-yl)acrylate (**9**)*

Brown solid; m.p.: 138-139 ºC, ^{1}H-NMR (400 MHz, DMSO-d_6, δ / ppm): 7.90 (*s*, 1H), 7.45 (*m*, 1H), 4.40 (*m*, 1H), 3.82 (*s*, 3H), 1.97-1.84 (*m*, 2H), 1.79-1.65 (*m*, 2H), 1.59-1.49 (*m*, 4H); ^{13}C-NMR (100 MHz, DMSO, δ / ppm): 161.61, 159.36, 157.92, 155.04, 133.87, 122.45, 109.53, 53.67, 52.85, 31.83, 341.48, 23.56, 23.31; IR (cm^{-1}): 3316.61, 2951.67, 1720.90; MS (ESI): *m/z*: $(M+H)^+$: 396.0; Anal. Calcd for $C_{13}H_{14}BrCl_2N_3O_2$: C, 39.52; H, 3.57; Br, 20.22; Cl, 17.95; N, 10.64. Found: C, 39.53; H, 3.56; Br, 20.24; Cl, 17.92; N, 10.67.

*Methyl 2,4-dichloro-7-cyclopentyl-7*H*-pyrrolo[2,3-d]pyrimidine-6-carboxylate (10)*

Light brownish powder; m.p.: 130-131 ºC; ^{1}H-NMR (400 MHz, DMSO-d_6), δ / ppm): 7.40 (*s*, 1H), 5.61-5.67 (*m*, 1H), 3.9 (*s*, 3H), 2.35-2.20 (*m*, 2H), 2.12-1.95 (*m*, 4H), 1.75-1.60 (*m*, 2H); ^{13}C-NMR (100 MHz, DMSO, δ / ppm): 165.45,

* Corresponding author. E-mail: ramakrishnads_chem@vssut.ac.in

154.37, 152.36, 152.06, 130.77, 114.87, 107.06, 57.01, 52.67, 30.60 (2C), 24.68. (2C); IR (cm^{-1}): 3433.39, 2956.30, 1727.99; MS (ESI): *m/z*: $(M+H)^+$: 314.0; Anal. Calcd for $C_{13}H_{13}Cl_2N_3O_2$: C, 49.70; H, 4.17; Cl, 22.57; N, 13.38. Found: C, 49.73; H, 4.12; Cl, 22.59; N, 13.36.

Spectra

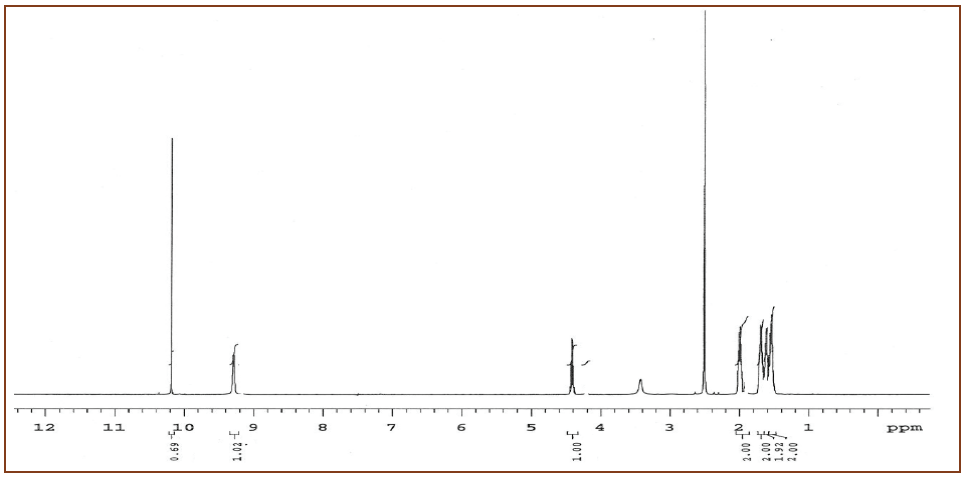

Fig. S-1. ^{1}H-NMR (400 MHz, DMSO) - **7**

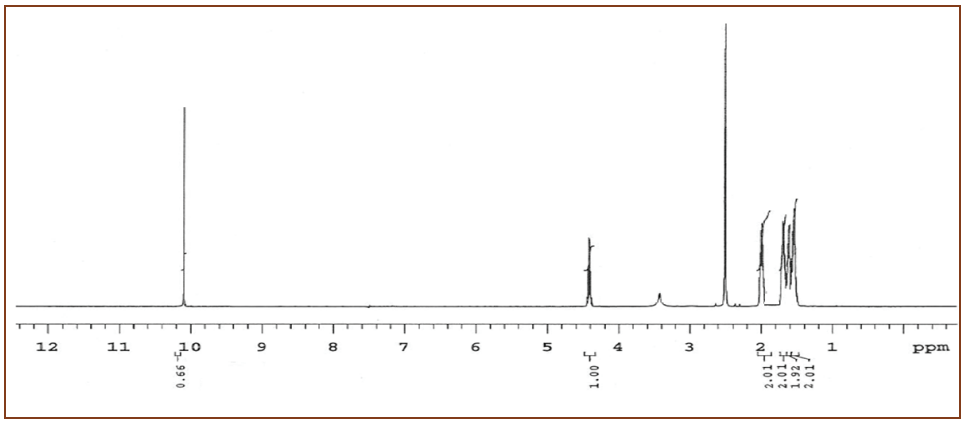

Fig. S-2. ^{1}H-NMR (400 MHz, DMSO, D_2O Exchange) - **7**

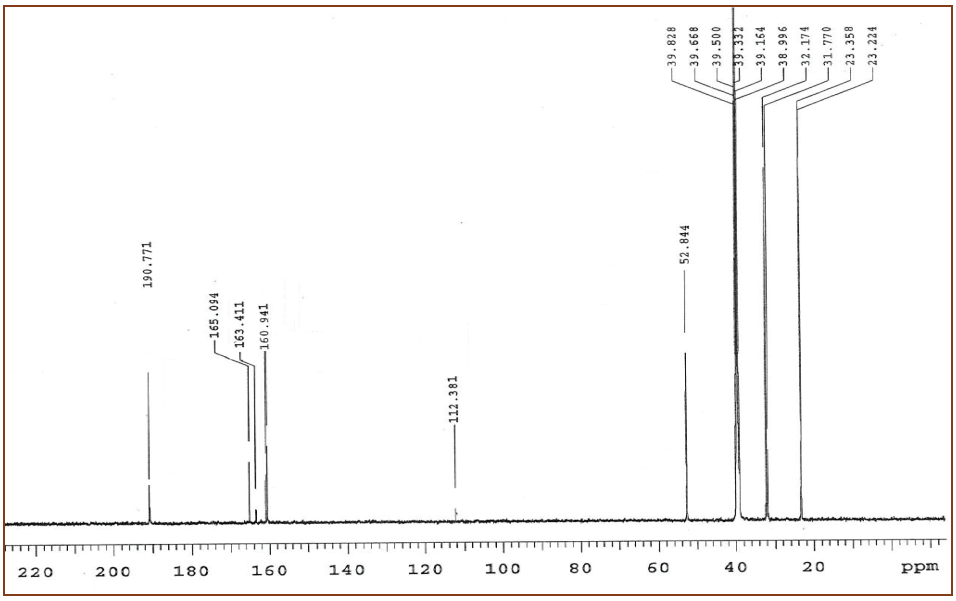

Fig. S-3. ^{13}C-NMR (100 MHz, DMSO) - **7**

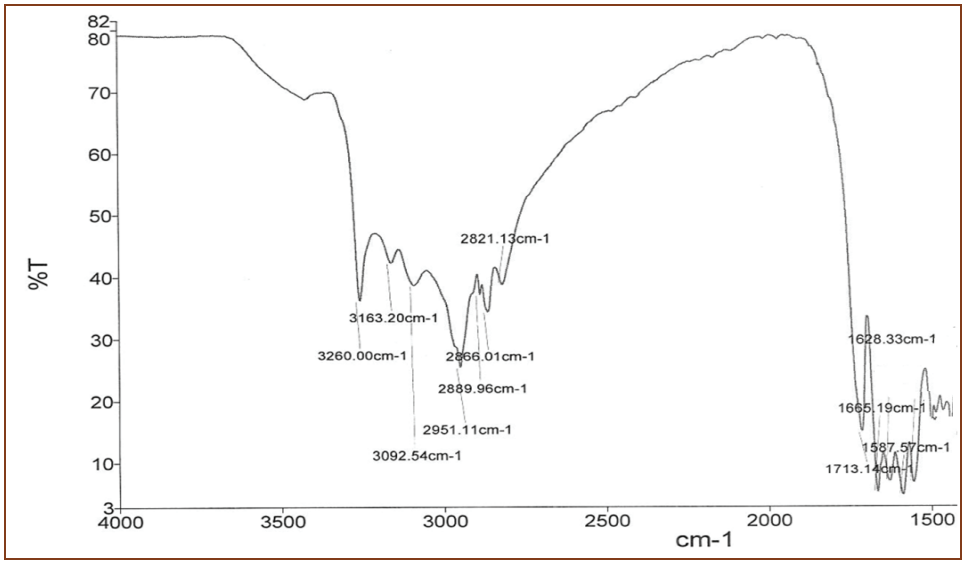

Fig. S-4. IR - **7**

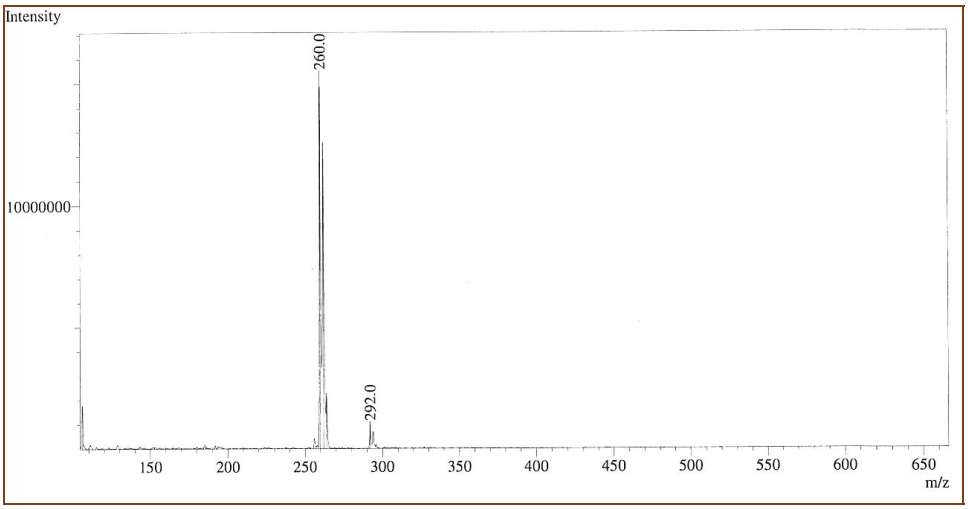

Fig. S-5. ESI-MS - **7**

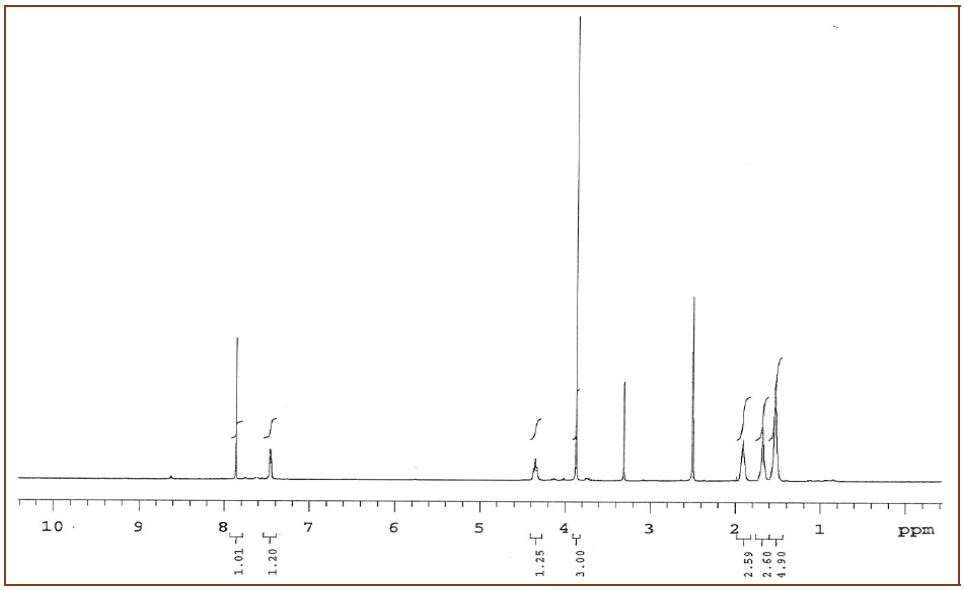

Fig. S-6. ^{1}H-NMR (400 MHz, DMSO) - **9**

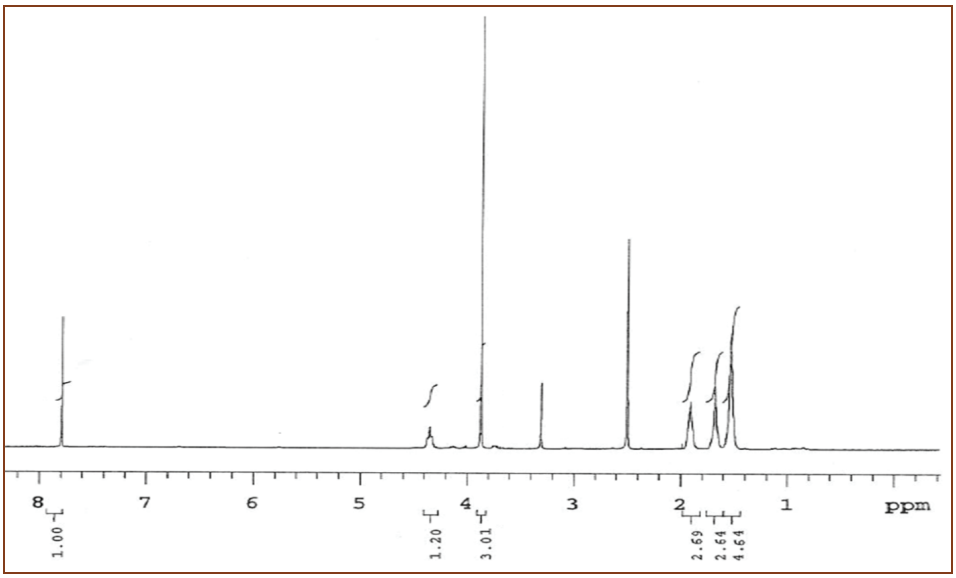

Fig. S-7. ^{1}H-NMR (400 MHz, DMSO, D_2O exchange) - **9**

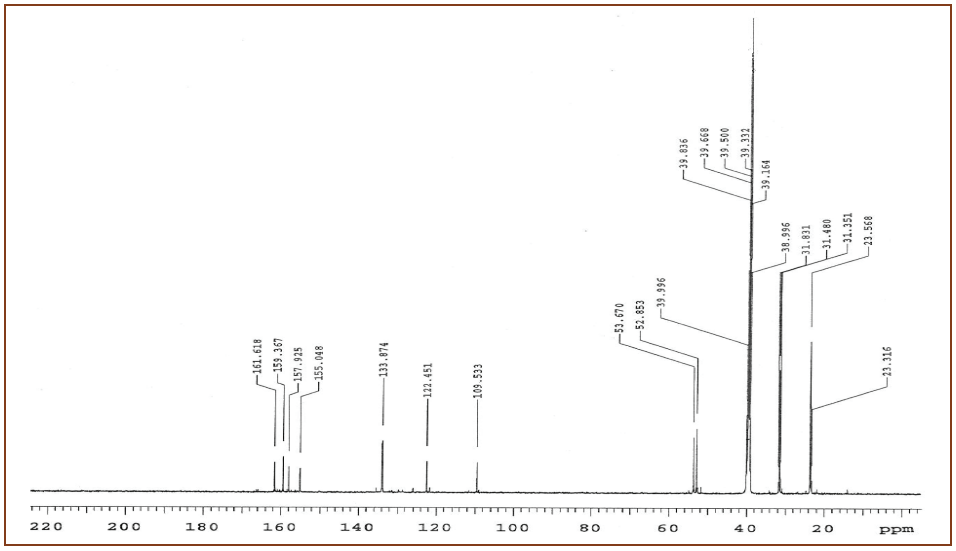

Fig. S-8. ^{13}C-NMR (100 MHz, DMSO) - **9**

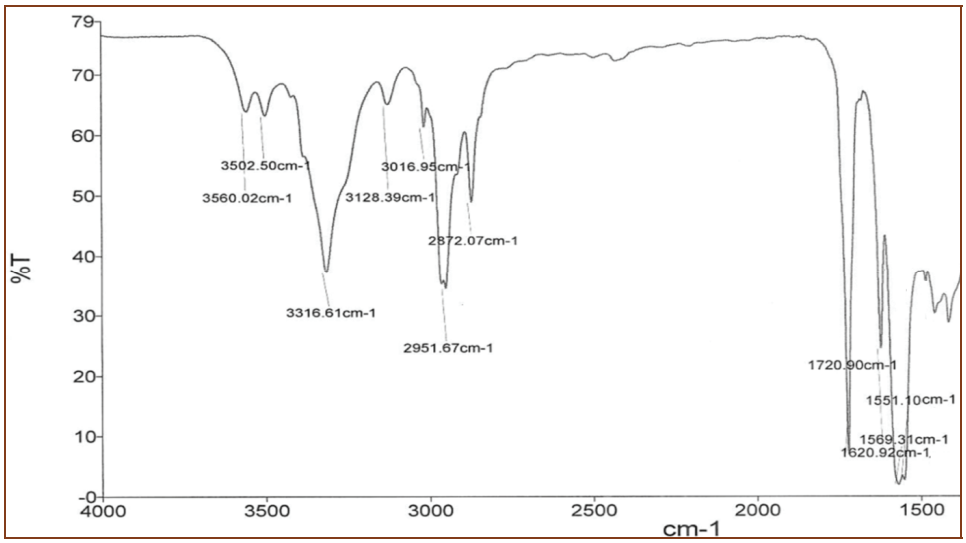

Fig. S-9. IR - **9**

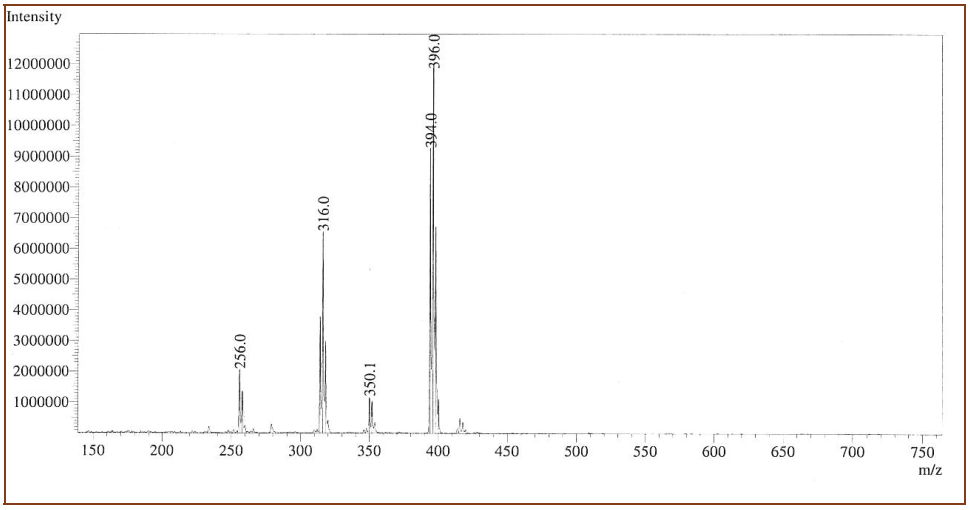

Fig. S-10. ESI-MS - **9**

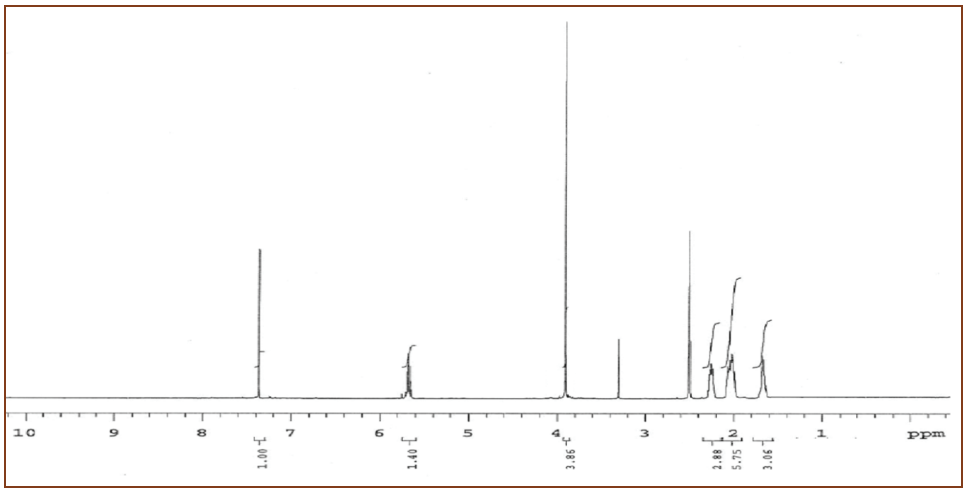

Fig. S-11. ^{1}H-NMR (400 MHz, DMSO) - **10**

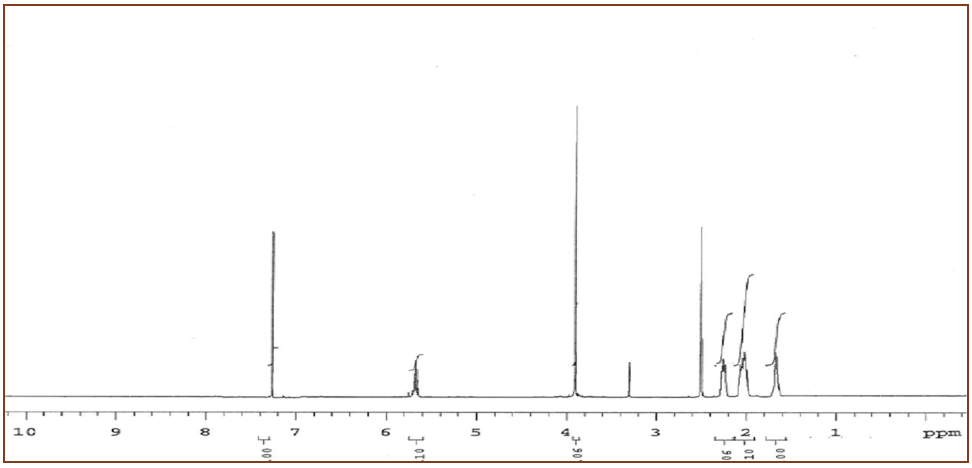

Fig. S-12. ^{1}H-NMR (400 MHz, DMSO, D_2OExchange) - **10**

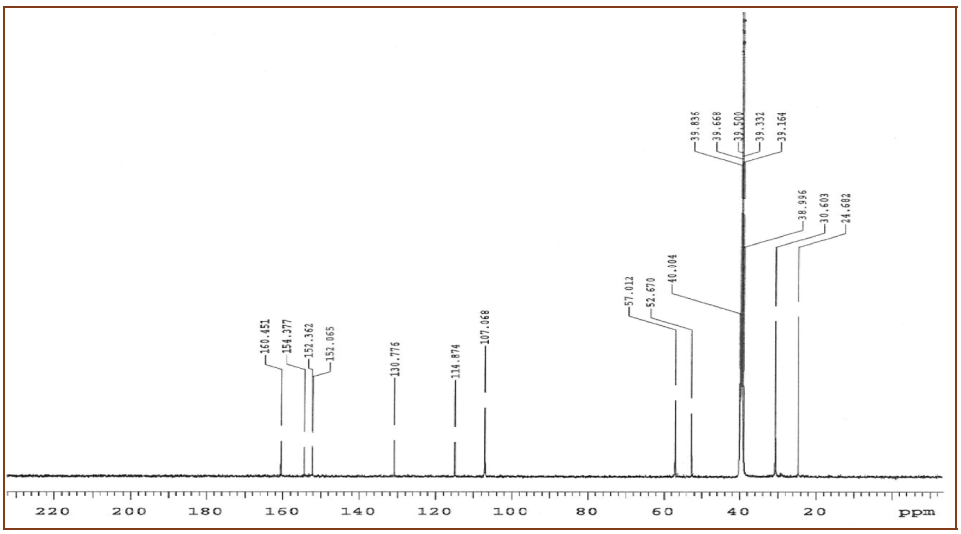

Fig. S-13. ^{13}C-NMR (100 MHz, DMSO) - **10**

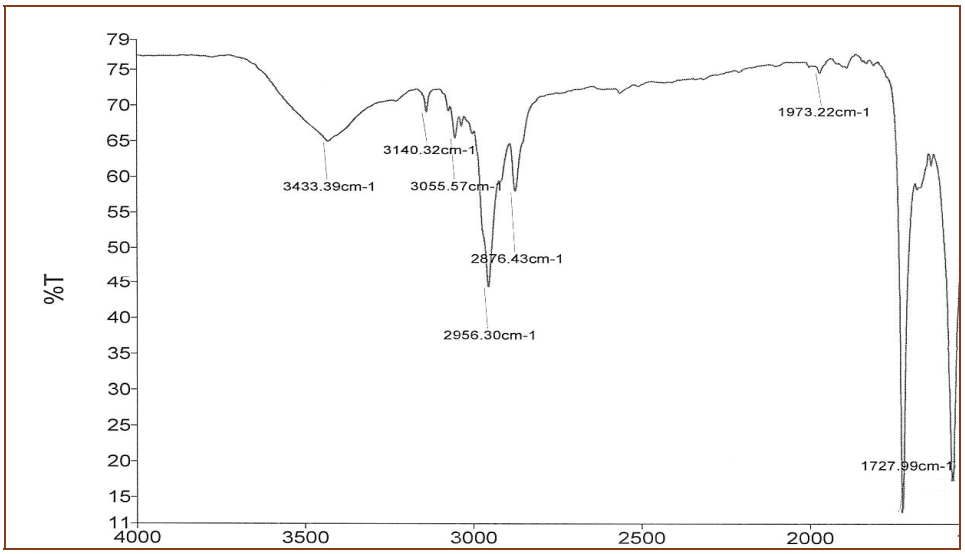

Fig. S-14. IR - **10**

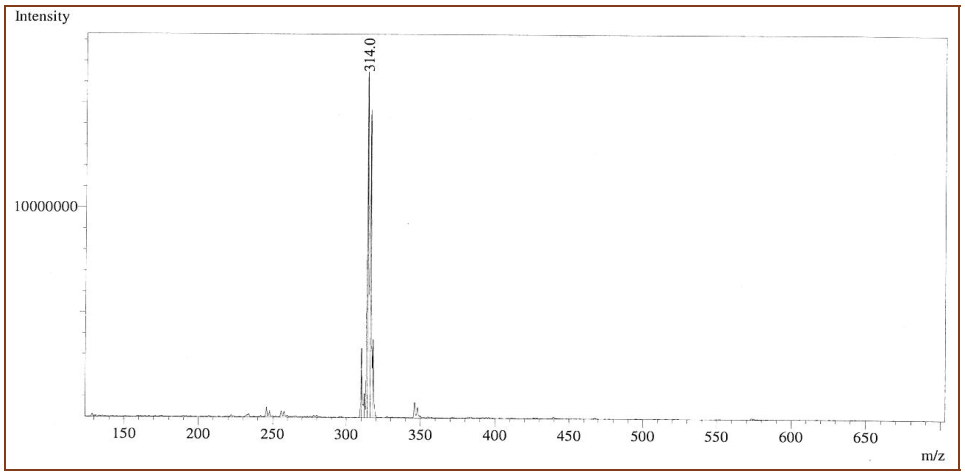

Fig. S-15. ESI-MS - **10**

Journal of the Serbian Chemical Society
JSCS-info@shd.org.rs • www.shd.org.rs/JSCS
J. Serb. Chem. Soc. *88* (1) 11–23 (2023)
JSCS–5607
Original scientific paper
Published 16 September 2022

The influence of different enzymatic preparations and skin contact time on aromatic profile of wines produced from autochthonous grape varieties Krstač and Žižak

VALERIJA MADŽGALJ[1], ALEKSANDAR PETROVIĆ[2], UROŠ ČAKAR[3], VESNA MARAŠ[1], IVANA SOFRENIĆ[4]* and VELE TEŠEVIĆ[4]

[1]"13. Jul Plantaže" ad., Bulevar Šarla de Gola 2, 81000 Podgorica, Montenegro, [2]Institute of Food Technology and Biochemistry, University of Belgrade – Faculty of Agriculture, Nemanjina 6, 11080 Belgrade, Serbia, [3]University of Belgrade – Faculty of Pharmacy, Department of Bromatology, Vojvode Stepe 450, 11000 Belgrade, Serbia and [4]University of Belgrade – Faculty of Chemistry, Studentski trg 12–16, 11000 Belgrade, Serbia

(Received 11 March, revised 11 June, accepted 29 June 2022)

Abstract: This study aimed to show aromatic profile of wines produced from two autochthonous grape cultivars Krstač (K) and Žižak (Z). During the wine production two enzymatic preparations (EP) Lallzyme cuvee blanc (CB) and Lallzyme enzymatic preparation β (EB) and different time of skin contact (4 and 8 h) were applied. Aromatic compounds were detected by GC/FID–MS analysis. Significantly higher content of total detected aromatic compounds compared to appropriate controls (168.54 and 161.72 mg L^{-1}) was observed for K EB4h (176.33 mg L^{-1}) and Z CB4h (177.29 mg L^{-1}) wines. Skin contact and usage of EP mostly increased content of 2-phenylethyl and isoamyl alcohols. Wines from both varieties showed higher content of hexanoic and octanoic acids compared to the control. It is interesting to emphasize that content of esters that are responsible for fruity aroma of wine which is important for pleasant taste (isoamyl acetate – banana, ethyl hexanoate – ripe banana, 2-phenylethyl acetate – powerful fruity rose like) were increased in all samples compared to the controls. The highest grades, after sensory evaluation, were obtained for K EB 8h (18.0 out of 20.0) and Z CB 8h (18.2 out of 20.0).

Keywords: aromatic compounds; autochthonous grapevine; GC/FID–MS analysis; must treatment; fruity aroma; sensory.

INTRODUCTION

Wine is rich source of different biologically active compounds. Among them it is possible to highlight polyphenols, which due to their beneficial health effects, are essential in healthy well balanced nutrition.[1] Beside phenolic com-

* Corresponding author. E-mail: ivanasofrenic@chem.bg.ac.rs
https://doi.org/10.2298/JSC220311056M

pounds it is important to emphasize those that are responsible for aromatic properties of wine. Wine quality mostly depends on aroma of wine.[2] The influence of wine aroma on organoleptic characteristics cannot be neglected too, since it is the key property which leads consumers to choose the wine.[3,4]

Different factors influence wine aromatic complexity, and the most significant are grape variety, pre-fermentative procedures, vinification procedures, fining, stabilization and aging.[5,6] Grape berry skin is one of the richest source of volatile compounds.[7] Prefermentative skin contact and pressure applied during the grape processing are winemaking procedures significantly affecting extraction of aromatic compounds.[8–11] Composition of grape juice and extraction process are responsible for content of aromatic compounds in wine.[12] White wine production process ordinarily includes skin removal to prevent excessive pass of polyphenols into the must which can cause enzymatic oxidative browning of wine. It is important to find balance between white wine skin contact and its removal.[13]

Aromatic compounds can be divided into the two groups, volatile and non-volatile compounds. Volatile compounds present in free form-directly contribute to the aroma, while non-volatile are in bound form.[14] Applying commercial enzymatic preparations which exhibit β-glucosidase activity it is possible to release aglycone from heteroside by cleavage of glycosidic bonds. This can affect the aromatic profile.[4,14] Application of enzymatic preparation especially during the maceration stage can significantly increase content of C_6 alcohols.[15]

White wine quality can be improved by must clarification.[16] It is also possible to improve quality of white wines by decreasing insoluble solids in the juice before fermentation.[12] Clarified musts, used for the production of white wines, can significantly improve organoleptic characteristics with emphasize on aroma.[17]

We have previously studied the influence of enzymatic preparations on the content of phenolic compounds in grape and fruit wines.[18,19] The influence of different enzymatic preparations and skin contact periods on aromatic profile of wines produced from Krstač and Žižak varieties was investigated in this study. For the first time data, regarding content and importance of aromatic compounds from wines produced from these two autochthonous varieties, will be published.

EXPERIMENTAL

Chemicals and plant material

In this study the following chemicals were used: methylene chloride, sodium sulfate anhydrous, methyl alcohol and 4-methyl-1-pentanol. All chemicals were obtained from Sigma–Aldrich, except methylene chloride which was obtained from Merck.

The autochthonous grape varieties Krstač and Žižak were investigated in this study. The grape varieties were grown in a vineyard on Ćemovsko polje in Montenegro. Among the white vine varieties, the most important are Krstač (grown on the “Pista” microlocality) and Žižak variety (grown on the “Bunar 17” microlocality). The training system of grape varieties Krstač and Žižak was a single Guyot, pruned to a mix of canes and spurs. All vines were evenly pruned, leaving one shoot growth on spur with two buds and an arc nine buds long.

Irrigation of the vine was carried out with a drip system. The yield of grapes per vine for the variety Krstač was 1.83 kg, while for Žižak 3.39 kg.

Winemaking

The grapes of Krstač (K) and Žižak (Z) varieties were harvested manually. Obtained grapes were in a state of full maturity and phytosanitary health 100 % (determined visually). The grapes of both varieties were manually destemmed, crushed, and sulfurized with 10 g $K_2S_2O_5$ per 100 kg mashed grapes. In vinification experiments were used: pure wine yeast culture *Saccharomyces cerevisiae* (ICV D47 Lallemand, Montreal, Canada), enzyme preparation Lallzyme Cuvee blanc (Lallemand, Montreal, Canada) which is mixture of pectinases and enzyme preparation Lallzyme β (Lallemand, Montreal, Canada) which is pectic enzyme complex. All experiments were divided into 5 treatments: Ctrl (control) – without skin contact and addition of enzymatic preparation, CB4h – with addition of enzymatic preparation Lallzyme Cuvee blanc and skin contact 4 h, CB8h – with addition of enzymatic preparation Lallzyme Cuvee blanc and skin contact 8 h, EB4h – with addition of enzymatic preparation Lallzyme β and skin contact 4 h, EB8h – with addition of enzymatic preparation Lallzyme β and skin contact 8 h. The amount of added enzymatic preparations was 2 g per 100 kg mashed grapes, and all skin contacts were performed at 5 °C temperature. After maceration of grape must in all 5 treatments grape juice was separated by static settling for 48 h and then racked. After that, all 5 treatments were inoculated with a pure culture of wine yeast *Saccharomyces cerevisiae* ICV D47 20 g hL^{-1} and left for fermentation. The alcoholic fermentation carried on for approximately 20 days at low temperature 15 °C. All obtained wines were dry (sugar content under 4 g L^{-1}). After sulphiting, racking and refilling vessels wines were prepared for GC–MS analysis.

GC/FID–MS analysis

Sample preparation was conducted by liquid–liquid extraction.[20] Volumes of 25 mL of wine sample and 5 mL of methylene chloride were stirred at 0 °C for 1 h. After one hour of extraction, the mixture was kept for 5 min in ultrasonic bath. Organic phase, which was collected after separation, was treated with sodium sulfate anhydrous to remove water and then filtrated. Subsequently, 0.6 mL of extracted wine sample was used for further GC/FID––MS analysis. Analysis of volatile compounds was conducted by using GC/FID–MS system according the previously described method, with some modifications.[21] The analysis was conducted on gas chromatograph (GC) system Agilent 7890A (Santa Clara, CA, USA). The device was equipped with Agilent 19091N-113 HP-INNOWax fused silica capillary column (30 m×0.32 mm i.d., 0.25 μm film thickness) which was used for separation. Injection was in split mode 3:1 with helium as carrier gas at 1.46 mL min^{-1}, and the injecting volume was 1 μL. The temperature of the GC oven was held at 40 °C for 5 min and then programmed to 220 °C at 10 °C min^{-1}, then held for 4 min at 220 °C. The instrument was equipped with dual detectors: mass selective detector (MSD) 5975C inert XL EI/CI MSD and flame ionization detector (FID) connected by capillary flow technology 2-way splitter with makeup gas. The ion source of the MSD and the transfer line were kept at 230 and 280 °C, respectively. Mass selective detector operated in the positive ion electron impact (EI) mode. Electron impact spectra in scan mode were recorded at 70 eV in mass range from 29 to 300 *m*/*z*. The FID detector was heated to 300 °C.

For quantitative evaluation the internal standard method was applied, with a known amount of 4-methyl-1-pentanol as an internal standard (IS). The (relative) percentages of the identified compounds were computed from the gas chromatography peak areas. The concen-

tration of each volatile was calculated with respect to the IS and presented as relative concentration of each component in analyzed sample.

The identification of the components was based on comparison with the reference spectra (Wiley and NIST databases). The percentages of the identified compounds were computed from the gas chromatography peak areas.

Statistical and sensory analysis

A one-way ANOVA was performed to compare the effect of using skin contact (4 and 8 h, 5 °C) and glycosidase enzyme preparations Lallzyme cuvee blanc and Lallzyme β, on each aromatic compounds separately. Tukey's post-hoc test with significant levels $p < 0.05$, was employed to conduct mean comparisons. The paired samples *T*-test was also applied. Statistical analysis was conducted using SPSS Statistical V20.0 software (IBM, Chicago, IL, USA).

The wine tasting panel, that consisted of three members, conducted sensory analysis of samples according to Bux–Baum method. For wine tasting the highest grade was 20 points.

RESULTS AND DISCUSSION

Effect of skin contact and usage of enzymatic preparation on the content of aromatic compounds in Krstač and Žižak wine

GC/FID–MS analysis of the wines showed that total content of detected aromatic compounds in Krstač samples were in range from 159.3 to 180.0 mg L^{-1}, while in Žižak from 161.7 to 192.5 mg L^{-1}. Statistical analysis, where paired samples *T*-test was applied, showed significant difference in the content of all detected aromatic compounds ($p < 0.05$), between Krstač Ctrl and Krstač EB4 wines (Table I) as well as for Ctrl and CB4 wines produced from Žižak variety (Table II). The concentrations of total detected volatile compounds obtained herein were similar to the literature data.[5,8,10] Wine fermentations of Emir grape cultivar resulted in 162.0 mg L^{-1} of volatiles in control and 187.0 mg L^{-1} of volatiles in skin contact sample.[8] Another study in which Muscat of Bornova wines were analyzed showed that control (158 mg L^{-1}) had lower content of total detected volatile compounds compared to 6 h (168 mg L^{-1}) and 12 h (172 mg L^{-1}) skin contact.[5]

Our findings are in line with the literature data which emphasized higher amounts of volatile compounds in skin contact wine compared to control (wine produced without skin contact).[10] After skin contact of 7 h at 15 °C Muscat of Alexandria wines were significantly enriched with aromatic compounds.[9] During the alcoholic fermentation compounds such as esters and alcohols are generated, and thus volatiles considerably increase in wine *vs.* juice.[8] Applied enzymatic preparation glycosidase during the maceration, cleave glycosidic bonds and so increase content of free form of different compounds potentially responsible for wine aroma.[6,22]

To the contrary, in Bical wines, produced after enzymatic preparation treatment, significant increase of total volatile compounds was not observed.[23]

TABLE I. The concentrations of aromatic compounds (mg L^{-1}) in Krstač wines using skin contact (4 and 8 h, 5 °C) and glycosidase enzyme preparations Lallzyme cuvee blanc and Lallzyme β with results of the one-way ANOVA along with the Tukey *post-hoc*; values are mean (n = 3) followed by different lowercase letters (a, b, c) indicate significant differences between treatments at the 5 % level; t = trace

Compounds	Sample					F	p
	K Ctrl	K CB4h	K CB8h	K EB4h[a]	K EB8h		
1-Hexanol	0.57 a	0.54 a	0.39 b	0.58 a	0.48 ab	12.4	0.001
Isobutyl alcohol	2.45 b	3.62 a	4.03 a	3.88 a	3.97 a	29.3	0.000
Isoamyl alcohol	91.19 bc	94.42 ab	99.14 a	94.32 abc	87.61 c	8.8	0.003
4-Methyl-1-pentanol	8.13	8.13	8.13	8.13	8.13		
3-Ethoxy-1-propanol	t	t	t	t	t		
2,3-Butanediol	t	t	0.12	0.14	0.10	1.7	0.259
3-(Methylthio)-1-propanol	0.22 b	0.22 b	0.25 ab	0.27 a	0.21 b	6.5	0.008
2-Phenylethyl alcohol	50.69 a	41.94 b	48.82 a	50.38 a	40.83 b	11.4	0.001
Total alcohols	153.25	148.87	160.87	157.69	141.33		
Hexanoic acid	1.98 b	2.52 ab	2.76 a	2.73 a	3.08 a	6.5	0.008
Octanoic acid	4.20 c	4.73 bc	5.56 a	5.34 ab	5.65 a	15.4	0.000
Decanoic acid	0.87 a	0.58 b	0.59 b	0.64 b	0.50 b	19.2	0.000
Isobutyric acid	t	0.24	t	0.25	0.26	0.2	0.863
9-Decenoic acid	1.30 a	0.56 b	0.51 b	0.64 b	t	8.7	0.007
Total acids	8.35	8.63	9.42	9.59	9.49		
Ethyl butyrate	0.89 c	1.12 b	1.35 a	1.22 ab	1.21 ab	20.7	0.000
Ethyl hexanoate	0.19 c	0.31 b	0.30 b	0.30 b	0.41 a	26.8	0.000
Ethyl (*S*)-(–) lactate	0.98 a	0.68 bc	0.89 ab	0.74 bc	0.64 c	9.7	0.002
Ethyl octanoate	t	0.16	0.20	0.18	0.25	2.1	0.178
Ethyl decanoate	t	0.19	0.17	t	t	1.7	0.267
Diethyl succinate	0.68 b	1.01 ab	1.07 a	1.07 a	1.00 ab	4.5	0.024
Ethyl 9-decenoate	t	t	t	t	t		
Ethyl 4-hydroxybutanoate	t	t	t	t	t		
Diethyl hydroxybutanedioate	t	t	t	t	t		
Ethyl ester 4-ethoxy benzoic acid	t	0.18	0.22	t	t	0.6	0.482
Ethyl hydrogen succinate	2.20 b	3.12 a	3.40 a	3.18 a	3.01 a	9.1	0.002
Isoamyl acetate	0.27 b	0.61 a	0.69 a	0.66 a	0.60 a	6.1	0.009
Hexyl acetate	t	t	t	t	t		
1,3-Propanediol diacetate	0.14 c	0.15 c	0.19 ab	0.21 a	0.17 bc	19.7	0.000
2-Phenylethyl acetate	0.16 b	0.25 a	0.30 a	0.28 a	0.26 a	8.9	0.002
γ-Butyrolactone	1.44 a	0.78 c	0.93 bc	1.21 ab	0.96 bc	12.3	0.001
Total ethyl esters, acetates and lactones	6.94	8.56	9.72	9.05	8.51		
Total aromatic compounds	168.54	166.06	180.01	176.33	159.33		

[a]Statistically significant difference (p<0.05) in the content of all detected aromatic compounds compared to K Ctrl

Alcohols

Among the alcohols, in Krstač and Žižak wines, the most predominant were higher alcohols, such as isoamyl alcohol, phenyl ethyl alcohol and isobutyl alco-

TABLE II. The concentrations of aromatic compounds (in mg L^{-1}) Žižak wines using skin contact (4 and 8 h, 5 °C) and glycosidase enzyme preparations Lallzyme cuvee blanc and Lallzyme β with results of the one-way ANOVA along with the Tukey *post-hoc*; values are mean (n = 3) followed by different lowercase letters (a, b, c) indicate significant differences between treatments at the 5 % level

Compound	Sample					*F*	*p*
	Z Ctrl	Z CB4h[a]	Z CB8h	Z EB4h	Z EB8h		
1-Hexanol	0.62 a	0.53 ab	0.39 b	0.68 a	0.73 a	8.49	0.003
Isobutyl alcohol	5.00 c	5.58 b	6.15 a	5.20 bc	5.58 b	20.77	0.000
Isoamyl alcohol	102.17 b	102.82 b	115.21 a	96.51 b	112.81 a	23.50	0.000
4-Methyl-1-pentanol	8.13	8.13	8.13	8.13	8.13		
3-Ethoxy-1-propanol	t	t	t	t	t		
2,3 Butanediol	0.20	0.36	0.33	0.30	t	0.92	0.474
3-(Methylthio)-1-propanol	0.24 ab	0.15 b	0.25 ab	0.26 ab	0.29 a	4.71	0.041
2-Phenylethyl alcohol	31.37 b	37.46 ab	41.58 a	41.09 ab	40.41 ab	3.79	0.040
Total alcohols	147.73	155.03	172.04	152.17	167.94		
Hexanoic acid	1.94 b	3.54 a	3.12 a	3.40 a	2.92 a	15.91	0.000
Octanoic acid	3.53 b	6.97 a	6.21 a	6.74 a	5.59 a	3.74	0.021
Decanoic acid	0.57	0.86	0.83	1.07	1.06	2.59	0.102
Isobutyric acid	0.34 ab	0.31 bc	0.38 a	0.36 ab	0.26 c	17.41	0.000
9-Decenoic acid	0.25 b	1.07 a	0.40 b	0.98 a	0.95 a	6.23	0.009
Total acids	6.63	12.75	11.23	12.55	10.78		
Ethyl butyrate	1.40 b	1.96 a	1.43 b	1.97 a	1.61 ab	11.34	0.001
Ethyl hexanoate	0.41 c	0.51 a	0.44 bc	0.50 ab	0.45 c	11.53	0.001
Ethyl (*S*)-(–) lactate	0.26 ab	0.15 b	0.19 ab	0.23 ab	0.32 a	3.62	0.045
Ethyl octanoate	0.19 b	0.25 a	0.22 ab	0.22 ab	0.26 ab	4.85	0.020
Ethyl decanoate	t	0.20	t	t	0.12	1.13	0.348
Diethyl succinate	0.45 b	0.84 a	0.96 a	0.85 a	0.74 a	10.11	0.002
Ethyl 9-decenoate	t	t	t	t	t		
Ethyl 4-hydroxybutanoate	1.21 c	1.43 b	1.30 bc	1.69 a	1.41 b	33.62	0.000
Diethyl hydroxybutanedioate	0.10 bc	0.08 bc	0.06 c	0.11 b	0.21 a	26.29	0.000
Ethyl ester 4-ethoxy benzoic acid	t	t	t	t	t		
Ethyl hydrogen succinate	1.63 a	2.29 a	2.33 a	2.23 a	0.54 b	4.18	0.030
Isoamyl acetate	0.69	0.71	1.13	0.79	0.83	2.72	0.091
Hexyl acetate	t	t	t	t	t		
1,3-Propanediol diacetate	0.23 ab	0.28 a	0.23 ab	0.28 a	0.23 b	3.53	0.048
2-Phenylethyl acetate	0.13 b	0.18 b	0.29 a	0.21 ab	0.17 b	6.85	0.006
γ-Butyrolactone	0.65	0.63	0.64	0.74	0.82	3.30	0.057
Total ethyl esters, acetates and lactones	7.36	9.51	9.22	9.83	7.71		
Total aromatic compounds	161.72	177.29	192.49	174.55	186.43		

[a]Statistically significant difference (p<0.05) in the content of all detected aromatic compounds compared to Z Ctrl

hol. The total detected alcohol content in K Ctrl was 153.3 mg L^{-1} (Table I), while in Z Ctrl 147.7 mg L^{-1} (Table II). It is important to highlight that literature data indicated higher alcohols as a major constituents of Muscat of Bornova

wines.[5] Almost 84 % of total free volatiles in wines were higher alcohols which indicated them as the most prominent compounds.[10]

The content of phenyl ethyl alcohol in wines produced from cultivar Krstač was from 40.8 to 50.7 mg L^{-1} (Table I) while in cultivar Žižak from 31.4 to 41.6 mg L^{-1} (Table II). Statistical analysis, where one-way ANOVA with the Tukey test was carried out, showed a statistically significant difference in the content of 2-phenylethyl alcohol ($p<0.05$) between Žižak Ctrl and Z CB8h, and Krstač Ctrl compared to K CB4h and K EB8h.

Study of Albariño wines, in which malolactic fermentation was not conducted, content of phenyl ethyl alcohol increased up to 20 mg L^{-1}.[2] Literature data suggested contribution of phenyl ethyl alcohol to pleasant wine aroma which reminds to rose.[5,12]

Our findings are supported by the literature data which indicated that skin contact and/or usage of enzymatic preparations, which possess glycosidase activity, generate higher content of free form of phenyl ethyl alcohol.[15] Application of enzymatic preparation in experiment with Bical wines did not significantly increase content of aromatic alcohols.[23] Wines produced in vinification with skin contact showed significantly higher content of phenyl ethanol and other fusel alcohols.[12] Muscat of Alexandria wines in which skin contact was applied significantly increased total level of alcohol.[9]

Prolonged maceration time and usage of enzymatic preparation Lallzyme β, in the wines produced from Krstač variety, decreased alcohol content. Generation of higher alcohols have been decreased with longer skin contact. It is important to point out that higher alcohol formation is mainly conducted by Ehrlich mechanism. Decrease of higher alcohols can be explained by the fact that Ehrlich mechanism blockage is result of higher levels of nitrogenous substances in vinifications.[6,24]

Concentration of 2,3-butanediol in Krstač wines were from 0.10 to 0.14 mg L^{-1} (Table I) while in Žižak wines were from 0.20 to 0.36 mg L^{-1} (Table II), respectively. There was no statistically significant difference between treatments as regards the content of 2,3-butanediol ($p>0.05$) in Krstač and Žižak wines. Krstač and Žižak wines produced by addition of various enzyme preparations (cuvee blanc, β-enzyme) and skin contact of 8 h had statistically significant higher content of isoamyl and isobutyl alcohols ($p<0.05$), as compared to the control wines (except K EB8h for isoamyl alcohol). The study, in which were analyzed Muscat of Bornova wines, reported almost similar results as in our study.[5]

Compounds with 6 carbon atoms can be formed from fatty acids in grapes during the pre-fermentative stage.[15] Significant increase of C_6 alcohols is a result of skin-contact process which ensures more fatty acids and lipoxygenase enzyme during fermentation.[8,12,15] Those compounds are responsible for herbaceous and leafy notes which are unfavourable for wine quality.[5,8] The content of 1-hexanol

was from 0.39 to 0.58 mg L^{-1} for Krstač wines, while for Žižak it ranged from 0.39 to 0.73 mg L^{-1}, respectively. Skin contact (8 h) and the use of Lallzyme enzyme β preparation, resulted in the higher content of 1-hexanol in Žižak wine (p<0.05), as compared to Z CB8h. The highest content of total detected alcohols, for both used grape cultivars, was observed when vinification was conducted by maceration, during the 8 hours, with enzymatic preparation Lallzyme cuvee.

Acids

Krstač wines obtained after applied skin contact (4 and 8 h) and usage of enzymatic preparation glycosidase showed higher content of hexanoic and octanoic acids (Table I). Wines obtained from cultivar Žižak, by the same vinification procedure, were enriched with hexanoic, octanoic and decanoic acids (Table II). Based on the Tukey test results, a statistically significant differences in the content of hexanoic and octanoic acids (p<0.05) between control (K Ctrl, Z Ctrl) and all other Krstač and Žižak skin contact wines (excluding K CB4h for hexanoic and octanoic acid) were found.

Our findings are in line with literature data which emphasized average content of 6 (3.7 mg L^{-1}), 8 (3.3 mg L^{-1}) and 10 (0.8 mg L^{-1}) carbon atoms fatty acids.[2] Another study reported almost similar values for content of 6 (3.3 mg L^{-1}), 8 (3.9 mg L^{-1}) and 10 (1.2 mg L^{-1}) carbon atoms fatty acids.[25] Skin contact Emir and Muscat of Bornova wines increased content of fatty acids.[5,8] Albariño wines produced with usage of enzymatic preparation during maceration showed almost double concentration of hexanoic and octanoic acids compared to other samples.[15]

Ethyl esters, acetates and lactones

Esters are important compounds which are responsible for fruity aroma (ethyl butanoate – pineapple, isoamyl acetate – banana, ethyl hexanoate – ripe banana, 2-phenyl ethyl acetate – powerful fruity, rose like).[5,12] It is important to emphasize that highest content of ethyl butyrate, ethyl hexanoate, diethyl succinate and ethyl hydrogen succinate was observed in wines produced from both grape cultivars. Significant concentrations of ethyl octanoate and ethyl 4-hydroxybutanoate were observed in wines produced from Žižak.

The literature data in which were studied other grape varieties reported similar findings related to esters.[5,6,9] The data related to ethyl esters and acetates content for Assyrtiko wines showed that skin contact has not significantly increased content of those compounds.[12]

A one-way Anova revealed that the use of maceration (4 and 8 h) and enzyme preparations led to a statistically significant increase in the content of ethyl butyrate, ethyl hexanoate, ethyl hydrogen succinate, isoamyl acetate and 2-phenylethyl acetate and a decrease in concentration of ethyl lactate and γ-butyrolactone (p<0.05) in all Krstač wines (except K CB8h for ethyl lactate and K EB4h for γ-butyrolactone). Literature data suggested that skin contact increase

content of ethyl hexanoate,[5,9] ethyl butanoate, 2-phenylethyl acetate,[9] ethyl octanoate, diethyl succinate and isoamyl acetate.[5] Our results are in agreement with findings which highlighted decrease of ethyl lactate[6] and γ-butyrolactone.[5,10]

Trace amounts of hexyl acetate, ethyl 9-decenoate, and 3-ethoxy-1-propanol are present in all wines. Skin contact caused an increase in hexyl acetate content in Albillo wines[6] and a decrease in 3-ethoxy-1-propanol concentration in Muscat of Bornova wines.[5] Addition of glycosidase enzyme preparations resulted in 3--ethoxy-1-propanol content rise in wines.[23] The highest effect on content of 3--ethoxy-1-propanol was exerted by a yeast strain used during the alcoholic fermentation.[26] C_6-alcohols and C_6-aldehydes are precursors to hexyl acetate.[27] In the literature, based on study of Chardonnay wines, concentrations of hexyl acetate vary between 0.020 and 0.068 mg L^{-1},[5,6] ethyl 9-decenoate 0.020 mg L^{-1},[28] and 3-ethoxy-1-propanol 0.099 mg L^{-1},[5] which is in line with our research.

Skin contact (4 h) and the use of cuvee blanc enzyme preparation resulted in the higher content of ethyl octanoate in Žižak wine (p<0.05) as compared to Žižak Ctrl.

Diethyl hydroxybutanedioate (diethyl malate) and ethyl 4-hydroxybutanoate are present in Žižak wines, and their trace amounts are found in Krstač wines. By using the Tukey *post-hoc* test, the highest statistically significant difference in the content of ethyl 4-hydroxybutanoate (p<0.05) between Z CB4h and Z EB4h was established. Vinification with skin contact of 8 h and the use of Lallzyme β enzyme preparation increased content of diethyl hydroxybutanedioate (p<0.05), as compared to Z CB8h and Z EB4h wines. The concentration is considerably higher in skin contact wine (Z EB8h) than in the control wine, which is in line with the data found in the literature.[9]

The precursor of diethyl hydroxybutanedioate is malic acid.[29] The correlation between diethyl hydroxybutanedioate and its precursor indicates potential reason for the different content of this compound in Žižak and Krstač varieties.

Higher ethyl 4-hydroxybutanoate content in Žižak wines, as compared to Krstač wines, may be interpreted as a result of glutamic acid higher concentration in Žižak grape juice. Ethyl 4-hydroxybutanoate is produced from glutamic acid through 4-hydroxybutanoic acid.[26,30]

Žižak wines produced by addition of Lallzyme β enzyme preparation and skin contact of 4 h had statistically significant higher content of 1,3-propanediol diacetate (p < 0.05), as compared to wine which was produced with the same enzyme preparation and prolonged skin contact time (8 h).

Content of isoamyl acetate was higher in Z Ctrl wine (0.69 mg L^{-1}) compared to K Ctrl wine (0.27 mg L^{-1}). Obtained results are in line with the literature data which reported similar findings.[25] It is interesting to emphasize that higher concentration of isoamyl acetate could contribute to “banana” nuance aroma of wines.[15]

Concentration of 2-phenylethyl acetate in Krstač wines was from 0.16 to 0.30 mg L^{-1} while in Žižak from 0.13 to 0.29 mg L^{-1}. Similar content was observed in Muscat of Alexandria wine[9] while the study of Loureira wines reported 0.26 to 0.30 mg L^{-1}.[25] Diethyl succinate content in Krstač wines was in the range from 0.68 to 1.07 mg L^{-1} while in Žižak from 0.45 to 0.96 mg L^{-1}. Our findings are in accordance with the literature data related to content of diethyl succinate.[2] Only one lactone detected in this study, γ-butyrolactone, had higher concentration in Krstač wines compared to Žižak.

Sensory evaluation of wines produced from Krstač and Žižak varieties

Wine samples produced from Krstač variety after skin contact (4 and 8 h, 5 °C) and usage of enzymatic preparations (Lallzyme Cuvee blanc and Lallzyme enzymatic preparation β) have had bright yellow colour and were without any difference in colour between different vinifications. Aroma intensity increased from K Ctrl wine to K EB8h wine which was the most intense. The taste of wine from different vinification showed remarkable difference. Wine obtained after vinification in which skin contact was applied during the 8 h and Lallzyme enzymatic preparation β had the soft taste and long-lasting aroma. Vinification with skin contact during the 8 h and Lallzyme Cuvee blanc influenced the production of wine without bitterness and hardness, while control showed the most intense sharp and bitter taste. Krstač wine samples, obtained after skin contact during the 8 h, have had higher grades after sensory evaluation compared to 4 h skin contact. The lowest grades, after sensory evaluation, were recorded for control vinification (without skin contact and enzymatic preparations, Fig. 1).

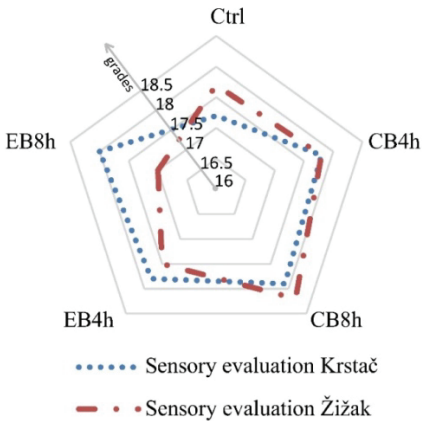

Fig. 1. Sensory evaluation Krstač and Žižak wines.

Žižak variety wines produced after skin contact (4 and 8 h, 5 °C) and usage of enzymatic preparations (Lallzyme Cuvee blanc and Lallzyme enzymatic preparation β) have had pale gold colour almost same intensity in all samples. All samples have had fruity aroma. Aroma increased in samples in which was skin

contact prolonged. The most intense aroma was in Z CB8h sample, while lowest intensity was observed for Z Ctrl. The taste of Z CB8h wine characterized as the most fruity and the softest. Žižak wines obtained after vinification, in which was applied Lallzyme enzymatic preparation β, have had softer taste without bitterness and astringency. Generally, the best taste characteristics showed Z CB8h wine (Fig. 1). Observing all samples from both varieties the highest grades, after sensory evaluation, were obtained after 8 h skin contact K EB8h (18.0 out of 20.0) and Z CB8h (18.2 out of 20.0, Fig. 1).

CONCLUSION

The wines produced with skin contact showed mostly higher content of 2-phenylethyl, isoamyl and other fusel alcohols. Krstač wines obtained after applied skin contact (4 and 8 h) and usage of enzymatic preparation showed higher content of hexanoic and octanoic acids. Significant concentrations of ethyl octanoate and ethyl 4-hydroxybutanoate were observed in wines produced from Žižak. Skin contact (4 and 8 h) and usage of enzymatic preparation increased content of ethyl butyrate, ethyl hexanoate, ethyl octanoate, diethyl succinate, isoamyl acetate and 2-phenylethyl acetate in wines produced from both cultivars. Observing all samples from both varieties the highest grades, after sensory evaluation, were obtained after 8 h skin contact K EB8h and Z CB8h.

Acknowledgements. This work was funded by the Scientific Research Grant from the Ministry of Education, Science and Technological Development of the Republic of Serbia No. TR31020, Grant Agreement between Ministry of Education, Science and Technological Development, Republic of Serbia and University of Belgrade – Faculty of Pharmacy, No. 451--03-68/2022-14/200161 and grant Agreement between Ministry of Education, Science and Technological Development of Republic of Serbia and University of Belgrade – Faculty of Chemistry, Contract number: 451-03-68/2022-14/200168.

ИЗВОД

УТИЦАЈ РАЗЛИЧИТИХ ЕНЗИМСКИХ ТРЕТМАНА И ВРЕМЕНА КОНТАКТА ПОКОЖИЦЕ НА АРОМАТСКЕ ПРОФИЛЕ ВИНА ПРОИЗВЕДЕНИХ ОД АУТОХТОНИХ СОРТИ ГРОЖЂА КРСТАЧ И ЖИЖАК

ВАЛЕРИЈА МАЦГАЉ[1], АЛЕКСАНДАР ПЕТРОВИЋ[2], УРОШ ЧАКАР[3], ВЕСНА МАРАШ[1], ИВАНА СОФРЕНИЋ[4] и ВЕЛЕ ТЕШЕВИЋ[4]

[1]"13. Јули Плантаже" ад., Булевар Шарла де Гола 2, 81000 Подгорица, Црна Гора, [2]Институт за прехрамбену технологију и биохемију, Универзитет у Београду – Пољопривредни факултет, Немањина 6, 11080 Београд, [3]Универзитет у Београду – Фармацеутски факултет, Војводе Степе 450. 11000 Београд и [4]Универзитет у Београду – Хемијски факултет, Студентски трг 12-16, 11000 Београд

Ова студија је имала за циљ да прикаже профиле ароматичних једињења вина произведених од аутохтоних сорти грожђа Крстач (K) и Жижак (Z). Током производње вина од обе сорте коришћени су ензимски препарати (EP): Lallzyme cuvee blanc (CB), Lallzyme enzymatic preparation β (EB) и различито време контакта покожице (4 и 8 h). Ароматична једињења су анализирана GC/FID–MS техником. За вина K EB4h (176,33 mg L^{-1}) и Z CB4h (177,29 mg L^{-1}) уочава се значајно већи садржај укупних ароматичних једи-

њења у поређењу са одговарајућим контролним винима (168,54 and 161,72 mg L^{-1}). Продужење времена контакта покожице и употреба EP углавном повећава садржај 2-фенилетил- и изоамил-алкохола. Вина обе сорте су показала већи садржај хексанске и октанске киселине у односу на контролна вина. Занимљиво је поменути да је у свим узорцима повећан садржај естара који су одговорни за воћну арому вина, која је заслужна за пријатан укус (изоамил-ацетат – банана, етил-хексаноат – зрела банана, 2-фенилетил-ацетат – јак воћни мирис руже), у поређењу са контролним винима. Највише оцене, након сензорног оцењивања, добијене су за K EB 8h (18,0 од максималних 20,0) и Z CB 8h (18,2 од максималних 20,0).

(Примљено. 11. марта, ревидирано 11. јуна, прихваћено 29. јуна 2022)

REFERENCES

1. U. Čakar, S. Šobajić, B. Vidović, B. Djordjević, *Progr. Nutr.* **20** (2018) 38 (https://doi.org/10.23751/pn.v20i1.5435)
2. E. Falqué, P. Darriet, E. Fernández, D. Dubourdieu, *Int. J. Food Sci. Technol.* **43** (2008) 464 (https://doi.org/10.1111/j.1365-2621.2006.01474.x)
3. M. J. Gómez-Míguez, M. Gómez-Míguez, I. M. Vicario, F. J. Heredia, *J. Food Eng.* **79** (2007) 758 (https://doi.org/10.1016/j.jfoodeng.2006.02.038)
4. E. Sánchez-Palomo, R. Alonso-Villegas, M. A. González-Viñas, *Food Chem.* **173** (2015) 1195 (https://doi.org/10.1016/j.foodchem.2014.10.148)
5. S. Selli, A. Canbas, T. Cabaroglu, H. Erten, Z. Günata, *Food Chem.* **94** (2006) 319 (https://doi.org/10.1016/j.foodchem.2004.11.019)
6. E. Sánchez-Palomo, M. A. González-Viñas, M. C. Díaz-Maroto, A. Soriano-Pérez, M. S. Pérez-Coello, *Food Chem*. **103** (2007) 631 (https://doi.org/10.1016/j.foodchem.2006.08.033)
7. E. García, J. L Chacón, J. Martínez, P. M. Izquierdo, *Food Sci. Tech. Int*. **9** (2003) 33 (https://doi.org/10.1177/1082013203009001006)
8. T. Cabaroglu, A. Canbas, R. Baumes, C. Bayonove, J. P. Lepoutre, Z. Günata, *J. Food Sci.* **62** (1997) 680 (https://doi.org/10.1111/j.1365-2621.1997.tb15434.x)
9. T. Cabaroglu, A. Canbas, *Acta Aliment. Hung.* **31** (2002) 45 (https://doi.org/10.1556/aalim.31.2002.1.5)
10. S. Selli, A. Canbas, T. Cabaroglu, H. Erten, J. P. Lepoutre, Z. Günata, *Food Control* **17** (2006) 75 (https://doi.org/10.1016/j.foodcont.2004.09.005)
11. D. Kechagia, Y. Paraskevopoulos, E. Symeou, M. Galiotou-Panayotou, Y. Kotseridis, *J. Agric. Food Chem.* **56** (2008) 4555 (https://doi.org/10.1021/jf073550q)
12. M. Maggu, R. Winz, P. A. Kilmartin, M. C. T. Trought, L. Nicolau, *J. Agric. Food Chem.* **55** (2007) 10281 (https://doi.org/10.1021/jf072192o)
13. E. García, J. L. Chacón, J. Martínez, P. M. Izquierdo, *Food Sci. Tech. Int.* **9** (2003) 33 (https://doi.org/10.1177/1082013203009001006)
14. S. C. Diéguez, L. C. Lois, E. F. Gómez, M. L. G. de la Peña, *LWT – Food Sci. Technol.* **36** (2003) 585 (https://doi.org/10.1016/S0023-6438(03)00064-1)
15. L. Armada, E. Fernández, E. Falqué, *LWT – Food Sci. Technol.* **43** (2010) 1517 (https://doi.org/10.1016/j.lwt.2010.06.009)
16. M. Ferrando, C. Güell, F.López, *J. Agric. Food Chem.* **46** (1998) 1523 (https://doi.org/10.1021/jf9703866)

17. V. M. Burin, T. M. Gomes, V. Caliari, J. P. Rosier, M. T. B. Luiz, *Microchem. J.* **122** (2015) 20 (https://doi.org/10.1016/j.microc.2015.03.011)
18. U. Čakar, A. Petrović, M. Janković, B. Pejin, V. Vajs, M. Čakar, B. Djordjević, *Eur. J. Hortic. Sci.* **83** (2018) 49 (https://doi.org/10.17660/eJHS.2018/83.1.7)
19. N. Lisov, A. Petrović, U. Čakar, M. Jadranin, V. Tešević, Lj. Bukarica-Gojković, *Maced. J. Chem. Chem. Eng.* **39** (2020) 185 (http://dx.doi.org/10.20450/mjcce.2020.2060)
20. V. Avram, C. G. Floare, A. Hosu, C. Cimpoiu, C. Măruţoiu, Z. Moldovan, *Anal. Lett.* **48** (2014) 1099 (https://doi.org/10.1080/00032719.2014.974054)
21. S. Veljović, N. Tomić, M. Belović, N. Nikićević, P. Vukosavljević, M. Nikšić, V. Tešević, *Food Technol. Biotechnol.* **57** (2019) 408 (https://doi.org/10.17113/ftb.57.03.19.6106)
22. T. Cabaroglu, S. Selli, A. Canbas, J. P. Lepoutre, Z. Günata, *Enzyme Microb. Tech.* **33** (2003) 581 (https://doi.org/10.1016/S0141-0229(03)00179-0)
23. S. M. Rocha, P. Coutinho, I. Delgadillo, A. D. Cardoso, M. A. Coimbra, *J. Sci. Food Agric.* **85** (2005) 199 (https://doi.org/10.1002/jsfa.1937)
24. A. Rapp, G. Versini, *Developments in food science, influence of nitrogen compounds in grapes on aroma compounds of wines*, San Michele all'Adige, 1995, p. 1659 (https://doi.org/10.1016/S0167-4501(06)80257-8)
25. E. Falqué, E. Fernández, D. Dubourdieu, *J. Agric. Food Chem.* **50** (2002) 538 (https://doi.org/10.1021/jf010631s)
26. A. Antonelli, L. Castellari, C. Zambonelli, A. Carnacini, *J. Agric. Food Chem.* **47** (1999) 1139 (https://doi.org/10.1021/jf9807317)
27. E. G. Dennis, R. A. Keyzers, C. M. Kalua, S. M. Maffei, E. L. Nicholson, P. K. Boss, *J. Agric. Food Chem.* **60** (2012) 2638 (https://doi.org/10.1021/jf2042517)
28. H. Li, Y. S. Tao, H. Wang, L. Zhang, *Eur. Food Res. Technol.* **227** (2008) 287 (http://dx.doi.org/10.1007/s00217-007-0722-9)
29. L. Khvalbota, A. Machyňáková, J. Čuchorová, K. Furdíková, I. Špánik*, J. Food Comp. Anal.* **96** (2021) (https://doi.org/10.1016/j.jfca.2020.103719)
30. L. Dufossé, A. Latrasse, H. E. Spinnler, *Sci. Aliments* **14** (1994) 17 (https://hal.archives-ouvertes.fr/hal-02637614).

Journal of the Serbian Chemical Society
JSCS@tmf.bg.ac.rs • www.shd.org.rs/JSCS

J. Serb. Chem. Soc. *88* (1) 25–39 (2023)
JSCS–5608

Original scientific paper
Published 14 December 2022

Design of benzimidazoles, benzoxazoles, benzothiazoles and thiazolopyridines as leukotriene A_4 hydrolase inhibitors through 3D-QSAR, docking and molecular dynamics

MARCOS LORCA[1], MARIO FAÚNDEZ[2], C. DAVID PESSOA-MAHANA[2], GONZALO RECABARREN-GAJARDO[2,3], BENJAMIN DIETHELM-VARELA[2], DANIELA MILLÁN[4], ISMAIL CELIK[5], MARCO MELLADO[6], ILEANA ARAQUE[1], JAIME MELLA[1,7]* and JAVIER ROMERO-PARRA[8]**

[1]*Institute of Chemistry and Biochemistry, Faculty of Science, University of Valparaíso, Valparaíso 2360102, Chile,* [2]*Faculty of Chemistry and Pharmacy, Pontifical Catholic University of Chile, Santiago 7820436, Chile,* [3]*Interdisciplinary Center for Neurosciences, Pontifical Catholic University of Chile, Santiago 8330024, Chile,* [4]*Integrative Center for Biology and Applied Chemistry, Bernardo O'Higgins University, Santiago 8370854, Chile,* [5]*Department of Pharmaceutical Chemistry, Faculty of Pharmacy, Erciyes University, Kayseri 38039, Turkey,* [6]*Instituto de Investigación y Postgrado, Facultad de Ciencias de la Salud, Universidad Central de Chile, Santiago 8330507, Chile,* [7]*Chilean Pharmacopeia Research Center, University of Valparaíso, Valparaíso 2360134, Chile and* [8]*Department of Organic Chemistry and Physical Chemistry, Faculty of Chemistry and Pharmaceutical Sciences, University of Chile, Santiago 8380544, Chile*

(Received 27 April, revised 1 August, accepted 18 August 2022)

Abstract: Human leukotriene A_4 hydrolase enzyme (LTA_4H) catalyses the biotransformation of the inactive precursor leukotriene A_4 (LTA_4) to the bioactive Leukotriene B_4 (LTB_4), which causes many inflammatory responses in the human body. Therefore, the selective inhibition of this enzyme becomes a useful strategy for the treatment of several illnesses such as asthma, allergic rhinitis, cardiovascular diseases, and cancer. Herein we report a 3D-QSAR/ /CoMFA and CoMSIA study on a series of 47 benzimidazoles, benzoxazoles, benzothiazoles and thiazolopyridines reported as potent LTA_4H inhibitors. Good statistical parameters were obtained for the best model (q^2 = 0.568, r^2_{ncv} = 0.891 and r^2_{test} = 0.851). A new series of 10 compounds capable of inhibiting leukotriene A_4 hydrolase with high potency was presented. All designed inhibitors showed low IC_{50} in nano- and sub-nanomolar ranges, when they were evaluated in 3D-QSAR models. Subsequently, the designed molecules, as well as the least and most active compounds were subjected to docking and molecular dynamics studies into LTA_4H. In conclusion, we summarised a thorough structure–activity relationship (SAR) of LTA_4H inhibitors of

* Corresponding authors. E-mail: (*)jaime.mella@uv.cl; (**)javier.romero@ciq.uchile.cl
https://doi.org/10.2298/JSC220427068L

heterocyclic structure. These models can be used for the rational proposal of new inhibitors.

Keywords: CoMFA; CoMSIA; binding free energy calculation; CADD; inflamemation; allergy.

INTRODUCTION

Leukotrienes (LTs) are lipid mediators synthesised primarily in leukocytes (mast cells, eosinophils, basophils, macrophages and so on).[1] The imbalance in the biosynthesis or metabolism of LTs is associated with inflammatory processes, asthma, cardiovascular diseases, chronic obstructive pulmonary disease (COPD), and cancer.[2] LTA_4 is the common inactive precursor that produces the bioactive leukotrienes by Human LTA_4 Hydrolase enzyme (LTA_4H). Given the importance of LTA_4H, obtaining novel and potent LTA_4H inhibitors is useful to treat various inflammatory diseases. Nowadays there is only a few drugs with the ability to modulate the leukotriene system, such as zileuton, zafirlukast and montelukast.[3]

Currently a number of LTA_4H inhibitors with several chemotypes different than heterocycles have been described, Kelatorphan is an example of these[4] (Fig. 1). Other relevant compounds are JNJ-26993135 and the thiazolopyridine JNJ--40929-837 developed by Johnson & Johnson Pharmaceutical Research (Fig. 1).[5,6]

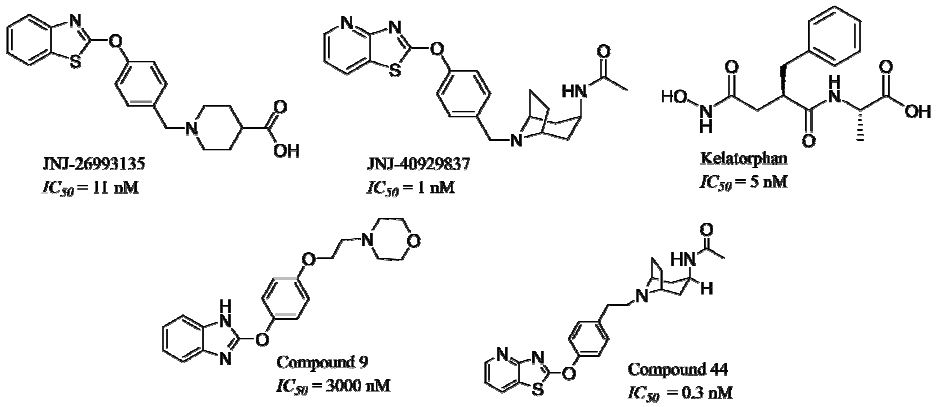

Fig. 1. Leukotriene A_4 hydrolase inhibitors. Kelatorphan represents a different class of non-heterocyclic inhibitor (*N*-hydroxyamide), whereas JNJ-26993135 and JNJ-40929837 are heterocyclic inhibitors developed by Johnson & Johnson Pharmaceutical Research. The least (**9**) and most active (**44**) compounds of the study are also displayed.

Pontiki *et al.* have reviewed some QSAR works on 5-LO inhibitors.[7] Bernstein[8] performed a QSAR of different antagonists of the cysteinyl leukotriene receptors (cysLT). Likewise, Sonawane *et al.*[9] built a QSAR of a series of phenylmethylphenoxypropylamino propanoic acid derivatives, and Sundarapandian *et*

al.[10] published a QSAR study of 142 compounds with substantial chemical diversity. Nevertheless, in none of them were applied a three-dimensional quantitative structure–activity relationship (3D-QSAR), comparative molecular field analysis (CoMFA) and comparative molecular similarity index analysis (CoMSIA) models. Accordingly, to date, no 3D-QSAR reports of any specific heterocyclic LTA_4H inhibitors are available.

In this study, we have compiled a series of 47 reported benzimidazoles, benzoxazoles, benzothiazoles and thiazolopyridines developed by Johnson & Johnson Pharmaceutical Research.[5,11,12] We performed a robust statistical 3D-QSAR of these large series of heterocyclic compounds to obtain a rational design and synthesis of promising new molecules through a CoMFA and CoMSIA. Later, we proposed a design of 10 new molecules as LTA_4H inhibitors (**1x**–**10x**). Furthermore, these 10 proposed compounds in conjunction with the most and least active inhibitors of the series (the compounds **9** and **44**) were subjected to docking and molecular dynamics assays over the human LTA_4H (PDBID:3FTS),[13] finding the agreement between 3D-QSAR and docking studies. All proposed designed compounds showed good inhibitory activities in a low and sub nanomolar range.

EXPERIMENTAL

Data selection and LTA_4H inhibitory activity

CoMFA and CoMSIA studies were performed on a set of 47 different heterocycles reported by Johnson & Johnson Pharmaceutical Research[5,11,12] (Table S-I, Supplementary material to this paper). Compounds were randomly divided into training and test sets. The distribution of pIC_{50} values for the complete set are shown in Fig. S-1 (Supplementary material). In all cases, the biological activity followed a Gaussian distribution where most compounds lie in the pIC_{50} range between 5.5 and 9.5.

CoMFA and CoMSIA calculations

CoMFA and CoMSIA studies were performed with Sybyl X-1.2 software. To derive the CoMFA and CoMSIA descriptor fields, the aligned molecules (Fig. S-2, Supplementary material) were subjected to the standard protocol, as it has been previously published by our research group.[14] PLS analysis was used to construct a linear correlation between the CoMFA and CoMSIA descriptors (independent variables) and the activity values (dependent variables). To select the best model, the cross-validation analysis was performed using the leave-one-out (LOO) method. Furthermore, the external predictive power of the developed 3D-QSAR models using the test set was examined by considering r^2_{test} and r^2_m. To confirm that the results are not obtained by a chance correlation, the Y-random test was carried out. Finally, the applicability domain (AD) was evaluated based on the simple standardisation method reported by Roy *et al.*[15]

Docking and molecular dynamics calculations

The molecular docking was performed according to the standard protocols as it is reported by our group using the leukotriene A_4 hydrolase PDBID:3FTS[14] in Autodock 4.2. The zinc atom was designated as the centre of the grid. The volumes chosen for the grid maps

were made up of 60×60×60 points, with a grid-point spacing of 0.0375 nm. The results were visualised in Visual molecular dynamics program (VMD).

Molecular dynamics simulation was performed with Gromacs 2020.4 version (Groningen machine for chemical simulations) to examine the leukotriene A_4 hydrolase – compound **7x**, **9x** and **10x** complexes stability. The molecular dynamics system input files were created following the same standard protocol reported by our group. Graphs were generated with GraphPad Prism. The binding free energy calculation by molecular mechanics Poisson–Boltzmann surface area (MM-PBSA) was performed between 80 and 100 ns using RashmiKumari's g_mmpbsa packages.[16] The average binding free energy was calculated using the "MmPbSaStat" Python script provided in "g_mmpbsa".

RESULTS AND DISCUSSION

Contour maps analysis and docking results

For the description and analysis of the CoMFA and CoMSIA contour maps, the least and the most active compounds of the series were used as a template (**9** and **44**, respectively). Both molecules are shown in Figs. 2 and 3 surrounded by different coloured polyhedrons, which represent the electrostatic, steric, hydrophobic, and hydrogen-bond donor–acceptor fields. The main interactions found in the docking studies are discussed along this section.

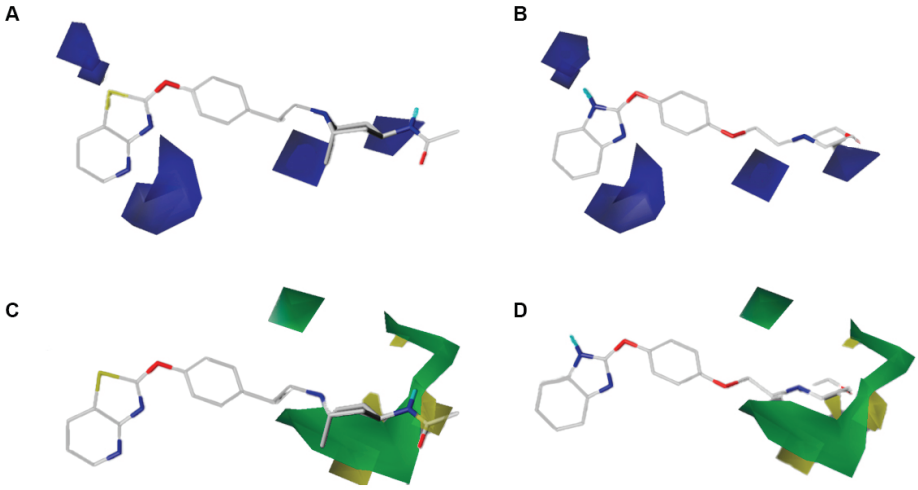

Fig. 2. CoMFA electrostatic (A and B) and steric (C and D) contour maps around compounds **44** (A and C) and **9** (B and D), the most active and less active of the series, respectively.

CoMFA electrostatic and steric contour maps

The electrostatic contour map shows two blue polyhedrons far from position 1, 3, and 4 of each heterocyclic cores of the compounds **9** and **44** (Fig. 2A and B). The incorporation of chains which contain electron-deficient atoms or groups projected toward that zone could favour the inhibitory activity over the enzyme. Even though all LTA_4H inhibitors shown in Table S-I (the compounds **1**–**47**) pos-

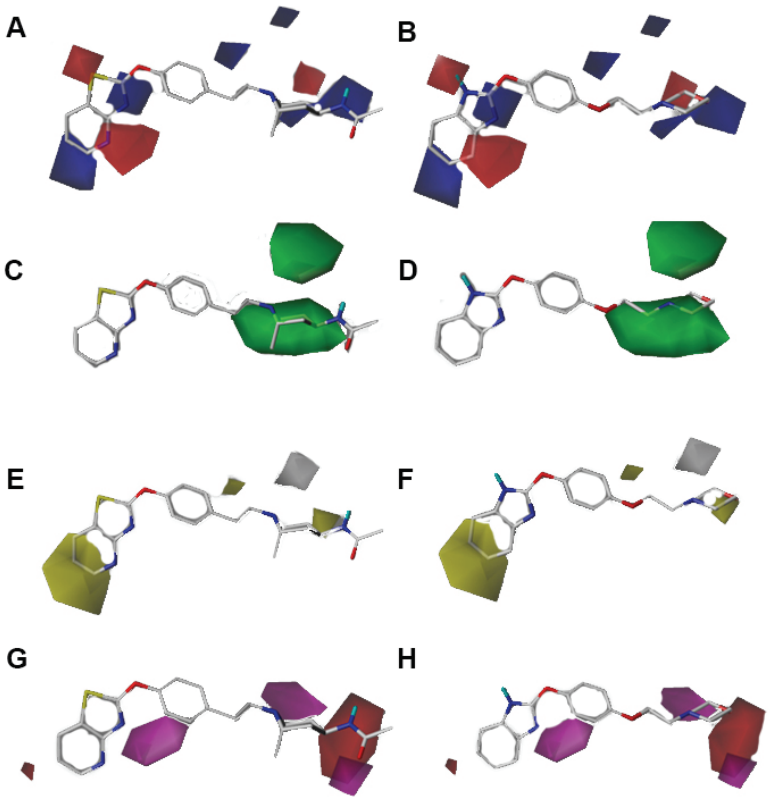

Fig. 3. CoMSIA electrostatic (A and B), steric (C and D), hydrophobic (E and F) and acceptor (G and H) contour maps around compounds **44** (A, C, E and G) and **9** (B, D, F and H), the most active and less active of the series, respectively.

sess electronegative atoms, such as sulphur, nitrogen or oxygen in their aromatic heterocyclic moieties, these are incapable of reaching contact with the blue polyhedrons mentioned above. In fact, the evidence demonstrates that these heteroatoms grant good inhibitory activities in all compounds. Considering this information, sulphur and nitrogen atoms were incorporated at positions 1 and 3, respectively, of all thiazolopyridine rings in the proposed compounds **1x**–**10x** (see Fig. 4). Furthermore, the latter were corroborated by our docking studies, where a hydrogen bond interaction can be seen between the hydroxyl group of Tyr378 and the sp^2 nitrogen atom at position 3 of the compounds **9**, **44**, **1x** and **3x**–**6x**, (Fig. S-3, Supplementary material). It should be noted that the hydrogen bond interaction described with Tyr378 can be confirmed at the hydrogen bond acceptor contour map of the CoMSIA model (see below). The compounds **2x**, **7x** and **8x** did not show this hydrogen bond interaction due to their heterocyclic thiazolopyridine rings being inverted into the catalytic site of the LTA_4H (Fig. S-3, Supplementary material).

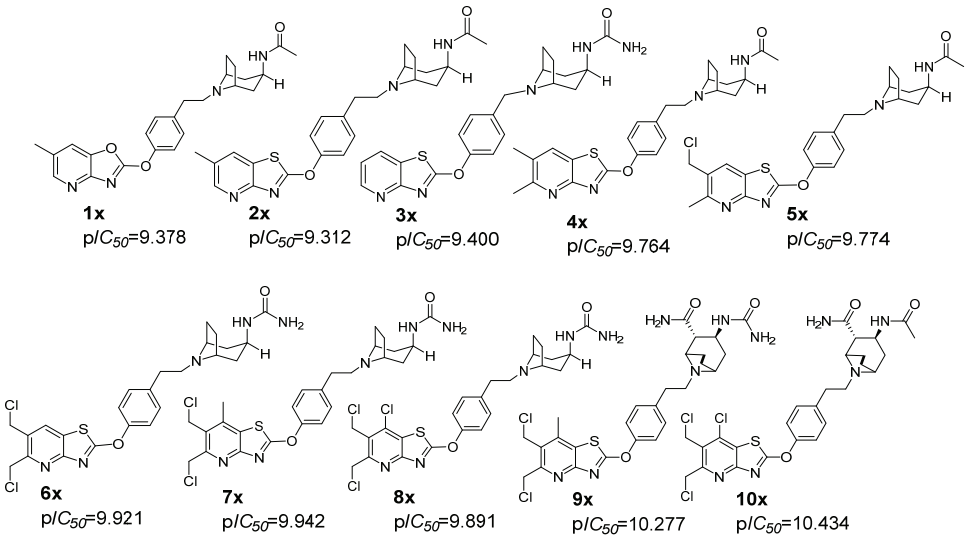

Fig. 4. Proposed structures of new molecules and their predicted pIC_{50} values.

A blue polyhedron can be seen intersecting the nitrogen atom in the amide group of the most active compound **44** (Fig. 2A) indicating that the amide function, and especially the hydrogen atom, would be favourable. This is corroborated by the high inhibitory activity that the compound **47** shows, with a pIC_{50} = = 9.000. The proposed designed structures **1x**–**10x** of Fig. 4 bear amide or urea groups, which is in line with these results. In addition, docking studies revealed that the structures **44** and **1x**–**9x** (except **10x**) showed a hydrogen bond interaction between the amides or urea groups and the carboxylate of amino acid Glu384, suggesting that they are the important functions for the inhibition of LTA_4H.

On the other hand, the less active compound **9** (Fig. 2B) shows its oxygen atom of the aliphatic morpholine ring projected towards the polyhedron, which would explain the lower inhibitory activity of this derivative. Docking assays have shown a hydrogen bond interaction between the oxygen of the morpholine ring and the Lys565 residue of the enzyme. However, this bond would not be enough to grant a good biological activity. In fact, those derivatives that have shown that the lowest inhibitory profiles, such as the compound **8** (pIC_{50} = = 6.456) bear an electron-rich oxygen group projected towards this blue polyhedron. This data was considered for the proposal of the designed compounds, establishing a functional amide or urea group in the vicinity of the blue polyhedron, which achieves an interaction with Glu384 of the catalytic site of LTA_4H.

The steric contour map (Figs. 2C and D) shows a large green polyhedron surrounding the cycloalkyl portions of the compounds **9** and **44**, meaning that

large rings or bulky groups at this part of the molecules would be beneficial for biological activity. As can be seen from Table S-I, the most active compounds, **44** and **47,** have a bulky azabicyclooctane ring in their structures, whereas the least active compounds (**9**, **34** and **35**) have less bulky rings, such as morpholine or piperidine. Considering this, the new molecules proposed **1x**–**10x** (Fig. 4), were designed maintaining the azabicyclooctane ring on their structures. Additionally, particularly in the derivatives **9x** and **10x,** a new amide group was added into the azabicyclooctane with the aim of increasing the volume and performing a hydrogen bond interaction through the oxygen atom of the amide with Lys565 of the enzyme. It is worth mentioning that more distant yellow polyhedrons surrounding the green regions are observed, which suggests a restriction of increasing the volume in this area.

CoMSIA electrostatic, steric, hydrophobic and hydrogen-bond acceptor contour maps

On the electrostatic map (Fig. 3A and B) it can be seen, unlike in the CoMFA in Fig. 2, a red polyhedron intersecting the sulphur and nitrogen atoms (or carbon atom in benzimidazole) at positions 1 and 4 of the thiazolopyridine and benzimidazole rings in the compounds **44** and **9,** respectively. This suggests that the electronegative atoms at those positions could be beneficial for the inhibitory activity. This explains why the most active compounds (**33**, **44** and **47**) exhibit sulphur atoms at position 1 and a nitrogen atom at position 4 in their aromatic heterocyclic cores, whereas the less active compounds (**9** and **15**) exhibit a nitrogen atom at position 1 (NH chemical group) and a carbon atom at position 4. It is noteworthy that thiazolopyridines, in contrast to benzimidazole, benzoxazole and benzothiazole inhibitors, showed the best inhibitory activities, which could be attributed to the nitrogen atom at position 4 of the heterocyclic framework. The latter is the reason why we have not considered the design of benzimidazoles in our proposed structures shown in Fig. 4.

Considering the well predicted pIC_{50} of designed compounds **1x**–**10x**, it could be a consequence of each one of them being thiazolopyridines bearing a nitrogen atom at position 4. In addition, is possible that this pyridine nitrogen atom of the thiazolopyridine ring could be involved, in some derivatives, in carrying out a π–π interaction with the amino acid Tyr383, as was demonstrated by our docking studies for the proposed derivatives **9x** and **10x** (Fig. S-3, Supplementary material), with these compounds having the best predicted pIC_{50} values (10.277 and 10.434, respectively). This could be explained because the Tyr383 residue has a hydroxyl group, which donates its electron density via resonance to the conjugated phenyl system, stimulating the π–π interaction with the pyridine ring of the thiazolopyridines, which have a low electron density in the presence of the nitrogen atom.

Positions 5 and 6 of the aromatic heterocycles of **9** and **44** in the electrostatic contour map (Figs. 3A and 3B)3 show a blue polyhedron nearby, indicating that the electropositive atoms projected to that region could be favourable for the inhibitory activity. For this reason, in the design of the proposed compounds shown in Fig. 4, chloromethylene groups on derivatives **5x**–**10x** were incorporated at those positions, leading to good pIC_{50} values due to the addition of electronegative atoms (chlorine) adjacent to the methylene carbons.

On the other hand, a blue polyhedron, analogous to one observed previously in the CoMFA analysis, surrounded the nitrogen atom of the amide in the compound **44** and the oxygen atom of the morpholine in the compound **9** (Figs. 3A and B, respectively). This emphasises that the presence of urea, amide or similar chemical group in this region could perform an interaction with Glu384 of the catalytic site of the enzyme.

The CoMSIA steric contour map (Figs. 3C and D) shows a similar situation as in the CoMFA analysis. Two green polyhedrons are surrounding the cycloalkyl portions of compounds **9** and **44**, which implies that bulky rings are preferred instead of planar rings or low bulky groups (see also the CoMFA steric contour map in Figs. 2C and D).

As can be seen in Figs. 3E and F, the hydrophobic contour map displays yellow polyhedral surfaces intersecting positions 5, 6 and 7 of the benzimidazole and thiazolopyridine rings in compounds **9** and **44**. The latter means that the increasing lipophilicity on those positions of the heterocyclic rings would be beneficial for the inhibitory activity. Therefore, this suggests that the insertion of methyl, halogen or alkyl-halogen groups could be a good strategy to increase the inhibitory activity over LTA_4H. Consequently, the proposed compounds **1x**, **2x** and **4x**–**10x** were designed while considering the functional groups mentioned above; thus, they bear those groups on their structures and show good predicted pIC_{50} values.

Furthermore, a small yellow polyhedron laying close to the oxygen atom of morpholine ring in compound **9** can be seen in Fig. 3F. This result means that the presence of polar hydrophilic atoms at that position would be detrimental for the inhibitory activity, which would explain some of the reasons for the reduced ability to inhibit the LTA_4H showed by **9** in comparison with the other compounds tested by Johnson & Johnson Pharmaceutical Research.[5,11,12]

On this contour map, magenta and red polyhedral surfaces can be seen (Figs. 3G and H). Magenta polyhedrons indicate that the presence of hydrogen bond acceptor groups is favourable for the biological activity, whereas the red polyhedrons indicate that hydrogen bond acceptor groups is unfavourable. A magenta polyhedron is nearby to the nitrogen atom at position 3 of the benzimidazole and thiazolopyridine rings in the compounds **9** and **44**, respectively (Figs. 3G and H), suggesting that an unprotonated nitrogen atom on that position would be appro-

priate. This would explain the low inhibitory activity showed by the benzimidazole derivatives such as **3**, **6**, **9** or **15**. The benzimidazole ring shows a tautomerism phenomenon between the nitrogen atoms at positions 1 and 3 of the heterocyclic system; therefore, the hydrogen atom, which is initially on the nitrogen 1, is constantly moving between both heteroatoms at positions 1 and 3 in the benzimidazole core. For this reason, we have dismissed the presence of the benzimidazole framework from the design of the novel derivatives **1x**–**10x** (Fig. 4), proposing only thiazolopyridine derivatives, which bear a sp^2 nitrogen atom at position 3, and show low basicity properties. as they remained unprotonated at physiological conditions. In addition, as we already have analysed for the CoMFA-electrostatic contour maps (see above), and considering the obtained results from docking assays, the magenta polyhedron nearby to the nitrogen atom at position 3 of the heterocycles agrees with the hydrogen bond interaction showed between the hydroxyl group of Tyr378 and this nitrogen atom at position 3. This corroborates the correlation between our 3D-QSAR models, and the docking experiments performed.

Another magenta polyhedron can be seen close to the azabicyclooctane ring of the compound **44** and to the morpholine scaffold of the compound **9** (Figs. 3G and H), suggesting that the insertion of hydrogen bond acceptor groups on this core could be favourable for biological activity. Taking this into account, the compounds **9x** and **10x** in Fig. 4 were designed bearing an extra amide group in the azabicyclooctane framework, resulting in being the most active compounds with the highest predicted pIC_{50} values of 10.277 and 10.434, respectively) when they were evaluated in the 3D-QSAR models. As was already mentioned above at the CoMFA-steric contour map, the amide groups in **9x** and **10x** perform hydrogen bond interactions through the carbonyl oxygen of the amides and the protonated amine of Lys565 (NH_3^+), supporting the favourability of hydrogen bond acceptors groups at this area.

Finally, there is a magenta polyhedral surface adjacent to the carbonyl oxygen atom of the amide group at the position 4 of the azabicyclooctane ring in the compound **44** (Fig. 3G). This suggests that a carbonyl group is highly favourable for the enzymatic inhibitory activity. Furthermore, there is also a red polyhedron near the nitrogen atom of the amide group in the derivative **44**. Likewise, the same polyhedron is represented close to the oxygen atom of the morpholine group in the compound **9** (Fig. 3H). Therefore, the presence of a hydrogen bond acceptor on that area should be avoided, whereas a hydrogen donor chemical function would be favourable. The latter agrees with our docking results achieved for the compounds **44** and **1x**–**9x,** which interact through the amide group by a hydrogen bond relation with the carboxylate function of Glu384 into the catalytic site of the enzyme.

Design of novel derivatives and molecular dynamics

Based on the information provided by the CoMFA and CoMSIA models, we have designed a series of compounds as leukotriene A_4 hydrolase inhibitors. Fig. 4 shows the proposed compounds with their predicted pIC_{50} values. The designed compounds **1x**–**8x** showed IC_{50} values in the nanomolar range, whereas the compounds **9x** and **10x** showed sub-nanomolar ranges in their IC_{50} values of the ability to inhibit LTA_4H. The compounds **1x**–**3x** had pIC_{50} values like the most active compound (compound **44**, Table S-I). Nonetheless, the compounds **4x**–**10x** exhibited better pIC_{50} values, and therefore, promising inhibitory activities over the enzyme. The best inhibitory profiles for the designed compounds **1x**–**10x** were obtained considering the following structural criteria: 1) incorporation of an aromatic thiazolopyridine or oxazolpyridine rings; 2) insertion of electropositive groups (chlorine contiguous to the methylene carbons) at positions 5 and 6 of the heterocycles (oxazolpyridine or thiazolopyridine) with the ability to increase the lipophilicity of this scaffold; 3) maintenance of the phenyl framework in order to obtain a certain distance between the thiazolopyridine and the bulky azabicyclooctane ring; 4) azabicyclooctane rings possessing at least one polar hydrogen bond acceptor chemical group, such as an amide or urea.

Then, we carried out a docking and molecular dynamics study of compounds **7x**, **9x** and **10x**. These derivatives had the highest predicted pIC_{50} values (9.942, 10.277 and 10.434, respectively). To examine the changes in the protein–inhibitor system, RMSD and RMSF trajectory analyzes were performed based on the backbone atoms. In protein–inhibitor complex MD simulations, *RMSD* measurements allow us to comment on the stability and the changes of protein and ligand. The strong interaction of the inhibitor with the enzyme makes the protein more stable. As seen in Fig. S-4A (Supplementary material), after 15 ns the system stabilized and continued with constant small shifts. Average *RMSD* values of 0.3, 0.24 and 0.19 nm were measured for LTA_4H–**7x**, LTA_4H–**9x** and LTA_4H–**10x** protein–ligand complexes, respectively. According to this result, the compound **10x** made the target LTA_4H enzyme more stable. *RMSF* corresponds to another analysis parameter that provides information about fluctuations and conformational changes of the protein–inhibitor complex. Residues with a high *RMSF* value indicate that they are more mobile, while those with a low *RMSF* value indicate that they are more stable. As seen in Fig. S-4B, the compound **9x** moved away from amino acids 290-310, its fluctuation in this region was higher than **7x** and **10x**. Therefore, the derivative **10x** was more stable interacting with the amino acids of the active site. The compound **10x** establishes a H bond with Tyr378.

The inhibitor binding modes and protein-inhibitor interaction diagrams of **7x**, **9x** and **10x** at the end of 100 ns are shown in Fig. 5, each one of them representing the change of the ligand at the catalytic site during the MD simulation process. Through its hydrogen atoms the amide group of the compound **7x** per-

forms two hydrogen bond interactions with Met270 and Gln143, respectively. On the other hand, Fig. 5 demonstrates that the compound **9x** carry out two hydrogen bond interactions between the oxygen atoms of both carbonyl functions of the amide groups at the azabicyclic moiety with Arg563, as well as an extra hydrogen bond interaction through the hydrogen atom between one of its amides with Pro266. Finally, the compound **10x** showed the ability to form a hydrogen bond interaction with Tyr378 and the amide function that bears in its structure. Although there were some changes according to the binding poses obtained from molecular docking, the compounds **7x**, **9x** and **10x** continued to interact with the LTA_4H catalytic site.

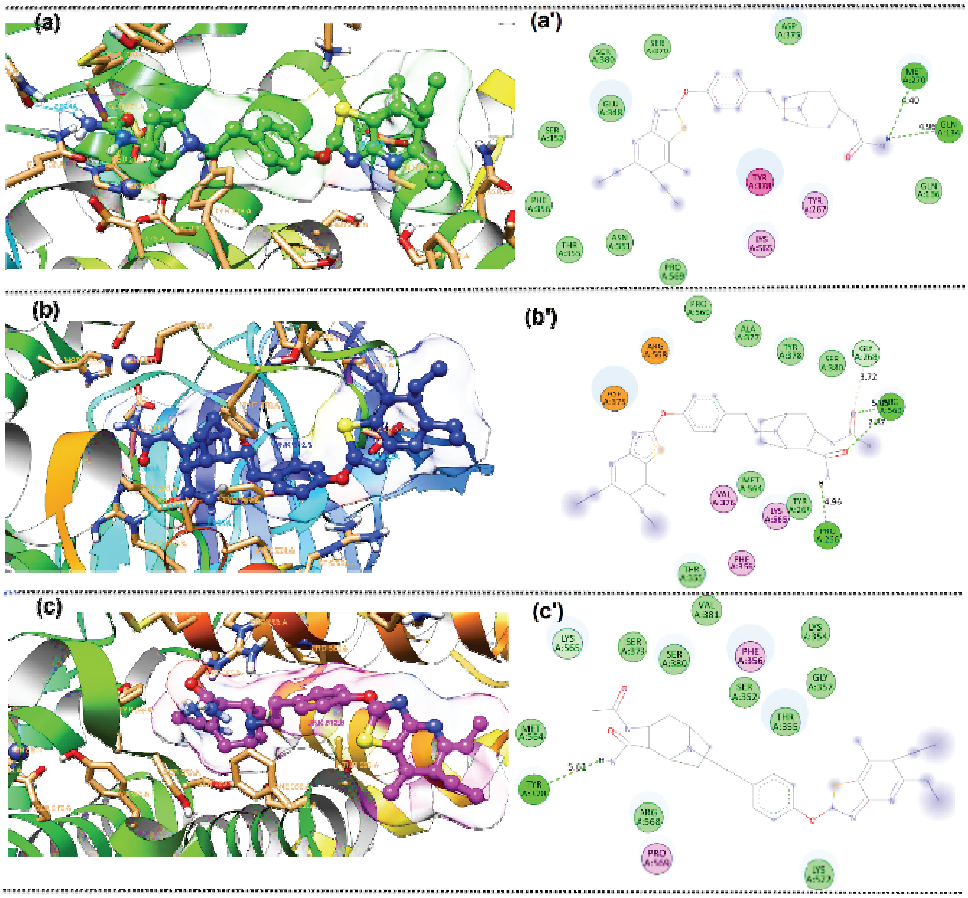

Fig. 5. Binding pose and protein-inhibitor schematic interactions of compound **7x** (a and a'), **9x** (b and b') and **10x** (c and c') in the LTA_4H catalytic site after 100 ns of molecular dynamics simulations.

Another important way to evaluate the protein–ligand interaction strength is by measuring the theoretical binding free energy. The latter parameter is obtained from the energy of the protein–inhibitor complex by subtracting the energies of the protein and ligand in single state, and the sum of the energies of van der Waals, electrostatic, polar solvation and solvent accessible surface area (*SASA*). As shown in Table I, the compounds **7x**, **9x** and **10x** gave mean BFE values of –205.40, –252.51 and –281.24 kJ/mol, respectively. In parallel with the *RMSD* and *RMSF* measurements, the compound **10x** showed the strongest interactions with the enzyme, corroborating its great potential as a LTA_4H inhibitor.

TABLE I. Results of MM-PBSA binding free energies (kJ/mol) between leukotriene A_4 hydrolase (LTA_4H) with compounds **7x**, **9x** and **10x**

Parameter	Complex		
	LTA_4H–**7x**	LTA_4H–**9x**	LTA_4H–**10x**
van der Waals	–121.43	–137.49	–174.21
Electrostatic	–542.03	–702.96	–235.00
Polar solvation	480.11	608.91	147.84
SASA	–22.06	–20.97	–19.86
Theoretical binding free energy	–205.40	–252.51	–281.24

Finally, considering the CoMFA, CoMSIA, docking studies and molecular dynamics simulation, we have summarised the structure–activity relationship in Fig. 6.

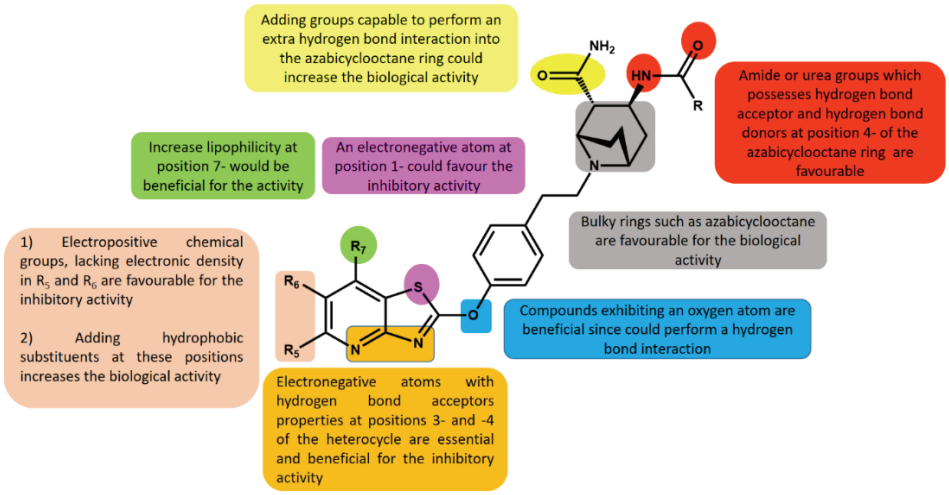

Fig. 6. Main structure–activity relationship found in this study. Substitution patterns were aimed to enhance the inhibitory activity over the human leukotriene A_4 hydrolase (LTA_4H).

CONCLUSION

Herein, we presented the construction of two QSAR models based on reported benzimidazole, benzoxazoles, benzothiazole and thiazolopyridine leukotriene A_4 hydrolase inhibitors (LTA_4H inhibitors). The models were externally validated. The best models presented q^2 values greater than 0.5. However, the CoMSIA model turned out to be superior, since it did not present outliers and exhibited a better external predictability coefficient (r^2_{test} = 0.851). Both models showed steric, electrostatic, hydrophobic and H-bond acceptor equilibria in the biological activity contribution. Using the information from the QSAR models, a new series of compounds were designed and presented (**1x**–**10x**). The predicted biological inhibitory activities for these new derivatives were high, exhibiting low IC_{50} in the nano- and sub-nanomolar ranges. Furthermore, the least active compound (**9**) and the most active compound (**44**), used to build the QSAR models, as well as **1x**-**10x** were subjected to docking assays with the human LTA_4H. In addition, the molecular dynamics simulations were carried out for the best compounds **7x**, **9x** and **10x**. The compound **10x** presented the best values of pIC_{50} (10.424), and the best binding profile according to the molecular dynamics and binding free energy calculations (-281.24 kJ/mol). Therefore, this compound represents an interesting lead compound for the development of new LTA_4H inhibitors.

SUPPLEMENTARY MATERIAL

Additional data and information are available electronically at the pages of journal website: https://www.shd-pub.org.rs/index.php/JSCS/article/view/11812, or from the corresponding author on request.

Acknowledgements. This work was financially supported by Conicyt/Fondecyt projects: Fondecyt de Iniciación en Investigación N° 11190145, Fondecyt grant 11130701; M.L thanks Beca Conicyt-PFCHA/Doctorado Nacional/2018-21180427; JRP acknowledge MRPF, GERR, GARP and CCRP. M.M. thanks to Fondecyt postdoctorado 2018 N° 3180408. All MD simulations presented here were carried out using resources provided by TÜBTAK (Turkish Scientific and Technological Research Council), ULAKBIM (Turkish Academic Network and Information Center) and TRUBA (High Performance and Grid Computing Center).

ИЗВОД

ДИЗАЈНИРАЊЕ БЕНЗИМИДАЗОЛА, БЕНЗОКСАЗОЛА, БЕНЗОТИАЗОЛА И ТИАЗОЛОПИРИДИНА КАО ИНХИБИТОРА ЛЕУКОТРИЕН A_4 ХИДРОЛАЗЕ, ПУТЕМ 3D-QSAR ДОКИНГА И МОЛЕКУЛСКЕ ДИНАМИКЕ

MARCOS LORCA[1], MARIO FAÚNDEZ[2], C. DAVID PESSOA-MAHANA[2], GONZALO RECABARREN-GAJARDO[2,3], BENJAMIN DIETHELM-VARELA[2], DANIELA MILLÁN[4], ISMAIL CELIK[5], MARCO MELLADO[6], ILEANA ARAQUE[1], JAIME MELLA[1,7] и JAVIER ROMERO-PARRA[8]

[1]Institute of Chemistry and Biochemistry, Faculty of Science, University of Valparaíso, Valpa¬ra¬íso 2360102, Chile, [2]Faculty of Chemistry and Pharmacy, Pontifical Catholic University of Chile, Santiago 7820436, Chile, [3]Interdisciplinary Center for Neurosciences, Pontifical Catholic Uni¬versity of Chile, Santiago 8330024, Chile, [4]Integrative Center for Biology and Applied Che¬mi¬stry, Bernardo O'Higgins University, Santiago 8370854, Chile, [5]Department of Pharma¬ceu¬ti¬cal Chemistry, Faculty of Pharmacy, Erciyes University, Kayseri 38039, Turkey, [6]Instituto de Inves¬tigación y Postgrado, Facultad de Ciencias de la Salud, Universidad Central de Chile, Santiago 8330507, Chile, [7]Chilean Pharmacopeia Research Center, University of Valparaíso, Valparaíso 2360134, Chile and [8]Department of Organic Chemistry u [8]Physical Chemistry, Faculty of Chemistry and Pharmaceutical Sciences, University of Chile, Santiago 8380544, Chile

Хумани ензим леукотриен A_4 хидролаза (LTA_4H) катализује биотрансформацију инактивног прекурсора леукотриена A_4 (LTA_4) у биоактивни леукотриен B4 (LTB_4), који изазива многе упалне одговоре у људском телу. Зато је селективна инхибиција овог ензима постале корисна стратегија за лечење разних болести као што су астма, алергијски ринитис, кардиоваскуларне болести и канцер. Овде приказујемо 3D-QSAR/ /CoMFA и CoMSIA студију на серији од 47 бензимидазола, бензоксазола, бензотиазола и тиазолопиридина за које се зна да су моћни LTA_4H инхибитори. Добијени су добри статистички параметри за најбољи модел (q^2 = 0,568, r^2_{ncv} = 0,891 и r^2_{test} = 0,851). Предложена је нова серија од 10 једињења која великом снагом могу да инхибирају леукотриен A_4 хидролазу. Сви дизајнирани инхибитори показују ниску IC_{50} у нано и субнаномоларним областима, када су оцењивани са 3D-QSAR моделима. Након тога, дизајнирани молекули, као и најмање и највише активна једињења су подвргнута студијама докинга и молекулске механике са LTA_4H. У закључку смо сажели темељиту релацију структуре и активности (SAR) за LTA_4H инхибиторе хетероцикличне структуре. Ови модели се могу искористити за рационално предлагање нових инхибитора.

(Примљено.27. априла, ревидирано 1. августа, прихваћено 18. августа 2022)

REFERENCES

1. J. Z. Haeggström, A. Rinaldo-Matthis, C. E. Wheelock, A. Wetterholm, *Biochem. Biophys. Res. Commun.* **396** (2010) 135 (https://doi.org/10.1016/j.bbrc.2010.03.140)
2. R. J. Snelgrove, *Thorax* **66** (2011) 550 (https://doi.org/10.1136/thoraxjnl-2011-200234)
3. N. Gueli, W. Verrusio, A. Linguanti, W. De Santis, N. Canitano, F. Ippoliti, V. Marigliano, M. Cacciafesta, *Arch. Gerontol. Geriatr.* **52** (2011) e36 (https://doi.org/10.1016/j.archger.2010.04.014)
4. T. D. Penning, L. J. Askonas, S. W. Djuric, R. A. Haack, S. S. Yu, M. L. Michener, G. G. Krivi, E. Y. Pyla, *Bioorg. Med. Chem. Lett.* **5** (1995) 2517 (https://doi.org/10.1016/0960-894X(95)00441-U)
5. N. L. Rao, P. J. Dunford, X. Xue, X. Jiang, K. A. Lundeen, F. Coles, J. P. Riley, K. N. Williams, C. A. Grice, J. P. Edwards, *J. Pharmacol. Exp. Ther.* **321** (2007) 1154 (https://doi.org/10.1124/jpet.106.115436)

6. W. Barchuk, J. Lambert, R. Fuhr, J.Z. Jiang, K. Bertelsen, A. Fourie, X. Liu, P.E. Silkoff, E.S. Barnathan, R. Thurmond, *Pulm. Pharmacol. Ther.* **29** (2014) 15 (https://doi.org/10.1016/j.pupt.2014.06.003)
7. E. Pontiki, D. Hadjipavlou-Litina, *Med. Res. Rev.* **28** (2008) 39 (https://doi.org/10.1002/med.20099)
8. P. R. Bernstein, *Am. J. Respir. Crit. Care. Med.* **157** (1998) S220 (https://doi.org/10.1164/ajrccm.157.6.mar-3)
9. L. V. Sonawane, S. B. Bari, *Acta Pharm. Sin., B* **45** (2010) 615 (http://www.ncbi.nlm.nih.gov/pubmed/20931764)
10. T. Sundarapandian, J. Shalini, S. Minky, A. Venkatesh, W. L. Keun, *Future Med. Chem*. **5** (2013) 27 (https://doi.org/10.4155/fmc.12.184)
11. V. M. Tanis, G. M. Bacani, J. M. Blevitt, C. C. Chrovian, S. Crawford, A. De Leon, A. M. Fourie, L. Gomez, C. A. Grice, K. Herman, *Bioorg. Med. Chem. Lett.* **22** (2012) 7504 (https://doi.org/10.1016/j.bmcl.2012.10.036)
12. C. A. Grice, K. L. Tays, B. M. Savall, J. Wei, C. R. Butler, F. U. Axe, S. D. Bembenek, A. M. Fourie, P. J. Dunford, K. Lundeen, *J. Med. Chem.* **51** (2008) 4150 (https://doi.org/10.1021/jm701575k)
13. D. R. Davies, B. Mamat, O. T. Magnusson, J. Christensen, M. H. Haraldsson, R. Mishra, B. Pease, E. Hansen, J. Singh, D. Zembower, *J. Med. Chem.* **52** (2009) 4694 (https://doi.org/10.1021/jm900259h)
14. M. Lorca, Y. Valdes, H. Chung, J. Romero-Parra, C.D. Pessoa-Mahana, J. Mella, *Int. J. Mol. Sci.* **20** (2019) 2510 (https://doi.org/10.3390/ijms20102510)
15. K. Roy, S. Kar, P. Ambure, *Chemometr. Intell. Lab. Syst.* **145** (2015) 22 (https://doi.org/10.1016/j.chemolab.2015.04.013)
16. R. Kumari, R. Kumar, A. Lynn, *J. Chem. Inf. Model.* **54** (2014) 1951 (https://doi.org/10.1021/ci500020m).

Journal of the Serbian Chemical Society
JSCS@tmf.bg.ac.rs • www.shd.org.rs/JSCS
J. Serb. Chem. Soc. *88* (1) S10–S25 (2023) *Supplementary material*

SUPPLEMENTARY MATERIAL TO

Design of benzimidazoles, benzoxazoles, benzothiazoles and thiazolopyridines as leukotriene A_4 hydrolase inhibitors through 3D-QSAR, docking and molecular dynamics

MARCOS LORCA[1], MARIO FAÚNDEZ[2], C. DAVID PESSOA-MAHANA[2], GONZALO RECABARREN-GAJARDO[2,3], BENJAMIN DIETHELM-VARELA[2], DANIELA MILLÁN[4], ISMAIL CELIK[5], MARCO MELLADO[6], ILEANA ARAQUE[1], JAIME MELLA[1,7]* and JAVIER ROMERO-PARRA[8]**

[1]Institute of Chemistry and Biochemistry, Faculty of Science, University of Valparaíso, Valparaíso 2360102, Chile, [2]Faculty of Chemistry and Pharmacy, Pontifical Catholic University of Chile, Santiago 7820436, Chile, [3]Interdisciplinary Center for Neurosciences, Pontifical Catholic University of Chile, Santiago 8330024, Chile, [4]Integrative Center for Biology and Applied Chemistry, Bernardo O'Higgins University, Santiago 8370854, Chile, [5]Department of Pharmaceutical Chemistry, Faculty of Pharmacy, Erciyes University, Kayseri 38039, Turkey, [6]Instituto de Investigación y Postgrado, Facultad de Ciencias de la Salud, Universidad Central de Chile, Santiago 8330507, Chile, [7]Chilean Pharmacopeia Research Center, University of Valparaíso, Valparaíso 2360134, Chile and [8]Department of Organic Chemistry and Physical Chemistry, Faculty of Chemistry and Pharmaceutical Sciences, University of Chile, Santiago 8380544, Chile

J. Serb. Chem. Soc. *88* (1) (2023) 25–39

Table S-I. Chemical structure and pIC_{50} values of the studied LTA_4H inhibitors

N°	Structure	IC_{50} / nM	pIC_{50}
1	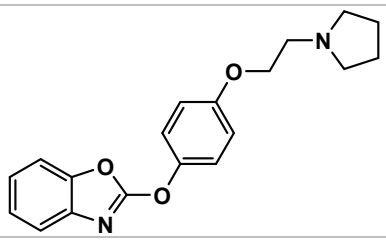	7	8.155

* Corresponding authors. E-mail: (*)jaime.mella@uv.cl; (**)javier.romero@ciq.uchile.cl

N°	Structure	IC_{50} / nM	pIC_{50}
2	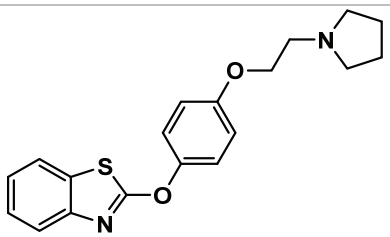	14	7.854
3	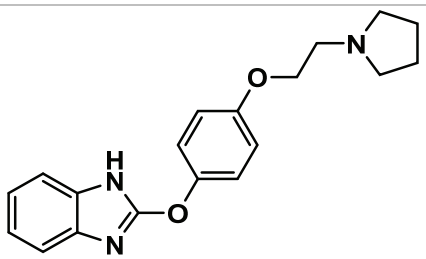	84	7.076
4	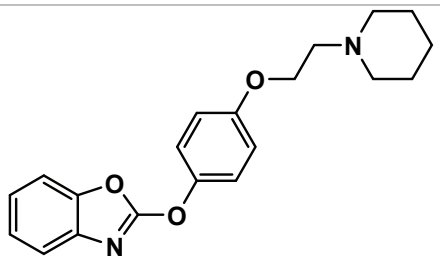	11	7.959
5	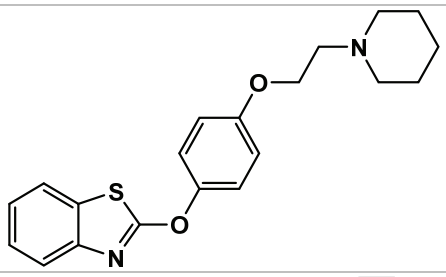	54	7.268
6	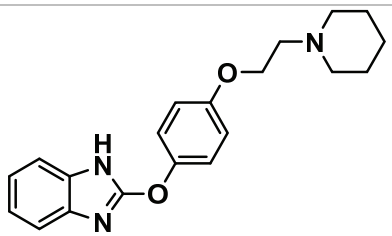	110	6.959

N°	Structure	IC_{50} / nM	pIC_{50}
7	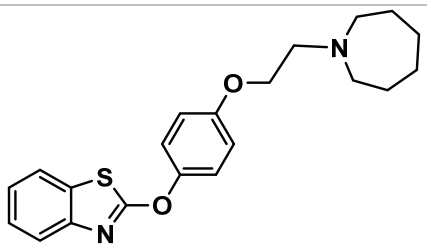	66	7.180
8	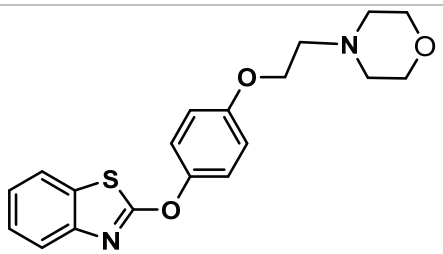	350	6.456
9	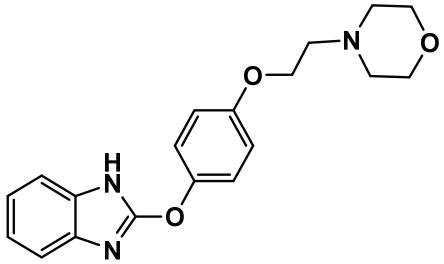	3000	5.523
10	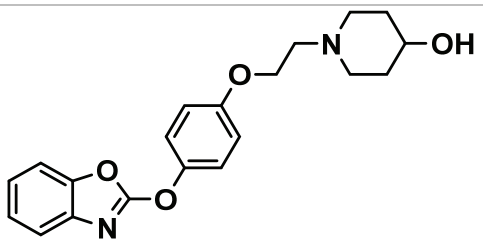	9	8.046
11	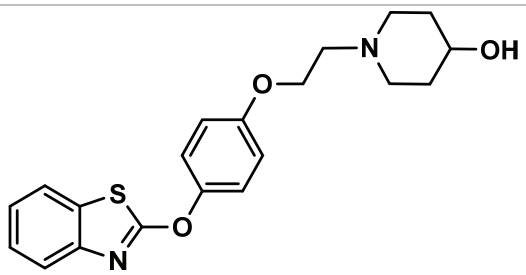	31	7.509

N°	Structure	IC_{50} / nM	pIC_{50}
12	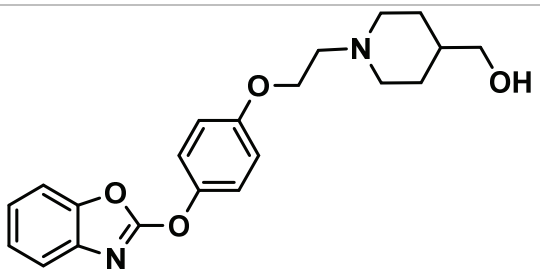	14	7.854
13	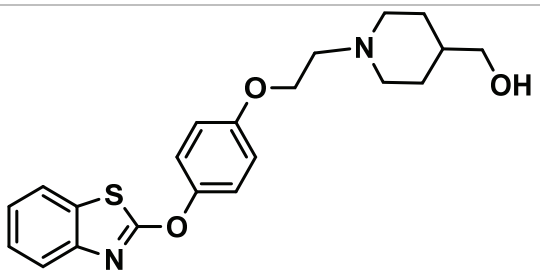	13	7.886
14	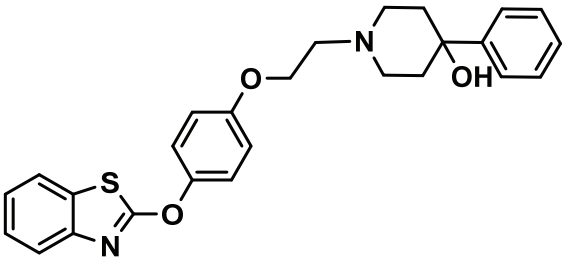	66	7.180
15	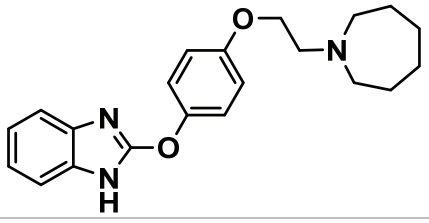	140	6.584
16	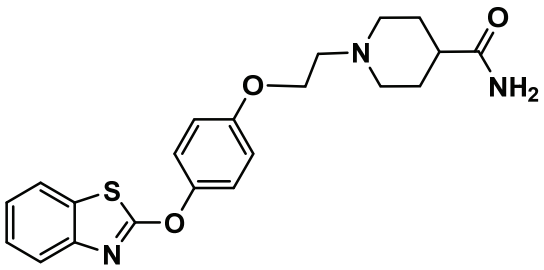	13	7.886

N°	Structure	IC_{50} / nM	pIC_{50}
17	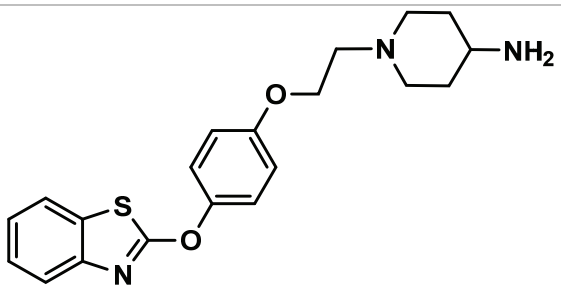	66	7.180
18	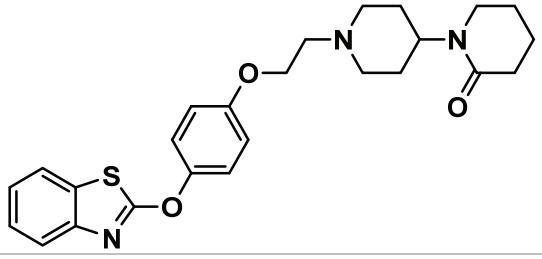	70	7.155
19	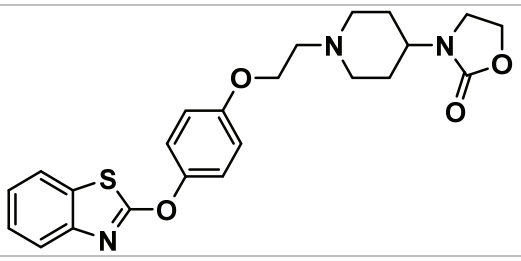	11	7.959
20	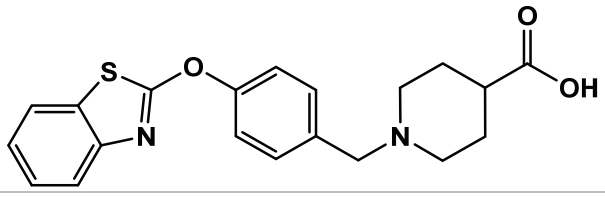	11	7.959
21	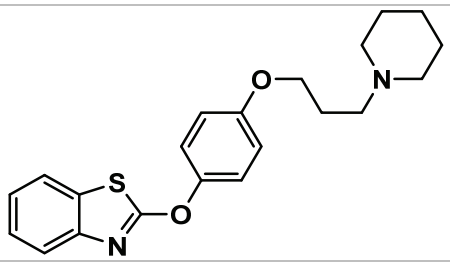	87	7.060

N°	Structure	IC_{50} / nM	pIC_{50}
22	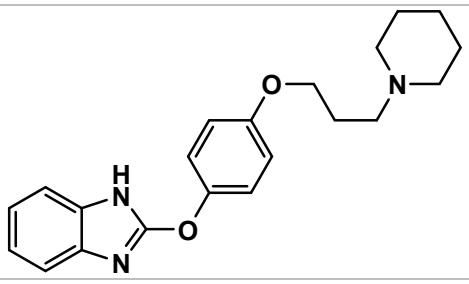	140	6.854
23	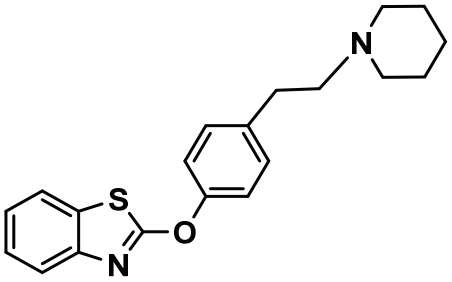	17	7.770
24	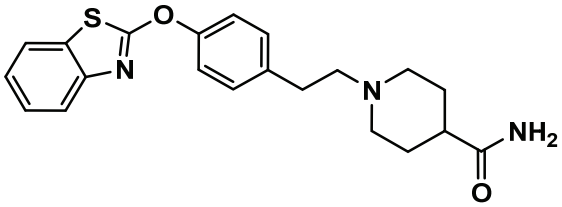	28	7.553
25	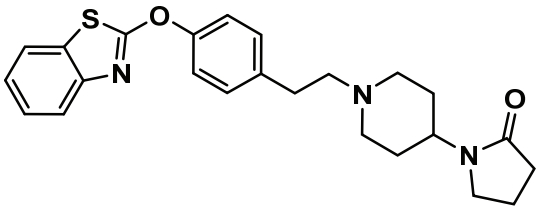	13	7.886
26	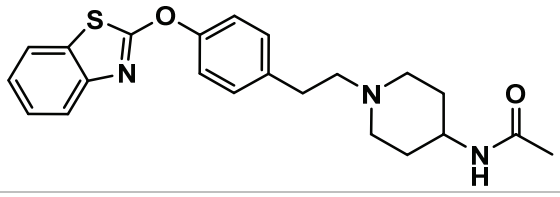	35	7.456

N°	Structure	IC_{50} / nM	pIC_{50}
27	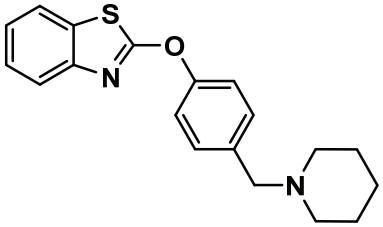	59	7.229
28	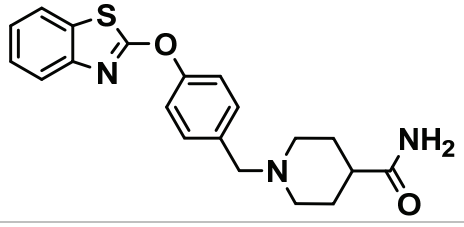	17	7.770
29	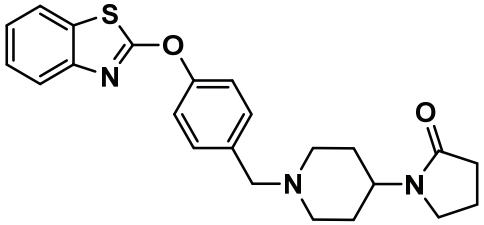	12	7.921
30	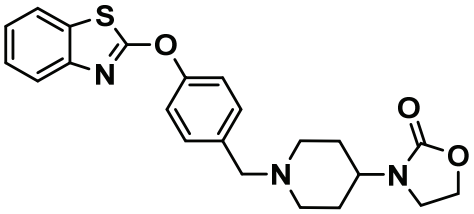	10	8.000
31	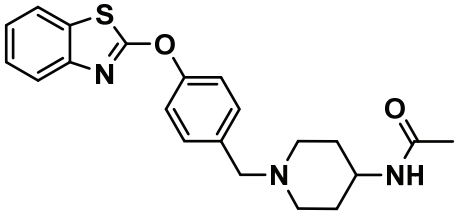	12	7.921
32	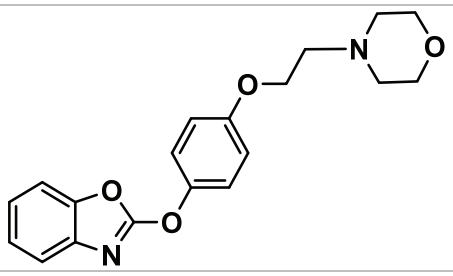	58	7.237

N°	Structure	IC_{50} / nM	pIC_{50}
33	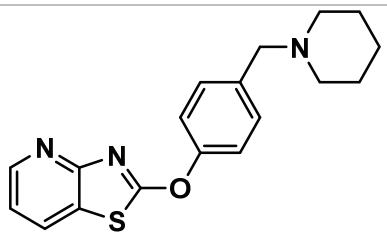	3	8.523
34	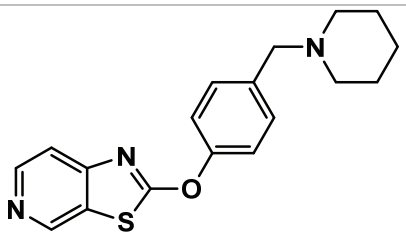	614	6.212
35	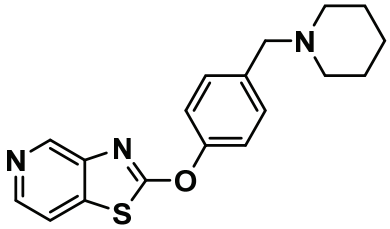	1800	5.745
36	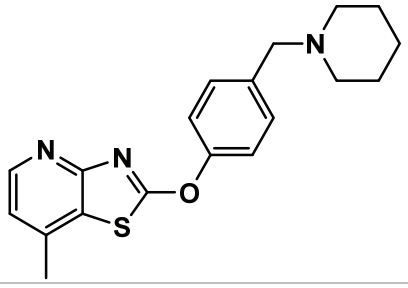	33	7.481
37	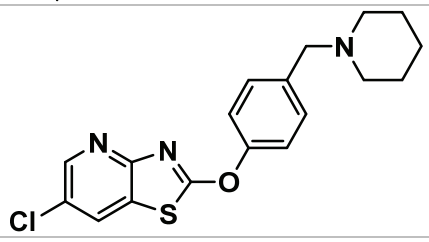	40	7.398

N°	Structure	IC_{50} / nM	pIC_{50}
38	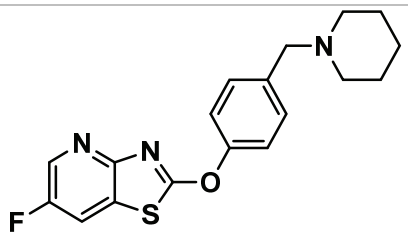	29	7.538
39	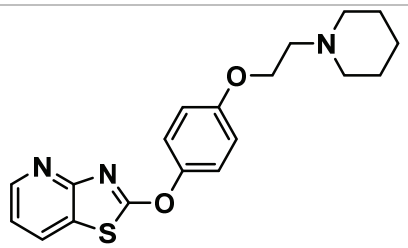	8	8.097
40	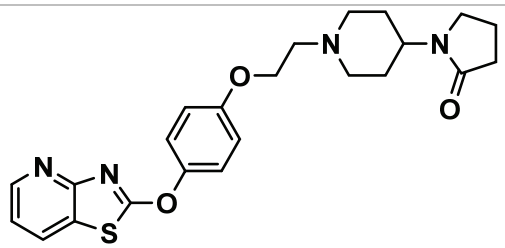	6	8.222
41	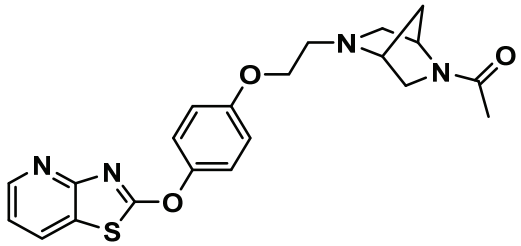	7	8.155
42	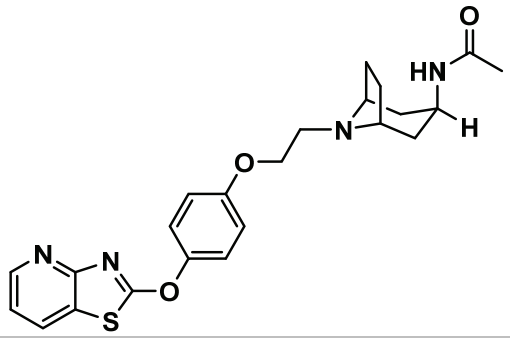	4	8.398

N°	Structure	IC_{50} / nM	pIC_{50}
43	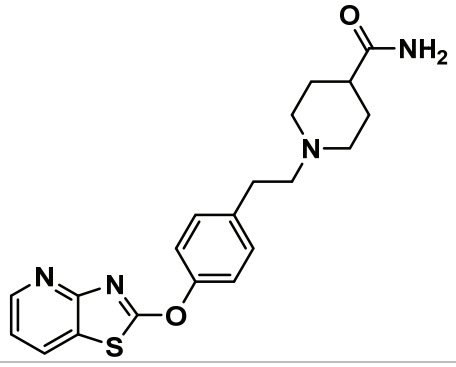	11	7.959
44	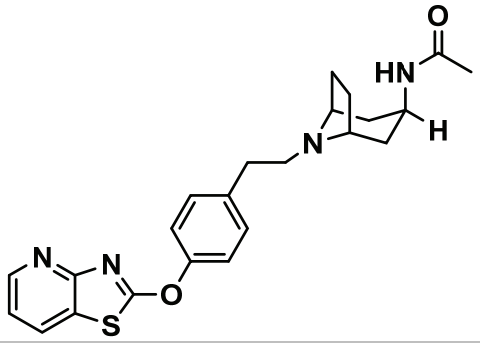	0.3	9.523
45	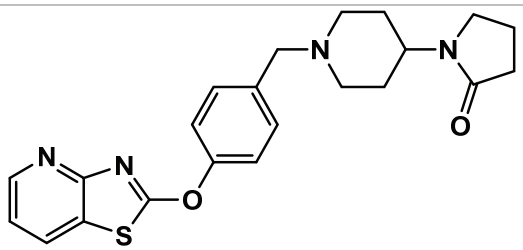	6	8.222
46	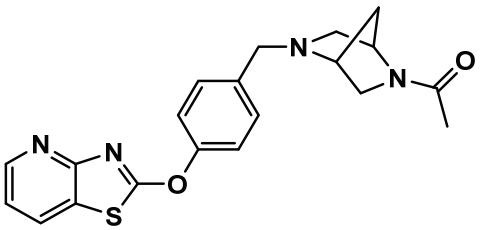	5	8.301

N°	Structure	IC_{50} / nM	pIC_{50}
47	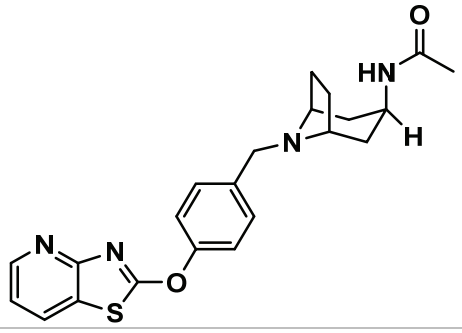	1	9.000

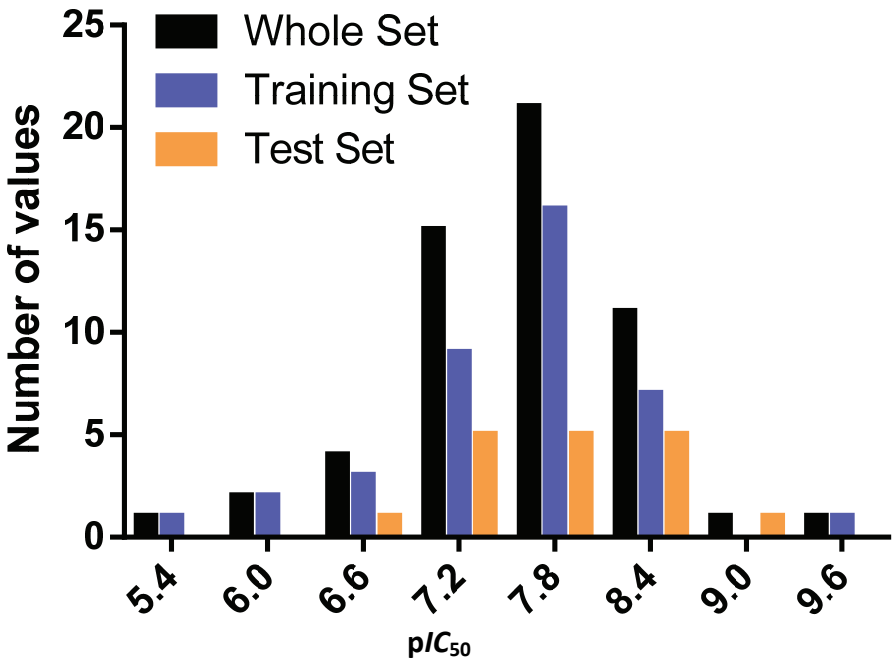

Fig. S-1. Histogram of frequency data portraying a uniform distribution of the pIC_{50} values of every inhibitory heterocyclic compound. Blue columns represent the training set molecules, orange columns represent the test set molecules and black columns represent the complete set molecules.

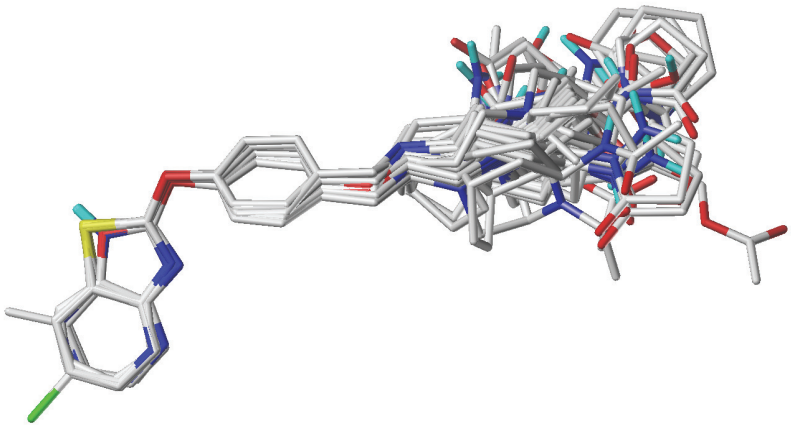

Fig. S-2. Superimposed structures of all compounds used in CoMFA/CoMSIA models.

Docking supplementary information

After the CoMFA and CoMSIA models were successfully built, 10 molecules (**1x–10x**) were designed as proposed inhibition compounds and tested with both models to obtain the new predicted pIC_{50} values. Subsequently, the docking assays of the compounds **9**, **44** and **1x–10x** were performed over the human LTA_4H (PDB_{ID}: 3FTS).[1] LTA_4H is made up of three distinctive domains, namely, *N*-terminal (residues 1–207), catalytic domain (residues 208–450), and *C*-terminal (residues 461–610).[2,3] The catalytic binding pocket is located at the interface of these domains, mostly towards the catalytic domain. Whereas the *N*-terminal is completely composed of long-stranded β-sheets, the other two domains are made of α-helices. The metal ion-binding site is formed by amino acid residues only from the catalytic domain such as His295, His299 and of Glu318.[2] The grid where **9**, **44** and the proposed compounds **1x–10x** were docked was established based on the putative amino acids of the catalytic site, such as Arg563, Lys565 and Tyr383,[2,4-6] with the zinc atom as the centre of the grid in order to obtain the binding mode of every compound and the docking descriptors.

Compounds **9** and **44** were chosen to be docked since they were the least and the most active LTA_4H inhibitors of the reported studied series, respectively. Therefore, to validate our docking assays, we compared the binding energies of the inhibitors **9** and **44** given by our docking experiments with their reported IC_{50} values. Results showed that the compound **9,** which has the highest IC_{50} value (3000 nM), displayed a deficient binding energy of -32.17 kJ/mol, which would explain the lower ability of **9** to inhibit the enzyme compared to the other molecules in table 1. Likewise, the most active inhibitory compound, the derivative **44**, had the lowest IC_{50} value (0.3 nM) and displayed an efficient binding energy of -43.14 kJ/mol, demonstrating a good correlation between the

experimental evidence and the theoretical information by our docking assays. Besides, the proposed compounds **1x–10x** also displayed efficient binding energies when they were docked into the catalytic site of the enzyme. Indeed, their values are comparable to the most active inhibitory compound (**44**).

The most active inhibitor **44** and the least active inhibitor **9** showed similar types of interactions but they were not exactly the same. Compound **44** formed a hydrogen bond interaction with Glu384, while compound **9** formed a hydrogen bond with Lys565. These different interactions could explain their different IC_{50} values and their different binding energies. Pharmacological compounds or inhibitors could exhibit multiple binding modes and contribute similarly to the overall affinity,[7] but when ligands are a part of a same chemical family, they often exhibit different sorts of affinity, potency, or pharmacological response, even if they settle into a biological target in a similar manner and performed similar interactions.[8]

Molecular docking of the compounds **9**, **44** (Fig. S-3), **1x**, **3x-6x**, **9x** and **10x** showed that all these derivatives are arranged in the same manner into the catalytic site of the LTA_4H enzyme, and all their thiazolopyridine rings overlap, that is to say the sulphur and nitrogen atoms at position 1- and 3- coincided, respectively (Fig. S-3). The compounds **9**, **44**, **1x**, **3x–6x** exhibited a hydrogen bond interaction with Tyr378 through the nitrogen atom at position 3- of their thiazolopyridine rings. The compounds **2x**, **7x** and **8x** were also arranged in the same manner as the other derivatives designed and shown in table 5, that is with their thiazolopyridine rings overlapping at the same direction within the catalytic site. Nonetheless, there is no coincidence of **2x**, **7x** and **8x** between the sulphur and nitrogen atoms with respect to the compounds **9**, **44**, **1x**, **3x–6x**, **9x** and **10x**, with these atoms being in opposite positions (Fig. S-3). The fact that the thiazolopyridine rings of the derivatives **2x**, **7x** and **8x** were inverted led to the loss of the hydrogen bond interaction between the amino acid Tyr378 and the nitrogen atom at position 3- of the heterocycles. Notwithstanding, the lack of this hydrogen bond interaction is balanced by the formation of a π-π interaction in **2x**, **7x** and **8x** between the pyridine rings of thiazolopyridines and the Tyr383 residue of the enzyme (Fig. S-3).

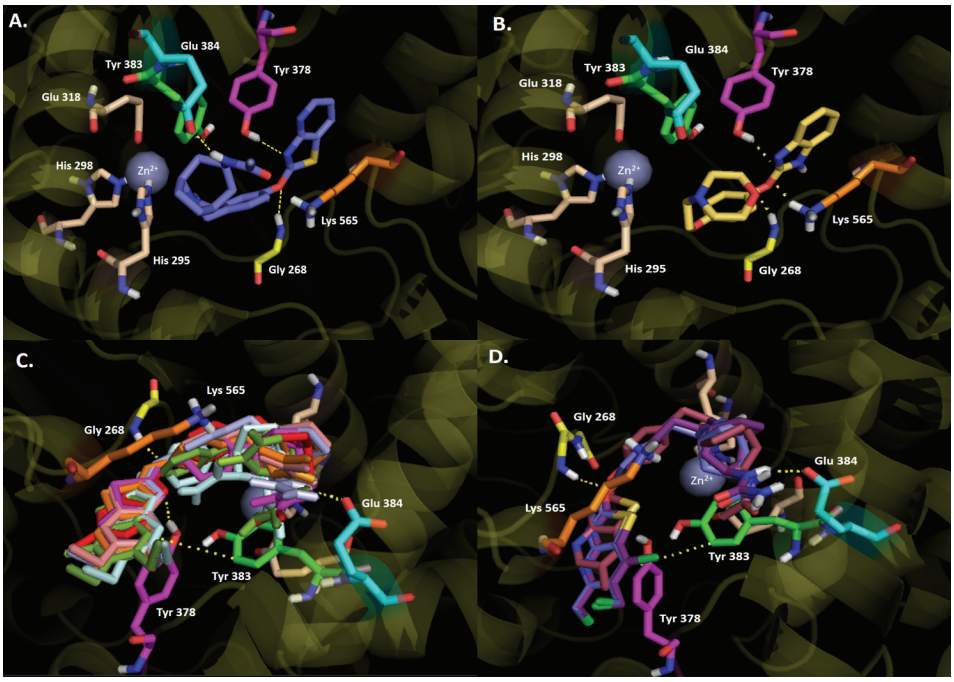

Fig. S-3. Predicted binding mode and predicted intermolecular interactions among **44**, **9**, **1x–10x** and the residues of the catalytic site of human LTA_4H. A. Compound **44** (most active inhibitor; H-bonding with Gly268, Tyr378 and Glu384). B. Compound **9** (least active inhibitor; H-bonding with Gly268, Tyr378 and Lys 565). C. Compounds **1x**, **3x–6x**, **9x** and **10x** (H-bonding with Gly268, Tyr378, Glu384 and Lys565 for **9x** and **10x**; π-π interaction with Tyr383 for **9x** and **10x**). D. Compounds **2x**, **7x** and **8x** (H-bonding with Gly268 and Glu384; π-π interaction with Tyr383)

All docked derivatives were shown to carry out a hydrogen bond interaction with Gly268 and Glu384 (except **10x**). The first one occurs due the oxygen atom between the phenyl rings and the thiazolopyridines, and the second one occurs through the hydrogen atoms of the amides or ureic groups placed at position 4- of the azabicyclooctane rings that all molecules contain (Fig. S-3).

The proposed compounds **9x** and **10x** did not perform a hydrogen bond interaction with Tyr378 (like the analogues **9**, **44**, **1x**, **3x–6x**), because their thiazolopyridine frameworks are slightly inclined to disfavouring the formation of this interaction. Notwithstanding, these molecules showed a π-π interaction through the amino acid Tyr383 and the pyridine rings of their thiazolopyridines. In addition, these molecules possess a second amide group at the azabicyclooctane core, which carried out an extra hydrogen bond interaction between the oxygen atom of the carbonyl group of the second amide and Lys565 residue. Therefore, these two different interactions could balance the lack of a hydrogen bond with Tyr378. Indeed, in the case of the hydrogen bond interaction

with Lys565, our CoMFA-steric contour map and CoMSIA-hydrogen bond acceptor contour map have demonstrated that the inclusion of an extra amide group in **9x** and **10x** led to a better inhibitory activity over the enzyme.

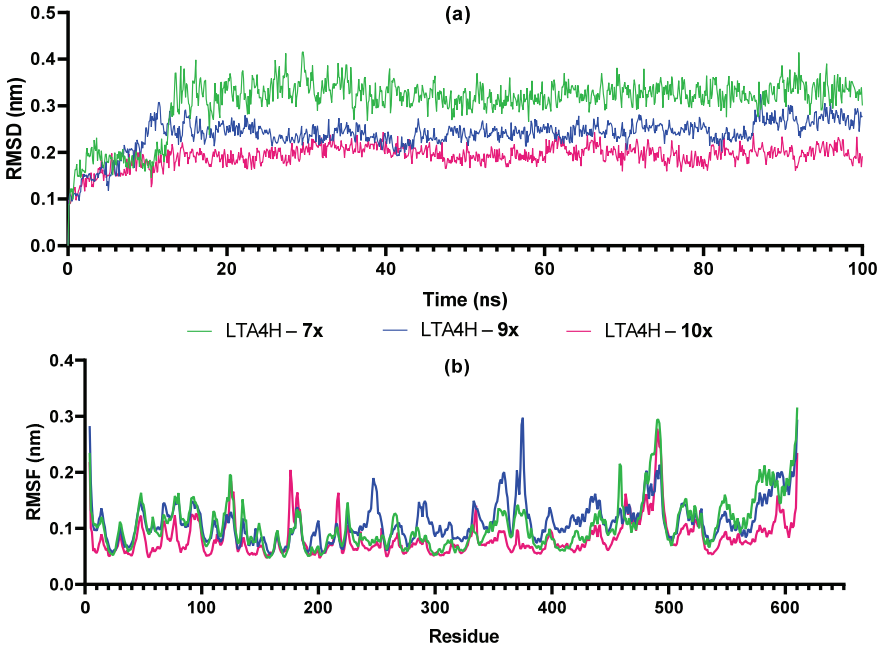

Fig. S-4. Trajectory analysis of molecular dynamics simulation of leukotriene A_4 hydrolase (LTA_4H) and compounds **7x, 9x** and **10x**. (a) RMSD of compound LTA_4H – **7x,** LTA_4H – **9x** and LTA_4H – **10x** complexes, (b) RMS fluctuation values during the period of 100 ns simulation

REFERENCES

1. D. R. Davies, B. Mamat, O. T. Magnusson, J. Christensen, M. H. Haraldsson, R. Mishra, B. Pease, E. Hansen, J. Singh, D. Zembower, H. Kim, A. S. Kiselyov, A. B. Burgin, M. E. Gurney, L. J. Stewart, *J. Med. Chem.* **52** (2009) 4694 (https://doi.org/10.1021/jm900259h)
2. M. M. Thunnissen, P. Nordlund, J. Z. Haeggström, *Nat. Struct. Biol.* **8** (2001) 131 (https://doi.org/10.1038/84117)
3. A. Rinaldo-Matthis, J.Z. Haeggstrom, *Biochimie* **92** (2010) 676 (https://doi.org/10.1016/j.biochi.2010.01.010)
4. P. C. Rudberg, F. Tholander, M. Andberg, M. M. Thunnissen, J. Z. Haeggström, *J. Biol. Chem* **279** (2004) 27376 (https://doi.org/10.1074/jbc.M401031200)
5. R. J. Snelgrove, *Thorax* **66** (2011) 550 (https://doi.org/10.1136/thorajxnl-2011-200234)
6. A. Wetterholm, J. F. Medina, O. Rådmark, R. Shapiro, J. Z. Haeggström, B. L. Vallee, B. Samuelsson, *Proc. Natl. Acad. Sci. U. S. A.* **89** (1992) 9141 (https://doi.org/10.1073/pnas.89.19.9141)

7. E. Stjernschantz, C. Oostenbrink, *Biophys. J.* **98**, (2010) 2682 (https://doi.org/10.1016/j.bpj.2010.02.034)
8. G. J. Kersh, E. N. Kersh, D. H. Fremont, P. M. Allen, *Immunity* **9** (1998) 817 (https://doi.org/10.1016/S1074-7613(00)80647-0).

Journal of the Serbian Chemical Society
JSCS-info@shd.org.rs • www.shd.org.rs/JSCS
J. Serb. Chem. Soc. *88* (1) 41–54 (2023)
JSCS–5609
Original scientific paper
Published 23 November 2022

Electrochemical properties of carbonized bentonite

NATAŠA P. JOVIĆ-JOVIČIĆ[1], DANICA V. BAJUK BOGDANOVIĆ[2#], TATJANA B. NOVAKOVIĆ[1], PREDRAG T. BANKOVIĆ[1], ALEKSANDRA D. MILUTINOVIĆ-NIKOLIĆ[1#] and ZORICA D. MOJOVIĆ[1]*

[1]*University of Belgrade – Institute of Chemistry, Technology and Metallurgy, Department of Catalysis and Chemical Engineering, Njegoševa 12, 11000 Belgrade, Serbia and* [2]*Faculty of Physical Chemistry, University of Belgrade, Studentski Trg 12–16, 11000 Belgrade, Serbia*

(Received 27 January, revised 22 March, accepted 26 March 2022)

Abstract: Organomodified bentonites were obtained by modification of bentonite clay from local mine Bogovina, with four different alkylammonium ions in the amounts that correspond to cation exchange capacity. Carbonized bentonites, obtained by pyrolyzing the organomodified bentonites in the flow of nitrogen, were characterized using XRD, low-temperature N_2 physisorption and Raman spectroscopy. Structural and textural properties of carbonized bentonites depended on the arrangement of alkylammonium cations in the paternal organomodified bentonite, while the Raman spectroscopy confirmed the presence of amorphous carbon. The obtained carbonized bentonites were used for modification of the carbon paste electrode. The modified electrodes were investigated using cyclic voltammetry and electrochemical impedance spectroscopy. The electrosorption of chloride and sulfate anions on carbonized bentonites was studied by chronocoulometry. The results were interpreted in the terms of surface groups and textural properties of the carbonized bentonites.

Keywords: $Fe(CN)_6^{3-/4-}$; electrosorption; chlorides; sulfates.

INTRODUCTION

Clays are materials with a wide range of application, present in plentiful deposits on or near the surface of the Earth. The smectite type of clays, such as bentonite, is of particular interest. Because of the properties such as high cation exchange capacity, surface area, and hydration characteristics, smectites can easily undergo a vast variety of modifications.[1]

Clay-modified electrodes have been investigated for a couple of decades to alter the electrode surface, consequently facilitating the reactions that occur on that surface.[2–5] Differently treated clays were used for electrode modification.

* Corresponding author. E-mail: zorica.mojovic@ihtm.bg.ac.rs
# Serbian Chemical Society member.
https://doi.org/10.2298/JSC220127030J

The most used are acid activation,[6] pillaring[7] and modification by organic compounds.[8] Each of these modifications brought new properties to the composite material broadening the range of their applications (as electrochemical sensors for a variety of analytes,[9] electrodes for energy storage applications, ion-selective electrodes). Among these applications, the electrochemical sensors for pharmaceutical[10] and food quality[11] can be singled out as the most advanced ones.

Further improvement of clay electrodes has been attempted through the synthesis of carbon-clay composites.[12–14] The carbon-clay composites combined a relatively high specific surface area of the clay with a good electrical conductivity of carbon and can open new possible applications of these hybrid materials.

Carbon electrodes are used for capacitive deionization of water, among other applications. This area of investigation acquired great attention in the last years due to worldwide problems regarding the lack of clean freshwater.[15] This work aims to establish the potential usability of carbonized bentonites for capacitive deionization. In the previous publication of this group of authors[16] carbon-clay composites were obtained by carbonizing clays modified with different amounts of hexadecyltrimethylammonium (HDTMA) ion. The performance of carbonized samples and parenting organomodified samples was compared. The results showed that the amount of present organic precursor had a significant influence on the electrochemical properties of the resulting carbonized clay. It was concluded that the electroactivity of carbonized clay-based electrodes depended on the porosity, ion-exchange capacity, and carbon-clay interface contact. One of the important parameters for efficient electrosorption is the behaviour of the electrode/electrolyte interface. The pore size distribution, rather than specific surface area, is one of the main factors influencing the formation of an electric double layer, and therefore the efficiency of electrosorption.[17] In this work the influence of different organic precursors on the electrochemical properties of resulting carbonized bentonite was investigated. Bentonite clay from a local deposit (Bogovina, Serbia) was modified with four different alkylammonium anions. The response of the obtained carbonized bentonites was tested toward negatively charged redox probe as well as for the electrosorption of chloride and sulfate ions.

EXPERIMENTAL

Bentonite (clay from Bogovina, coal and bentonite mine, Serbia) fraction with a particle size of up to 74 μm, enriched with sodium using the ion-exchange procedure, was employed for modification with different organic cations. The procedure for organo-bentonite preparation was adopted according to Baskaralingam.[18] Four alkylammonium ions (hexadecyltrimethylammonium (HDTMA), dodecyltrimethylammonium (DDTMA), benzyltrimethylammonium (BTMA) and trimethylammonium (TMA), all acquired from Sigma–Aldrich) were introduced in the amounts which correspond to the value of cation exchange capacity (*CEC*) of the clay. The *CEC* value was previously estimated by ammonium acetate procedure (EPA, Method 9080)[19] to be 63.3 mmol of monovalent cation per 100 g of dry clay.[20] The obtained organomodified bentonites were heated at the rate of 5 °C min^{-1} until 400 °C was

reached. The temperature was held at 400 °C for 30 min. Subsequently, the samples were let to cool down to room temperature. The cycle of heating and cooling was performed in the stream of nitrogen. The samples were designated as c-HDTMA-B, c-DDTMA-B, c-BTMA-B and c-TMA-B, per the applied parental material.

The XRD analysis was performed using a Rigaku Smart Lab automatic multipurpose X-ray diffractometer (equipped with low background Si sample holder support; 1D D/teX 250 Ultra detector in XRF mode) and Cu anode (λ = 0.1542 nm). The diffractograms of the samples were obtained in the 2θ range from 2 to 45°, with the scanning rate of 0.3° min^{-1}, and scanning step of 0.01°.

Textural properties were assessed from nitrogen adsorption-desorption isotherms recorded at −196 °C and relative pressure in the range $0.05 < p/p_0 < 0.98$ using a Sorptomatic 1990, Thermo Finnigan. Samples were degassed at 150 °C for 10 h under vacuum. The specific surface area of the samples was calculated according to the Brunauer, Emmett and Teller (BET) method from the linear part of the nitrogen adsorption isotherms.[21–23] The pore size distribution has been computed from the desorption branch of the isotherms using Barrett, Joyner and Halenda (BJH) method.[21]

The Raman spectra were recorded using a Thermo DXR Raman microscope and laser excitation at the wavelength of 532 nm. Measurements were performed using the constant laser power of 9 mW, exposure time of 20 s, repetition of 10, grating with 900 lines mm^{-1}, and spectrograph aperture of 50 μm pinhole. The Thermo Scientific Omnic 9 software was used for the spectra acquisition and analysis. After the acquisition, the fluorescence background was subtracted from the Raman spectra using the fifth-order polynomial fit.

The electrochemical investigation of the samples was performed using modified a carbon paste electrode as the working electrode. Carbon pastes with the carbonized bentonite samples as modifiers were prepared manually by mixing 500 mg of a sample, 25 mg of carbon black (CB, Vulcan®-XC 72R), and 300 mg of paraffin oil. The paste was packed into a hollow (2 mm diameter) Teflon tube while the electrical contact was provided using a copper wire. The reference electrode was Ag/AgCl in 3 M KCl, while a platinum rod served as the counter electrode. The electrochemical measurements were performed using an Autolab electrochemical workstation (Autolab PGSTAT302N, Metrohm-Autolab BV, Netherlands). Impedance measurements were performed in 1 mM $K_4[Fe(CN)_6]$ in 0.2 M KCl, at open circuit potential using a 5 mV rms sinusoidal modulation in the 100 kHz–0.1 Hz frequency range. Cyclic voltammetry measurements were performed in the same electrolyte, at the scan rate of 50 mV s^{-1}. The electrosorption properties of carbonized clays were tested in 0.2 M NaCl and 0.2 M Na_2SO_4 solutions using chronocoulometry. Chronocoulometric curves were obtained by applying a potential of 0.5 V *vs*. Ag/AgCl for 20 s and recording the transient current.

RESULTS AND DISCUSSION

XRD analysis

The results of the XRD analysis for the carbonized samples are presented in Fig. 1.

The crystalline phases expected for bentonite were observed: smectite, quartz, feldspar and calcite.[24] It is well known that the incorporation of quaternary ammonium cations (QAC) into interlamellar space results in the increase of d_{001} values of smectite.[1] The previous studies of this group have shown that the incorporation of QAC in the different amounts corresponding to the cation exchange

capacity (*CEC*) of smectite leads to the formation of different molecular arrangements, depending on the structure and QAC alkyl chain length.[16,25–27] Short-chain QAC dominantly forms monolayers with characteristic $d_{001} \approx 1.4$ nm, while longer chain QAC make bilayers structure ($d_{001} \approx 1.8$ nm) with the alkyl chain axes parallel to the silicate layers.[1] Pseudo-trimolecular arrangement structures of kinked alkyl chains are observed with highly charged smectites and/or long surfactant cations and exhibit $d_{001} \approx 2.2$ nm.[1] The specific arrangements of organic cations in samples with the amount of QAC equal to *CEC* are summarized in Table I.

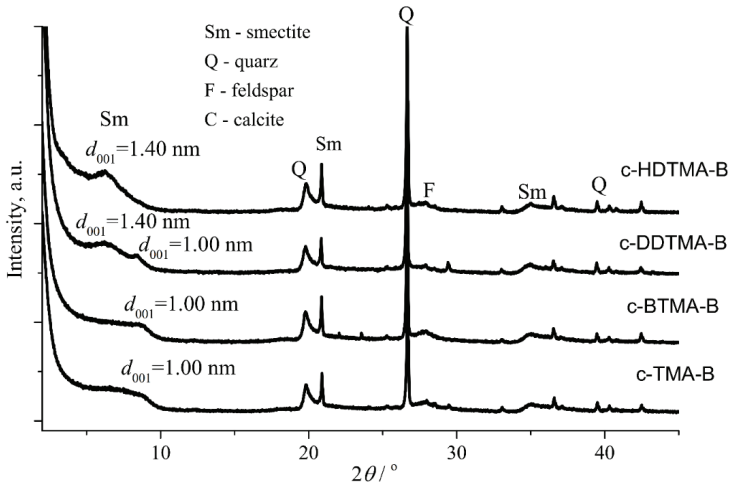

Fig. 1. X-ray diffractograms of carbonized bentonites (Sm – smectite, Q – quartz, F – feldspar and C – calcite).

TABLE I. Basal spacing values previously obtained for the samples with QAC incorporated in the amount equal to CEC

Sample	d_{001} / nm	QAC arrangement	Ref.
HDTMA-B	2.00	Pseudo-trimolecular layer	13
DDTMA-B	1.78	Bimolecular layer	22
BTMA-B	1.46	Monomolecular layer	23
TMA-B	1.40	Monomolecular layer	24

c-HDTMA-B, obtained by the carbonization of 1.0 HDTMA-B, showed $d_{001} = 1.40$ nm which is in agreement with the previous findings.[28] Taken into account that the elemental silicate sheet of Bogovina smectite is approx. 1.01 nm[28] the interlamellar distance of 0.40 nm is almost the same as reported by Ruiz-García *et al.*[29] for sucrose carbonated smectite.

The value of 0.40 nm is in good agreement with the formation of a carbon monolayer between smectite lamellae.[29,30] According to literature data, the type

of organic precursor and clay mineral had a strong impact on the formation of carbon structure and thickness.[29–31] The c-DDTMA-B besides the presence of d_{001} of 1.40 nm also showed the reflection that corresponded to collapsed structure with the characteristic basal spacing of ~1.0 nm.[1] Only the collapsed structure was detected for c-TMA-B and c-BTMA-B samples derived from the short--chain and the aromatic QAC precursors, respectively. Based on the obtained results, it seems that the samples with lower carbon content, either due to the smaller number of carbon atoms present in QAC precursor or lower loading of QAC,[16] led to the formation of the collapsed structure during the applied carbonization procedure at elevated temperature.

Textural properties

Nitrogen adsorption/desorption isotherms for carbonized bentonites (Fig. 2a) exhibited similar profiles.

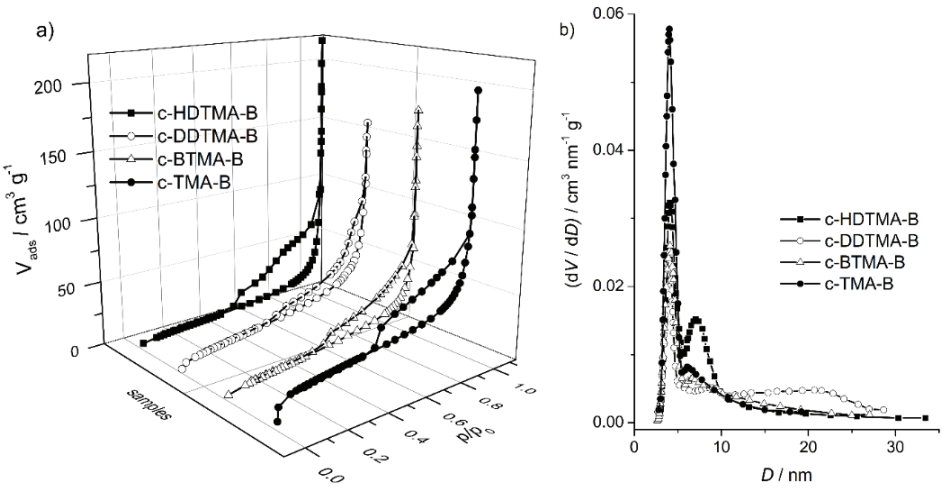

Fig. 2. a) Nitrogen adsorption/desorption isotherms recorded for carbonized bentonites; b) corresponding pore size distributions obtained by the Barrett–Joyner–Halenda (BJH) method.

All investigated samples were of Type IIb, according to the IUPAC classification, with the H3 type hysteresis loop.[21] The H3 loop is characteristic of powders and aggregates of plate-shaped particles, clays, and pigments. Hysteresis loops at higher relative pressures are the result of capillary condensation. Narrower hysteresis loops, such as those obtained for c-DDTMA-B and c-BTMA-B samples, usually indicate irregularly shaped aggregates.

The specific surface area and total pore volume (Table II) of the carbonized bentonites depended on the organic precursor used for the synthesis of organobentonites. The lowest value was obtained for c-HDTMA-B and the highest for

c-TMA-B reflecting the amount of carbon generated in the pores of bentonite upon the pyrolysis of the organic precursor.

TABLE II. Textural properties calculated from N_2 adsorption-desorption isotherms; S_{BET} is specific surface area; $V_{0.98}$ is total pore volume estimated from the amount of nitrogen adsorbed at the relative pressure of 0.98; D_{max} is the maximum pore diameter

Sample	S_{BET} / m^2 g^{-1}	$V_{0.98}$ / cm^3 g^{-1}	D_{max1} / nm	D_{max2} / nm	D_{max3} / nm
c-HDTMA-B	27	0.093	4.0	7.0	–
c-DDTMA-B	47	0.130	3.9	8.7	20.7
c-BTMA-B	34	0.102	4.1	6.7	–
c-TMA-B	89	0.127	4.0	6.1	–

The pore size distribution in the mesoporous region obtained by the BJH method (Fig. 2b) exhibits two peaks in the mesoporous region. The first peak had maxima at about 4.0 nm and is characteristic of clays rich in smectite.[32] The second peak had the maxima within the range from 6.1–8.7 nm and can be considered as the indicator of precursor influence. The third maximum at 20.7 appeared only for the c-DDTMA-B sample.

Raman spectroscopy

Raman spectra (Fig. 3) were recorded in the Raman shift range from 2200 to 800 cm^{-1}.

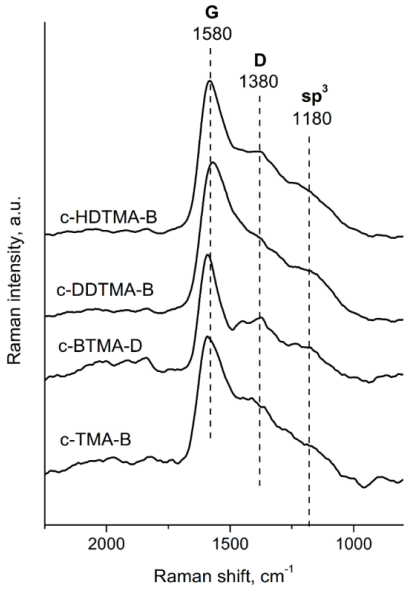

Fig. 3. Raman spectra of c-HDTMA-B, c-DDTMA-B, c-BTMA-B and c-TMA-B in the range between 2200 and 800 cm^{-1}.

The Raman spectra of the investigated carbonized clays were similar. The typical D and G bands can be observed at ~1580 and ~1380 cm^{-1} representing

the graphitized and disordered sp^2 structure. The G band corresponds to the in-plane, doubly degenerated E_{2g} phonon at the graphene Brillouin zone centre. The D peak is linked to the breathing modes of the sp^2 rings and requires a defect for its activation.[33] In addition, the band at 1180 cm^{-1} observed in all spectra could be attributed to the contribution of sp^3 carbon vibrations.[34] The appearance of the D peak is correlated to the presence of aromatic rings or the formation of clusters in the amorphous carbon.[35] The noticeable difference of the D peak in the c-HDTMA-B and c-DDTMA-B spectra are the result of different arrangements of the organic precursor in the smectite interlamellar space. HDTMA was arranged in a pseudo-trimolecular layer enabling the formation of more clusters. According to Ferrari and Robertson,[35] unlike in graphite, the development of the D peak in amorphous carbons indicates ordering. The same peak in the c-BTMA-B spectrum arose because of the presence of an aromatic ring.

Electrochemical properties of carbonized bentonite

The electrochemical properties of the carbonized bentonite were first tested using cyclic voltammetry in 1 mM potassium hexacyanoferrate (II) in 0.2 M KCl (Fig. 4a). All recorded cyclic voltammograms (CVs) showed the characteristic pair of peaks corresponding to the oxidation and the reduction of $[Fe(CN)_6]^{3-/4-}$. The response of anionic probe on cationic clay greatly depends on the modification of the clay. Smectite sheets have a permanent negative charge introduced by isomorphic substitution. It is expected that these charges would repel the anionic redox probe. However, the cationic sites present at the edges of clay particles[36] and/or introduced by clay modification provide the sites for interaction with the anionic probe. CVs recorded using c-HDTMA-B and c-DDTMA-B containing electrodes were similar, as expected, because of the similarity of molecules of the used organic precursors. The peak-to-peak separation was 0.43 V, I_a/I_c ratio was 1.05 and half-wave potential was 0.31 V. CV of c-BTMA-B electrode exhibited lower peak-to-peak separation of 0.23 V. The I_a/I_c ratio was 0.9 and the half-wave potential was 0.26 V. c-TMA-B electrode showed the highest current, although the peak corresponding to the oxidation of $[Fe(CN)_6]^{4-}$ was not well resolved. The estimated peak-to-peak separation and the half-wave potentials were 0.30 and 0.26 V, respectively. The shift of the half-wave potentials and peak-to-peak separation toward lower values for c-BTMA-B and c-TMA-B showed that $[Fe(CN)_6]^{4-}$ was more easily oxidized at these electrodes with faster electron transfer. The results of the CV of c-BTMA-B the I_a/I_c ratio to be below unity indicating better retention of the formed $[Fe(CN)_6]^{3-}$ at the electrode surface. The presence of $[Fe(CN)_6]^{3-}$ on the electrode surface additionally contributed to the repulsion, thus increasing the charge transfer resistance.

The response of the carbon paste electrode also depends on the source of carbon. In our previous publication,[37] we have investigated the influence of gra-

phite and carbon black on the response of carbon clay-based electrodes. Better results were obtained with carbon black, although the graphite-based electrodes showed improvement in comparison to the electrodes based only on carbon clay, without the addition of an external carbon source.

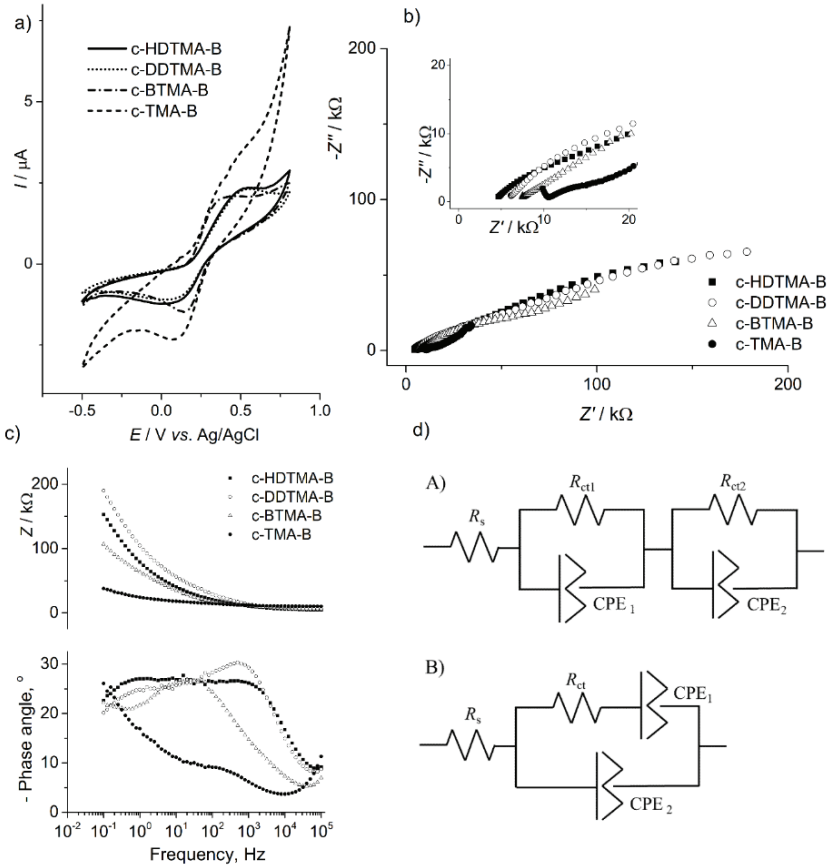

Fig. 4. Carbon paste electrodes modified with different clay samples: a) cyclic voltammograms recorded in 1 mM $K_4[Fe(CN)_6]$ + 0.2 M KCl at a scan rate of 50 mV s^{-1}; b) Nyquist plot recorded in the same solution in OCP; c) Bode plot recorded in the same solution in OCP; d) the equivalent electric circuit used to fit EIS data.

Further investigation was performed using the electrochemical impedance spectroscopy (EIS) in the same solution. The Nyquist plots obtained for the c--HDTMA-B and c-DDTMA-B electrodes (Fig. 4b) were similar to each other and consisted of two depressed semi-circles. The accompanying Bode plots (Fig. 4c) showed two relaxation time constants. Hence, these spectra were fitted with an equivalent circuit consisting of the series combination of an internal resistance R_s, a parallel R_{ct1}–CPE_1 and a parallel R_{ct2}–CPE_2 (equivalent circuit A). The

first R_{ct}–CPE pair corresponds to the charge transfer resistance and the capacitance accompanied with the charge transfer resistance. The second R_{ct}–CPE pair describes the second semi-circle at lower frequencies and corresponds to the ionic resistance in the electrode and the diffusion impedance. The Nyquist plots obtained for the c-BTMA-B electrode and the c-TMA-B electrode consisted of a semi-circle and the linear part. The accompanying Bode plots (Fig. 4c) exhibited one relaxation time constant. Hence, these spectra were fitted with a modified Randles circuit (equivalent circuit B) consisting of internal resistance (R_s) in a series with a parallel combination of a double-layer capacitance represented with a constant phase element (CPE_2) and an impedance of a faradaic reaction (serial combination of charge transfer resistance, R_{ct}, and a constant phase element (CPE_1)). The constant phase element (CPE) is often used to replace the double-layer capacitance (C_{dl}) and the Warburg impedance in the original Randles circuit. The capacitance element CPE will become the pure capacitance, pure resistance, and Warburg impedance when $n = 1$, $n = 0$ and $n = 0.5$, respectively. The resistor (R), capacitor (C) and Warburg impedance element (W) can, therefore, be considered to be a special case of CPE.[38] The results obtained using fitting with these circuits are presented in Table III. The highest value of charge transfer resistance was obtained for c-BTMA-B.

TABLE III. The electrochemical parameters obtained by fitting the EIS data recorded using the electrodes with the CB/clay ratio of 1:20 in 1 mM $K_4[Fe(CN)_6]$ in 0.2 M KCl

Electrode	R_s / kΩ	R_{ct1} / kΩ	Q_1[a] / μS s^{n_1}	n_1	R_{ct1} / kΩ	Q_2 /μS s^{n_2}	n_2
c-HDTMA-B	3.8	7.8	0.9	0.7	388	5.7	0.4
c-DDTMA-B	5.3	21.5	0.6	0.7	345	4.3	0.4
c-BTMA-B	7.0	105.0	25.7	0.6	4.1	–	0.5
c-TMA-B	9.8	12.5	29.3	0.5	9.1	–	0.4

[a]The impedance of constant phase element: $Z = 1/Y = 1/(i\omega)^n Q$; where Y is admittance, i is the imaginary unit, ω is the angular frequency, n is the exponent associated with the system inhomogeneity and Q has the numerical value of the admittance $1/|Z|$ at $\omega = 1$ rad/s

The behaviour of the redox probe $[Fe(CN)_6]^{3-/4-}$ is influenced by the electronic properties, microstructure, and surface properties of the electrode surface.[39] The investigated composites contained bentonite, and its negative surface charge repulses the negatively charged redox probe.[8] However, the positively charged pH-dependent sites enable the interaction of the clay-modified electrodes with the negatively charged redox probe.

At the pH of the used electrolyte (pH 5.5), >AlOH and >SiOH groups are present at the clay surface because of the deprotonation of $>AlOH_2^+$ and $>SiOH_2^+$ at lower pH values.[40] The PZC measurement[16] revealed that the contribution of a variable charge was less pronounced at carbonized clays, especially for those with higher carbon content. On the other hand, the carbonized bento-

nites showed to have a different distribution of surface groups in comparison with that of the starting bentonite. Besides that, they contain additional surface groups, such as >C=O, >COOH, >C-OH, $>NH_2$,[41,42] and some of them (>COOH groups) are shown to have an inhibitory effect on the electrochemistry of $Fe(CN)_6^{3-/4-}$.[43]

The intercept of the semicircle with the real axis at higher frequencies represents the internal resistance, R_S. The internal resistance mainly represents the resistance of the bulk electrolyte. The value of R_S increased in the following order: c-HDTMA-B < c-DDTMA-B < c-BTMA-B < c-TMA-B. The observed shift of the R_S to higher values can be ascribed to the increase of the ionic resistance of the electrode surface,[44] *i.e.*, the electrode layer adjacent to the bulk electrolyte. The increase of the thickness of this layer, *i.e.*, the increase of the depth of the electrolyte penetration into the electrode,[45] led to the increase of R_S.

The electrosorption properties of investigated carbonized bentonites were tested from 0.2 M NaCl and 0.2 M Na_2SO_4. The anodic polarization was applied to test the sorption of anions and the obtained chroncoulometric curves were normalized for the sake of comparison (Fig. 5).

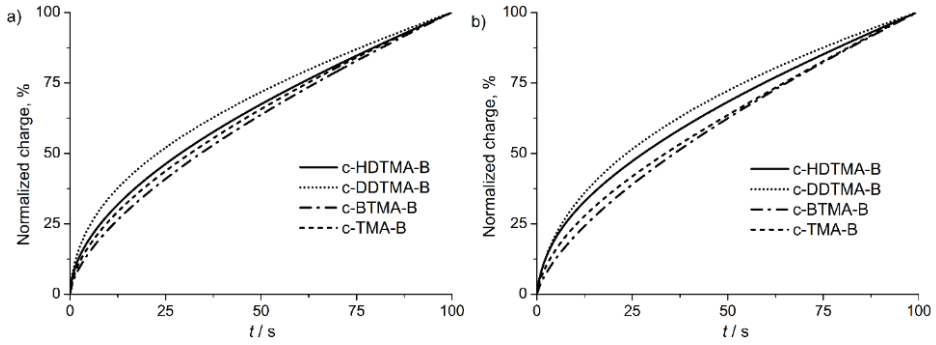

Fig. 5. Normalized chronocoulometric curves of carbonized bentonites in: a) 0.2 M NaCl and b) 0.2 M Na_2SO_4.

The time constant ($\tau = RC$) can be obtained by applying:[46]

$$-\ln\left(1-\frac{Q}{Q_0}\right)=\frac{t}{RC} \quad (1)$$

where Q_0 is the electrode's charge at the equilibrium, t is the time of the pulse, R is the resistance and C is the electrode's capacitance.

The time constant, obtained as a slope of the linear part of the plot, is presented in Table IV.

The electrosorption depends on the average pore dimensions,[47] the ionic charge and the hydrated radius.[48] The electrosorption was hindered by the pre-

sence of smaller pores resulting in the higher values of time constants. The values of the obtained time constants correlate with the values of the second maxima obtained from the N_2 adsorption-desorption isotherms: the higher the constant the smaller pore diameter. The shorter time constants were obtained for chlorides than for sulfates. The slower kinetics of electrosorption recorded for the sulfate ions is the consequence of their higher charge that caused stronger electrostatic interactions.

TABLE IV. Time constants (s) of the carbonized bentonite electrodes calculated from the chronocoulometric curves recorded in 0.2 M NaCl solution and 0.2 M Na_2SO_4 solution

Electrode	Solution	
	NaCl	Na_2SO_4
c-HDTMA-B	9.80	10.39
c-DDTMA-B	8.73	9.11
c-BTMA-B	10.29	11.33
c-TMA-B	10.75	11.40

CONCLUSION

Organomodified bentonite composite, prepared by the use of different alkylammonium salts (HDTMA, DDTMA, BTMA and TMA), was pyrolyzed and carbon-bentonite hybrid composites were obtained. The carbonized bentonites were characterized using the XRD, low-temperature N_2 physisorption and Raman spectroscopy. The structure with the defined d_{001} basal spacing was found only for HDTMA-derived sample, while the samples derived from organoclays with shorter chains showed the presence of collapsed structures. Extreme values of the specific surface area and pore volume were obtained for the carbonized clay originating from the bentonite modified with the surfactant with the highest and lowest numbers of carbon atoms. The Raman spectroscopy confirmed the formation of amorphous carbon in the carbonized bentonites.

Electrochemical impedance spectroscopy and cyclic voltammetry showed that the carbonized bentonite sample derived from TMA-clay exhibited the highest electrochemical activity toward the $Fe(CN)_6^{3-/4-}$ redox couple. The internal resistance of the samples increased with the decrease of the chain length of the used organic precursor. The chronocoulometry was used to study the electrosorption properties of carbonized bentonites toward chloride and sulphate ions. The electrosorption was hindered at the samples with smaller pores. The type of organic precursor influenced the pore size of the carbonized bentonite and their electrosorption properties.

Acknowledgment. This work was financially supported by the Ministry of Education, Science and Technological Development of the Republic of Serbia (Grant No. 451-03-9/2021--14/200026).

ИЗВОД

ЕЛЕКТРОХЕМИЈСКА СВОЈСТВА КАРБОНИЗОВАНИХ БЕНТОНИТА

НАТАША П. ЈОВИЋ-ЈОВИЧИЋ[1], ДАНИЦА В. БАЈУК БОГДАНОВИЋ[2], ТАТЈАНА Б. НОВАКОВИЋ[1], ПРЕДРАГ Т. БАНКОВИЋ[1], АЛЕКСАНДРА Д. МИЛУТИНОВИЋ-НИКОЛИЋ[1] и ЗОРИЦА Д. МОЈОВИЋ[1]

[1]Универзитет у Београду - Институт за хемију, технологију и металургију, Центар за катализу и хемијско инжењерство, Његошева 12, 11 000 Београд и [2]Факултет за физичку хемију, Универзитет у Београду, Студентски трг 12–16, 11 000 Београд

Органомодификовани бентонити су добијени модификацијом бентонита из локалног рудника Боговина са четири различита алкиламонијум јона у количини која је једнака његовом капацитету јонске измене. Карбонизовани бентонити, добијени пиролизом органомодификованих бентонита у струји азота, окарактерисани су помоћу дифракције X-зрачења (XRD), нискотемпературском физисорпцијом азота и Раманском спектроскопијом. Структурна и текстурална својства карбонизованих бентонита зависе од уређења алкиламонијум катјона у одговарајућем полазном органомодификованом бентониту. Резултати карактеризације су показали да особине узорака зависе од распореда алкиламонијум катјона у органомодификованом бентониту од ког су настали, док је Раманска спектроскопија потврдила присуство аморфног угљеника. Добијени карбонизовани бентонити су коришћени за модификацију електроде од пасте угљеника. Модификоване електроде су испитане помоћу цикличне волтаметрије и електрохемијске импедансне спектроскопије. Електросорпција хлорида и сулфата је проучавана помоћу хронокулонометрије. Резултати су протумачени на основу присутних површинских група и текстуралних својстава карбонизованих бентонита.

(Примљено 27. јануара, ревидирано 22. марта, прихваћено 26. марта 2022)

REFERENCES

1. M. F. Brigatti, E. Galán, B. K. G. Theng, in *Handbook of Clay Science, Developments in Clay Science*, F. Bergaya, G. Lagaly (Eds.), Elsevier, Amsterdam, 2013, pp. 21–81 (ISBN: 978-0-08-098259-5)
2. P.K. Ghosh, A.J. Bard, *J. Am. Chem. Soc.* **105** (1983) 5691 (https://doi.org/10.1021/ja00355a030)
3. S. M. Macha, A. Fitch, *Microchim. Acta* **128** (1998) 1 (https://doi.org/10.1007/BF01242184)
4. Z. Navratilova, P. Kula, *Electroanalysis* **15** (2003) 837 (https://doi.org/10.1002/elan.200390103)
5. I. K. Tonle, E. Ngameni, A. Walcarius, *Sensors Actuators, B* **110** (2005) 195 (https://doi.org/10.1016/j.snb.2005.01.027)
6. P. Falaras, F. Lezou, *J. Electroanal. Chem.* **455** (1998) 169 (https://doi.org/10.1016/S0022-0728(00)00133-9)
7. D. Petridis, P. De S. Kaviratna, T.J. Pinnavaia, *J. Electroanal. Chem.* **410** (1996) 93 (https://doi.org/10.1016/0022-0728(96)04541-X)
8. I. K. Tonle, E. Ngameni, F. M. M. Tchieno, A. Walcarius, *J. Solid State Electrochem.* **19** (2015) 1949 (https://doi.org/10.1007/s10008-014-2728-0)
9. P. R. Vernekar, N. P. Shetti, M. M. Shnbhag, S. J. Malode, R .S. Malladi, K. R. Reddy. *Microchim. J.* **159** (2020) 105441 (https://doi.org/10.1016/j.microc.2020.105441)

10. N. P. Shetti, S. J. Malode, D. S. Nayak, R. R. Naik, G. T. Kuchinad, K. R. Reddy, S. S. Shukla, T. M. Aminabhavi, *Michochim. J.* **155** (2020) 104727 (https://doi.org/10.1016/j.microc.2020.104727)
11. N. P. Shetti, D. S. Nayak, S. J. Malode, *Vacuum* **155** (2018) 524 (https://doi.org/10.1016/j.vacuum.2018.06.050)
12. P. Aranda, M. Darder, R. Fernández-Saavedra, M. Lopez-Blanco, E. Ruiz-Hitzky, *Thin Solid Films* **495** (2006) 104 (https://doi.org/10.1016/j.tsf.2005.08.284)
13. M. Darder, E. Ruiz-Hitzky, *J. Mater. Chem.* **15** (2005) 3913 (https://doi.org/10.1039/B505958E)
14. A. Gómez-Avilés, M. Darder, P. Aranda, E. Ruiz-Hitzky, *Angew. Chem. Int. Ed. Engl.* **46** (2007) 923 (https://doi.org/10.1002/anie.200603802)
15. C. Zhang, D. He, J. Ma, W. Tang, T. D. Waite, *Water Res.* **128** (2018) 314 (https://doi.org/10.1016/j.watres.2017.10.024)
16. N. Jović-Jovičić, M. Mojović, D. Stanković, B. Nedić-Vasiljević, A. Milutinović-Nikolić, P. Banković, Z. Mojović, *Electrochim. Acta* **296** (2019) 387 (https://doi.org/10.1016/j.electacta.2018.11.031)
17. S. Biniak, A. Swiatkowski, M. Pakuła, M. Sankowska, K. Kuśmierek, G. Trykowski, *Carbon* **51** (2013) (https://doi.org/10.1016/j.carbon.2012.08.057)
18. P. Baskaralingam, M. Pulikesi, D. Elango, V. Ramamurthi, S. Sivanesan, *J. Hazard. Mater.* **128** (2006) 138 (https://doi.org/10.1016/j.jhazmat.2005.07.049)
19. EPA, *Method 9080: Cation-exchange capacity of soils (ammonium acetate)*, https://www.epa.gov/sites/production/files/2015-12/documents/9080.pdf
20. N. Jović-Jovičić, A. Milutinović-Nikolić, M. Žunić, Z. Mojović, P. Banković, I. Gržetić, D. Jovanović, *J. Contam. Hydrol.* **150** (2013) 1 (https://doi.org/10.1016/j.jconhyd.2013.03.004)
21. F. Rouquerol, J. Rouquerol, K. S. W. Sing, P. Llewellyn, G. Maurin, *Adsorption by powders and porous solids, principles, methodology and applications*, Academic Press, New York, 2012 (https://doi.org/10.1016/B978-0-12-598920-6.X5000-3)
22. B. C. Lippens, B. G. Linsen, J. H. De Boer, *J. Catal.* **3** (1964) 32 (https://doi.org/10.1016/0021-9517(64)90089-2)
23. K. S. Sing, *Pure Appl. Chem.* **57** (1985) 603 (https://doi.org/10.1351/pac198557040603)
24. International Center for Diffraction Data, Joint Committee on Powder Diffraction Standards (JCPDS), Swarthmore, PA, 1990
25. N. Jović-Jovičić, A. Milutinović-Nikolić, P. Banković, B. Dojčinović, B. Nedić, I. Gržetić, D. Jovanović, *Acta Phys. Pol., A* **117** (2010) 849 (https://doi.org/10.12693/APhysPolA.117.849)
26. A. Abu Rabi-Stanković, A. Milutinović-Nikolić, N. Jović-Jovičić, P. Banković, M. Žunić, Z. Mojović, D. Jovanović, *Clays Clay Miner.* **60** (2012) 291 (https://doi.org/10.1346/CCMN.2012.0600306)
27. A. Abu Rabi-Stanković, Z. Mojović, A. Milutinović-Nikolić, N. Jović-Jovičić, P. Banković, M. Žunić, D. Jovanović, *Appl. Clay Sci.* **77**–**78** (2013) 61 (https://doi.org/10.1016/j.clay.2013.04.003)
28. P. Banković, A. Milutinovic-Nikolic, Z. Mojović, N. Jović-Jovičić, M. Perovic, V. Spasojevic, D. Jovanović, *Micropor. Mesopor. Mater.* **165** (2013) 247 (https://doi.org/10.1016/j.micromeso.2012.08.029)

29. C. Ruiz-García, J. Perez-Carvajal, A. Berenguer-Murci, M. Darder, P. Aranda, D. Cazorla-Amoros, E. Ruiz-Hitzky, *Phys. Chem. Chem. Phys.* **15** (2013) 18635 (https://doi.org/10.1039/C3CP53258E)
30. P Anadão, E. A. Hildebrando, I. L. R. Pajolli, K. R. de Oliveira Pereira, H. Wiebeck, F. R. V. Díaz, *Appl. Clay Sci.* **53** (2011) 288 (https://doi.otg/10.1016/j.clay.2011.04.022)
31. Q. Chen, R. Zhu, W. Deng, Y Xu, J. Zhu, Q. Tao, H. Hongping, *Appl. Clay Sci.* **100** (2014) 112 (https://doi.org/10.1016/j.clay.2014.04.011)
32. U. Kuila, M. Prasad, *Geophys. Prospect.* **61** (2013) 341 (https://doi.org/10.1111/1365-2478.12028)
33. O. Frank, G. Tsoukleri, I. Riaz, K. Papagelis, J. Parthenios, A. C. Ferrari, A. K. Geim, K.S. Novoselov, C. Galiotis, *Nat. Commun.* **2** (2011) 255 (https://doi.org/10.1038/ncomms1247)
34. J. Schwan, S. Ulrich, V. Batori, H. Ehrhardt, S. R. P. Silva, *J. Appl. Phys.* **80** (1996) 440 (https://doi.org/10.1063/1.362745)
35. A. C. Ferrari, J. Robertson, *Phys. Rev., B* **61** (2000) 14095 (https://doi.org/10.1103/PhysRevB.61.14095)
36. A. Fitch, *Clays Clay Miner.* **38** (1990) 391 (https://doi.org/10.1346/CCMN.1990.0380408)
37. C. Apetrei, I. M. Apetrei, J. A. De Saja, M. L. Rodriguez-Mendez, *Sensors* **11** (2011) 1328 (https://doi.org/10.3390/s110201328)
38. B.T. Mark, E. Orazem, *Electrochemical Impedance Spectroscopy*, John Wiley & Sons, Inc, Hoboken, NJ, 2008 (https://doi.org/10.1002/9780470381588)
39. R. L. McCreery, *Chem. Rev.* **108** (2008) 2646 (https://doi.org/10.1021/cr068076m)
40. A. Kriaa, N. Hamdi, E. Srasra, *Russ. J. Electrochem.* **43** (2007) 167 (https://doi.org/10.1134/S102319350702005X)
41. S. Gu, X. Kang, L. Wang, E. Lichtfouse, C. Wang, *Environ. Chem. Lett.* **17** (2019) 629 (https://doi.org/10.1007/s10311-018-0813-9)
42. L. Zhang, J. Cao, *J. Therm. Anal. Calorim.* **137** (2019) 1 (https://doi.org/10.1007/s10973-018-7947-7)
43. M. M. Lounasvuori, M. Rosillo-Lopez, C. G. Salzmann, D. J. Caruana, K. B. Holt, *Faraday Discuss.* **172** (2014) 293 (https://doi.org/10.1039/C4FD00034J)
44. H. Nara, D. Mukoyama, R. Shimizu, T. Mommaa, T. Osaka, *J. Power Sources* **409** (2019) 139 (https://doi.org/10.1016/j.jpowsour.2018.09.01)
45. Y. Abe, N. Hori, S. Kumagai, *Energies* **12** (2019) 4507 (https://doi.org/10.3390/en12234507)
46. M. Noked, E. Avraham, A. Soffer, D. Aurbach, *J. Phys. Chem., C* **113** (2009) 21319 (https://doi.org/10.1021/jp905987j)
47. G. Rasines, P. Lavel, C. Macías, M. Haro, C. O. Ania, J. L. Tirado, *J. Electroanal. Chem.* **671** (2012) 92 (http://dx.doi.org/10.1016/j.jelechem.2012.02.025)
48. Z. Chen, H. Zhang, C. Wu, Y. Wang, W. Li, *Desalination* **369** (2015) 46 (https://doi.org/10.1016/j.desal.2015.04.022).

Journal of the Serbian Chemical Society
JSCS@tmf.bg.ac.rs • www.shd.org.rs/JSCS
J. Serb. Chem. Soc. *88* (1) 55–68 (2023)
JSCS–5610
Original scientific paper
Published 1 August 2022

Highly selective water-compatible molecularly imprinted polymers for benzophenone-4

MILOŠ P. PEŠIĆ[1#], JUGOSLAV B. KRSTIĆ[2] and TATJANA Ž. VERBIĆ[1*#]

[1]*University of Belgrade – Faculty of Chemistry, Belgrade, Serbia and* [2]*University of Belgrade – Institute of Chemistry, Technology and Metallurgy – National Institute of the Republic of Serbia, Belgrade, Serbia*

(Received 25 March, revised 6 May, accepted 9 May 2022)

Abstract: Molecularly imprinting technology was applied for preparing selective sorbents for benzophenone-4 (BP4), an organic UV filter used in sunscreens and cosmetics. Several imprinted polymers were prepared by bulk polymerization, using BP4 as template. Combination of stability (mechanical and chemical), selectivity and robustness of the imprinted polymers with BP4 properties resulted in a successful imprinting process (imprinting factors in range 1.05–2.60). The prepared polymers were characterised by infrared spectroscopy, elemental analysis, conductometric titrations and nitrogen physisorption at 77 K. Adsorption capacities and selectivity towards 7 other organic UV filters (benzophenone-3, benzophenone-8, homosalate, butyl methoxydibenzoylmethane, ethyl hexyl salicylate, ethyl hexyl *p*-dimethylamino benzoate and ethyl hexyl *p*-methoxycinnamate) were determined, proving high adsorption capacity and high selectivity for BP4 binding. The highest adsorption capacity was observed for 4-vinylpyridine/ethylene glycol dimethacrylate co-polymer prepared in dimethyl sulfoxide (1.108 mmol g^{-1}). The imprinted polymer with the highest binding capacity was applied to solid phase extraction of BP4 from aqueous solutions with 98.5 % efficiency.

Keywords: UV filters; imprinting factor; binding selectivity.

INTRODUCTION

Molecularly imprinted polymers (MIPs) are smart synthetic materials which can be used for several applications:[1–4] as sorbents for solid phase extraction (SPE),[5–9] as stationary phase for chromatography,[10–15] as sensors,[16–18] artificial enzymes,[19–21] as systems for controlled drug delivery and release,[22–24] *etc.* Molecular imprinting technology (MIT) is based on interactions between template molecule and functional monomer in the presence of porogen. The chosen

* Corresponding author. E-mail: tatjanad@chem.bg.ac.rs
# Serbian Chemical Society member.
https://doi.org/10.2298/JSC22032540P

monomer should have at least one functional group which is likely to interact with the template. During the polymerization process monomer molecules, as present in excess, surround the template molecule, forming a pre-polymerization complex. Then, in the presence of a cross-linker, a rigid polymer network is formed usually by free radical polymerization. After the template is washed out, selective binding sites complementary to template molecules in size, shape and chemical characteristics remain in the polymer, enabling the template rebinding.[1] In some examples, only one monomer is used for the preparation of MIPs.[25,26] The above-described approach is known as non-covalent imprinting and presents the most commonly used approach in MIT. Interactions like van der Waals, hydrogen and ionic bonding are involved in non-covalent imprinting process and, later on, in template rebinding. Thus, the higher the variety and strength of monomer-template interactions, the more selective polymer with higher binding capacity is obtained.[1]

Imprinted polymers have good selectivity, chemical and mechanical stability; therefore, these materials can be universally applied in various fields of chemistry and biosciences.[2] Although extensive research is being done within the field, and many advances have been achieved in MIT in recent decades, MIPs are generally still lacking high binding efficiency. Most of the non-covalent MIPs described in the literature can bind only a small percent of the template amount initially used during polymerization.[25] Therefore, optimizing and fine tuning of polymerization conditions and the process itself to obtain highly selective polymers with high template binding efficiency is an on-going demand in MIT.[2]

The growing need for skin protection from the sun radiation has established UV filters as one of the emerging environmental contaminants.[27,28] Regularly used sunscreen cosmetic products contain a high amount of UV filters (up to 15 %). UV filters can be divided into inorganic (zinc oxide and titanium oxide) and organic (benzophenones, cinnamates, dibenzoylmethanes, triazole derivatives, salicylates, *etc*).[28]

Benzophenone-type UV-filters are major ingredients of sunscreen products nowadays. According to EU regulations, BP4 or sulisobenzone (Fig. 1) and its sodium salt, BP5, can be used in sunscreens up to 5%.[30] When released in the environment, several adverse effects have been noticed such as coral bleaching, estrogenic activity in fish and even endocrine disrupting effects are suspected.[27,31,32]

It is estimated that 40 % of coastal coral colonies worldwide are exposed to UV-filter pollution.[28,33] BP3 can cause oxidative stress in zooxanthellae, organisms that live in symbiosis with corals. The decrease of zooxanthellae causes the lightening of the brown colour of the corals.[27,32–34] BP4 was found in river, lake and sea water;[35] the EC_{50} value (half maximal effective concentration) of

BP4 is near 10 mg dm^{-3} in the *Isochrysis galbana*, *Scorpaenopsella armata*, *Paracentrotus lividus and Mytilus galloprovincialis*.[27,36]

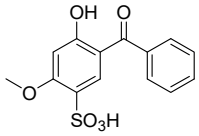

Fig. 1. Structure of benzophenone-4.

Although UV filters gained high attention with highly increased research interest in methods for pre-concentration and extractions from various samples with subsequent quantitation, only few papers describe MIT applied for development of UV filter imprinted polymers. Sun *et al*. described the application of MIP imprinted with BP2 for solid phase extraction (SPE) of four benzophenones from tap and river water. 4-vinylpyridine (4VP)/ethylene glycol dimetachrylate (EDMA) based polymer imprinted with benzophenone-2 (BP2) was successfully applied for the extraction of benzophenone-1 (BP1), BP2, benzophenone-4 (BP6) and benzophenone-8 (BP8).[37] Ayadi *et al*. described molecularly imprinted polyaniline on silica support for the selective adsorption of BP4 from aqueous media.[38] To the best of our knowledge, no other examples of polymers imprinted using BP-type UV-filters as templates were published so far.

Within this study, we used BP4 as the template molecule to prepare several imprinted polymers by bulk polymerization.[39] Different polymer constituents were used: monomers (*N,N*-dimethylaminoethyl methacrylate-DMAEM and 4VP), cross-linkers (divinylbenzene-DVB and EDMA), porogenic solvents (ACN and DMSO). Polymers were characterized using FT-infrared spectroscopy (FTIR), nitrogen adsorption and adsorption isotherms. Binding capacity and selectivity towards other UV-filters was determined. Elemental analysis (EA) and conductometric titrations were used in order to estimate total and accessible binding places. The goal was to prepare selective sorbents for BP4 with high binding capacity, which can be used as potential sorbents for BP4 extraction and pre-concentration during sample preparation.

EXPERIMENTAL

Apparatus

Infrared spectra were recorded using Thermo Scientific Nicolet 6700 FT-IR Spectrometer, ATR technique. HPLC measurements were done using Agilent Technologies HPLC instrument Series 1260 with quaternary pump, on-line degasser, auto sampler and diode array detector. Conductometric titrations were done using WTWCond330i with TetraCon325 conductometric cell. Elemental analysis was performed by combustion analysis on a Vario EL III C,H,N,S/O elemental analyzer (Elementar Analysesysteme, GmbH, Hanau, Germany). Chromabond vacuum manifold (Macherey-Nagel) was used for SPE extraction. For nitrogen physisorption Sorptomatic 1990 Thermo Finnigan analyzer was used. MultiBio RS24 (BioSan) rotator and Microspin 12 centrifuge (BioSan) were used for conducting binding experiments.

Reagents

Benzophenone-4 (BP4), benzophenone-3 (BP3), ethyl hexyl salicylate (OS), ethyl hexyl *p*-dimethylamino benzoate (PABA-O), *N,N*-dimethylaminoethyl methacrylate (DMAEM), divinylbenzene (DVB), azobisisobutyronitrile (AIBN) were purchased from Sigma Aldrich. HPLC grade methanol and acetonitrile were purchased from Fisher Scientific. Benzophenone-8 (BP8) was purchased from the Tokyo Chemical Industry. 4-vinylpyridine (4VP) and ethylene glycol dimethacrylate (EDMA) were purchased from Acros Organics. Butyl methoxydibenzoylmethane (AVB) and homosalate (HMS) were purchased from Merck.

Inhibitor remover (Sigma Aldrich) was used to remove polymerization inhibitors from 4VP, DMAEM and EDMA (5 mL of monomer/cross-linker was passed over 250 mg of inhibitor remover). DVB was purified using alumina, in the same way as EDMA. Commercially available BP4 is declared to have some percent of water bound. It was dried at 60 °C under vacuum, until no further change in mass was observed (color change from pale to clear lemon yellow was observed during drying). Other reagents were of analytical grade and used as received.

Preparation of imprinted and non-imprinted polymers

The imprinted polymers were prepared using bulk polymerization: template, monomer, cross-linker, porogen and polymerization initiator were placed in a glass vial. Upon dissolution, argon was purged through a pre-polymerization mixture for 5 min. AIBN was used as initiator (30 mg). Vials were tightly closed and left in an oil bath at 60 °C for 24 h. After polymerization was completed, the glass vials were broken and the polymer grounded in a mortar with pestle. The non-imprinted polymers were prepared as the imprinted ones, omitting the template presence. Composition of the prepared polymers is given in Table I.

TABLE I. Composition of prepared polymers

Polymer label	$m_{\text{BP4 template}}$ / mg (n / mmol)	V_{monomer} / μL (n / mmol)	$V_{\text{cross linker}}$ / mL	V_{porogen} / mL
NIP1	–	DMAEM 337 (2.0)	EDMA 1.888	ACN 2.730
MIP1	154.0 (0.5)	DMAEM 337 (2.0)	EDMA 1.888	ACN 2.730
NIP2	–	DMAEM 337 (2.0)	DVB 1.424	ACN 2.730
MIP2	154.0 (0.5)	DMAEM 337 (2.0)	DVB 1.424	ACN 2.730
NIP3	–	4VP 213 (2.0)	EDMA 1.888	DMSO 2.730
MIP3	154.0 (0.5)	4VP 213 (2.0)	EDMA 1.888	DMSO 2.730
NIP4	–	4VP 213 (2.0)	DVB 1.424	DMSO 2.130
MIP4	154.0 (0.5)	4VP 213 (2.0)	DVB 1.424	DMSO 2.130
NIP5	–	4VP 106.4 (1.0)	DVB 1.424	DMSO 2.000
MIP5	308.3 (1.0)	4VP 106.4 (1.0)	DVB 1.424	DMSO 2.000

Template was removed from the polymer by exhaustive washing using 2 % ammonia in methanol/water 1:1 volume ratio (process was monitored by HPLC supernatant analysis). The polymers were then washed several times with methanol and dried in an oven at 60 °C.

Binding experiments

Batch binding experiments were performed as follows: polymer 10.0±0.2 mg was weighed in a micro tube, and 2.000 mL of template solution in acetonitrile was added. The concentrations of template solution were 0.1–10 mmol dm^{-3} (0.1, 0.2, 0.5, 1.0, 2.0, 4.0, 6.0,

8.0 and 10.0). Micro tubes were shaken using a rotator for 60 min, centrifuged (10 min, 14,500 rpm) and template concentration in supernatant was determined by HPLC.

The adsorption capacity was determined according to:

$$Q = \frac{(c_0 - c_f)V}{m} \quad (1)$$

where Q stands for adsorption capacity (μmol g^{-1}), c_0 for total concentration of template at the beginning (mM), c_f – free concentration of template after binding (mmol dm^{-3}), V – volume of template solution used for binding experiment (mL) and m – mass of the polymer used for binding experiment (g)[25].

The imprinting factors were determined according to:[40]

$$IF = \frac{(n_{bound} / n_{free})_{MIP}}{(n_{bound} / n_{free})_{NIP}} \quad (2)$$

where IF stands for imprinting factor, n_{bound} / μmol – amount of the template bound to NIP/ /MIP and n_{free} / μmol – amount of the template free after binding.

Selectivity studies

10.0±0.2 mg of the imprinted polymer was weighed in a micro tube and 2.000 mL of 5.0 mmol dm^{-3} solution of selected UV filter was added. After 1 h of mixing, the polymer was removed by centrifugation, and UV filter concentration in supernatant was determined by HPLC according to procedure described in Section HPLC analysis.

HPLC analysis

BP4 was analyzed on Purospher Star RP18e 55-4 column, particle size was 3 μm, flow rate 1 mL min^{-1}, solvent A (1 % AcOH in water), solvent B (ACN), solvent volume ratio 80:20. Injection volume was 1.00 μL, column temperature 25 °C, detection wavelength 286 nm, retention time 3.30 min. Total method duration time was 4 min.

BP3 and BP8 were analyzed using Waters Symmetry C18 column, 3 mm×100 mm, 5 μm particle size. Flow rate was 0.6 mL/min, solvent A (water), solvent B (ACN), solvent volume ratio 30:70. Injection volume was 1.00 μL, column temperature 25 °C, total method duration time – 4 min. Retention times for BP3 and BP8 were: 2.27 and 1.46 min, respectively. For other UV filters, detection wavelengths were: 310 nm (OCT and PABA-O), 360 nm (AVB), 238 nm (OS and HMS). Retention times were OCT – 2,25 min, AVB – 2.09 min, OS – 2.64 min, HMS – 2.85 min and PABA-O – 2.32 min.

Solid phase extraction

100.0 mg of MIP4 was placed in an empty SPE cartridge with a frit on the bottom, PTFE filter (0.45 μm) was placed on the top of the polymer. Packed sorbent was washed with 1.000 mL of ACN, then 3 times with HPLC water (3×0.500 mL). 50 mL of BP4 solution (5.00 mg L^{-1}) was passed through the SPE cartridge at flow rate of approx. 1 mL min^{-1}. The sorption was repeated using the same solution (once already passed). BP4 concentration was determined in filtrate using HPLC.

Conductometric titrations

30–50 mg of polymer was placed in a titration cell, 20.0 mL of ACN added, suspension was stirred using a magnetic stirrer and titrated with 0.1024 M HCl solution at 25.0±0.5 °C. The amount of the N-containing group was calculated according to end-point HCl volume.

FTIR

FTIR spectra were recorded for NIPs, washed MIPs and MIPs that were washed and subsequently tested for template re-binding. Samples of polymers with bound template were obtained after binding experiments when a 10.0 mM template solution was used. After centrifugation, polymer was washed with a minimal volume of ACN, and dried in oven at 60 °C and atmospheric pressure for 24 h.

Nitrogen physisorption

Nitrogen physisorption was determined at 77 K. Samples were degassed for 1 h at room temperature and kept at 50 °C under vacuum for 24 h. The value of specific surface area of samples was determined using Braunauer, Emmet, Teller method (BET).

RESULTS AND DISCUSSION

Benzophenone 4 (Fig. 1) is a diprotic acid containing the sulfonic ($–SO_3H$) and the phenolic –OH group. Acting as a strong acid, sulfonic group can form ionic pairs with basic monomers. Hydroxyl group in ortho position is forming a pseudo six-membered ring with benzophenone group and, as such, it most probably doesn't significantly contribute to the stability of the pre-polymerization complex. Methoxy ($–OCH_3$) group in the position 4 can act as H-bond acceptor (HBA). Two basic monomers were used in our study – DMAEM and 4VP. Both were expected to form ionic pairs and hydrogen bonds with template molecules, as well as to establish π–π stacking interactions (in case of 4VP). EDMA and DVB were used as cross-linkers, expecting that through π–π interactions DVB would contribute more to the binding capacity of the polymers than EDMA. If so, polymers prepared with DVB would have higher adsorption capacity than EDMA polymers. This was confirmed by binding experiments (Section *Binding isotherms*).

ACN is a commonly used solvent for MIP preparation because it favours non-covalent interactions.[40] Thus, ACN was our first choice for porogenic solvent, but was not applicable to all polymers preparation. When a combination of 4VP and EDMA/DVB was used, not all components were soluble in ACN. It seems that the ionic pair between 4VP and BP4 (or complex in general) is not soluble in EDMA/ACN or DVB/ACN. Monomer/template complex forms immediately upon mixing of these two components, which is easily observed by the colour change – mixture turns red (Fig. 2), 4VP is colourless to pale yellow liquid and BP4 is yellow solid.

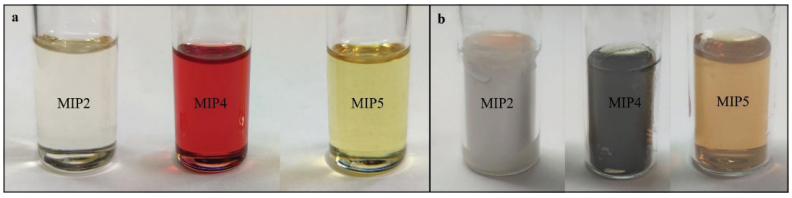

Fig. 2. MIP2, MIP4 and MIP5: a) pre-polymerization complexes and b) prepared polymers.

As this complex was not soluble in ACN, ACN/toluene mixtures, nor in acetone, other solvent had to be used. Therefore, dry DMSO was used even though it doesn't enable hydrogen bonding and is not the best choice for porogen. Pre-polymerization mixtures and obtained monolith polymers are shown in Fig. 2.

Binding isotherms

Binding of BP4 for NIPs and MIPs was conducted by batch binding experiments.[25] Binding isotherms were obtained as $Q = f(c_f)$[40] where Q stands for the adsorption capacity (μmol g^{-1}) and c_f for the free concentration of template after binding (mmol dm^{-3}), as defined in Eq. (1). Polymers showed very high capacities for binding BP4. As it can be seen on Fig. 3, BP4 binding capacity for each NIP is much lower than for the corresponding MIPs. Polymer MIP4 showed the highest binding capacity.

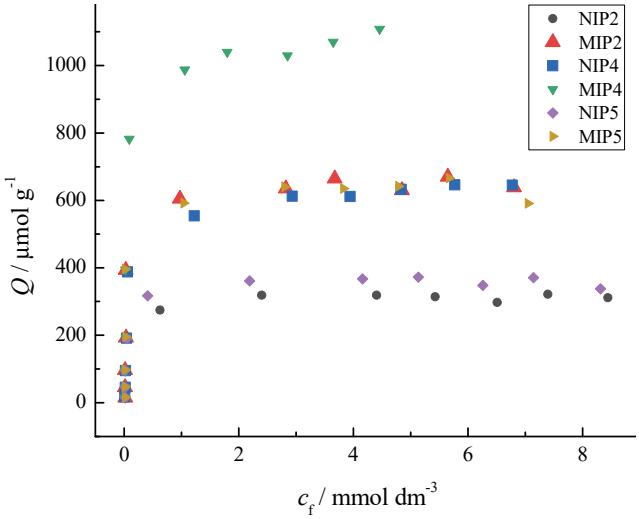

Fig. 3. Binding isotherms for selected polymers (Table I).

Obtained results imply that the imprinting process was successful. If template – monomer ionic pairs are formed, the formation of high-affinity binding sites is expected, as ionic interactions prevail as the dominant ones. Each available nitrogen-containing part of the polymer will bind the template. So, the only difference between the imprinted and the non-imprinted polymer is that MIP has more available monomer units than NIP because the template was present during polymerization.

Imprinting effect

Imprinting factor is calculated as ratio of the amount of template bound to imprinted *vs.* non-imprinted polymer. The imprinting factors for polymer pairs

MIP/NIP 2, 4 and 5, in ACN/water mixtures and ACN are shown in Table II. It is interesting that the presence of water in rebinding medium has a more prominent effect on imprinted polymers.

TABLE II. Imprinting factors (*IF*) for MIP/NIP pairs in ACN (IF_{ACN}) and in aqueous solutions containing 20 vol. % of ACN ($IF_{ACN\text{-}water}$)

Polymer	IF_{ACN}	$IF_{ACN\text{-}water}$ (20 vol. % ACN)	Improvement ($IF_{ACN\text{-}water}/IF_{ACN}$)
MIP1:NIP1	1.05	1.14	1.10
MIP2:NIP2	2.53	2.64	1.04
MIP3:NIP3	1.40	1.75	1.25
MIP4:NIP4	2.60	3.17	1.22
MIP5:NIP5	2.10	3.43	1.63

The imprinting factors in aqueous medium, for DVB polymers, are higher than in ACN, but the binding percentage (Table III) of the template to the polymer is lower. If water is present in porogen, some interactions between the template and the monomer, like hydrogen bonding, are disrupted. This leads to lower binding efficiency, but to higher imprinting factor. However, as the imprinted polymers have specific (imprinted) binding sites, the effect of water is lower than in non-imprinted ones. The improvement of imprinting factors in aqueous media compared to ACN is also shown in Table II (calculated as $IF_{ACN\text{-}water}/IF_{ACN}$). High imprinting factors in aqueous medium are of considerable importance when the application of these polymers in aqueous samples is considered.

TABLE III. Binding of BP4 to studied polymers calculated as the amount of bound BP4 relative to starting BP4 concentration (10 mmol dm^{-3})

Polymer	Binding of BP4 (ACN) / %	Binding of BP4 (20 % ACN, *V*/*V*) / %
NIP1	29.54	26.64
MIP1	30.52	29.38
NIP2	15.57	11.05
MIP2	31.94	24.69
NIP3	30.88	18.89
MIP3	38.61	28.96
NIP4	32.25	16.31
MIP4	55.41	38.22
NIP5	16.89	10.70
MIP5	29.54	29.10

Adsorption capacities

The measured adsorption capacities for imprinted polymers were in the range 0.591–1.108 mmol g^{-1} of BP4. These capacities are much higher than those described in literature for "regular" MIPs for other templates. Ayadi *et al.*[39]

described polymers for BP UV filters binding which had a capacity of 27.90 or 96.06 μmol g^{-1}.

The adsorption capacities obtained from binding experiments were compared to those calculated from the polymer composition (based on monomer composition), but also those obtained from elemental analysis and conductometric titrations (Fig. 4).

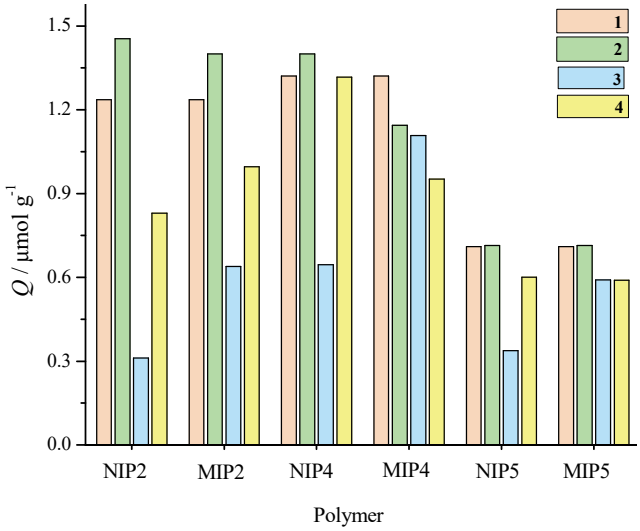

Fig. 4. 1: Calculated content of N – based on monomer composition, 2: N content determined by EA, 3: adsorption capacity – determined from adsorption isotherms, 4: monomer content determined by conductometric titration – HCl consumption.

According to the elemental analysis results (Supplementary material to this paper, Table S-V), polymers have adsorption capacity in the range 0.714 mmol g^{-1} (MIP5) up to 1.454 mmol g^{-1} (MIP4). Capacity was calculated according to the content of nitrogen (%) in the polymer, as all nitrogen in the polymer originates from the functional monomer. As can be seen in Fig. 4, all polymers have lower experimentally determined adsorption capacity than obtained from elemental analysis or based on the monomer and cross-linker composition. The only exception is polymer MIP4, where the adsorption capacity is very close to the determined content of N (EA data) and similar to the calculated nitrogen content, proving the most successful imprinting process for MIP4. To the best of our knowledge, this represents a unique example in the literature published so far.

Conductometric titrations were done to check the accessibility of monomer units in the polymer. Accessible binding sites were calculated according to 0.1 mol dm^{-3} HCl titration volume (titration graphs shown in Supplementary material, Figs. S-1 and S-2). The values obtained by conductometric titrations are

in between the calculated and the determined N, on one side, and the adsorption capacity on the other side. This can be explained as follows: not all monomer units are available for the template binding, but also, there are units not available for titration with HCl during the applied equilibration time. Again, there is one exception – MIP4.

BET surface (Supplementary material, Table S-VIII) areas are larger for MIPs compared to NIPs. However, it can be seen that binding capacity is not in direct correlation with specific surface area, *i.e.*, MIP4 (663 m^2 g^{-1}) and MIP5 (634 m^2 g^{-1}) have very similar BET areas, but the binding capacity for these two polymers differ almost twice (1.108 mmol g^{-1} for MIP4, 0.591 mmol g^{-1} for MIP5). MIP2/NIP2 are found to be mesoporous materials, while MIP4/NIP4 and MIP5/NIP5 seem to be microporous.

Selectivity studies

Selectivity of the prepared polymers was studied by comparison of the binding of UV filters from few groups of organic UV filters. In Fig. 5, the adsorption capacities are shown for template and other studied UV filters when binding was done using 5 mM solutions.

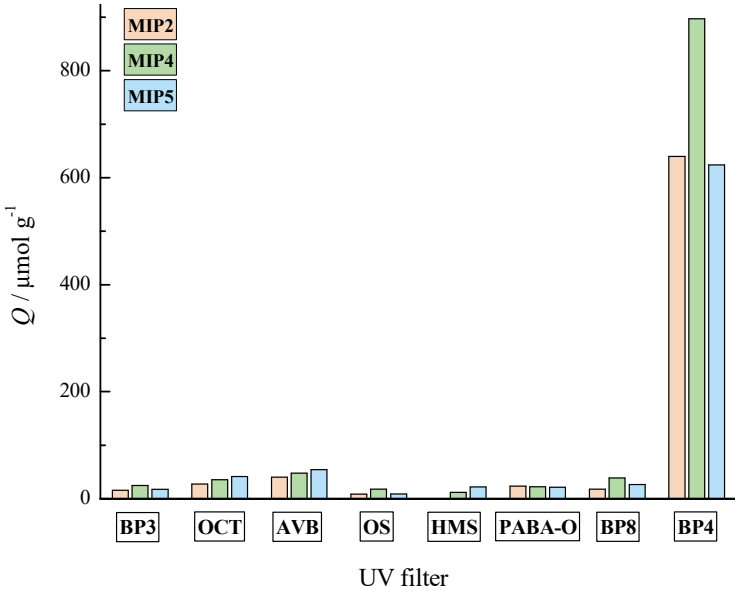

Fig. 5. Selectivity of imprinted polymers towards other UV filters.

As it can be seen, the binding of BP4 (55.4 %) compared to other UV filters (<5.5 %) is much higher due to different type of interactions between template and polymer: the template is bound to the polymer by strong ionic interactions between sulfonic group of the template and pyridine core (or amino group of

DMAEM) in the polymer. Stronger binding is also a consequence of hydrogen bonding between the –OH group of the template and pyridine core, even though the –OH group is at least partially bound in pseudo-six-membered ring with benzophenone oxygen. None of other UV filters have the acidic group as BP4 has, so the rest of the examined compounds bind to polymers mainly by hydrogen bonding.

Solid-phase extraction of BP4 from aqueous solutions

With MIP4 as a sorbent, 95.0 % of BP4 was adsorbed after the first elution. If the same BP4 solution was passed over MIP4 for the second time, the total of 98.5 % of BP4 adsorption was achieved. The obtained results indicate that the prepared imprinted polymer can be successfully applied for BP4 removal from aqueous solutions. The possibility of extraction from aqueous solutions is crucial for the application in real samples analysis as BP4 can be found in water ecosystems.[36]

Infrared spectroscopy

There is no difference between MIP4 (Fig. 6a) and NIP4 (Fig. 6c) in FTIR spectra, indicating that the removal of the template molecule from the imprinted polymer was fully achieved by the applied washing procedure.

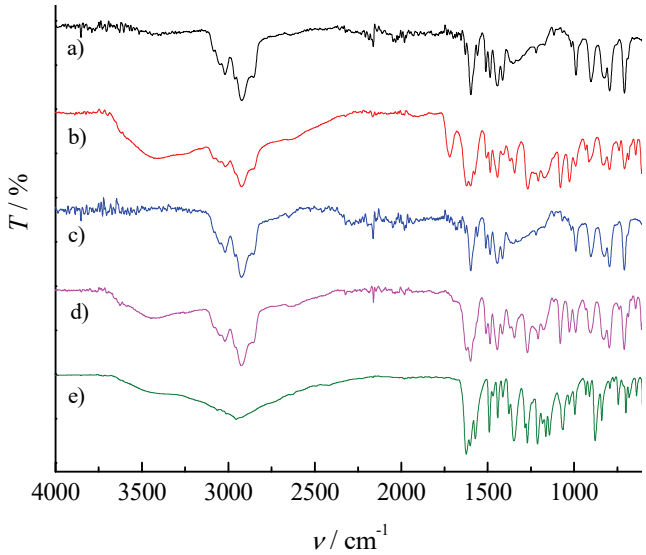

Fig. 6. Infrared spectra for selected polymers: a) MIP4; b) MIP4 with re-bound BP4; c) NIP4; d) NIP4 with bound BP4; e) BP4.

The difference within 1500–1700 cm^{-1} region between polymers with re--bound template (Fig. 6b and d) and unbound ones (Fig. 6a and c) confirms the

presence of the template when compared to the spectra of pure template (Fig. 6e). Furthermore, the presence of the re-bound template in spectra of Fig. 6b and d is visible within hydrogen bonds region (3300–3500 cm^{-1}). This is probably due to moisture traces present in BP4.

CONCLUSION

Benzophenone 4 (BP4) is one of the most commonly used organic UV filter in sunscreen lotions and other cosmetic products. As an emerging environmental contaminant, the need for quantitative determination upon environmental sample preconcentration has pointed out the need for BP4 selective sorbents development. Five polymer pairs of molecularly imprinted (MIPs) and nonimprinted polymers (NIPs) were prepared within this study. The polymers were characterized by template binding studies, infrared spectroscopy, elemental analysis, conductometric titrations and nitrogen adsorption analysis. All MIPs were successfully imprinted with BP4. However, the imprinting factor was higher in polymers containing DVB (2.10–2.60) compared to EDMA (1.05–1.40) polymers. The prepared polymers have high adsorption capacity for template binding – up to 1.108 mmol g^{-1} (MIP4). Binding of the template to prepared MIPs was compared to binding of 7 other organic UV filters, proving high BP4 MIPs selectivity. The nitrogen physisorption showed that differences in adsorption capacity are not the consequence of different specific surface areas. Finally, MIP4 was used as a sorbent for solid phase extraction of BP4 from aqueous solution, with 98.5 % sorption efficiency. The obtained results are promising for the application of MIPs as solid phase extraction sorbents for BP4 preconcentration from real samples, which is the subject of our ongoing study.

SUPPLEMENTARY MATERIAL

Additional data and information are available electronically at the pages of journal website: https://www.shd-pub.org.rs/index.php/JSCS/article/view/11718, or from the corresponding author on request.

Acknowledgement. The authors would like to thank the Ministry of Education, Science and Technological Development of Republic of Serbia (Grant No: 451-03-68/2022-14/200168 and 451-03-68/2022-14/200026) for financial support.

ИЗВОД

ВИСОКО СЕЛЕКТИВНИ ВОДОКОМПАТИБИЛНИ МОЛЕКУЛСКИ ОБЕЛЕЖЕНИ ПОЛИМЕРИ ЗА БЕНЗОФЕНОН-4

МИЛОШ П. ПЕШИЋ[1], ЈУГОСЛАВ Б. КРСТИЋ[2] и ТАТЈАНА Ж. ВЕРБИЋ[1]

Универзитет у Београду – Хемијски факултет, Београд и [1]Универзитет у Београду – Институт за хемију, технологију и металургију – Институт од националног значаја за Републику Србију, Београд

Технологија молекулског обележавања примењена је у синтези селективних сорбената за бензофенон-4 (BP4), органски UV филтер који се користи у кремама за сунчање и другим козметичким производима. Полимери су добијени полимеризацијом у маси,

користећи (BP4) као матрицу. Комбинацијом стабилности (механичке и хемијске), селективности и робусности молекулски обележених полимера са својствима BP4 извршено је успешно обележавање (фактор обележавања 1,05–2,60). Карактеризација добијених полимера је извршена применом инфрацрвене спектроскопије, елементалне анализе, кондуктометријских титрација и физисорпције азота на 77 K. Адсорпциони капацицети и селективност испитани су за 7 других органских UV филтера (бензофенон-3, бензофенон-8, хомосалат, бутилметоксидибензоилметан, етилхексил-салицилат, етилхексил-*p*-диметиламинобензоат и етилхексил-*p*-метоксицинамат), потврђујући велики адсорпциони капацитет и високу селективност за везивање BP4. Највећи адсорпциони капацитет показао је ко-полимер 4-винилпиридина и дивинилбензена добијен коришћењем диметил-сулфоксида као порогена (1,108 mmol/g). Полимер са највећим капацицетом за везивање BP4 примењен је као сорбент за екстракцију чврстом фазом BP4 из водених раствора са ефикасношћу од 98,5 %.

(Примљено 25. марта, ревидирано 6. маја, прихваћено 9. маја 2022)

REFERENCES

1. B. Sellergren, *Molecularly Imprinted Polymers: Man-Made Mimics of Antibodies and Their Applications in Analytical Chemistry*, Elsevier, Amsterdam, 2001. (ISBN: 978-0444547859)
2. *Handbook of Molecularly Imprinted Polymers*, C. Alvarez-Lorenzo, A. Concheiro (Eds.), Smithers Rapra, Shrewsbury, 2013 (ISBN: 978-1847359605)
3. *Molecularly Imprinted Materials: Science and Technology*, M. Yan, O. Ramström (Eds.), Marcel Dekker, New York, 2005 (ISBN: 978-0367578190)
4. *Molecular Imprinting of Polymers*, Landes Bioscience, S. Piletsky, A.P.F. Turner (Eds.), Georgetown, TX, 2006 (ISBN: 978-1587062193)
5. D. Sun, Z. Song, Y. Zhang, Y. Wang, M. Lv, H. Liu, L. Wang, W. Lu, J. Li, L. Chen, *Front. Environ. Chem*. **2** (2021) 703961 (https://doi.org/10.3389/fenvc.2021.703961)
6. F. Qiao, H. Sun, H. Yan, K. Row, *Chromatographia* **64** (2006) 625 (https://doi.org/10.1365/s10337-006-0097-2)
7. M. Sanagi, S. Salleh, W. Ibrahim, A. Naim, D. Hermawan, M. Miskam, I. Hussain, H. Aboul-Enein, *J. Food Composit. Anal*. **32** (2013) 155 (https://doi.org/10.1016/j.jfca.2013.09.001)
8. M. Lasakova, P. Jandera, *J. Sep. Sci*. **32** (2009) 799 (https://doi.org/10.1002/jssc.200800506)
9. F. Tamayo, E. Turiel, A. Martin-Esteban, *J. Chromatogr., A* **1152** (2007) 32 (https://doi.org/10.1016/j.chroma.2006.08.095)
10. Y. Huang, C. Zheng, Z. Liu, *Curr. Org. Chem*. **15** (2011) 1863 (https://doi.org/10.2174/138527211795656651)
11. W. Cheong, S. Yang, F. Ali, *J. Sep. Sci.* **36** (2013) 609 (https://doi.org/10.1002/jssc.201200784)
12. W. Cheong, F. Ali, J. Choi, J. Lee, K. Sung, *Talanta* **106** (2013) 45 (https://doi.org/10.1016/j.talanta.2012.11.049)
13. O. Baltrons, M. Lopez-Mesas, C. Palet, F. Derf, F. Porter-Koltalo, *Anal. Methods* **5** (2013) 6297 (https://doi.org/10.1039/C3AY41227J)
14. M. Malik, H. Shaikh, G. Mustafa, M. Bhanger, *Sep. Purif. Rev*. **48** (2019) 179 (https://doi.org/10.1080/15422119.2018.1457541)
15. T. Hishiya, H. Asunama, M. Komiyama, *Polym. J*. **35** (2003) 440 (https://doi.org/10.1295/polymj.35.440)
16. Y. Saylan, S. Akgonullu, H. Yavuz, S. Unal, *Sensors* **19** (2019) 1279 (https://dx.doi.org/10.3390%2Fs19061279)

17. K. Haupt, K. Mosbach, *Chem. Rev*. **100** (2000) 2495 (https://doi.org/10.1021/cr990099w)
18. N. Leibl, K. Haupt, C. Gonzato, L. Duma, *Chemosensors* **9** (2021) 123 (https://doi.org/10.3390/chemosensors9060123)
19. H. Lan, *PhD Thesis*, Iowa state University, 2018 (https://dr.lib.iastate.edu/entities/publication/baf42fc0-5fec-465e-a78e-d8a0524c44f7)
20. D. Mathew, B. Thomas, K. Devaky, *Artif. Cells Nanomed. Biotechnol*. **47** (2019) 1149 (https://doi.org/10.1080/21691401.2019.1576703)
21. X. li, M. Zangiabadi, Y. Zhao, *J. Am. Chem. Soc*. **143** (2021) 5172 (https://doi.org/10.1021/jacs.1c01352)
22. S. Zaidi, *Mater. Sci. Technol*. **3** (2020) 2589 (https://doi.org/10.1016/j.mset.2019.10.012)
23. S. He, L. Zhang, S. Bai, H. Yang, Z. Cui, X. Zhang, Y. Li, *Eur. Polym. J.* **143** (2021) (https://doi.org/10.1016/j.eurpolymj.2020.110179)
24. R. Liu, A. Poma, *Molecules* **26** (2021) 3589 (https://doi.org/10.3390/molecules26123589)
25. M. Pesic, M. Todorov, G. Becskereki, G. Horvai, T. Verbic, B. Tóth, *Talanta* **217** (2020) 121075 (https://doi.org/10.1016/j.talanta.2020.121075)
26. M. Sibrian-Vazquez, D. Spivak, *J. Am. Chem. Soc.* **126** (2004) 7827 (https://doi.org/10.1021/ja038961b)
27. L. L. R. de Miranda, K. E. Harvey, A. Ahmed, S. C. Harvey, *Environ. Monit. Assess.* **193** (2021) 1 (https://doi.org/10.1007/s10661-021-09626-6)
28. Y. Huang, P. Wang, J. C. F. Law, Y. Zhao, Q. Wei, Y. Zhou, Y. Zhang, H. Shi, K. S. Y. Leung, *Environ. Int*. **143** (2020) 105961 (https://doi.org/10.1016/j.envint.2020.105961)
29. Y. Huang, J. C. F. Law, T. K. Lam, K. S. Y. Leung, *Sci. Total. Environ*. **755** (2021) 142486 (https://doi.org/10.1016/j.scitotenv.2020.142486)
30. *Regulation (EC) No. 1223/2009 of the European Parliament and of the Council of 30 November 2009*, Official Journal of the European Union (2009) L 342/59–L 342/209 (http://data.europa.eu/eli/reg/2009/1223/oj)
31. C. A. Downs, E. Kramarsky-Winter, J. E. Fauth, R. Segal, O. Bronstein, R. Jeger, Y. Lichtenfeld, C. M. Woodley. P. Pennington Y. Loya, *Ecotoxicol.* **23** (2014) 175 (https://doi.org/10.1007/s10646-013-1161-y)
32. C. Corinaldesi, F. Marcellini, E. Nepote, E. Damiani, R. Danovaro, *Sci. Total Environ*. **637** (2018) 1279 (https://doi.org/10.1016/j.scitotenv.2018.05.108)
33. C. A. Downs, E. Kramarsky-Winter, R. Segal, J. Fauth, S. Knutson, O. Bronstein, F. R. Ciner, R. Jeger, Y. Lichtenfeld, C. M. Woodley, P. Pennington, K. Cadenas, A. Kushmaro, Y. Loya, *Arch. Environ. Contam. Toxicol*. **70** (2016) 26 (https://doi.org/10.1007/s00244-015-0227-7)
34. O. Ben-Zvi, G. Eyal, Y. Loya, *Hydrobiologia* **759** (2015) 15 (https://doi.org/10.1007/s10750-014-2063-6)
35. B. Kasprzyk-Hordern, R. Dinsdale, A. Guwy, *Water Research* **43** (2009) 363 (https://doi.org/10.1016/j.watres.2008.10.047)
36. E. Paredes, S. Pérez, R. Rodil, J. B. Quintana, R. Beiras, *Chemosphere* **104** (2014) 44 (https://doi.org/10.1016/j.chemosphere.2013.10.053)
37. H. Sun, Y. Li, C. Huang, J. Peng, J. Yang, X. Sun, S. Zang, J. Chen, X. Zhang, *J. Sep. Sci.* **38** (2015) 3412 (https://doi.org/10.1002/jssc.201500419)
38. C. Ayadi, A. Anene, R. Kalfat, Y. Chevalier, S. Hbaieb, *Colloids Surfaces A* **567** (2019) 32 (https://doi.org/10.1016/j.colsurfa.2019.01.042)
39. Z. Dorko, A. Szakolczai, T. Verbic, G. Horvai, *J. Sep. Sci.* **38** (2015) 4240 (https://doi.org/10.1002/jssc.201500874)
40. *Molecularly Imprinted Polymers in Biotechnology*, B. Mattiasson, L. Ye (Eds.), Springer International Publishing, 2015 (ISBN: 978-3319207292).

Journal of the Serbian Chemical Society
JSCS@tmf.bg.ac.rs • www.shd.org.rs/JSCS
J. Serb. Chem. Soc. *88* (1) S26–S29 (2023) *Supplementary material*

SUPPLEMENTARY MATERIAL TO

Highly selective water-compatible molecularly imprinted polymers for benzophenone-4

MILOŠ P. PEŠIĆ[1], JUGOSLAV B. KRSTIĆ[2] and TATJANA Ž. VERBIĆ[1]*

[1]*University of Belgrade – Faculty of Chemistry, , Belgrade, Serbia and* [2]*University of Belgrade – Institute of Chemistry, Technology and Metallurgy – National Institute of the Republic of Serbia, Belgrade, Serbia*

J. Serb. Chem. Soc. *88* (1) (2023) 55–68

Table S-I. NIP2 adsorption isotherm data

c_0 / mmol dm^{-3}	0.10	0.25	0.50	1.00	2.00	4.00	6.00	7.00	8.00	9.00	10.00
c_f / mmol dm^{-3}	0.03	0.02	0.02	0.03	0.63	2.41	4.41	5.43	6.51	7.39	8.44
Q / μmol g^{-1}	13.93	45.58	96.12	193.29	274.39	318.78	318.60	314.03	297.59	321.21	311.38

Table S-II. MIP2 NIP2 adsorption isotherm data

c_0 / mmol dm^{-3}	0.10	0.25	0.50	1.00	2.00	4.00	5.00	6.00	7.00	8.00	9.00	10.00
c_f / mmol dm^{-3}	0.03	0.02	0.02	0.04	0.03	0.98	1.80	2.82	3.68	4.85	5.65	6.81
Q / μmol g^{-1}	14.86	45.73	96.51	192.98	393.87	604.90	639.80	635.30	664.65	629.83	669.76	638.89

Table S-III. NIP4 adsorption isotherm data.

c_0 / mmol dm^{-3}	0.10	0.25	0.50	1.00	2.00	4.00	6.00	7.00	8.00	9.00	10.00
c_f / mmol dm^{-3}	0.01	0.02	0.03	0.04	0.06	1.23	2.94	3.94	4.83	5.77	6.77
Q / μmol g^{-1}	17.09	45.55	94.65	191.36	387.67	554.28	612.31	611.27	633.01	646.06	645.06

Table S-IV. MIP4 adsorption isotherm data

c_0 / mmol dm^{-3}	0.10	0.25	0.50	1.00	2.00	4.00	5.00	6.00	7.00	8.00	9.00	10.00
c_f / mmol dm^{-3}	0.02	0.03	0.03	0.04	0.03	0.09	0.51	1.06	1.80	2.85	3.65	4.46
Q / μmol g^{-1}	15.11	44.66	94.65	192.72	394.69	781.84	897.53	987.70	1039.79	1029.14	1069.46	1108.14

Table S-V. NIP5 adsorption isotherm data

c_0 / mmol dm^{-3}	0.10	0.25	0.50	1.00	2.00	4.00	6.00	7.00	8.00	9.00	10.00
c_f / mmol dm^{-3}	0.02	0.02	0.02	0.05	0.41	2.19	4.16	5.14	6.26	7.14	8.31
Q / μmol g^{-1}	15.55	46.42	96.29	190.11	317.22	361.49	367.37	372.58	347.90	371.22	337.98

* Corresponding author. E-mail: tatjanad@chem.bg.ac.rs

Table S-VI. MIP5 adsorption isotherm data

c_0 / mmol dm^{-3}	0.10	0.25	0.50	1.00	2.00	4.00	5.00	6.00	7.00	8.00	9.00	10.00
c_f / mmol dm^{-3}	0.02	0.02	0.01	0.03	0.02	1.04	1.88	2.80	3.83	4.79	5.67	7.05
Q / μmol g^{-1}	15.88	46.85	97.16	194.67	395.85	591.76	624.18	639.79	634.64	641.82	666.08	590.73

c_0 – total concentration of BP4, c_f – free concentration of BP4 after binding, Q – adsorption capacity

Table S-VII. Elemental analysis data for polymer pairs NIP/MIP2, NIP4/MIP4 and NIP5/MIP5

Element	Content, %		
	C	H	N
NIP2	84.05	8.47	2.04
MIP2	83.11	8.59	1.96
NIP4	88.14	8.13	1.96
MIP4	79.26	7.26	1.64
NIP5	85.78	7.80	1.00
MIP5	89.74	8.01	1.00

Table S-VIII. Capacity data for polymer pairs NIP/MIP2, NIP4/MIP4 and NIP5/MIP5.

Polymer	c_N/ mmol g^{-1}		Adsorption capacity, mmol g^{-1}	Content of N (cond), mmol g^{-1}	Specific surface area (BET), m^2 g^{-1}
	Calculated	Determined			
NIP2	1.236	1.454	0.311	0.830	290
MIP2	1.236	1.400	0.639	0.996	339
NIP4	1.321	1.400	0.645	1.317	539
MIP4	1.321	1.145	1.108	0.952	663
NIP5	0.710	0.714	0.338	0.601	551
MIP5	0.710	0.714	0.591	0.590	634

Calculated content of N – based on monomer composition, determined content of N – N determined by EA, adsorption capacity – determined from adsorption isotherms, N content determined by conductometric titration – based on HCl consumption

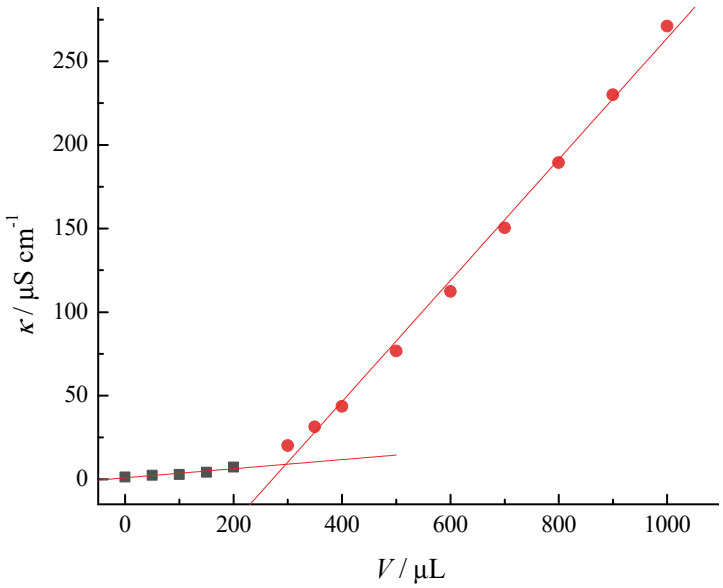

Figure S-1. Example of titration graph for conductometric titration of MIP5 with HCl. 52.6 mg of polymer was placed in a titration cell, 20.0 mL of ACN added, suspension was stirred using a magnetic stirrer and titrated with 0.1024 mol dm^{-3} HCl solution at 25.0±0.5 °C

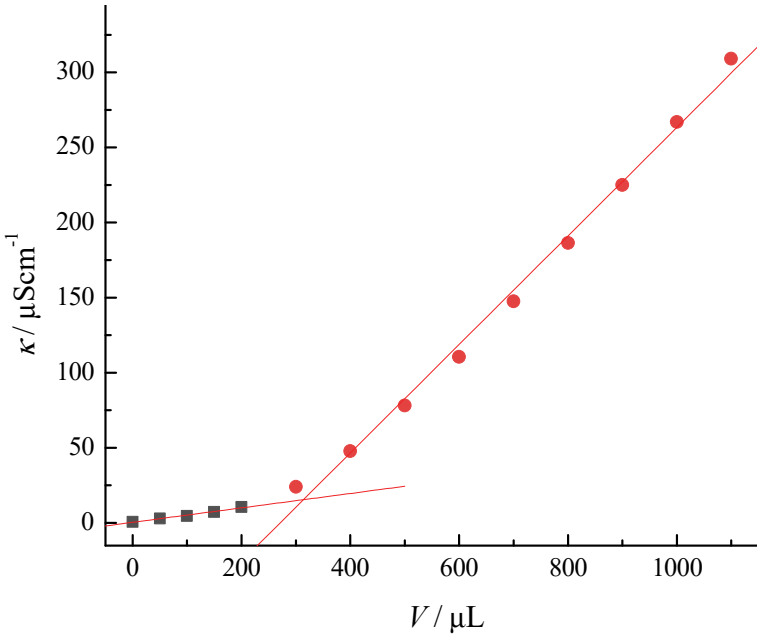

Figure S-2. Example of titration graph for conductometric titration of NIP5 with HCl. 50.2 mg of polymer was placed in a titration cell, 20.0 mL of ACN added, suspension was stirred using a magnetic stirrer and titrated with 0.1024 mol dm^{-3} HCl solution at 25.0±0.5 °C

Table S-IX. Selectivity data for binding of UV filters to MIP2

Compound	BP3	OCT	AVB	OS	HMS	PABA-O	BP8	BP4
c_0 / mmol dm^{-3}	5.00	5.00	5.00	5.00	5.00	5.00	5.00	5.00
c_f / mmol dm^{-3}	4.92	4.86	4.80	4.96	0.00	4.88	4.91	1.80
Q / μmol g^{-1}	15.90	27.51	40.14	8.40	0.00	23.80	18.19	639.80

Table S-X. Selectivity data for binding of UV filters to MIP4

Compound	BP3	OCT	AVB	OS	HMS	PABA-O	BP8	BP4
c_0 / mmol dm^{-3}	5.00	5.00	5.00	5.00	5.00	5.00	5.00	5.00
c_f / mmol dm^{-3}	4.88	4.82	4.76	4.91	4.94	4.89	4.81	0.51
Q / μmol g^{-1}	24.41	35.31	47.82	18.04	11.82	22.64	38.86	897.53

Table S-XI. Selectivity data for binding of UV filters to MIP5

Compound	BP3	OCT	AVB	OS	HMS	PABA-O	BP8	BP4
C_0 / mmol dm^{-3}	5.00	5.00	5.00	5.00	5.00	5.00	5.00	5.00
C_f / mmol dm^{-3}	4.91	4.79	4.73	4.95	4.89	4.89	4.87	1.88
Q / μmol g^{-1}	17.60	41.72	54.54	9.22	21.84	21.24	26.35	624.16

c_0 – total concentration of BP4, c_f – free concentration of BP4 after binding, Q – adsorption capacity

Journal of the Serbian Chemical Society
JSCS-info@shd.org.rs • www.shd.org.rs/JSCS
J. Serb. Chem. Soc. *88* (1) 69–82 (2023)
JSCS–5611
Original scientific paper
Published 30 September 2022

Synthesis of activated carbons from water hyacinth biomass and its application as adsorbents in water pollution control

AHMAD HAKKY MOHAMMAAD* and MIRJANA KIJEVČANIN#

University of Belgrade Faculty of Technology and Metallurgy, Karnegijeva 4, 11000 Belgrade, Serbia

(Received 5 December 2021, revised 10 February, accepted 11 February 2022)

Abstract: The water hyacinth biomass was used for the synthesis of activated carbons in a process of chemical activation with $ZnCl_2$, followed by controlled pyrolysis. The applied impregnation weight ratios $ZnCl_2$ and dry hyacinth biomass were in the range of 0.5–3.5. The carbonization was conducted at four different temperatures (400–700 °C) under an inert atmosphere. The highest yield of activated carbon was obtained for the impregnation ratio of 0.5 and carbonization temperature of 400 °C. The samples were characterized using elemental analysis, adsorption–desorption isotherms of nitrogen and SEM analysis. The activated carbon obtained with an impregnation ratio 2.0 and carbonization temperature of 500 °C ($2.0AC_{500}$) showed the highest values of specific surface area and total pore volume of 1317 m^2 g^{-1} and 0.697 cm^3 g^{-1}, respectively. The adsorption of glyphosate, pesticide with a strong negative environmental impact, was a fast process, with the equilibrium time of 120 min. The adsorption isotherms were fitted with Langmuir and Freundlich model. The Langmuir adsorption capacity of q_{max} = 240.8 mg g^{-1} for $2.0AC_{500}$ classified the selected adsorbent as a very efficient one. The tested adsorption process followed the kinetics of the pseudo-second-order model.

Keywords: carbonization; characterization; pyrolysis; pesticide removal; adsorption; modelling.

INTRODUCTION

One of the leading environmental problems in Africa and Asia is the presence of water hyacinth (*Eichhornia crassipes*) in natural waters (mostly rivers and lakes). Water hyacinth forms dense and impenetrable floating mats on water surfaces, causing considerable problems in aquatic ecosystems. This plant has shown a strong negative impact on the biodiversity of the aquatic system in many

* Corresponding author. E-mail: ahmadhakky59@gmail.com
# Serbian Chemical Society member.
https://doi.org/10.2298/JSC212121006M

ways: its presence leads to a significant reduction in the amount of light in the water, prevents access to wildlife (birds in particular) thereby disrupting the normal functioning of fauna and representing a suitable environment for mosquitoes breeding.[1]

Utilization of water hyacinth biomass as source of lignocellulose for the activated carbon production can be one of the strategies in water pollution control. Using activated carbon obtained from lignocellulose biomass instead of fossil coal will reduce the production of greenhouse gasses and therefore represents a green approach in the synthesis of materials that can be used in process of pollutant removal.[2] The water hyacinth is characterized by a high content of lignocellulose biomass, including 48 % hemicellulose as the major component, along with 20 % cellulose and with 10 % of average lignin content, so it can be potentially employed as a proper carbon source.[3–5]

The activated carbons have been used as adsorbents of a wide range of contaminants such as pharmaceuticals, metallic and non-metallic pollutants and dyes from aqueous solutions.[2,6] In comparison with other adsorbents (zeolites, clays and polymers) activated carbons show better performance and stability in terms of adsorption.[7] The chemical activation of raw lignocellulose precursor material is usually a one-step method for the activated carbons preparation. Among many chemical agents, the $ZnCl_2$ is one of the most effective chemicals used for producing activated carbons with highly developed porosity.[8,9] This activation agent has a high activating capability, and it is relatively expensive. In process of chemical activation, the $ZnCl_2$ contributes to the pore development by localized decomposition of organic matter, inhibiting tar formation and enhancing the carbon yield.[8,9]

Water hyacinth has already been used as a precursor for activated carbon synthesis. The activation processes were dominantly performed by KOH[10] or H_3PO_4[11] under various and well-studied experimental approach. On the other hand, $ZnCl_2$ activation of water hyacinth has been applied,[4,12] but the impact of amount of the activation agent has not been sufficiently studied.

Pesticides are chemical substances used for the increase of the agricultural production. As artificial organic compounds, pesticides can remain in the environment for many years and may be transported over a long distance.[13] Among many pesticides, glyphosate-based herbicides as systemic, broad-spectrum herbicides are widely used, therefore contributed to concerns about their environmental impact.[14] International Agency for Research on Cancer and World Health Organization classify glyphosate as substance that is “probably carcinogenic to humans” (group 2A).[15] According to the author’s best knowledge, there is lack in the existing literature about application of activated carbons obtained from water hyacinth bio waste as adsorbents of glyphosate.

The main objective of the present work was to obtain activated carbons with a high surface area from water hyacinth biomass, using different amounts of $ZnCl_2$ and applying different carbonization temperatures. The selected activated carbon was further evaluated as adsorbent for glyphosate removal.

EXPERIMENTAL

Materials

The water hyacinth (WH) plant (Karbala, Iraq) was used as raw material for obtaining the activated carbon. The raw WH was washed with distilled water. The roots and stalks without leaves were chopped and dried in an oven for 24 h. The dried WH was boiled in 0.25 M hydrochloric acid to remove metallic oxides, rinsed with distilled water, and finally dried in vacuum freeze dryer for 24h. The dry WH was crushed and ground in rotary mill, and finally sieved in order to obtain particles sized 1.4–2.0 mm.

The $ZnCl_2$ (≥98 %), supplied from Sigma–Aldrich, was used as activating agent in process of chemical activation during the activated carbons synthesis.

The herbicide glyphosate – GPh (≥99 %), used in adsorption study, was purchased from Merck.

Activated carbons synthesis

The activated carbon (AC) based on dry water hyacinth biomass was prepared by chemical activation of dry WH with $ZnCl_2$ according to the procedure described in literature.[16] The impregnation ratio was calculated as the ratio of the weight of $ZnCl_2$ in solution to the weight of the dry WH. The impregnation ratio was 0.0, 0.5, 1.0, 1.5, 2.0, 2.5 and 3.0.

The 40 g of dry WH sample was added to 150 ml of solution with the appropriate mass of $ZnCl_2$ and stirred at 60 °C for 4 h. The solid and liquid phases were separated by filtration through Buchner funnel and dried at 105 °C during 24 h. The drying process was applied prior to carbonization in order to avoid the loss of sample caused by rash steam development. The carbonization of activated WC was carried out in electrical furnace with nitrogen flowing (150 cm^3 min^{-1}) and at heating rate of 15 °C min^{-1}. The carbonization during 80 min was conducted at following temperatures: 400, 500, 600 and 700 °C.

The obtained activated carbon was rinsed with 0.5 M HCl in order to remove the activating agent, washed with hot distilled water until neutral pH and finally dried at 110 °C for 12 h. The dry samples were weighted in order to calculate the yield.

The synthetized activated carbons were denoted according to impregnation ratio and carbonization temperature, *e.g.*, $0.5AC_{400}$ means that the impregnation ratio and the carbonization temperature were 0.5 and 400 °C, respectively.

The yield of activated carbons was calculated from mass ratio between activated carbon and starting WH after drying process:

$$Y = 100\frac{m_{AC}}{m_{dryWHAC}} \quad (1)$$

where Y / % is yield of the synthesis, m_{AC} / g is the mass of activated carbon and m_{dryWH} / g is the mass of dry WH.

Characterization methods

The synthetized ACs were characterized using elemental analysis, nitrogen adsorption-desorption isotherms and scanning electron microscopy (SEM).

The elemental analysis was used in order to determinate the content of carbon, hydrogen, nitrogen and sulphur in raw materials and activated carbons. The analysis was performed using elemental analyser instrument (Thermo Scientific – FlashEA1112 automatic elemental analyzers). Prior to analysis, the samples were dried in an oven at 110 °C.

The textural properties of activated carbons were obtained from adsorption-desorption nitrogen isotherms at –196 °C (Micromeritics' ASAP® 2020). Prior to analysis the samples were outgassed at 110 °C during 12 h. The specific surface area (S_{BET}) was calculated according to Brunner–Emmett–Teller method,[17] the total pore volume (V_T) was estimated from N_2 adsorption isotherm according to Gurvich rule, and represents the liquid molar volume adsorbed at pressure p/p_0 of 0.999.[18,19] The volumes of micropores and mesopores were calculated using Dubinin–Radushkevich method[20] and Barrett, Joyner, Halenda (BJH) method,[21] respectively.

The morphology of activated carbons was characterized by scanning electron microscopy (SEM-JEOL, JSM 6360 LV).

Adsorption study

The herbicide glyphosate (GPh) was used as a model of pesticide pollutant. During adsorption study, the GPh concentration was determinated by UV–Vis spectrophotometer (UV––Vis 1800 Shimadzu) at λ_{max} = 264 nm.

The volume of GPh solution of 75 cm^3 was introduced into the glass flasks and mixed with 20 mg of adsorbents. After the adsorption process, the GPh concentration in the supernatant was analyzed, with previous separation of the solid phase by centrifugation at 12,000 rpm for 20 min.

The effect of surface development of activated carbons on the adsorption efficiency was performed using GPh starting concentration of 100 mg dm^{-3} for the adsorption time of 240 min. The adsorption was performed from a solution with pH 3.55, which represents the unbuffered pH value of GPh solution for the investigated concentration.

The effect of contact time on the GPh adsorption was monitored at predetermined time intervals between 5 min and 240 min, at 25 °C, with starting GPh concentration of 100 mg dm^{-3}.

The adsorption isotherms were constructed at equilibrium adsorption time at 25 °C with GPh initial concentration in range 50–250 mg dm^{-3}.

The amount of the adsorbed herbicide (q_t / mg g^{-1}) was calculated according to:

$$q_t = \frac{(c_i - c_t)V}{m} \tag{2}$$

where c_i is the initial concentration of GPh /mg dm^{-3}, c_t / mg dm^{-3} is the concentration of GPh in time t, V / dm^{-3} is the volume of GPh solution and m / g is the mass of the adsorbent.

Adsorption data analysis

Two well-known isotherm models Langmuir[22] and Freundlich[23] were used for modelling the adsorption data, while the adsorption kinetics data were fitted with both, pseudo-first[24] and pseudo-second order[25] kinetics' models. The applied isotherm and kinetics model have been frequently used for heterogeneous adsorption systems that consist of solid adsorbent and dissolved adsorbate molecule.[26]

RESULTS AND DISCUSSION

Results of characterization

The yield of activated carbons obtained after chemical activation with $ZnCl_2$ and carbonization process is given in Fig. 1.

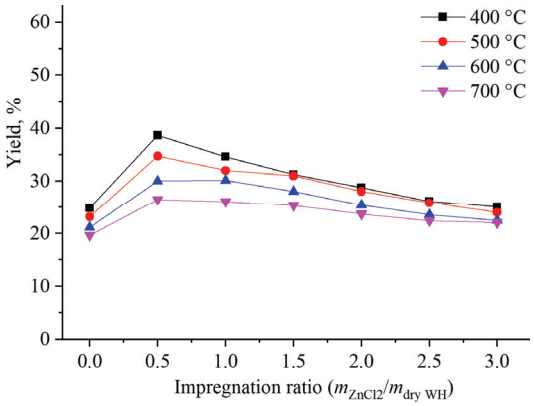

Fig. 1. The influence of impregnation ratio and carbonization temperature on yield of activated carbons prepared from water hyacinth dry material.

It was observed that activated carbons obtained with the impregnation ratio 0 (*i.e.*, without applied $ZnCl_2$) and the temperature range 400–700 °C had relatively low yield in the range of 19.6–24.9 %. This fact can be related to a high content of volatile matter and relatively low lignin content in raw WH material used for the preparation of activated carbons. According to the literature, the activated carbons obtained by pyrolisis without prior activation showed significant weight loss attributed to gasses extraction (CO, CO_2 and CH_4).[27] The activation agent and applied carbonization temperature have a significant impact on the yield of activated carbons (Fig. 1). Generally, the best yields were obtained for the lowest carbonization temperature (400 °C). With the temperature increase the yield of activated carbon decreased regardless the amount of applied $ZnCl_2$, which was explained by the promotion of tar volatilization by higher temperature.[28] For each carbonization temperature it was observed that the amount of the activation agent has a similar impact on yield, *i.e.*, the activated carbon yields continually decreased with the impregnation ratio higher than 0.5 (Fig. 1). This observation can be explained by larger evolution of volatiles compounds affected by dehydration agent – $ZnCl_2$.[29]

In order to estimate the effect of the amount of activation agent – $ZnCl_2$, on surface development, the specific surface area (S_{BET}) of samples obtained on the carbonization temperature of 400 °C was correlated with the impregnation ratio (from 0.0 to 3.0) and shown in Fig. 2.

The activated carbon obtained without impregnation showed the lowest value of S_{BET}. This result was expected since the $ZnCl_2$ works as a dehydration reagent during the carbonization process, which leads to carbon charring, form-

ations of the aromatic, porous structure, and restricts the formation of the tar.[29] The introduction of $ZnCl_2$ led to development of specific surface and this trend continued up to impregnation ratio 2.0, and after that decreased for higher impregnation ratios. These results are in accordance with literature data.[27,29,30]

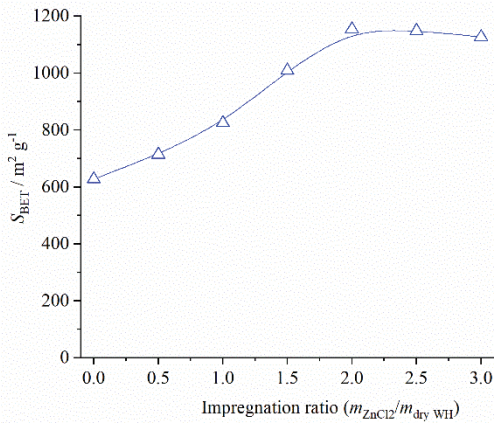

Fig. 2. The influence of impregnation ratio ($m_{ZnCl_2}/m_{dry\ WH}$) on specific surface area of carbons obtained by carbonization at 400 °C.

The more detailed textural properties analysis was applied on the activated carbon samples with impregnation ratio 2.0, since the carbons with highest S_{BET} values (Fig. 2) were obtained using $ZnCl_2$ in this impregnation ratio.

The effect of temperature (400–700 °C) on the specific surface area (S_{BET}), micropore (V_{mic}) and mesopore volume (V_{meso}) as well as on total pore volume (V_{tot}) of the activated carbons with impregnation ratio 2.0 are presented in Table I.

TABLE I. Surface area and pore volumes of activated carbons with impregnation ratio 2.0 obtained at different carbonization temperatures

T / °C	S_{BET} / m^2 g^{-1}	V_{tot} / cm^3 g^{-1}	V_{mic} / cm^3 g^{-1}	V_{meso} / cm^3 g^{-1}
400	1154	0.602	0.301	0.298
500	1317	0.697	0.152	0.541
600	1284	0.670	0.135	0.527
700	1163	0.605	0.113	0.485

The most of the investigated textural properties increased with the rise of final carbonization temperature from 400 to 500 °C, while further increase of temperature led to surface development decreasing. Increasing temperature from 400 to 500 °C had strong positive impact on mesoporosity development, while temperatures higher than 500 °C led to slight decrease of mesopore volume. Besides that, all investigated carbonization temperatures above 400 °C reduced microporosity of activated carbons. Similar trends can be found in literature,[27,28,31] According to Rodriguez-Reinoso and Molina-Sabio,[27] $ZnCl_2$ has an important role in the development of micro- and mesoporosity in the carboniz-

ation process up to 500 °C, but at higher temperatures the reaction of $ZnCl_2$ with the char is negligible. The decrease in textural properties at temperatures higher than 500 °C can also be attributed to a sintering effect at high temperature, followed by the shrinkage of the char, and the realignment of the carbon structure.[32]

Sentilkumar *et al.*[12] applied the weight of $ZnCl_2$ that corresponded to 10 % of raw water hyacinth and the synthetized activated carbon with S_{BET} = 579.94 $m^2 g^{-1}$ at high temperature of 900 °C. Boonpoke[4] produced the microporous activated carbon with a specific surface area of 1066 $m^2 g^{-1}$ at 600 °C using an equal amount of $ZnCl_2$ and raw water hyacinth (impregnation ratio 1:1). The present study applied different amounts of $ZnCl_2$ and found that the impregnation ratio 2:1 leads to obtaining the activated carbons with higher values of S_{BET} than those in previous studies at lower carbonization temperatures of 400 and 500 °C (Table I). Wu *et al.*[10] activate the raw water hyacinth with KOH and synthetized activated carbon with S_{BET} = 1380 $m^2 g^{-1}$, but on 800 °C. Yang and Qiu[33] showed that the activated carbons with the specific surface area of even 2000 $m^2 g^{-1}$ could be produced from pharmaceutics' herb residue, but synthesis required chemical activation with booth NaOH and $ZnCl_2$.

The elemental analysis was performed in order to evaluate the effect of temperature on the chemical composition of activated carbons. The result of the elemental analysis of dry WH and the activated carbons prepared with impregnation ratio of 2.0 are presented in Table II.

TABLE II. The results of the elemental analysis

Sample	Content of elements, wt. %				
	C	H	O[a]	N	Ash
Dry WH	41.22	6.23	47.07	1.54	3.94
AC400	80.31	3.37	15.16	0.32	0.84
AC500	81.57	3.15	14.20	0.27	0.81
AC600	83.24	2.98	12.79	0.24	0.75
AC700	84.15	2.75	12.23	0.19	0.68

[a]The oxygen content is calculated from the difference up to 100 %

The major organic elements in all investigated samples are carbon and oxygen. The WH has higher content of ash, consisting mainly of silica and metal oxides.[16]

The treatment with HCl after activation process led to leaching of metal cations and therefore the ash content was reduced. During the carbonization process, with temperature rise the content of carbon increased, which was expected.[16]

The scanning electron microscopy (SEM) was employed to show the difference in the morphology between the raw WH material and the activated carbons with impregnation ratio 2:1, obtained in the temperature range from 400–700 °C.

The SEM images were recorded using magnification of 3000× and presented in Fig. 3.

In Fig. 3 significant difference in surface morphology can be observed between raw WH and ACs. The surface of the raw WH is moderately developed with parts of a smooth area, but after impregnation and carbonization, the raw WH biomass turns to be more porous with more open structures (Fig. 3). The increase of the carbonization temperature led to a reduction in small cracks in the activated carbon surfaces which could be responsible for the reduce of textural properties. According to the textural analysis the mesopore formation was dominantly responsible for the surface development (Table I). Since the mesopores are those with diameter from 2–50 nm, they are not visible in Fig. 3, where macroporous structure can be noticed.

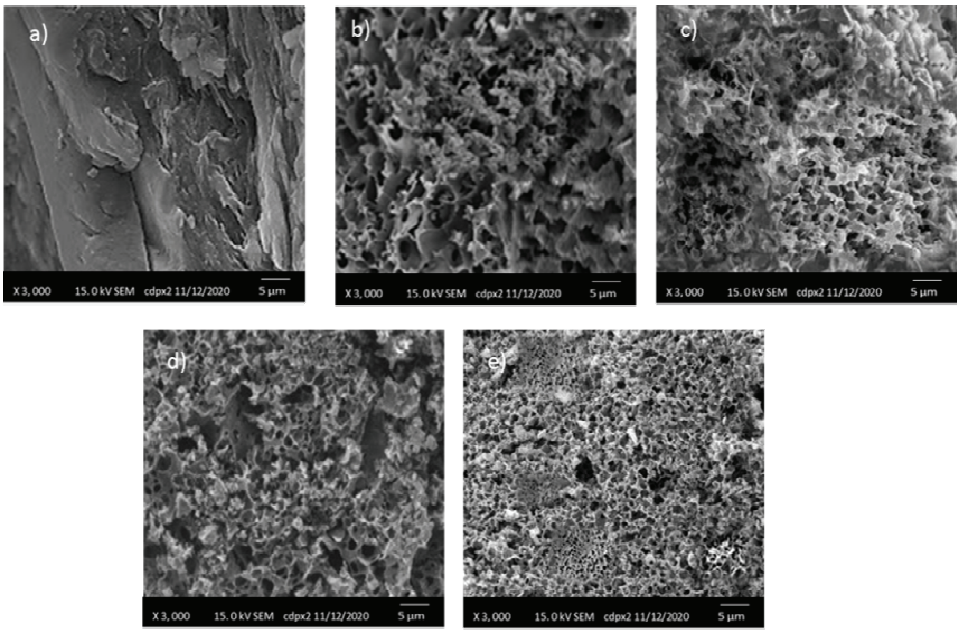

Fig. 3. The SEM images of: a) raw WH; b) $2.0AC_{400}$; c) $2.0AC_{500}$; d) $2.0AC_{600}$; e) $2.0AC_{700}$.

Adsorption study

The effect of surface development of activated carbons on adsorption efficiency. The aim of this adsorption study was to select the activated carbon with the best adsorption properties toward GPh. The effect of surface development of the activated carbons (impregnation ratio 2.0, T_{carb} = 400 to 700 °C) on the amount of adsorbed GPh for 240 min is presented in Fig. 4.

Although the specific surface area shows an impact on the amount of the adsorbed GPh, the difference in q_{240} for the samples with relatively close values

of S_{BET} was negligible. For example, the samples with S_{BET} values of 1317 and 1284 m^2g^{-1} adsorbed almost the same amount of GPh with values 153 and 151 mg g^{-1}, respectively. The obtained results suggested that the increasing S_{BET} values of ~30 m^2 g^{-1} did not lead to a significant increase in the efficiency of GPh removal. Herath *et al*[34] found that both physisorption and chemisorption mechanisms affected the adsorption of glyphosate onto the activated carbon, but that physical interactions dominantly increase with the rise of surface development.

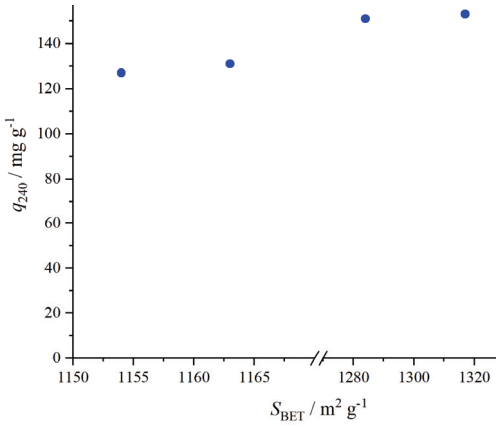

Fig. 4. The influence of specific surface area (S_{BET}) on the amount of the adsorbed glyphosate (q_{240}) for 240 min.

Although $2.0AC_{500}$ and $2.0AC_{600}$ showed almost the same amount of adsorbed GPh for the adsorption time of 240 min, the $2.0AC_{500}$ was selected for further adsorption study, since its synthesis requires lower carbonization temperature.

Kinetic study

The effect of contact time on GPh adsorption on selected adsorbent $2.0AC_{500}$ was performed in order to estimate the equilibrium time of adsorption (Fig. 5).

The uptake of GPh increased gradually up to 120 min and after this time the amount of adsorbed GPh was almost constant. For the investigated process, the time of 120 min can be considered as equilibrium, since there is no significant change in the amount of the adsorbed GPh for longer times. The amount of adsorbed GPh in equilibrium time was found to be q_e = 151.87 mg g^{-1}. In order to describe the kinetics of the process, the experimental data (Fig. 5) were fitted with pseudo-first and pseudo-second-order kinetic models. The calculated kinetic parameters for both models are given in Table III.

The results presented in Table III revealed that the experimental data show better fit with pseudo-second order kinetic model than with pseudo-first order model. The amount of adsorbed GPh in equilibrium calculated from pseudo-sec-

ond order kinetic model was q_e = 156.3 mg g^{-1} which is very close to the experimental value of q_e = 151.87 mg g^{-1}. According to many authors, pseudo-second order model indicates that the possible mechanism of investigated process included chemisorption of pollutants on adsorbent surface.[35]

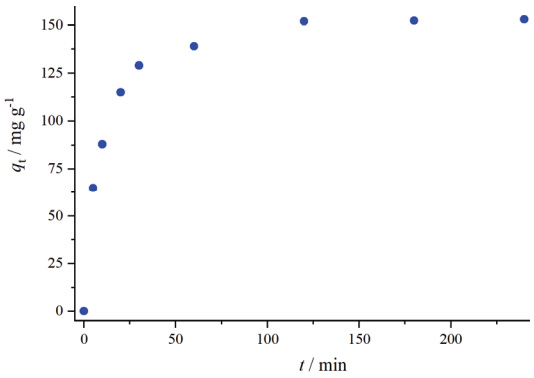

Fig. 5. The effect of contact time on GPh adsorption using activated carbon 2.0AC$_{500}$.

TABLE III. The parameters of pseudo-first and pseudo–second order kinetic models

Pseudo-first order	q_e / mg g^{-1}	k_1 / min^{-1}	R^2
	214.9	0.0773	0.944
Pseudo-second order	q_e / mg g^{-1}	k_2 / g mg^{-1} min	R^2
	156.3	0.0011	0.994

Adsorption isotherm models

The experimental isotherm data together with nonlinear fits of Langmuir and Freundlich models are presented in Fig. 6, while the calculated isotherm's parameters are listed in Table IV.

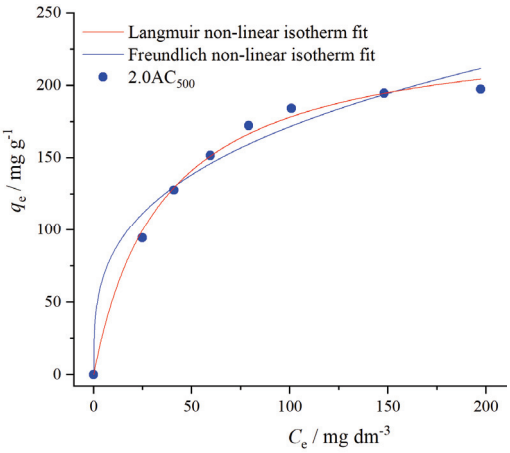

Fig. 6. The adsorption isotherm for GPh adsorption on 2.0AC$_{500}$ on 25 °C, fitted with Langmuir and Freundlich isotherm model.

Table IV. Calculated isotherm parameters for Langmuir and Freundlich model for GPh adsorption on $2.0AC_{500}$

Langmuir	K_L / dm^3 mg^{-1}	q_{max} / mg g^{-1}	R^2
	0.0284	240.8	0.995
Freundlich	K_F / (mg g^{-1})(dm^3 mg^{-1})$^{1/n}$	n	R^2
	41.15	3.23	0.965

Both investigated models generally could be applied to describe the GPh adsorption onto $2.0AC_{500}$ process, since coefficients of determination are $R^2 > > 0.900$ (Table IV). However, the Langmuir model showed better fitting with the experimental data, having $R^2 = 0.995$. The agreement of adsorption data with Langmuir model indicated that surface of investigated adsorbent is energetically homogenous and the binding sites are uniformly distributed with the same affinity. The adsorption process occurs until monolayer surface coverage and after saturation there is no additional interaction between adsorbate molecules. The monolayer adsorption capacity (q_{max}) according to the Langmuir model was 240.8 mg g^{-1}.

The literature review of glyphosate adsorption on carbons derived from different type of biomass and other adsorbents is presented in Table V.

TABLE V. Comparison of glyphosate adsorption capacity of different adsorbents

Adsorbent	Adsorption parmeters	q_{max} / mg g^{-1}	Reference
$2.0AC_{500}$	S_{BET} = 1317 m^2 g^{-1};pH 3.55; T = 25 °C, C_{GPh}, 50–250 mg dm^{-3}	240.8	Current study
Rice husk char	S_{BET} = 229 m^2 g^{-1}; pH < 4; C_{GPh}, 0–100 mg dm^{-3}	123.03	34
Carbon derived from waste newspapers	S_{BET} = 535 m^2 g^{-1};pH 2.5; T = 28 °C; C_{GPh}, 5–100 mg dm^{-3}	48.4	36
Eucalyptus *camaldulensis* bark-mediatedchar	pH 10.18, C_{GPh} = 20.28 mg L^{-1}, contact time 78.42 min; T = 303.23 K	66.76	37
Carbon obtained from sugar cane bagasse	C_{GPh}, 0.338–2.704 g L^{-1}	161.3	38
Zr-MOF	pH 3–6; C_{GPh}, 20–70 mg L^{-1}; contact time: 1–180 min, T, 308–3018 K	256.54	39
Resin D301	T, 303.15–318.15 K; C_{GPh}, 5–50 mg/L; pH 4	833.33	40

Although Chen *et al.*[40] found that Resin D301 as adsorbent showed extraordinary efficiency for glyphosate removal, the adsorption capacity for $2.0AC_{500}$ of 240.8 mg g^{-1} is close to the adsorption capacity of Zr–MOF adsorbent[39] and still higher than q_{max} of the most reported carbon-based adsorbents. Therefore the $2.0AC_{500}$ could be classified as efficient and tested in real wastewaters treatments.

CONCLUSION

The water hyacinth biomass was used as starting material for the production of activated carbons. The activated carbons were synthetized using chemical activation with $ZnCl_2$ followed by controlled carbonization. On carbonization at various carbonization temperatures: 400, 500, 600 and 700 °C the different impregnation ratios of $ZnCl_2$ in range of 0.5–3.5 were applied. The chosen synthesis parameters showed significant impact on activated carbons yield and surface development. The impregnation ratio of 0.5 and temperature of 400 °C led to the highest yield of activated carbons. On the other hand, the textural properties showed that the most developed surface of 1317 $m^2\ g^{-1}$ and the total pore volume of 0.697 $cm^3\ g^{-1}$ has the activated carbon obtained with the impregnation ratio 2.0 and the carbonization temperature of 500 °C. This activated carbon with the best textural properties was used as an adsorbent for glyphosate, pesticide with strong negative environmental impact. Experiments showed that the adsorption takes place very fast and the equilibrium time was estimated at 120 min. The adsorption isotherms were fitted with Langmuir and Freundlich model, and Langmuir model showed better fit indicating that adsorption occurs in the form of monolayer on energetically equal and homogenously distributed adsorption sites. The Langmuir adsorption capacity of q_{max}=240.8 mg g^{-1} classified selected adsorbent as very efficient one. The adsorption kinetics study revealed that glyphosate adsorption follows the pseudo-second order kinetics, which indicates possible chemisorption mechanism.

ИЗВОД

СИНТЕЗА АКТИВНОГ УГЉА ИЗ БИОМАСЕ ВОДЕНОГ ЗУМБУЛА И ЊЕГОВА ПРИМЕНА КАО АДСОРБЕНАТА У КОНТРОЛИ ЗАГАЂЕЊА ВОДЕ

АНМАД НАККУ МОНАММААД и МИРЈАНА КИЈЕВЧАНИН

Универзитет у Београду Технолошко–металуршки факултет, Карнегијева 4, 11000 Београд

Биомаса воденог зумбула је коришћена за синтезу активног угља у процесу хемијске активације са $ZnCl_2$, након чега је уследила контролисана пиролиза. Примењени масени односи импрегнације $ZnCl_2$ и суве биомасе зумбула били су у распону од 0,5–3,5. Карбонизација је спроведена на четири различите температуре (400–700 °C) у инертној атмосфери. Највећи принос активног угља добијен је за однос импрегнације 0,5 и температуру карбонизације 400 °C. Узорци су карактерисани применом елементалне анализе, адсорпционо–десорпционих изотерми азота и СЕМ анализе. Активни угаљ добијен за однос импрегнације 2,0 и температуру карбонизације 500 °C ($2.0AC_{500}$) показао је вредности специфичне површине и укупне запремине пора од 1317 и 0,697 $cm^3\ g^{-1}$, редом. Адсорпција глифосата, пестицида са јаким негативним утицајем на животну средину, била је брз процес, са равнотежним временом од 120 min. Изотерме адсорпције су корелисане Langmuir и Freundlich моделом. Langmuir адсорпциони капацитет q_{max} = 240,8 mg g^{-1} за $2.0AC_{500}$ класификовао је одабрани адсорбент као веома ефикасан. Тестирани процес адсорпције пратио је кинетику модела псеудо-другог реда.

(Примљено 5. децембра 2021, ревидирано 10. фебруара, прихваћено 11. фебруара 2022)

REFERENCES

1. M. A. Bote, V. R. Naik, K. B. Jagadeeshgouda, *Mater. Sci. Energy Technol*. **3** (2020) 397 (https://doi.org/10.1016/j.mset.2020.02.003)
2. M. Bilal, J. Ali, N. Hussain, M. Umar, S. Shujah, D. Ahmad, *J. Serb. Chem. Soc*. **85** (2020) 265 (https://doi.org/10.2298/JSC181108001B)
3. A. Saning, S. Herou, D. Dechtrirat, C. Ieosakulrat, P. Pakawatpanurut, S. Kaowphong, C. Thanachayanont, M. M. Titirici, L. Chuenchom, *RSC Adv.* **9** (2019) 24248 (https://doi.org/10.1039/C9RA03873F)
4. A. Boonpoke, *J. Environ. Biol.* **36** (2015) 1143 (http://www.jeb.co.in/journal_issues/201509_sep15/paper_15.pdf)
5. C. A. Riyanto, E. Prabalaras, *J. Phys.: Conf. Ser.* **1307** (2019) 012002 (https://doi.org/10.1088/1742-6596/1307/1/012002)
6. M. I. Din, S. Ashraf, A. Intisar, *Sci. Prog.* **100** (2017) 299 (https://doi.org/10.3184/003685017X14967570531606)
7. A. Regti, M. R. Laamari, S. E. Stiriba, M. El-Haddad, *J. Assoc. Arab Univ. Basic Appl. Sci.* **24** (2017) 10 (https://doi.org/10.1016/j.jaubas.2017.01.003)
8. Z. Hu, M. P. Srinivasan, *Micropor. Mesopor. Mater*. **43** (2001) 267 (https://doi.org/10.1016/S1387-1811(00)00355-3)
9. Z. Yue, J. Economy, *Micropor.Mesopor. Mater*. **96** (2006) 314 (https://doi.org/10.1016/j.micromeso.2006.07.025)
10. K. Wu, B. Gao, J. Su, X. Peng, X. Zhang, J. Fu, P. K. Chu, *RSC Adv*. **6** (2016) 29996 (https://doi.org/10.1039/C5RA25098F)
11. Y. Huang, L. Shunxing, C. Jianhua, Z. Xueliang, C. Yiping, A*ppl. Surf. Sci.* **293** (2014) 160 (https://doi.org/10.1016/j.apsusc.2013.12.123)
12. S. T. Senthilkumar, R. Kalai Selvan, Y. S. Lee, J. S. Melo, *J. Mater. Chem., A* **1** (2013) 1086 (https://doi.org/10.1039/c2ta00210h1086)
13. M. T. Scholtz, E. Voldner, A. C. McMillan, B. J. Van Heyst, *Atmos. Environ.* **36** (2002) 5005 (https://doi.org/10.1016/S1352-2310(02)00570-8)
14. M. Schweizer, K. Brilisauer, R. Triebskorn, K. Forchhammer, H. R. Köhler, *Peer J.* **7** (2019) 7094 (https://doi.org/10.7717/peerj.7094)
15. W. Morley, S. Seneff, *Surg. Neurol. Int.* **5** (2014) 134731 (https://doi.org/10.4103/2152-7806.134731)
16. T. H. Liou, *Chem. Eng. J.* **158** (2010) 129 (https://doi.org/10.1016/j.cej.2009.12.016)
17. J. Rouquerol, P. Llewellyn, F. Rouquerol, *Stud. Surf. Sci. Catal.* **160** (2007) 49 (https://doi.org/10.1016/S0167-2991(07)80008-5)
18. S. J. Gregg, K. S. W. Sing, *Adsorption, Surface Area, and Porosity 2*, Academic Press, London, 1982, pp. 41–105 (https://doi.org/10.1002/bbpc.19820861019)
19. F. Rouquerol, J. Rouquerol, K. Sing, *Absorption by powders and porous solids, Principles, Methodology and Applications*, Academic press, London, 1999, pp. 165–189 (https://doi.org/10.1016/B978-0-12-598920-6.X5000-3)
20. M. M. Dubinin, *J. Colloid Interface Sci*. **23** (1967) 487 (https://doi.org/10.1016/0021-9797(67)90195-6)
21. E. P. Barrett, L. G. Joyner, P. P. Halenda, *J. Am. Chem. Soc.* **73** (1951) 373 (https://doi.org/10.1021/ja01145a126)
22. I. Langmuir, *J. Am. Chem. Soc.* **40** (1918)1361 (https://doi.org/10.1021/ja02242a004)

23. H. M. F. Freundlich, *Z. Phys. Chem. A* **57** (1906) 385 (https://doi.org/10.1515/zpch-1907-5723)
24. S. Lagergren, *Handlingar* **24** (1898) 1 (https://doi.org/10.1002/andp.18983000208)
25. Y. S. Ho, J. C. Y. Ng, G. McKay, *Sep. Purif. Meth.* **29** (2000) 189 (https://doi.org/10.1081/SPM-100100009)
26. A. Ivanovska, L. Pavun, B. Dojčinović, M. Kostić, *J. Serb. Chem. Soc.* **86** (2021) 885 (https://doi.org/10.2298/JSC210209030I)
27. F. Rodriguez-Reinoso, M. Molina-Sabio, *Coloids Surfaces, A* **241** (2004) 15 (https://doi.org/10.1016/j.colsurfa.2004.04.007)
28. Q. Qian, M. Machida, H. Tatsumoto, *Bioresour. Technol*. **98** (2007) 353 (https://doi.org/10.1016/j.biortech.2005.12.023)
29. 29. S. Yorgun, N. Vural, H. Demiral, *Micropor. Mesopor. Mater.* **122** (2009) 189 (https://doi.org/10.1016/j.micromeso.2009.02.032)
30. A. C. Lua, T. Yang, *J. Colloid Interf. Sci.* **290** (2005)505 (https://doi.org/10.1016/j.jcis.2005.04.063)
31. M. M. Gómez-Tamayo, A. Macías-García, M. A. Díez, E. M. Cuerda-Correa, *J. Hazard. Mater.* **153** (2008) 28 (https://doi.org/10.1016/j.jhazmat.2007.08.012)
32. K. Mohanty, D. Das, M. N. Biswas, *Adsorption* **12** (2006) 119 (https://doi.org/10.1007/s10450-006-0374-2)
33. J. Yang, K. Qiu, *Chem. Eng. J*. **167** (2011) 148 (https://doi.org/10.1016/j.cej.2010.12.013)
34. I. Herath, P. Kumarathilaka, M. I. Al-Wabel, A. Abduljabbar, M. Ahmad, A. R. A. Usman, M. Vithanage, *Micropor. Mesopor. Mater*. **225** (2016) 280 (https://doi.org/10.1016/j.micromeso.2016.01.017)
35. B. H. Hameed, R. R. Krishni, S. A. Sata, *J. Hazard. Mater.* **162** (2009) 305 (https://doi.org/10.1016/j.jhazmat.2008.05.036)
36. M. M. Nourouzi, T. G. Chuah, T. S. Y. Choong, *Desalin. Water Treat*. **24** (2010) 321 (https://doi.org/10.5004/dwt.2010.1461)
37. K. Sen, J. K. Datta, N. K. Mondal, *Appl. Water Sci*. **9** (2019) 162 (https://doi.org/10.1007/s13201-019-1036-3)
38. D. C. Nguyena, A. I. Vezentseva, P. V. Sokolovskiyc, A. A. Greishc, *Russ. J. Phys. Chem., A* **95** (2021) 1212 (https://doi.org/10.1134/S0036024421060194)
39. Q. Yang, J. Wang, X. Chen, W. Yang, H. Pei, N. Hu, Y. Li, Y. Suo, T. Lic, J. Wang, *J. Mater. Chem.* **6** (2018) 2184 (https://doi.org/10.1039/C7TA08399H)
40. F. Chen, C. Zhou, G. Li, F. Peng, *Arab. J. Chem.* **9** (2016) S1665 (https://doi.org/10.1016/j.arabjc.2012.04.014).

Journal of the Serbian Chemical Society
JSCS-info@shd.org.rs • www.shd.org.rs/JSCS
J. Serb. Chem. Soc. *88* (1) 83–95 (2023)
JSCS–5612
Original scientific paper
Published 18 November 2022

Controlling reactions during heavy metal leaching from municipal solid waste incineration fly ash

WEIFANG CHEN*, YEGUI WANG, MINZHU HU, YONGLUN LI and GUILIN FANG

School of Environment and Architecture, University of Shanghai for Science and Technology, 516 Jun Gong Road, Shanghai 200093, China

(Received 5 May, revised 26 July, accepted 1 August 2022)

Abstract: This research aimed to characterize the physical and chemical properties of municipal solid waste (MSW) incineration fly ash, as well as to investigate the leaching of heavy metals during toxicity characteristics leaching procedure (TCLP) process. To understand the leaching behaviour, concentrations of heavy metals, chloride, sulphate and calcium at various leaching, time was monitored together with pH of the leaching solution. Results showed that the chemical compositions of fly ashes led to differences in leaching environment. For the two fly ashes under study, one resulted in a leaching environment with pH of 10–12 while the other had pH about 6–7. Based on pH, anions and cations concentrations, Minteq software was employed to investigate the speciation of heavy metals. Results showed that the shift in precipitation/dissolution balance of carbonate and hydroxides of heavy metals could explain the fluctuation in metal concentrations during the leaching process, which indicates that leaching was probably controlled by these reactions. On the other hand, addition of EDTA changed the controlling reactions. Chelating reactions between heavy metals and EDTA led to much higher leaching toxicity due to the presence of heavy metals, showing that the presence of chelating organics in natural environment may facilitate heavy metal leaching.

Keywords: characterization; toxicity characteristics leaching procedure; Minteq; precipitation/dissolution.

INTRODUCTION

Industrialization and urbanization in recent decades had led to alarming rises in the generation of municipal solid waste. It was reported that, in 2020, China produced 242 million tons of MSW which were mainly disposed of by landfill and incineration.[1] The disposal by landfill was intensive and the leaching of heavy metals into groundwater was problematic.[2] Incineration, on the other hand,

* Corresponding author. E-mail: chenweifang@usst.edu.cn
https://doi.org/10.2298/JSC220505065C

was effective in reducing both volume (up to 90 %) and mass (up to 70 %) while generating electricity.[3,4] Therefore, it was considered a promising method and had witnessed rapid developments.

However, air pollution and generation of residues are some of the concerns related to incineration. Solid residues from MSW incineration include bottom ash and fly ash.[5] Between them, fly ash is considered hazardous as it contains large amount of heavy metals and toxic organics.[6] Besides residues from MSW incineration, fly ash also contained reagents and products from flue gas neutralization. Therefore, the main elements in fly ash include O, Cl, S Ca, Si, Al, Fe, Mg, Na and K, as well as toxic elements such as Pb, Cd, Cr, Ni, Zn, Cu, *etc*.[7]

MSW fly ash accounted for about 3–15 % of the MSW depending on the incineration technology.[8] This means that, in China, millions of tons of fly ash need to be processed annually. Due to the continuous growth in fly ash generation, many countries have called for reuse and recycling. Fan *et al.* believed that MSW fly ash is basically an aluminosilicate material.[9] Therefore, it could be reused as cementitious materials, soil amendment or light-weight aggregate in construction and road pavement materials.[10]

However, it is important to remove harmful elements before fly ash can be reused. Luo *et al*. classified the fly ash treatment into three categories, that is, chemical and physical separation, stabilization/solidification and thermal treatment.[11] The purposes of these treatments are to re-configure ashes (*e.g.*, vitrification or sintering) to remove pollutants (*e.g.*, washing), or to immobilize pollutants (*e.g.*, solidification, geo-polymerization).[12–15]

Toxicity leaching tests were often conducted to compare the effects of heavy metal removal or immobilization. The most commonly used method was toxicity characteristics leaching procedure (TCLP) recommended by US EPA. Leaching of heavy metal was a complicated process. Many reactions, involving precipitation/dissolution, diffusion, sorption and surface coating, *etc.*, could occur during leaching.[16] That is why physical and chemical factors could all influence the leaching of heavy metals. The former includes particle size, shape and porosity, temperature, time, *etc*., while the later includes pH, redox, complexation or sorption conditions and leaching kinetics, *etc*.[17,18] Therefore, the conditions of leaching tests have to be specified so that the results are comparable. Sample preparation, composition of leachant, mixing method, liquid to solid ratio, time, temperature and filtration method were all elucidated in the TCLP method. Still, researchers have argued that TCLP may not be able to truly reflect the leaching behaviour of ashes of high alkalinity. Lu *et al*. compared the leaching potentials of raw and cement-solidified bottom ashes *via* TCLP, multi-pH TCLP and EDTA-mediated TCLP and found that TCLP underestimated the leaching of heavy metal.[19] They recommended that EDTA-mediated TCLP may be more

suitable for the evaluation the heavy metal leaching by alkaline materials, especially in the environment where organic acid may be present.

This research intended to study the properties of two fly ashes and investigate the heavy metal leaching characteristics during TCLP tests. pH, heavy metal, chloride, sulphate, carbonate and calcium concentrations in leaching solutions were monitored. Software Minteq 3.1 was used to calculate the metal speciation and solubility under the leaching conditions. At the same time, the leaching of heavy metal with addition of EDTA was also studied for comparison. Our ultimate goal was to study the feature of heavy metal leaching in fly ashes and advance the understanding of interaction between fly ash and leachant in order to pave the way for a better prediction of heavy metal impact on the environment.

EXPERIMENTAL

Fly ashes

Fly ashes employed in this research were from municipal solid waste incineration plants in Zhejiang and Guangdong Provinces of China. The samples were designated as FA1 and FA2, respectively.

Fly ash characterization

The moisture content was determined according to the national standard method of China (GB/T212-2008). The proximate analysis was conducted according to ASTM standard method E1131-08. The chemical compositions of the samples were determined by X-ray fluorescence spectroscopy (XRF-1800, Shimadzu, Japan) and the crystalline phases were characterized by X-ray diffraction (XRD, Rigaku UItima IV, Japan) with a CuKα radiation at 40 kV and 30 mA, as 2θ ranging from 5 to 90°, while FTIR analysis was carried out *via* Nicolet iS10 (Thermo Scientific, Germany).

pH and the acid neutralization capacity (*ANC*) of fly ash were measured according to the methods proposed by Liu *et al*.[20] Specifically, 1 g of fly ash and 100 mL of deionized water were put into a 300 mL conical flask and stirred at 200 r/min for 15 min and pH was measured. Half of the mixture was next titrated with 1 mol/L acetic acid to pH 7.0. The amount of acetic acid consumed was the *ANC*.

Analysis of heavy metal contents

The contents of heavy metals in fly ash were measured based on a standard method of China (HJ803-2016) which was designed specifically for the analysis of metal in soil/sediments, *via* digestion with nitric acid/chloric acid. Heavy metals in the digested solution were determined by inductively coupled plasma optical emission spectrometry (ICP-OES, Optima8000, PerkinElmer, US) after pretreatment.

Heavy metal leaching toxicity tests

Fly ash was dried and sieved with a 200-mesh sieve before use. TCLP (USEPA method 1311) and an EDTA-modified TCLP were adopted to analyse the leaching toxicity potentials of fly ashes for comparison. With EDTA-modified TCLP, the concentration of EDTA in the leachant was set at 1 mmol/L. All other procedures were conducted as stipulated by the TCLP method. To study the leaching behaviour of heavy metal during TCLP tests, instead of the 18 h recommended by the standard method, leaching time was set at 2, 4, 6, 8, 10, 12, 14, 16 and 18 h, respectively. After mixing for the pre-determined amount of time, the mixture was fil-

tered and the filtrate analyzed for pH, chloride, sulfate, calcium, carbonate and heavy metal concentrations.

RESULTS AND DISCUSSION

Fly ash characterization

The proximate analysis was carried out on both fly ashes to understand their basic properties as shown in Table I. 78 and 89 % of FA1 and FA2 were ash. This is reasonable as fly ashes were the results of high temperature incineration and most of the volatiles or organics were burned off. The high ash contents could be attributed to Ca, Si compounds and other residual metals.[21] According to the proximate analysis, about 22 and 11 % of the fly ash were volatile and fixed carbon indicated the residual organics.

TABLE I. Physicochemical properties of FA1 and FA2

Sample	Proximate content[a], wt. %			Moisture content, %	pH	*ANC* / mL g^{-1}
	Volatiles	Fixed carbon	Ash			
FA1	9	13	78	0.34	12.7	7.3
FA2	3	8	89	0.34	12.4	3.8

[a]Content of fixed carbon = 100 – Content of ash – Content of volatiles

Besides the proximate analysis, Table I also listed the moisture content, pH and ANC of these ashes. Both ashes had low moisture contents (only 0.34 %) but high in pH and acid neutralization capacity (*ANC*). The pH measured here was the natural pH in contact with water. Fly ashes in this research originated from bag filters which were used to treat flue gas. Lime was sprayed to neutralize acidic gases. Therefore, the high pH was most likely caused by the neutralization products or CaO and $Ca(OH)_2$ that remained. *ANC* was measured to evaluate the presence of alkaline compounds and their availability and reactivity.[22] Although both fly ashes showed similar pHs as shown in Table I, their *ANC* values differed. FA1 had a much higher *ANC* indicating that the alkalinity in FA1 may be more readily neutralized by acetic acid.

XRF and XRD analysis were next performed to further clarify the chemical compositions and crystalline structures of fly ashes. The XRF results are presented in Table II.

XRD results in Fig. 1 proved the presence of chloride salts, *i.e.*, NaCl and KCl. Other crystals observed include portlandite ($Ca(OH)_2$), anhydrite ($CaSO_4$), calcium hydrochloride (CaCl(OH)), calcite ($CaCO_3$) and silica (SiO_2). XRF and XRD results were consistent with the high pH and ANC values of both fly ashes in Table II. Due to the presence of these calcium-containing compounds, raw fly ashes manifested strong alkalinity.[21]

FTIR spectrograms were obtained to investigate the surface functional groups as shown in Fig. 2. The wideband at 3445 cm^{-1} corresponded to the stretching

vibration of –OH in hydration water, while the band at 1634 cm^{-1} was its bending vibrations.[24] Absorbances centred at 2510, 2360, 1795, 1451 and 875 cm^{-1} were caused by vibrations of CO_3^{2-} (carbonates).[25] Peaks at 1120 and 660 cm^{-1} indicated vibration stretching of S–O bonds and SO_3^{2-}, respectively.[26] Besides, Si–O bonds were observed at 560 cm^{-1}.[27] It appears that that SiO_2, SO_4^{2-} and CO_3^{2-} salts were all found to be present in these fly ashes.

TABLE II. Element compositions of FA1 and FA2 *via* XRF (wt. %)

Item	Ash	
	FA1	FA2
Ca	55.74	50.97
Cl	14.27	11.44
O	11.41	12.70
K	7.01	5.68
Na	4.22	4.32
Mg	1.79	0.64
S	1.32	2.38
Si	0.68	1.70
Fe	1.31	2.65
Al	0.36	0.78
Ti	0.33	0.76
Br	0.18	1.02
P	0.13	0.20

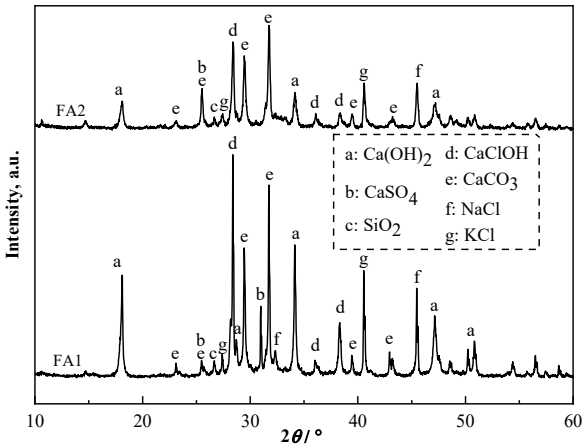

Fig. 1. XRD pattern of FA1 and FA2.

Overall, the characterizations showed that both ashes were high in alkalinity with an abundance of chemicals such as Ca-containing compounds, salts of chloride, sulphate and carbonate, and oxides (*e.g.*, SiO_2). However, the exact amount of these elements differed as their origins varied. This variability could be added to the difficulty in fly ash treatment.

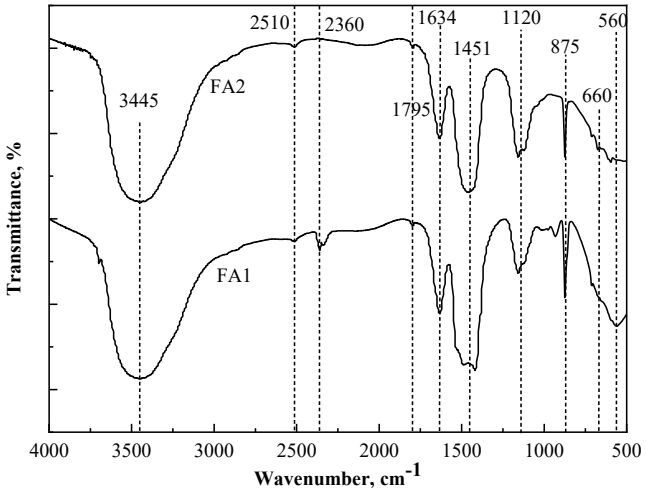

Fig. 2. FTIR spectra of FA1 and FA2.

Heavy metal contents

Heavy metals were of the most concern for their toxicity. Digestion+ICP--OES analysis was employed to analyse the heavy metal contents in fly ashes. This method was able to detect even trace amount of heavy metals in solids.

Table III lists the contents of 6 major heavy metals in fly ashes. Contents of other metals such as As and Sb, were also detected, but their contents were extremely low and were not of concern here. Studies have shown that many heavy metals were transported in the form of volatile chloride and condensed into fly ash particles.[28,29] FA1 had 1.08 g/kg of Pb and 7.90 g/kg of Zn. By comparison, the contents of Cu, Cr and Cd were much smaller. However, the heavy metals contents also varied with fly ash. FA2 showed a much higher metal contents than FA1, probably due to the difference in solid wastes compositions in different city. The municipality where FA1 came from implemented a more stringent garbage sorting practice.

TABLE III. Contents of major heavy metals in FA1 and FA2

Sample	Heavy metal content, g kg^{-1}					
	Cr	Ni	Cu	Zn	Pb	Cd
FA1	0.25	0.06	0.53	7.90	1.08	0.18
FA2	2.22	0.69	1.98	26.74	2.46	0.25

Heavy metal leaching toxicity

The main purpose of this research was to investigate the leaching behaviour of fly ashes by studying the leaching of heavy metals at different time point and exploring the important factors affecting the leaching behaviour.

TCLP leaching. Fig.3a shows the changes of pH and heavy metals concentrations at different leaching time. As shown in Fig. 3a, pH of the FA1 leaching solution rose quickly from the original 2.88 to about 10 after just 2 h. It continued to climb gradually, from 10 at 2 h to about 12 at 10 h. The changes in pH were caused by the consumption of acetic acid by the alkalinity in fly ash. For FA1, Cr, Ni, Cu, Zn and Cd concentrations remained low and stable during the whole leaching process. On the contrary, there is an obvious increase in Pb leaching as time was extended.

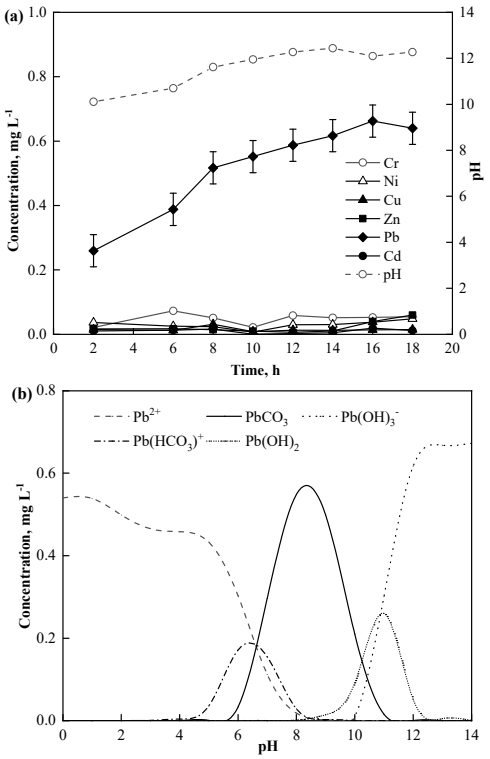

Fig. 3. Leaching of heavy metals FA1 during TCLP test (a); speciation of metals in leaching environment *via* Minteq (b).

To understand the different leaching phenomena of metals, besides heavy metals, other anion and cation concentrations in leaching solution were also monitored. As shown by XRD, XRF and FTIR analysis, fly ashes contained a variety of carbonate, sulphate and chloride salts and metal oxides. The release of these compounds into leaching solution could change the leaching environment thus affecting the release of heavy metals. Results showed that high concentrations of potassium, sodium, chloride, sulphate, carbonate and calcium were detected in leaching liquid. For instance, the leaching solution of FA1 contained a

total inorganic carbon (*TIC*) of about around 123.3 mg/L with a sulphate concentration about 120 mg/L. The release of carbonate would not only change the acidity of leaching solution but also reacting with heavy metals to form different compounds thus affecting the solubility of metals.

Software Minteq 3.1 was used to elaborate the speciation of metals in the leaching environment. Concentrations of heavy metals, calcium, chloride, sulphate and carbonate and pH were entered into the software. Minteq results showed that Cr, Ni, Cu, Zn and Cd mainly existed as carbonate or hydroxide precipitates at the pHs of the leaching solution (10–12). For example, for Cd, $CdCO_3$ and $Cd(OH)_2$ precipitates dominated at high pH. This is in accordance with the low leaching of these metals shown in Fig. 3a. That is, the high alkalinity of FA1 resulted in a very alkaline leaching solution. Metals Cr, Ni, Cu, Zn and Cd were bound up in carbonate or hydroxides precipitates.

The only exception is Pb, which has an obvious trend of increasing leaching. This can also be explained by the reactions occurring during leaching process. Fig. 3b represents the speciation of Pb-containing compounds at different pHs at the presence of carbonate, calcium, sulphate and other heavy metals. Only major species were presented here. Concentrations of other species such as $PbOH^+$, $Pb(HCO_3)^+$ and $PbSO_4$, were negligible. Unlike Cr, Ni, Cu, Zn and Cd, Pb existed mainly as $PbCO_3$ at pH 6–10, while $Pb(OH)_3^-$ became dominant as pH rose to higher than 10. It seems that as the pH of leaching solution increased, Pb was dissolved gradually to form species the like of $Pb(OH)_3^-$.

Fig. 4a shows the leaching concentrations of heavy metals and pH changes during leaching of FA2. pH of the leaching solution reached 5.2 after 2 h, then rose to 6.0 at 6 h and fluctuated between 6.5 and 7.2 after that. FA2 had a much lower alkalinity and acid neutralization capacity. Thus, the leaching solution remained acidic to near neutral.

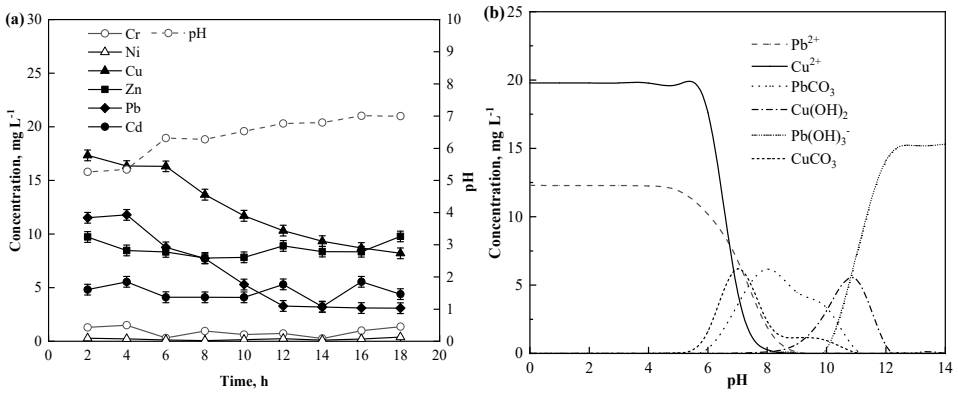

Fig. 4. Leaching concentrations of heavy metal against leaching time (a) and speciation Pb and Cu at different pH *via* Minteq (b).

The characterization of FA2 (Table III) showed that FA2 contained much higher amount of heavy metals. Therefore, higher leaching was observed for all metals. For instance, the leaching of Zn at 18 h from FA1 was 0.022 mg/L, while that from FA2 reached as high as 8.21 mg/L.

However, the behaviour of metal leaching also was different from that of FA1. Cr, Ni, Zn and Cd leaching stabilized after 4 h. As with FA1, Minteq software was employed to calculate the predominant species. Results showed that Cr^{3+}, Ni^{2+}, Zn^{2+} and Cd^{2+} were the dominant species in the whole range of pH during the FA2 leaching. The formation of carbonate precipitate was very low at the pH range. Cr, Ni, Zn and Cd compounds that could be dissolved by acetic acid in TCLP were leached out at the first 4 h, after which time the leaching stabilized.

However, for Cu and Pb, at the first stage of leaching (2–10 h), pH fluctuated between 5 and 6. According to the calculation *via* Minteq, the predominant species at this stage were Cu^{2+} and Pb^{2+}, respectively (Fig. 4b). As leaching progressed, pH increased to about 7, and $PbCO_3$ and $CuCO_3$ precipitates became predominant. This is consistent with the decline in Pb and Cu leaching in Fig. 4a after 10 h.

Overall, it appears that the heavy metals leaching was a complicated process. Besides heavy metals, other chemicals from fly ash were also released, which changed the leaching environment. Of the two fly ashes under investigation, one was much more alkaline that the other, which resulted in two different leaching environments. However, the analysis *via* Minteq showed that regardless of the differences, the precipitation/dissolution of metal carbonate and hydroxides seemed to be the controlling reactions of heavy metal leaching, as the changes in metals containing compounds affected the extent of leaching.

EDTA-modified TCLP. As shown by TCLP leaching, the fly ash compositions could greatly affect leaching behaviour by changing the leaching environment where chemical reactions (mainly precipitation/dissolution) occurred. For the two fly ashes under study, their original difference in chemical composition, and other characteristics such as alkalinity, led to difference in conditions of leaching solutions. Thus, heavy metals behaved differently. In their study of the merit and demerit of TCLP for the leaching toxicity evaluation, Lzquierdo and Querol believed high alkalinity in fly ash led to a rise in pH of the leaching solution.[30] The leaching of metal was often repressed. Fly ash in natural landfill environment came into contact with an environment with a much lower pH and presence of organics. Thus, TCLP test may underestimate the real leaching potentials. Studies above already showed that the precipitation/dissolution reactions were related to the pH of leaching environment.

To investigate the leaching behaviour when organics were present, EDTA was used to represent chelating organics and its concentration was set at 1 mmol/L.

Fig. 5 shows the heavy metal leaching by FA1 and FA2 *via* EDTA-modified TCLP.

The addition of EDTA did not change pH of the leaching solution but increased the leaching of all metals. Cu and Cd leaching at 18 h for FA1 almost doubled. Other metals also observed various degree of increase. This proved that the chelating capability of EDTA facilitated the release of metals. Another proof of EDTA's chelating effects is the leaching of Pb and Cu from FA2. Without EDTA, the leaching of Pb and Cu declined as leaching progress (Fig. 4a). With the presence of EDTA, Pb leaching continued to increase from 2–8 h and stabilized after 10 h. These results showed that the chelating effects from EDTA changed the behaviour of metals. When acetic acid alone was used as leachant, the leaching process was controlled by the precipitation/dissolution of carbonate and hydroxides of metals. With the addition of merely 1 mmol/L of EDTA, chelating reactions also played a significant role. This shows that the presence of chelating organics in natural condition may have significant effects on the leaching of metals and had to be taken into consideration.

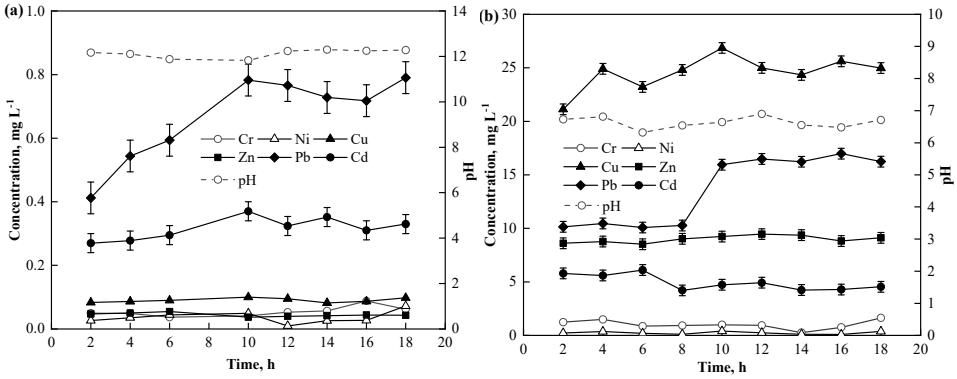

Fig. 5. Heavy metal leaching *via* EDTA-modified TCLP: a) FA1; b) FA2.

CONCLUSIONS

Fly ashes had high alkalinity because of the presence of various Ca-bearing compounds, though the strength of alkalinity and their acid neutralization capacity varied. Other major chemical composition in ashes include NaCl, KCl, SiO_2 and heavy metals such as Cr, Ni, Cu, Zn, Pb and Cd, *etc*. The exact contents of these chemicals could differ based on the compositions of municipal solid waste, incineration conditions and flue gas treatment method.

Study of heavy metals (Cr, Ni, Cu, Zn, Pb and Cd) leaching behaviour via TCLP showed that the process was complicated. The precipitation/dissolution reactions had significant effects on leaching. Because of the alkalinity in fly ash, pH of the leaching solution was raised. Calculations based on Minteq software

showed that the shifts in the precipitation/dissolution equilibrium of carbonate and hydroxides compound of heavy metals could explain the leaching of metals over time. The differences in characteristics of fly ash (alkalinity and heavy metal content, *etc*.) resulted in the variation of leaching environment and the concentrations of heavy metals. But it seems that the precipitation/dissolution reactions controlled the release of heavy metals from fly ash in TCLP test.

On the other hand, the addition of EDTA introduced chelating effects. Chelating of Pb with EDTA resulted in continuous leaching of Pb for 10 h. The amount of leaching was greatly increased, indicating that TCLP may lead to underestimation of the metal concentrations in natural environment.

Acknowledgements. This work was supported by Shanghai Natural Science Foundation (14ZR1428900) and National Natural Science Foundation of China (21707090).

ИЗВОД

КОНТРОЛИСАЊЕ РЕАКЦИЈА ТОКОМ ЛУЖЕЊА ТЕШКИХ МЕТАЛА ИЗ ЛЕТЕЋЕГ ПЕПЕЛА ОД СПАЉИВАЊА КОМУНАЛНОГ ЧВРСТОГ ОТПАДА

WEIFANG CHEN, YEGUI WANG, MINZHU HU, YONGLUN LI и GUILIN FANG

School of Environment and Architecture, University of Shanghai for Science and Technology, 516 Jun Gong Road, Shanghai 200093, China

Ово истраживање је имало за циљ да окарактерише физичка и хемијска својства летећег пепела од спаљивања комуналног чврстог отпада и истражи лужење тешких метала током процеса TCLP (енгл. *Toxicity Characteristics Leaching Procedure* – поступак лужења са карактеристикама токсичности). Да би се разумело понашање током лужења, праћене су концентрације тешких метала, хлорида, сулфата и калцијума у различитим временима лужења, и pH вредности раствора за испирање. Резултати су показали да је хемијски састав летећег пепела довео до разлика у окружењу за лужење. Од два летећа пепела која су проучавана, један је резултирао pH вредношћу од 10–12 у окружењу за лужење, док је други имао pH од око 6–7. Софтвер Minteq је коришћен за истраживање специјације тешких метала на основу pH вредности и концентрације анјона и катјона. Резултати су показали да промена у равнотежи таложења/растварања карбоната и хидроксида тешких метала може објаснити флуктуацију концентрација метала током процеса лужења, што указује на то да је лужење вероватно контролисано овим реакцијама. С друге стране, додавање EDTA је променило контролне реакције. Реакције хелирања између тешких метала и EDTA довеле су до много веће токсичности лужења тешких метала, показујући да присуство хелирајућих органских материја у природном окружењу може олакшати лужење тешких метала.

(Примљено. 5. маја, ревидирано 26. јула, прихваћено 1. августа 2022)

REFERENCES

1. M. A. Al-Ghouti, M. Khan, M. S. Nasser, K. Al-Saad, O. E. Heng, *Environ. Technol. Inn.* **21** (2021) 101267 (https://doi.org/10.1016/j.eti.2020.101267)
2. B. C. Liu, L. Zhang, Q. S. Wang, *Waste Manage.* **134** (2021) 42 (https://doi.org/10.1016/j.wasman.2021.08.007)

3. P. F. Ren, T. C. Ling, K. H. Mo, *J. Hazard. Mater.* **424** (2022) 127457 (https://doi.org/10.1016/j.jhazmat.2021.127457)
4. R. Voss, R. P. Lee, L. Seidl, F. Keller, M. Frohling, *Waste Manage.* **134** (2021) 206 (https://doi.org/10.1016/j.wasman.2021.07.040)
5. R. V. Silva, J. Brito, C. J. Lynn, R. K. Dhir, *Resour. Conserv. Recycl.* **140** (2019) 23 (https://doi.org/10.1016/j.resconrec.2018.09.011)
6. Y. B. Fan, S. J. Li, Y. B. Li, H. Q. Liang, M. X. Tang, K. K. Huang, L. Zhu, *J. Build. Eng.* **44** (2021b) 103427 (https://doi.org/10.1016/j.jobe.2021.103427)
7. Y. M. Wei, T. Shimaoka, A. Saffarzadeh, F. Takahashi, *J. Hazard. Mater.* **187** (2011) 534 (https://doi.org/10.1016/j.jhazmat.2011.01.070)
8. F. Huber, J. Fellner, *Resour. Conserv. Recycl.* **139** (2018), 17 (https://doi.org/10.1016/j.resconrec.2018.08.003)
9. C. C. Fan, B. M. Wang, H. M. Ai, Y. Qi, Z. Liu, *J. Clean. Prod., A* **319** (2021) 128790 (https://doi.org/10.1016/j.jclepro.2021.128790)
10. S. Y. Han, T. Y. Ju, Y. Meng, Y. F. Du, H. L. Xiang, A. Aihemaiti, J. G. Jiang, *J. Clean. Prod.* **321** (2021) 128922 (https://doi.org/10.1016/j.jclepro.2021.128922)
11. H. W. Luo, D. Q. He, W. P. Zhu, Y. C. Wu, Z. T. Chen, E. H. Yang, *Waste Manage., B* **84** (2019) 83 (https://doi.org/10.1016/j.wasman.2018.11.037)
12. S. L. Pei, T. L. Chen, S. Y. Pan, Y. L. Yang, Z. H. Sun, Y. J. Li, *J. Hazard. Mater.* **398** (2020), 122959 (https://doi.org/10.1016/j.jhazmat.2020.122959)
13. D. H. Yan, Z. Peng, L. F. Yu, Y. Z. Sun, R. Yong, K. H. Karstensen, *Waste Manage.* **76** (2018) 106 (https://doi.org/10.1016/j.wasman.2018.03.006)
14. S. K. Nath, S. Kumar, *J. Non-Cryst. Solids* **505** (2019) 241 (https://doi.org/10.1016/j.jnoncrysol.2018.11.007)
15. N. Ogawa, T. Amano, Y. Nagai, K. Hagiwara, T. Honda, Y. Koike, *Waste Manage.* **124** (2021) 154 (https://doi.org/10.1016/j.wasman.2021.02.016)
16. F. Liu, S. H. Ma, K. Ren, X. H. Wang, *Sci. Total Environ.* **708** (2020) 135095 (https://doi.org/10.1016/j.scitotenv.2019.135095)
17. H. W. Wang, X. X. Fan, Y. Wang, W. H. Li, Y. J. Sun, M. L. Zhan, G. Z. Wu, *J. Environ. Manage.* **208** (2018) 15 (https://doi.org/10.1016/j.jenvman.2017.11.071)
18. X. Wang, K. Zhu, L. Zhang, A. Li, C. Chen, J. Huang, Y. Zhang, *J. Environ. Manage.* **301** (2022) 113856 (https://doi.org/10.1016/j.jenvman.2021.113856)
19. C. C. Lu, M. H. Hsu, Y. P. Lin, *J. Hazard. Mater.* **368** (2019) 336 (https://doi.org/10.1016/j.jhazmat.2019.01.066)
20. Z. Y. Liu, Y. Yue, M. Lu, J. Zhang, F. C. Sun, X. Huang, J. Z. Zhou, G. R. Qian, *Waste Manage.* **84** (2019) 329 (http://dx.doi.org/10.1016/j.wasman.2018.11.049)
21. H. W. Luo, Y. Cheng, D. Q. He, E. H. Yang, *Sci. Total Environ.* **668** (2019a) 90 (https://doi.org/10.1016/j.scitotenv.2019.03.004)
22. Y. Yue, Z. Y. Liu, Z. Z. Liu, J. Zhang, M. Lu, J. Z. Zhou, G. R. Qian, *J. Environ. Manage.* **238** (2019) 144 (https://doi.org/10.1016/j.jenvman.2019.02.098)
23. E. Atanes, B. Cuesta-Garcia, A. Nieto-Marquez, F. Fernandez-Martinez, *J. Environ. Manage.* **240** (2019) 359 (https://doi.org/10.1016/j.jenvman.2019.03.122)
24. H. Yi, Z. Ai, Y. L. Zhao, X. Zhang, S. X. Song, *Sol. Energy Mater. Sol. Cells* **204** (2020) 110233 (https://doi.org/10.1016/j.solmat.2019.110233)
25. X. Y. Zhan, G. M. Kirkelund, *J. Hazard. Mater.* **412** (2021) 125220 (https://doi.org/10.1016/j.jhazmat.2021.125220)

26. W. P. Zhu, X. Chen, L. J. Struble, E. H. Yang, *J. Clean. Prod.* **192** (2018) 782 (https://doi.org/10.1016/j.jclepro.2018.05.049)
27. J. K. Prusty, B. Pradhan, *Constr. Build. Mater.* **241** (2020) 118049 https://doi.org/10.1016/j.conbuildmat.2020.118049
28. F. H. Wang, F. Zhang, Y. J. Chen, J. Gao, B. Zhao, *J. Hazard. Mater.* **300** (2015) 451 (https://doi.org/10.1016/j.jhazmat.2015.07.037)
29. D. C. W. Tsang, I. M. C. Lo, *Environ. Sci. Technol.* **40** (2006) 6655 (https://doi.org/10.1021/es060625i)
30. M. Lzquierdo, X. Querol, *Int. J. Coal Geol.* **94** (2012) 54 (https://doi.org/10.1016/j.coal.2011.10.006).

Journal of the Serbian Chemical Society
JSCS@tmf.bg.ac.rs • www.shd.org.rs/JSCS
J. Serb. Chem. Soc. *88* (1) 97–111 (2023)
JSCS–5613
Original scientific paper
Published 30 September 2022

Pictorial based learning: Promoting conceptual change in chemical kinetics

HABIDDIN HABIDDIN[1]*, HERUNATA HERUNATA[1], OKTAVIA SULISTINA[1], ACENG HAETAMI[2], MAYSARA MAYSARA[2] and DUŠICA RODIĆ[3#]

[1]*Department of Chemistry, Universitas Negeri Malang, Indonesia,* [2]*Department of Chemistry Education, Universitas Halu Oleo, Kendari, Indonesia and* [3]*Department of Chemistry, Biochemistry and Environmental Protection, University of Novi Sad, Novi Sad, Serbia*

(Received 3 April, revised 18 August, accepted 19 August 2022)

Abstract: This study aimed to examine the effect of pictorial based learning (PcBL) on conceptual change in the topic of chemical kinetics. The four-tier instrument (FTDICK) previously developed was deployed to map conceptual change within chemical kinetics concepts. First-year chemistry students at an Indonesian university formed an experimental and a control group. The experimental group experienced the PcBL approach while the control one experienced direct instruction (DI). The conceptual changes demonstrated by the two groups are classified into four categories, namely complete, partial, false and random. Complete conceptual change (CCC) had the highest occurrence rate among the four categories. However, generalising that PcBL and DI are influential in promoting conceptual change in the field of chemical kinetics may be too ambitious. Therefore, further research is needed to reach that conclusion. The effectiveness of PcBL and DI in promoting conceptual change in this study was almost equal. However, in answering the FTDICK questions, the PcBL students showed a better performance reflecting more sound scientific understanding than DI students did.

Keywords: pictorial representation; direct instruction; four-tier instrument; misconception.

INTRODUCTION

The topic of chemical kinetics is a challenge for many students at both secondary and university levels.[1] Similar to other physical chemistry topics, chemical kinetics demands the integration of conceptual understanding and mathematical ability as well as a correlation with other chemistry topics such as thermodynamics, the theory of molecular kinetics, and other aspects of chemical react-

* Corresponding author. E-mail: habiddin_wuni@um.ac.id
# Serbian Chemical Society member.
https://doi.org/10.2298/JSC220403070H

ivity. Many studies have revealed that students can successfully acquire knowledge on chemical phenomena following the elaboration of the associated academic content. However, they may still harbour ingrained misconceptions.[2,3] Efforts to promote conceptual changes in situations where students hold misconceptions have been made over the last few decades[4] and they constitute an important part of chemistry teaching. Conceptual change presupposes a restructuring or modification of existing knowledge[2,5–7] such that it becomes a solid piece of scientific knowledge.[2]

Various teaching strategies relevant to the theory of conceptual change can be applied to modify students' conceptions.[2] The implementation of such material related to acids and bases resulted in significant conceptual changes as well as changes in students' attitudes toward chemistry.[4] Another study[8] employed the predict-discuss-explain-observe-discuss-explain (PDEODE) teaching model to promote a conceptual change related to the concept of evaporation.

Another study revealed that the conceptual change on inorganic chemistry was successful in overcoming students' misconceptions related to the topic of the state of matter.[9]

Presenting a visual representation of relevant chemical concepts can be a way of challenging students' thinking processes. Many studies support the theory that a pictorial representation prompts meaningful learning, which helps students master scientific concepts and encourages concept management, concepts acquisition and integration underpinning the cognitive activities.[10] According to the cognitive psychology of instruction, the visualisation approach is a helpful strategy in aiding students to solve multistep tasks.[11] Thus, the use of pictorial representations can be helpful in teaching and learning,[12] including promoting conceptual change. Scientific concepts, including chemical concepts, can be presented, and communicated in many formats, including visual representations (pictures, graphs, photographs, diagrams), tables and mathematical formulae.[12] Depicting chemical concepts within appropriate representations can stimulate students' cognitive development and promote their information processing abilities.[13]

In some studies, the advantage of pictorial representation over verbal-based learning has produced some contradictory results. One study revealed that pictorial and verbal-based instruction had an equal effect on student achievement.[14] Another study reported that verbal-based learning resulted in better student achievement than pictorial-based learning,[15] while the other revealed that students who experienced pictorial-based learning performed better on a pictorial-based test but not on a verbal or multiple-choice one.[16] Arnold and Dwyer[17] found that the implementation of pictorial representations in teaching and learning produced higher student attainment.

Regardless of the small number of contradictory results, the majority of research established those pictorial representations promoted a more productive science learning environment.[17–19] Berg *et al.*[20] revealed that when students had been asked to draw a representational picture after observing a chemical process, they were more likely to produce a reasonable explanation of this process. In another study, macroscopic and sub-microscopic visualisations positively impacted students' discourse.[21] Pictorial representations emphasising the sub-microscopic level have been a tool to improve students' scientific understanding. Students' mastery of chemical concepts is profoundly affected by their ability to interpret abstract concepts.[22] Therefore, the practice in visualising and interpreting these abstract concepts should be incorporated in chemistry teaching.[23]

The PcBL in this study combined pictorial representations, involving the sub-microscopic level, with verbal explanations within the students' pair work class discussions, and written explanations.

EXPERIMENTAL

Research design and instrument

This quasi-experimental study applied the pre-test – post-test non-equivalent group design. It involved two groups of first-year chemistry students (with the age range of 19–21 years old) from an Indonesian university taking a fundamental chemistry course. One group with 23 students was chosen as the experimental group, and the other with 25 students as the control group. The allocation of students in each class within the university is managed by the department. Students are distributed equally in terms of their academic background to ensure homogeneity between classes. This procedure explains the equal prior knowledge between the two groups. Both groups completed a pre-test and post-test with identical questions in the form of the Four-tier diagnostics instrument of chemical kinetics (FTDICK) developed in our previous study.[24] FTDICK is a four-tier assessment tool having answer reason tiers along with attached confidence rating indices (*CRI*) on each tier. The full features of the FTDICK instruments are provided in the Supplementary material to this paper.

The pre-test was carried out simultaneously for both groups, while the post-test was conducted separately. Due to Covid-19 precautions, the post-test for the control group was carried out online using the zoom platform. To ensure that students answered the questions independently, they were requested to turn on the video during the test. The post-test for the experimental group was conducted when the government regulation for delivering all the classes online had not been applied.

PROCEDURE

This study encompassed the following steps.

Pre-test

Within the pre-testing, the students from experimental and control groups completed the FTDICK test, which provided insight into the misconception that students held before they embarked on the chemical kinetics course. Several common misconceptions were uncovered and used to design the pictorial representations to be implemented in chemical kinetics teaching. The most prevalent misconceptions demonstrated by 8.70–45.60 % of students were

found in the successive half-lives of first-, second- and zero-order reactions, the effect of concentration on the rate of chemical reaction, and the process of catalysis.

Intervention

Within this study, the experimental group was exposed to PcBL that aimed to address the misconceptions revealed by the pre-test, while the students in the control group learned through DI. The teaching textbooks and duration of teaching for the two groups was the same. The PcBL process was initiated at the start of the kinetics course by presenting images or graphics representing the sub-microscopic processes occurring in various chemical reaction scenarios. The pictorial representations functioned as a cognitive trigger for students. Below is an example of a pictorial trigger presented at the beginning of the session on successive half-lives in chemical reactions.

Fig. 1 provides pictorial representations of successive half-lives for first- and second-order reactions and was used as the trigger at the start of instruction related to the concept of half-lives. In the next step of the procedure, students worked in pairs to extract information

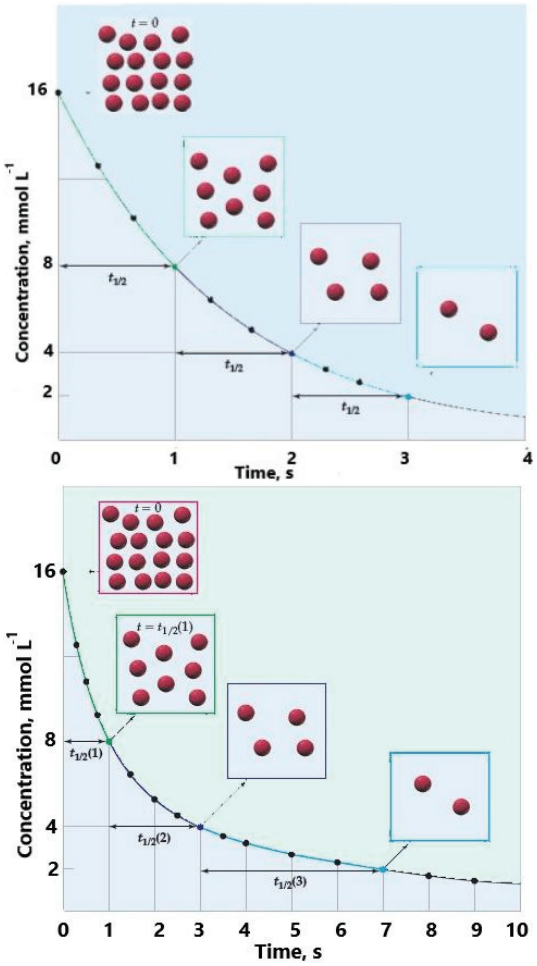

Fig. 1. The pictorial trigger for the concept of successive half-lives of first and second orders.

from the two figures and make comparisons. The information gained from the pictorial representation was discussed in class. This resulted in the conclusion that the time for each half-life is different for first- and second-order reactions. Similar steps were applied in the teaching of other concepts.

Direct instruction (DI) in this study was initiated by a brief review of the previous topic from the last class, followed by teaching on the current topic. Subsequently, students carried out exercises individually or in small groups depending on the tasks' complexity. The teacher then provided constructive feedback and a brief review of concepts covered within that lesson. As explained previously, the textbook for DI group was the same with the textbook for PcBL class. However, the pictorial presentations within the textbook were only used for additional information to support the teacher's explanation.

Post-test

The post-test was employed to explore conceptual changes demonstrated by the students from the experimental and control groups. Eleven questions of the original FTDICK were removed to leave nine questions that focussed on concepts for which students had demonstrated misconceptions. The instrument is provided in Supplementary material.

Data analysis

There are four possible combinations of students' responses to the FTDICK, namely: correct answer correct reason (CACR), correct answer wrong reason (CAWR), wrong answer correct reason (WACR) and wrong answer wrong reason (WAWR). CACR combinations reflect students' scientific understanding of the concepts under investigation. WAWR is the primary indicator of students' misconceptions related to these concepts. Confidence rate index (*CRI*) for each combination is the average of the *CRI* for the A-tier and the R-tier. It reflects the level of students' scientific and unscientific reasoning, as outlined in Table I.

TABLE I. The criteria for classification of students' misconceptions[12]

No.	*CRI* of a WAWR combination	Category
1.	>4.00–5.00	Strong
2.	>2.75–4.00	Moderate
3.	>2.00–2.75	Weak
4.	>1.00–2.00	Lack of knowledge
5.	>0.00–1.00	Guesswork

Students' responses to the pre-test and post-test were graded according to the following procedures. Score 1 was attributed to a CACR combination, while score 0 was attributed to the other combinations (WACR, CAWR and WAWR). The number of students that demonstrated misconception on each question in both the pre-test and post-test, was calculated according to:

$$N = 100\frac{n\text{WAWR}}{Nt} \quad (1)$$

N represents the number of students with misconceptions. nWAWR is the number of students providing WAWR combinations in each question. Nt is the total number of students participating in this study.

The criteria for classification of students' misconceptions

The strength of students' misconceptions is reflected by students' *CRI* when providing WAWR combinations. The *CRI* values are classified according to the criteria applied by Habiddin.[12] The criteria are presented in Table I.

The difference in performance between PCBL and DI students

The Mann–Whitney U test using SPSS software was employed to reveal the statistical difference in performance of PcBL and DI students on FTDICK. The non-parametric procedure (Mann–Whitney U test) was applied because the Shapiro–Wilk test prerequisite procedure revealed that the collected data were not normally distributed.

RESULTS AND DISCUSSION

Pictorial based learning (PcBL): Addressing students' misconceptions

The misconceptions demonstrated by students on the pre-test were used to develop teaching material for PcBL. As discussed in the method section, PcBL intervention in this study was conducted using a pictorial representation of chemical kinetics' concepts as a trigger for students' cognitive and thinking processes. The PcBL was initiated by giving a pictorial presentation of a specific chemical concept. Following this, students worked in pairs to extract meaningful information from the representation and associated teaching. For example, where more than one image associated with a concept was provided, students were instructed to compare the similarities and differences between the pictorial representations. To overcome the misconception that "the duration of the first- and second half-life is identical (which they are not in any but first-order reactions)", the PcBL was initiated through the pictorial representation presented in Fig. 1.

This misconception was uncovered from students' responses when given a question in which they had to determine the concentration of a reactant in its first- and second half-life. In answering such a question, some students considered that the concentration within the first- and the second half-life is the same. Therefore, Fig. 1 provides a cognitive challenge to students. Fig. 1 was employed to prompt students understand that the time needed for each half-life for a second-order reaction is not a constant as in the case of first-order reaction. This figure is intended to overcome the misconception that the duration of successive half-lives within second-order reaction is identical and draw students' attention to the fact that the constant duration of successive half-lives is only applicable for the first-order reactions. Fig. 2 is the pictorial trigger to overcome the misconception that "a catalyst does not remain chemically unchanged after the reaction is completed." The figure shows that the catalyst, represented by the two red spheres, is not consumed and remain chemically unchanged even though it took part in the reaction, as shown in the central box. The involvement of the catalyst is confirmed by the separation of two red spheres and their recombination.

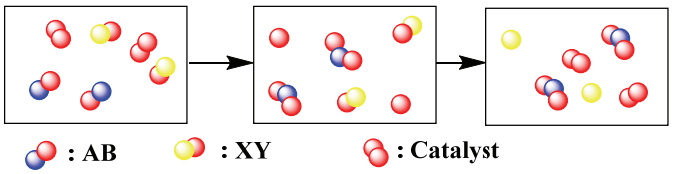

Fig. 2. The Pictorial trigger for the concept of catalyst.

Fig. 3 provides several pictorial clues that the presence of a catalyst increases the reaction rate. The figure is the pictorial trigger to overcome a misconception that "the presence of a catalyst decreases the rate." Fig. 3a depicts the decomposition of HCOOH without the presence of a catalyst. Fig. 3b illustrates the decomposition of HCOOH using the catalyst H^+. The figure shows that the presence of the catalyst lowers the activation energy and leads to a higher reaction rate in comparison to the uncatalysed reaction (Fig. 3a). The figure also indicates another scientific information: the presence of a catalyst provides a different reaction mechanism as depicted by the different steps in the same reaction and multiple transition states in the presence of the catalyst. Some concepts are difficult to display pictorially, and so verbal descriptions had to be used. For example, Table II was used to overcome the belief that "the power of the reactants in the rate law expression for a given chemical reaction is equal to the stoichiometric coefficients in the balanced equation of that reaction." It also demonstrates that the rate law expression cannot be obtained by applying the same procedure as for the equilibrium constant expression. Both of these theories are commonly held misconceptions.[25]

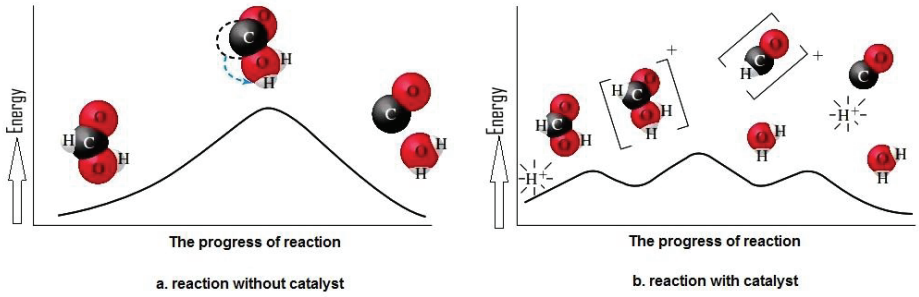

Fig. 3. The Pictorial trigger for the concept of catalyst.

It is likely that the misconception that the rate law expression is obtained from the stoichiometric equation derives from the nature of the examples used during the teaching. If within the examples that the students were given the values of the stoichiometric coefficients and exponents in the rate law expression were identical, this could have led to the conclusion that the latter could be obtained directly from the former. Table II provides examples demonstrating that

the rate law is determined experimentally and does not depend on the balanced stoichiometric equation. This table also demonstrates that the rate law expression and the equilibrium-constant expression are different concepts.

TABLE II. The triggering table for the concept of rate law

No.	Chemical equation	Rate law
1.	$CO(g) + NO_2(g) \rightarrow CO_2(g) + NO(g)$	Rate = $kc_{CO}c_{NO2}$
2.	$2H_2O_2(aq) \rightarrow 2H_2O(l) + O_2(g)$	Rate = kc_{H2O2}
3.	$2NO(g) + Cl_2(g) \rightarrow 2NOCl(g)$	Rate = $kc_{NO2}c_{Cl2}$
4.	$2NH_3(g) \rightarrow N_2(g) + 3H_2(g)$	Rate = $kc_{(NH3)}{}^0 = k$
5.	$Pt(NH_3)_2Cl_2(aq) + H_2O(l) \rightarrow [Pt(NH_3)_2O)Cl]^+(aq) + Cl^-(aq)$	Rate = $kc_{Pt(NH3)2Cl2}$

The figures and table were presented at the beginning of elaboration of the concept of interest. Following this, students worked in pairs to extract valuable pieces of information and relate them to the targeted concept. In the next step, students shared their conclusions with the whole class, and this was followed by a class discussion led by the class teacher.

The process of extracting valuable information from a picture or table, relating the information to the relevant concept and sharing and discussing ideas is expected to trigger students' cognitive processes and finally lead to the conceptual change. These activities are appropriate to the following components of scientific practices formulated by The National Research Council,[26] namely: asking questions, analysing and interpreting data, constructing explanations and designing solutions, engaging in discussion based on evidence, and also obtaining, evaluating and communicating information. These scientific practices were in the focus of science education research over the last decade.[27–29]

Description of conceptual change occurrence rates

Students' conceptual change as a result of the implementation of PcBL and DI approach is determined based on the shift from students' misconceptions demonstrated on the pre-test to a scientific understanding and decrease in the frequency of occurrence of these misconceptions on the post-test. Table III shows the percentages of students holding misconceptions before and after the implementation of the abovementioned teaching approaches. The table presents the complete conceptual change (CCC), partial conceptual change (PCC), false conceptual change (FCC) and random conceptual change (RCC) occurrence rates. CCC means that all the students who previously held misconceptions demonstrated a full scientific understanding given on the post test. PCC means that a only certain portion of the students demonstrated a scientific understanding of given concept on the post-test. A smaller portion of students is still retaining the misconception. FCC means that the number of students demonstrating misconception (MC) on the post-test is even higher compared to the pre-test. RCC

means the number of students holding the misconception decreased, but their *CRI* increased and *vice versa*. The comparison of the conceptual change occurrence rates among PcBL and DI students is depicted in Fig. 4.

TABLE III. Conceptual change occurrence rates

Misconception (MC)	Pre-test			Post-test					
				PcBL			DI		
	N %	*CRI*	Category	*N* %	*CRI*	Category	*N* %	*CRI*	Category
MC1: the terminalogy of the first half-life and the second half-life means the same	21.74	3.3	Moder-ate	5.26	1.5	Lack of knowledge	4.17	1.5	Lack of knowledge
MC2: the reaction rate always increases with a decrease in concentration of reactant	21.74	2.8	Moder-ate	0	0	Over-come	25	4.5	Strong
MC3: the $t_{1/2}$ value of each successive half-life for the first- and the second-order reactions is identical	26.09	3.1	Moder-ate	36.84	3.9	Moder-ate	8.33	4.0	Strong
MC4: the duration of the half-lives of a second-order reaction is constant	23.91	3.6	Moder-ate	36.84	3.5	Moder-ate	25	3.0	Moder-ate
MC5: the power of the reactants in the rate law expression for a given chemical reaction is equal to the stoichiometric coefficients in the balanced equation of that reaction	8.70	2.0	Weak	5.26	1.5	Lack of knowledge	8.33	3.5	Moder-ate
MC6: the equilibrium-constant expression can be used to derive the rate law expression	45.65	3.3	Moder-ate	10.52	3.0	Moder-ate	16.67	3.3	Moder-ate
MC7: the rate law equation can only be expressed in terms of the rate of disappearance of reactants	26.09	3.3	Moder-ate	0	0	Over-come	0	0	Over-come
MC8: a catalyst does not remain chemically unchanged after the reaction is completed	17.39	3.1	Moder-ate	0	0	Over-come	0	0	Over-come
MC9: the presence of a catalyst decreases the reaction rate	13.04	3.8	Moder-ate	5.26	5.0	Strong	4.17	1.0	Lack of knowledge
MC10: the reaction rate always decreases with time	10.87	2.5	Weak	0	0	Over-come	0	0	Over-come

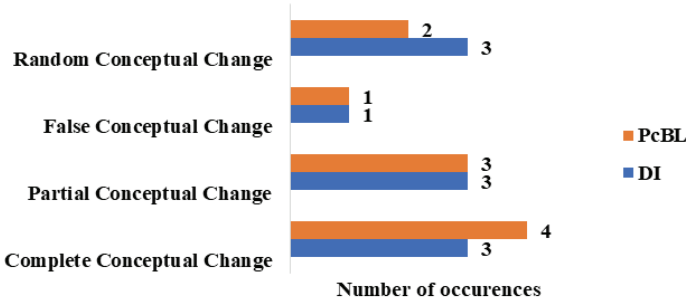

Fig. 4. A comparison of occurrence rates of the four types of conceptual change among students from PcBL and DI groups.

The CCC is the most frequent type of conceptual change demonstrated by PcBL students, whereas the occurrence rates of CCC and PCC are equal within the DI students. The CCC for PcBL students is detected for MC2, MC7, MC8, while for the DI students it occurred in relation to MC10 and MC7, MC8 and MC10. Before the intervention, 21.74 % of PcBL students with a *CRI* of 2.80 held the misconception that the rate always increases with a decrease in concentration (MC2). After the intervention, all PcBL students held a correct scientific understanding regarding this concept. The opposite phenomenon, *i.e.*, FCC, is shown by DI students. The number of students holding the misconception that fell in the "strong" category increased after the intervention. For MC7, MC8 and MC10, both groups demonstrated a CCC. Within MC8, students assumed that "a catalyst does not remain chemically unchanged after the reaction is completed."

After the interventions encompassing Fig. 2, they realised that the catalyst remains chemically unchanged even after it took part in the reaction. The absence of the two connected red spheres representing a catalyst in the central box implies that the catalyst is involved in the reaction. The two connected red spheres in the final box indicated the correct scientific idea to the PcBL students, which is that the catalyst is not consumed in the reaction and that it remains chemically unchanged after it. This study confirmed the work published by Canpolat *et al.*[30] that students taught by a conceptual change approach performed better than those taught by a more traditional approach. The successful conceptual change was also reported in relation to the teaching about acid and base.[4] The improvement in students' understanding after implementing pictorial representations has also been reported in regard to the other chemistry topics.[20,21,31,32]

A PCC was detected in relation to MC1, MC5, and MC6 for PcBL students. A significant decrease in a number of students holding the misconceptions to successive half-lives after experiencing PcBL is strong evidence of conceptual change regarding MC1. Fig. 1 shows that the label $t_{1/2}$ at every point where the concentration of the reactant is half the previous one triggered students' aware-

ness that half-life terminology is applicable every time the concentration is halved. The 5.26 % of students who still held this misconception after the intervention showed a very low *CRI* of 1.5, which falls in the "lack of knowledge" category.

Another significant decrease in the number of students holding the misconception that "used the equilibrium-constant expression to derive the rate law" is revealed in MC6. However, the remaining 10.52 % of students who still held this misconception showed a moderate *CRI*.

Meanwhile, a small decrease in the number of students holding the misconception that "the power of the reactants in the rate law expression for a given chemical reaction is equal to the stoichiometric coefficients in the balanced equation of that reaction" is revealed for MC5. Providing various chemical equations accompanied by their rate law expressions (Table II) did not totally overcome students' misconceptions in regard to this concept. PCC for DI students appears for MC1, MC6 and MC9. As explained before, PCC for MC1 and MC6 also appear for PcBL students. At MC9, a small portion of DI students (4.17 %) still held the misconception that "the presence of a catalyst decreases the rate" but with a very low *CRI* falling in the lack of knowledge category. Some unexpected results regarding FCC are found in relation to MC3 for PcBL students. Even after experiencing PcBL and studying Fig. 1, some students still firmly believed that "the $t_{1/2}$ value of each successive half-life for the first- and the second-order reactions is identical."

Although the *CRI* of those misconceptions remained in the "moderate" category, the number of students holding them increased. This phenomenon confirms the strong familiarity of students with the concept of constant half-life in first-order reactions.[12] Greater emphasis on first-order reactions in chemistry textbooks could be the cause of this misunderstanding.[12] This could also explain the unexpected in finding related to MC4, namely, "the duration of the half-lives of a second-order reaction is constant." This finding is in line with the one published by Tirr *et al.*[15] DI students demonstrated an RCC in this instance. The number of students holding the misconception decreased significantly, but the CRI of those still holding it increased significantly, falling into the "strong category." The RCC is demonstrated by PcBL students regarding MC9 related to the misconception that "the presence of a catalyst decreases the reaction rate."

This misconception is a novel finding. Fig. 3 was used to explore this point with an additional question designed to establish a link between the energies of the different transition states and the relative rates of each reaction. A discussion of the different mechanisms was also instigated. After experiencing PcBL, a complete conceptual change was also demonstrated regard to this concept. The number of students demonstrating this misconception significantly decreased, but the *CRI* of those holding it also increased, falling in the "strong" category.

The fact that PcBL in this study did not completely remediate students' misconception could have a variety of explanations. Firstly, students may not yet be familiar with this teaching approach. Students may need more practice in extracting meaningful information from visual prompts. Secondly, the PcBL approach implemented in this study was provided by the lecturers (who are also the authors). The approach may be enhanced by asking students to draw their pictorial representations of the relevant concepts.[33] Thirdly, the ways in which students initially develop their misconceptions needs to be explored[2] in order to develop better strategies to overcome them. Further studies should consider these shortcomings.

PcBL vs. *DI students' performances*

The results of this study imply that it is not possible to determine which of the two approaches (PcBL and DI) is better in promoting conceptual change. As displayed in Fig. 4, the CCC occurrence rate for PcBL students is higher than that for the DI students. The occurrence rate of PCC and FCC is equal for the two groups. The DI students demonstrate higher RCC occurrence rates compared to the PcBL students. Reflecting on these facts, it seems that PcBL students showed only a slightly better performance than DI students did in terms of the conceptual change. This phenomenon is in line with the work of Wang,[34] who compared inquiry-based teaching and DI.

In terms of students' performance of FTDICK, the Mann Whitney U test revealed that the mean rank of the PcBL students (29.16) is higher than that of the DI students (16.33). Specifically, the U statistic and the asymptotic significance (2-tailed) p-value show that PcBL students' performance in answering FTDICK questions was significantly higher compared to the DI students (U = = 92.000, p = 0.001). This result reinforces the finding that PcBL is effective in achieving CCC for most students who experience it.

CONCLUSION

The implementation of PcBL and DI triggers a conceptual change among students who previously harboured misconceptions in regard to chemical kinetics. Complete conceptual change (CCC) had the highest occurrence rate among the PcBL students, while CCC and PCC occurred with equal frequency among the DI students. FCC also occurred with the same frequency among the students for the two groups, but at the same time, this type of conceptual change was least frequently observed. The existence of PCC, RCC, and even FCC reflects that the implementation of PcBL may not instantly provide a complete conceptual change. To achieve this more practice, particularly in developing students' ability to interpret pictures, graphics and tables, and finally extract valuable information from these representations, is needed. In dealing with pictorial representations, some students face two challenging issues, which are: *i*) difficulty in extracting

the relevant information[12,35] and *ii*) errors in transforming the information extracted from the pictorial context into chemical behaviour.[35] Providing more opportunities for students to deal with pictorial representations both in teaching and learning and in the evaluation process will encourage students to become more familiar with such exercise and more confident in their ability to deal with them. A study has shown a link between students' confidence in chemistry with their achievement in chemical kinetics.[36]

Although the results show that the frequency of CCC among the PcBL students is slightly higher in comparison to the DI students, we don't attempt to generalize the conclusions of this study in regard to PcBL for the entire field of chemistry teaching, or even the field of chemical kinetics. However, the conclusions reached within this study may prompt further studies with larger sample sizes and in other chemistry topics and a more readily generalizable inference can be reached in the future. In terms of students' answers to FTDICK questions, the PcBL students demonstrated a better performance in comparison to the DI students. This may infer that the PcBL approach is more potent in improving students' understanding of chemical kinetics than the DI approach.

SUPPLEMENTARY MATERIAL

Additional data and information are available electronically at the pages of journal website: https://www.shd-pub.org.rs/index.php/JSCS/article/view/11740, or from the corresponding author on request.

Acknowledgement. We thank Universitas Negeri Malang for providing the grant of this research with the grant number 20.3.169/UN32.14.1/LT/2019.

ИЗВОД

УЧЕЊЕ ЗАСНОВАНО НА ИЛУСТРАЦИЈАМА: ПРОМОВИСАЊЕ КОНЦЕПТУАЛНЕ ПРОМЕНЕ У ОКВИРУ ТЕМЕ ХЕМИЈСКА КИНЕТИКА

HABIDDIN HABIDDIN[1], HERUNATA HERUNATA[1], OKTAVIA SULISTINA[1], ACENG HAETAMI[2], MAYSARA MAYSARA и ДУШИЦА РОДИЋ[3]

[1]Department of Chemistry, Universitas Negeri Malang, Indonesia, [2]Department of Chemistry Education, Universitas Halu Oleo, Kendari, Indonesia и [3]Дейартман за хемију, биохемију и заштиту животне средине, Природно-математички факултет, Универзитет у Новом Саду, Нови Сад

Ова студија је имала за циљ да испита утицај учења заснованог на илустрацијама (PcBL) на концептуалне промене у оквиру теме Хемијска кинетика. За мапирање концептуалних промена у оквиру концепата хемијске кинетике, коришћен је претходно развијени четворослојни инструмент (FTDICK). Студенти прве године хемије на једном универзитету у Индонезији формирали су експерименталну и контролну групу. Експериментална група је обучавана применом PcBL методе, док је контролна група обучавана применом директне инструкције (DI). Концептуалне промене које су уочене у оквиру ове две групе класификоване су у четири категорије: потпуне, парцијалне, лажне и насумичне. Потпуна концептуална промена (CCC) је имала највећи степен учесталости од четири наведене категорије. Међутим, било би исувише амбициозно генерализовати да су и PcBL и DI ефикасни у поспешивању концептуалних промена у области хемијске кинетике. Да би се извео такав закључак, потребна су додатна истраживања.

Ефикасност PcBL и DI методе у поспешивању концептуалних промена у овој студији била је готово једнака. Међутим, у решавању задатака на FTDICK, студенти PcBL групе су остварили бољи учинак од студената DI групе и тиме показали боље научно разумевање.

(Примљено.3. априла, ревидирано 18. августа, прихваћено 19. августа 2022)

REFERENCES

1. K. Bain, M. H. Towns, *Chem. Educ. Res. Pract.* **17** (2016) 246 (https://doi.org/10.1039/C5RP00176E)
2. G. C. Weaver, in *Chemistsћ Guide to Effective Teaching, Vol. 2*, N. J. Pienta, M. M. Cooper, T. J. Greenbowe, Eds., Pearson Education, Inc., Upper Saddle River, NJ, 2009, p. 35
3. V. Talanquer, *J. Chem. Educ.* **94** (2017) 1805 (https://doi.org/10.1021/acs.jchemed.7b00427)
4. G. Demircioglu, A. Ayas, H. Demircioglu, *Chem. Educ. Res. Pract.* **6** (2005) 36 (https://doi.org/10.1039/B4RP90003K)
5. A.-M. Rusanen, *Sci. Educ.* **23** (2014) 1413 (https://doi.org/10.1007/s11191-013-9656-8)
6. G. J. Posner, K. A. Strike, P. W. Hewson, W. A. Gertzog, *Sci. Educ.* **66** (1982) 211 (https://doi.org/10.1002/sce.3730660207)
7. M. Schneider, X. Vamvakoussi, W. Van Dooren, in *Encyclopedia of the Sciences of Learning*, N.M. Seel, Ed., Springer US, Boston, MA, 2012, p. 735 (https://doi.org/10.1007/978-1-4419-1428-6_352)
8. B. Coştu, A. Ayas, M. Niaz, *Chem. Educ. Res. Pract.* **11** (2010) 5 (https://doi.org/10.1039/C001041N)
9. R. S. Rohmah, F. Fariati, S. Ibnu, in *Proceedings of The 3rd International Conference on Mathematics And Science Education (ICOMSE)*, (2019), Malang, Indonesia, AIP Conf. Proc., American Institute of Physics, Melville, New York, 2020, p. 20020 (https://doi.org/10.1063/5.0000492)
10. K. M. Edens, E. F. Potter, *Stud. Art Educ.* **42** (2001) 214 (https://doi.org/10.2307/1321038)
11. D. C. Orlich, R. J. Harder, R. C. Callahan, M. S. Trevisan, A. H. Brown, *Teaching Strategies: A Guide to Effective Instruction*, 9th ed,. Wadsworth Publishing, Boston, MA, 2010
12. Habiddin, *PhD Thesis*, University of Reading, 2018
13. T. Gegios, K. Salta, S. Koinis, *Chem. Educ. Res. Pract.* **18** (2017) 151 (https://doi.org/10.1039/C6RP00192K)
14. J. Snowman, D. J. Cunningham, *J. Educ. Psychol.* **67** (1975) 307 (https://doi.org/10.1037/h0076934)
15. W. C. Tirr, L. Manelis, K. L. Leicht, *J. Read. Behav.* **11** (1979) 99 (https://doi.org/10.1080/10862967909547313)
16. K. L. Alesandrini, J. W. Rigney, *J. Res. Sci. Teach.* **18** (1981) 465 (https://doi.org/10.1002/tea.3660180509)
17. T. C. Arnold, F. M. Dwyer, *Percept. Mot. Skills* **40** (1975) 369 (https://doi.org/10.2466/pms.1975.40.2.369)
18. J. Rigney, K. Lutz, *J. Educ. Psychol.* **68** (1976) 305 (https://doi.org/10.1037/0022-0663.68.3.305)
19. W. G. Holliday, *J. Res. Sci. Teach.* **12** (1975) 77 (https://doi.org/10.1002/tea.3660120111)

20. A. Berg, D. Orraryd, A. J. Pettersson, M. Hultén, *Chem. Educ. Res. Pract.* **20** (2019) 710 (https://doi.org/10.1039/C8RP00288F)
21. V. Hunter, I. Hawkins, A. J. Phelps, *Chem. Educ. Res. Pract.* **20** (2019) 851 (https://doi.org/10.1039/C9RP00064J)
22. R.B. Kozma, J. Russell, *J. Res. Sci. Teach.* **34** (1997) 949 (https://doi.org/10.1002/(SICI)1098-2736(199711)34:9<949::AID-TEA7>3.0.CO;2-U)
23. B. Bucat, M. Mocerino, in *Multiple Representations in Chemical Education*, J.K. Gilbert, D.F. Treagust, Eds., Springer Netherlands, Dordrecht, 2009, pp. 11
24. H. Habiddin, E. M. Page, *Indones. J. Chem.* **19** (2019) 720 (https://doi.org/10.22146/ijc.39218)
25. T. Turányi, Z. Tóth, *Chem. Educ. Res. Pract.* **14** (2013) 105 (https://doi.org/https://doi.org/10.1039/C2RP20015E)
26. N. R. Council, *A Framework for K-12 Science Education: Practices, Crosscutting Concepts, and Core Ideas*, The National Academies Press, Washington DC, 2012
27. M. Evagorou, S. Erduran, T. Mäntylä, *Int. J. STEM Educ.* **2** (2015) 11 (https://doi.org/10.1186/s40594-015-0024-x)
28. J. Osborne, *J. Sci. Teacher Educ.* **25** (2014) 177 (https://doi.org/10.1007/s10972-014-9384-1)
29. R. S. Schwartz, N. G. Lederman, F. Abd-el-Khalick, *Sci. Educ.* **96** (2012) 685 (https://doi.org/10.1002/sce.21013)
30. N. Canpolat, T. Pınarbaşı, S. Bayrakçeken, O. Geban, *Res. Sci. Technol. Educ.* **24** (2006) 217 (https://doi.org/10.1080/02635140600811619)
31. M. Baptista, I. Martins, T. Conceição, P. Reis, *Chem. Educ. Res. Pract.* **20** (2019) 760 (https://doi.org/10.1039/C9RP00018F)
32. G. Eymur, Ö. Geban, *Int. J. Sci. Math. Educ.* **15** (2017) 853 (https://doi.org/10.1007/s10763-016-9716-z)
33. V. M. Williamson, T. J. Jose, in *Chemists' Guide to Effective Teaching, Vol. 2*, N. J. Pienta, M.M. Cooper and T. J. Greenbowe, Eds., Pearson Education, Inc., Upper Saddle River, NJ, 2009, p. 71
34. J. Wang, *Int. J. Sci. Math. Educ.* **18** (2020) 1063 (https://doi.org/10.1007/s10763-019-10010-7)
35. H. Habiddin, E. M. Page, *Int. J. Sci. Math. Educ.* **19** (2021) 65 (https://doi.org/10.1007/s10763-019-10037-w)
36. H. Habiddin, E. M. Page, H. Herunata, O. Sulistina, W. Winartiasih, M. Muarifin, M. Maysara, in *Proceedings of The 3rd International Conference on Mathematics and Science Education (*ICOMSE*)*, (2019), Malang, Indonesia, AIP Conf. Proc., American Institute of Physics, Melville, New York, 2020, p. 20006 (https://doi.org/10.1063/5.0000502).

Journal of the Serbian Chemical Society
JSCS@tmf.bg.ac.rs • www.shd.org.rs/JSCS
J. Serb. Chem. Soc. *88* (1) S30–S34 (2023) *Supplementary material*

SUPPLEMENTARY MATERIAL TO

Pictorial based learning: Promoting conceptual change in chemical kinetics

HABIDDIN HABIDDIN[1]*, HERUNATA HERUNATA[1], OKTAVIA SULISTINA[1], ACENG HAETAMI[2], MAYSARA MAYSARA[2] and DUŠICA RODIĆ[3#]

[1]*Department of Chemistry, Universitas Negeri Malang, Indonesia,* [2]*Department of Chemistry Education, Universitas Halu Oleo, Kendari, Indonesia and* [3]*Department of Chemistry, Biochemistry and Environmental Protection, University of Novi Sad, Novi Sad, Serbia*

J. Serb. Chem. Soc. *88* (1) (2023) 97–111

THE FTDICK INSTRUMENT

Consent form

We are conducting an investigation into students' understanding of chemical reaction kinetics. As you will be studying/have studied this topic we would like you to attempt the following questions and choose reasons for your answers. The results from the investigation will be used alongside the data from other students to gain a better understanding of students' understanding of reaction rates and may be published in the educational literature. The outcomes will be completely anonymous and no participants will be identifiable. If you would like your results to contribute to our investigation, please tick the box below:

○ I am happy to take part in this investigation and for my results to contribute to the investigation

Signed: Date:

* Corresponding author. E-mail: habiddin_wuni@um.ac.id

No.	Question
1.	A 64 mg sample of radioactive material decays by first order reaction. After 10 minutes two half-lives have passed. What is the mass of the sample that remains after 15 minutes? A. 24 mg B. 23 mg C. 16 mg D. 8 mg State the confidence rating of your answer 1. Very unconfident 2. Not very confident 3. Average 4. Quite confident 5. Very confident Which one of the following options is the reason for your answer to the question? After 10 minutes, half of the initial sample remained The rate of decay of this sample is a constant For each successive half-life, the mass change of sample is a constant The rate of decay of this sample increases as the mass of sample decreases For each successive half-life, the mass of sample decreases by a factor of 2 State the confidence rating of your answer 1. Very unconfident 2. Not very confident 3. Average 4. Quite confident 5. Very confident
2.	The decomposition of nitrogen dioxide to nitric oxide and oxygen at a certain temperature is shown pictorially below and is a second order reaction and the equation for the reaction is: $2NO_2(g) \rightarrow 2NO(g) + O_2(g)$ 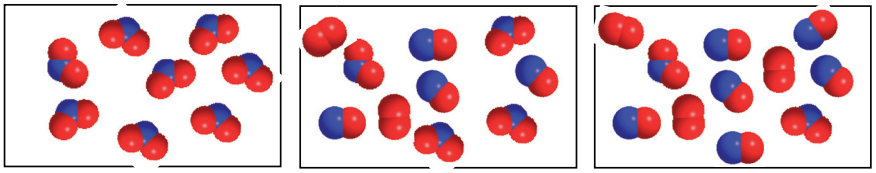 $t = 10\ s$ $t = 20\ s$ $t =$ .....? time The time at the final representation shown above is… A. 25 s B. 30 s C. 40 s D. 50 s State the confidence rating of your answer 1. Very unconfident 2. Not very confident 3. Average 4. Quite confident 5. Very confident Which one of the following options is the reason for your answer to the question? The value of each successive half-life is half the preceding one The value of t½ is constant The rate of disappearance of this sample increases with decrease in concentration The value of each successive half-life is twice the preceding one. State the confidence rating of your answer 1. Very unconfident 2. Not very confident 3. Average 4. Quite confident 5. Very confident
3.	The second order reaction of $H_2O_2(aq) + 3I^-(aq) + 2H^+(aq) \rightarrow 2H_2O(l) + I_3^-(aq)$ is first order in H_2O_2, first order in I^- and zero order in H^+. The rate law expression for this reaction is…. A. Rate = $k\, c_{H_2O_2} (c_{I^-})^3 (c_{H^+})^2$ B. Rate = $k\, c_{H_2O_2}\, c_{I^-}$ C. Rate = $k \frac{[C_{H_2O_2}]\ C_{I^-}}{\ }$ D. Rate = $k\, (c_{H_2O_2})^x (C_{I^-})^y (C_{H^+})^z$ (x, y, z are $\neq 0$) State the confidence rating of your answer 1. Very unconfident 2. Not very confident 3. Average 4. Quite confident 5. Very confident Which one of the following options is the reason for your answer to the question? The values of the exponents in the rate law are obtained from the coefficients in the balanced equation The rate law is expressed based on the law of mass action that describes the relationship between the concentrations of the reactants and products. The values of the exponents in the rate law are based on the order of the reactants which are determined experimentally The information which is provided in the question is inadequate to determine the rate law. State the confidence rating of your answer 1. Very unconfident 2. Not very confident 3. Average 4. Quite confident 5. Very confident

4. The decomposition of nitrogen dioxide to nitric oxide and oxygen takes place by second order kinetics:

$$2NO_2(g) \rightarrow 2NO(g) + O_2(g)$$

At time, t = 10 s the pressure of NO_2 is 10.66 kPa and after 5 seconds the pressure has dropped to 5.33 kPa. Determine the time at which the pressure of NO_2 is 2.66 kPa

A. 17.5 *s* B. 20 *s* C. 25 *s* D. 30 *s*

State the confidence rating of your answer

1. Very unconfident 2. Not very confident 3. Average 4. Quite confident 5. Very confident

Which one of the following options is the reason for your answer to the question?

The value of each successive half-life is half the preceding one

The value of t½ is constant

The rate of disappearance of this sample increases with decrease in concentration

The value of each successive half-life is twice the preceding one.

State the confidence rating of your answer

1. Very unconfident 2. Not very confident 3. Average 4. Quite confident 5. Very confident

5. The formation of HI(g) follows the reaction $H_2 + I_2 \rightarrow 2HI$. This reaction may occur with the following mechanism:

$$I_2 \underset{k_{-1}}{\overset{k_1}{\rightleftharpoons}} 2I \quad \text{fast}$$

$$I + I + H_2 \xrightarrow{k_2} 2HI \quad \text{slow}$$

The overall rate law of this reaction is….

A. Rate = $k_2 (C_I)^2 (C_{H2})$ B. Rate = $k \frac{(C_{HI})^2}{(C_I)^2 (C_{H_2})}$

C. Rate = $k_2 \frac{k_1}{k_{-1}} (C_{I2}) (C_{H2})$ D. Rate = $k_1 (C_{I2}) - k_{-1}(C_I)^2$

State the confidence rating of your answer

1. Very unconfident 2. Not very confident 3. Average 4. Quite confident 5. Very confident

Which one of the following options is the reason for your answer to the question?

The rate law is obtained directly from the slow step in the mechanism

The rate law is obtained from the fast step in the mechanism

The rate law is obtained from the law of mass action

The rate law is obtained from the slow step by considering any intermediates in preceding steps

State the confidence rating of your answer

1. Very unconfident 2. Not very confident 3. Average 4. Quite confident 5. Very confident

6. The following diagram depicts an imaginary two step mechanism of a reaction.

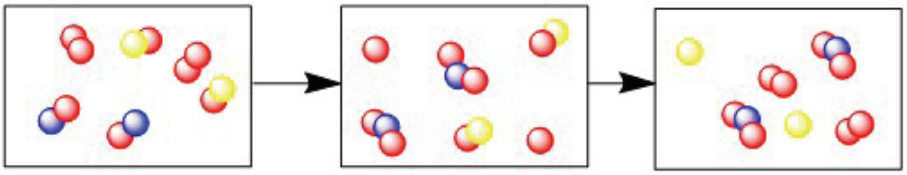

Based on the representation above, the substance that acts as a catalyst is….

X B. XZ C. X_2 D. XY

State the confidence rating of your answer

1. Very unconfident 2. Not very confident 3. Average 4. Quite confident 5. Very confident

Which one of the following options is the reason for your answer to the question?

The substance does not undergo a permanent chemical change and is reformed in the final product

The substance is formed in one elementary reaction and consumed in the next

The substance increases the rate without being involved chemically in the reaction

The substance is not present in the final product

State the confidence rating of your answer

1. Very unconfident 2. Not very confident 3. Average 4. Quite confident 5. Very confident

7. The variation in partial pressure of HCOOH for the decomposition of formic acid {HCOOH(g) → CO_2(g) + H_2(g)} in the gas phase as a function of time at 838 K is described in the graph below.

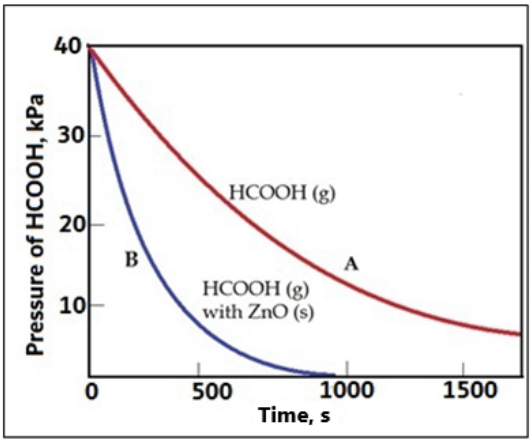

A graph of the partial pressure of HCOOH versus time is shown as the red curve, A. Assuming that ZnO(s) is the catalyst, when a small amount of solid ZnO is added, the partial pressure of HCOOH versus time varies as shown by the blue curve, B. Based on this information, which is the correct statement below?

This is an example of homogeneous catalysis and the rate of B is higher than the rate of A
This is an example of heterogeneous catalysis and the rate of B is higher than the rate of A
This is an example of homogeneous catalysis and the rate of A is higher than the rate of B
This is an example of heterogeneous catalysis and the rate of A is higher than the rate of B

State the confidence rating of your answer

1. Very unconfident 2. Not very confident 3. Average 4. Quite confident 5. Very confident

Which one of the following options is the reason for your answer to the question?

HCOOH, CO_2 and H_2 are in the same phase and the presence of ZnO increases the rate
HCOOH and ZnO are in different phases and the presence of ZnO decreases the rate
HCOOH, CO_2 and H_2 are present in the same phase and the presence of ZnO decreases the rate
HCOOH and ZnO are in different phases and the presence of ZnO increases the rate

State the confidence rating of your answer

1. Very unconfident 2. Not very confident 3. Average 4. Quite confident 5. Very confident

8. The hypothetical reaction G → H is depicted pictorially below. Each blue sphere represents 0.2 moles of G and each red sphere represents 0.2 moles of H, and the container has a volume of 1.00 L.

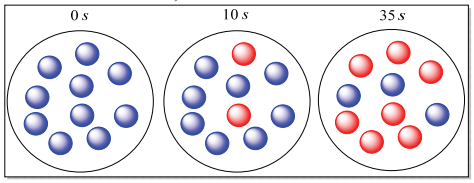

The number of moles of G and H respectively in the mixture after 32 s is….

A. 1.280 mol; 0.720 mol B. 0.544 mol; 1.456 mol C. 0.720 mol; 1.280 mol D. 1.456 mol; 0.544 mol

State the confidence rating of your answer

1. Very unconfident 2. Not very confident 3. Average 4. Quite confident 5. Very confident

Which one of the following options is the reason for your answer to the question?

As time increases, the rate of conversion of G molecules to H molecules also increases
As time increases, the rate of conversion of G molecules to H molecules decreases
The rate of conversion of G molecules to H molecules per second is a constant

State the confidence rating of your answer

1. Very unconfident 2. Not very confident 3. Average 4. Quite confident 5. Very confident

9.	The decomposition of N_2O_5 in a solvent occurs according to the following equation $N_2O_5 \rightarrow 2NO_2 + ½\ O_2$ In the interval between 20 minutes and 40 minutes, the $[N_2O_5]$ decreases from 0.1 M to 0.080 M. Which of the following options is the correct expression of the average reaction rate? A. Rate = $\Delta C_{N2O5}/\Delta t$ = 0.001 M min^{-1} B. Rate = $\Delta C_{NO2}/\Delta t$ = 0.001 M min^{-1} C. Rate = $\Delta C_{O2}/\Delta t$ = 0.0005 M min^{-1} D. Rate = $\Delta C_{NO2}/\Delta t$ = - 0.002 M min^{-1} State the confidence rating of your answer 1. Very unconfident 2. Not very confident 3. Average 4. Quite confident 5. Very confident Which one of the following options is the reason for your answer to the question? O_2 is produced twice as fast as N_2O_5 is consumed NO_2 is produced a half as fast as N_2O_5 is consumed The rate law can only be expressed by the rate of disappearance of N_2O_5 N_2O_5 is consumed twice as fast as NO_2 is produced NO_2 is consumed twice as fast as N_2O_5 is consumed O_2 is produced a half as fast as N_2O_5 is consumed State the confidence rating of your answer 1. Very unconfident 2. Not very confident 3. Average 4. Quite confident 5. Very confident

Note: The complete FTDICK instrument used in the pre-test is available in the previous paper of Habiddin and Page.[1]

REFERENCES

1. H. Habiddin, E. M. Page, *Indones. J. Chem.* **19** (2019) 720–736 (https://doi.org/10.22146/ijc.39218).